SERIES OF BOOKS

ON

ELECTRONIC VALVES

The series of books on electronic valves includes:

Book I **Fundamentals of Radio Valve technique**
547 pages 6″ × 9″, 384 illustrations, cloth bound

Book II **Data and Circuits of Radio Receiver- and Amplifier Valves**
1933/39, 424 pages, 531 illustrations

Book III **Idem**
1940/41, 220 pages, 267 illustrations

Book IIIA **Idem**
1945/50, ± 480 pages, 500 illustrations (in preparation)

Book IV **Application of the Electronic Valve in Radio Receivers and Amplifiers** (Vol. I)
1. R.F. and I.F. amplification; 2. Frequency changing; 3. Determination of the padding curve; 4. Interference and distortion due to bend in characteristics of the receiving valves; 5. Detection — 467 pages 6″ × 9″, 256 illustrations

Book V **Application of the Electronic Valve in Radio Receivers and Amplifiers** (Vol. II)
6. A.F. amplification; 7. The output stage; 8. Power supply — 450 pages, 343 illustrations

Book VI **Application of the Electronic Valve in Radio Receivers and Amplifiers** (Vol. III)
9. Inverse feedback; 10. Control devices; 11. Stability and instability of circuits; 12. Parasitic feedback; 13. Interference phenomena; 14. Calculations of receivers and amplifiers (in preparation)

Book VII **Transmitting Valves**
320 pages, 256 illustrations

BOOK VII

TRANSMITTING VALVES

TRANSMITTING VALVES

THE USE OF PENTODES, TETRODES AND TRIODES IN TRANSMITTER CIRCUITS

621.396.615 : 621.396.694

BY

J. P. HEYBOER †
Graduate of the Technical University, Delft

REVISED BY

P. ZIJLSTRA
Graduate of the Technical University, Delft

WITH A FOREWORD BY

H. A. THOMAS, D.Sc., M.I.E.E., M.I.R.E.
Research Department Lever Brothers and Unilever Limited

PHILIPS' TECHNICAL LIBRARY

THE ENGLISH TRANSLATION OF THIS WORK IS BY
G. DUCLOUX — SUTTON (ENGLAND)

DUTCH AND GERMAN VERSION HAS ALREADY APPEARED

FIRST PUBLISHED 1951

PRINTED IN THE NETHERLANDS

FOREWORD

TO THE ENGLISH EDITION

There are a great many books on radio valves and their applications to telecommunication. In most of these books the greatest attention is given naturally to receiving valves and associated circuitry because of their wide applications; usually, somewhat cursory consideration is given to transmitting valves, high-frequency transmitters, high-power modulators and frequency changers.

The appearance of a well presented book devoted entirely to transmitting valves and the theory of the circuitry associated with them is, therefore, most welcome to the electronic and radio engineer; when the late author was a member of the scientific staff of an international organisation with the high reputation of Philips and has been writing about a subject in which he was an expert, the reader naturally has confidence that the information given is up to date and authoritative.

The various aspects of transmitting valves, as amplifiers, modulators, oscillators and frequency changers, are all successively presented in a lucid manner; the text is not overburdened with mathematics and is well illustrated by over 200 carefully prepared illustrations; furthermore, the high technical standard expected of publications by the Philips organisation is well maintained.

This volume is a valuable contribution to electronic technology and can unreservedly be recommended both to the advanced student and to the professional engineer.

H. A. THOMAS, D.Sc., M.I.E.E., M.I.R.E.
Research Department,
Lever Brothers and Unilever Limited.

PREFACE

The author of this book, Johannes Pieter Heyboer, was a victim of the armies of occupation and did not live to see its publication. Honest and straightforward as was his nature, he could not but offer resistance to the injustice meted out to the allied peoples during the years of the 2nd world war. On January 30th 1945, when he was staying in Amsterdam in order to apply his knowledge of radio to the best possible advantage there, he and a number of his colleagues were taken by the enemy and on April 14th were put to death.

After the liberation his remains, together with those of many others who had given their lives for the freedom of their country, were removed to the Cemetery of Honour at Bloemendaal in Holland.

The manuscript of this book had been completed in 1944, and the publication of the Dutch edition in 1946 was made possible by the author's former colleagues. The rapid advances of technical science during the war years, details of which were only made known some years later, necessitated a complete revision of the original text for the English edition. This task was undertaken by the undersigned.

The main object of Mr. Heyboer was to prepare a complete study of transmitting valves and their applications, passing in turn to modulation, oscillation and frequency multiplication, in each case deriving the more important theoretical quantities for the characteristics of the valve, partly by calculation and partly by graphical means. During the last few years many books have been published on the subject of the operation of special valves with such high frequencies that the transit time of the electrons is an important factor in the mechanism of amplification.

The present book has been purposely limited to the treatment of valves in which the transit time is of minor importance, since the theoretical knowledge of valves which exhibit transit-time effects has not yet gained that degree of maturity that is to be found in the case of the more "classical" types of transmitting valves.

A publication, such as the present book, in which the properties of those "classical" transmitting valves have been treated in detail, will undoubtedly fill a long-felt want; it is in fact rather strange that a comprehensive study of the subject has not so far been published. We anticipate that the many users of transmitting valves, as well as students who wish to become more conversant on the subject, will adopt it.

The publisher intends to prepare a separate book, within the framework of the Philips' Series on Electronic Valves, about valves which do involve transit-time effects, as soon as the development and understanding of the working of those valves have reached completion.

P. ZIJLSTRA

CONTENTS

INTRODUCTION

Comparison of transmitting valves with receiving valves

Although there is no difference between receiving and transmitting valves as far as their action is concerned, it is nevertheless necessary to place them in separate categories, since the requirements to be met by the high-vacuum valves in a receiver differ so very much from those relating to the valves of a transmitter.

After all, the function of a receiver is to amplify and rectify the modulated R.F. signal in order to produce a sufficiently undistorted A.F. signal.

The object of a transmitter, on the other hand, is to convert a given amount of D.C. energy, obtained in turn from a source of direct voltage (mains rectifier, or battery with converter), into R.F. energy, and to modulate the latter with an A.F. signal, with the least possible degree of distortion. Further, for reasons of economy, this conversion must take place as efficiently as possible: a transmitter should therefore be regarded more as a converter. In effect, the anode current of a transmitting valve does not flow in the straight part of the static characteristic; the so-called impulse excitation employed causes the anode current to pass only for a period equal to less than half the alternating grid-voltage cycle. In receiving valves, as far as R.F. and I.F. amplifiers are concerned, this excitation method is not practicable, by reason of the high degree of distortion it produces. There is therefore no alternative in this case but to employ the straight part of the static characteristic, which means not only that a certain standing current must be accepted, but also that the optimum anode alternating current will be on the low side, and these two factors tend to reduce both output power and efficiency.

The latter, in view of the low output power, is of no significance, but, at the same time, the ultimate object is to amplify to the greatest possible extent the very weak grid signal: the receiving valve as used for R.F. or I.F. amplification should therefore be looked upon as a voltage amplifier.

This implies that the anode circuit of an R.F. or I.F. receiving valve works in conjunction with the highest possible external resistance, in the form of high-quality tuned circuits, whereas the anode of the transmitting valve usually only carries a fairly low loading resistance to handle the R.F. power developed, the work of the anode circuit proper being to prevent unwanted components of the anode current, arising from the impulse excitation, from passing through this loading resistance. The anode circuit of a transmitting valve thus functions as a filter for the harmonics and, as such, is made to include considerable capacitance. In the case of a receiving valve, on the other hand, the capacitance of the anode circuit must be kept relatively low, to ensure high parallel resistance.

So much, then, concerning the use of high-vacuum valves as R.F. amplifiers for reception and transmission.

In reception work the valve also serves as a mixing device, two R.F. signals being applied to different grids, to produce at the anode a signal of which the frequency is equal to the difference between the frequencies of the two R.F. signals: the principle employed in this process is based on the non-linear relationship between the anode current and the voltages on the grids in question.

The same principle is adopted for the superposition of the A.F. signal to be transmitted upon the R.F. signal in a transmitting valve; this is termed modulation, referring to the form assumed by the R.F. aerial signal as a function of time.

Frequency mixing in a receiving valve, however, is very different from the mixing process in transmission: firstly, in reception the applied signals are both of radio frequency, whereas in transmission one of these is a low-frequency signal; secondly, one of the R.F. signals of the receiving valve is modulated at various low frequencies, while in transmission the A.F. signal itself is composed of various frequencies. Thirdly, the modern receiving valve generates its own second or local frequency; the transmitting valve has to obtain its A.F. signal from a separate amplifier. In reception technique, then, the octode, with 6 grids, has been evolved, whereas transmission technique has not gone beyond the pentode with its three grids.

Further, it may be said that the receiver generally incorporates an I.F. amplifier as well as a detector for the A.F. signal, there being no equivalent of these in a transmitter: the A.F. amplifier of a receiver may

be compared with the modulation amplifier of a transmitter, with this difference that the output power of the latter is very much the higher. Lastly, the transmitter employs an oscillator as first stage for generating the transmission frequency; a similar function does not exist in the receiver.

In the following pages the first two chapters deal briefly with the technology and classification of transmitting valves from different aspects, after which the working of the high-vacuum valve under impulse excitation is discussed. Details are then given of the factors in transmitting technique that have led to the improvements upon the triode, namely the tetrode and pentode, passing in turn to a study of modulation and of the transmitting valve as oscillator and frequency multiplier.

chapter VIII contains certain special points of importance in the practical application of transmitting valves, and chapter IX introduces a number of problems encountered in the high frequencies.

Rectifier valves do not constitute part of the R.F. side of a transmitter and are therefore not discussed, but, although the same may be said of considerations regarding modulation valves, a few relevant remarks have been included in the Appendix, as it is felt desirable to say something of the manner in which the modulation power, referred to in chapter V, is obtained; this discussion, however, is confined to questions of power, efficiency and distortion, for as far as these factors are affected by the characteristics of the valve. Points relating to the frequency characteristics etc. of modulation amplifiers are considered to be outside the scope of the present work.

CHAPTER I

The Technology of Transmitting Valves

§ 1. The cathode

The heaters of early transmitting and receiving valves were manufactured from tungsten, as the use of this metal as a source of electronic emission had been prompted by the various requirements to be met by this source, as applicable to high-vacuum valves. On the one hand it is essential that emission be sufficiently high; on the other, evaporation of the metal at the working temperature should not be excessive if the life of the cathode is not to be so short as to present an uneconomical proposition. Rapid evaporation, moreover, would produce deposits of the metal on the other components of the valve, mainly the grids, with undesirable consequences, such as grid-emission, to mention only one. At the same time, cathode material must not be too brittle; otherwise it is easily damaged during transport of the valve.

Tungsten is a metal that meets these conditions fairly well, albeit a reasonable degree of emission is obtained only at elevated temperatures: the working temperature of the tungsten filament of a transmitting valve is in the region of 2550° K, at which level evaporation is sufficiently low to guarantee a reasonably long life. Naturally, the wattage needed to produce this high temperature is considerable, and a measure of the amount of power required, in comparison with cathodes made of other materials, is found in the specific emission, defined as the quotient of the saturation current and the heater power; a tungsten heater at a temperature of 2550 °K has a specific emission of 7 mA/W, and it will be shown in due course that this value contrasts very unfavourably with that of other kinds of cathodes.

For some time past, therefore, use has been made of other materials for the heaters of low-power valves. Even in transmitting valves for high-power output the tungsten heater is nowadays often superseded by carburized thoriated tungsten wire which requires very much less current to heat it.

Due to the low specific emission of tungsten, the heater wattage of the more highly powered valves sometimes assumes considerable proportions; for example, the TA 20/250, a water-cooled valve giving an R.F.

output of 250 kW at an anode potential of 20 kV, has a heater consumption of 14.7 kW (V_f = 35 V; I_f = 420 A): the saturation current of this heater is about 85 A.

Such high heater currents necessitate special constructions of both the heater and its leading-in conductors, and, in the case in point, the filament is composed of 12 wires, each 426 mm in length and arranged in two series groups of six parallel wires. The current per wire is thus 70 A, the thickness of the wire being 1.3 mm. Contact is established between the heater itself and the external terminals by means of thick copper rods, attached to the glass with robust chromium-iron flanges. Fig.1, depicting the head of the valve in question, clearly shows these heater connections, whilst in fig. 148 the same valve may be seen mounted in R.F. heating equipment.

As already stated above, thoriated tungsten is being employed more and more instead of plain tungsten for heaters, as this material ensures a considerable increase in the specific emission. These heaters are made of tungsten containing about 2% of thorium oxide.

This is subjected to a suitable thermal treatment in vacuo, whereby the oxide is reduced to thorium at the surface of the wire.

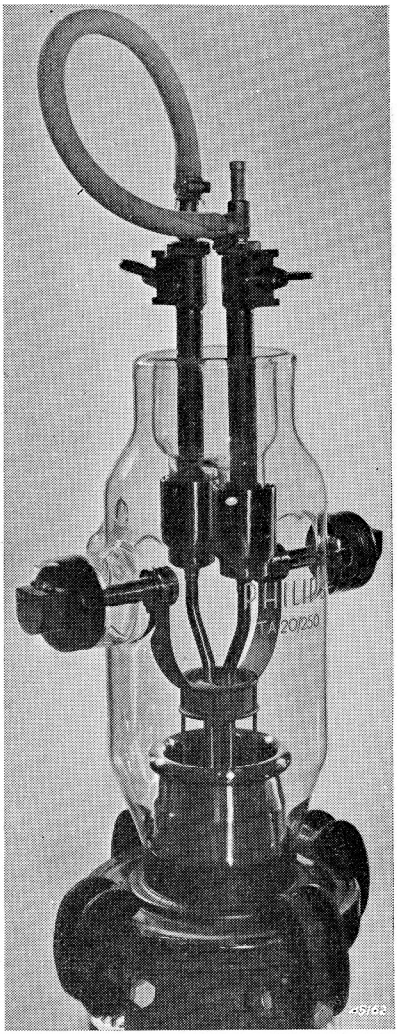

Fig. 1. Head of the water-cooled valve TA 20/250, showing the two connections for the heater and two for the grid.

Electronic emission is increased by this method to such an extent as to be much higher than that of the ordinary tungsten heater at even

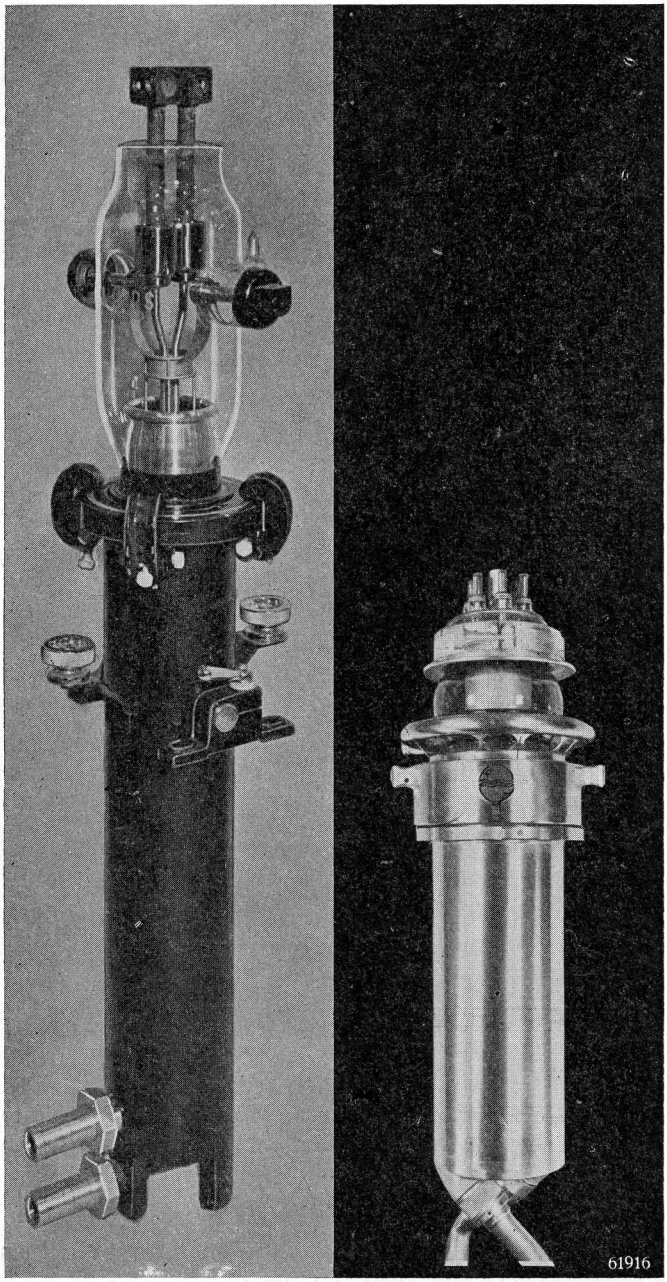

lower temperatures: at a working temperature of 2000° K the specific emission of thoriated tungsten lies between 70 and 100 mA/W. In practice, a certain quantity of carbon is introduced into the the tungsten wire by heating it for some time in hydrocarbon, since it is found that the presence of carbon accelerates reduction of the thorium oxide into thorium and so reduces the time required for activation of the

Fig 2a. Triodes with tungsten heater (TA 18/100) and with thoriated tungsten heater (TBW 12/100), both with water-cooled anode and delivering 100 kW.

wire. After carburizing, the outer layers of the tungsten filament consist of a compound of tungsten and carbon, and subsequent heating at a certain temperature under vacuum causes thorium to diffuse to the surface. It has been proved that evaporation of thorium from a tungsten-carbide core is very much less than in the case of non-carburized wire, irving to this and the life of the heater is improved.

Figs. 2a, b and c illustrate a number of triodes, some of which have the thoriated tungsten heater (TBW 12/100 and TBL 6/6000) and some the plain tungsten heater (TA 18/100, TA 12/35 and TAL 12/20). This last-mentioned valve is of the forced-air cooled type and has an anode dissipation of 20 kW.

The higher specific emission of thoriated tungsten heaters brings with it certain advantages in connection with the design of the valve, such as lower temperature and less heating of other parts of the valve due to radiation, less

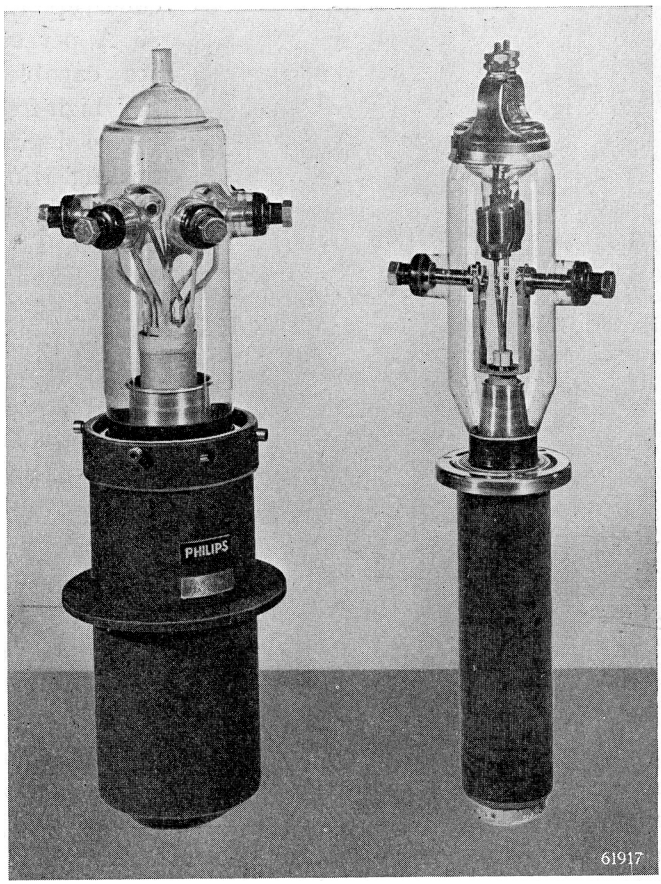

Fig. 2b. Triodes with tungsten heater: TA 12/35 and TAL 12/20. The first has a water-cooled anode, whilst the anode of the TAL 12/20 is air-cooled, the maximum dissipation being 20 kW.

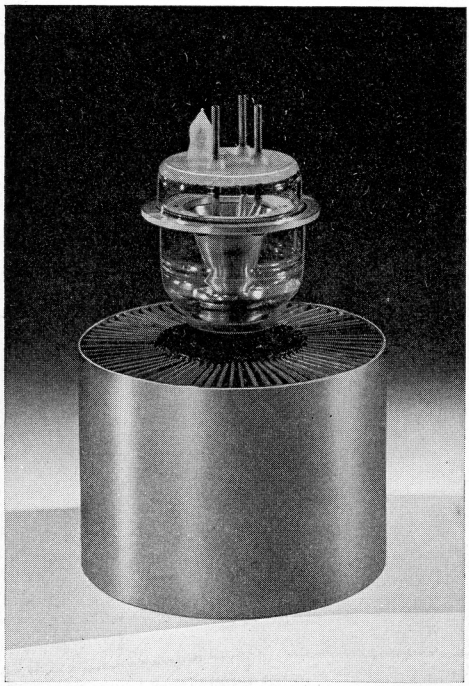

61918

Fig. 2c. Triode with thoriated tungsten heater: TBL 6/6000. The anode of this valve is forced-air cooled.

power required for heating purposes, lower current and consequently not so much trouble from ripple current caused by the magnetic field set up by the heater current. Compare for instance the TA 18/100 (tungsten) with the TBW 12/100 (thoriated tungsten); the first of these needs 7 kW for heating, with a current of 70 A per heater strand, whereas the second type takes only 3,6 kW at 33 A per strand. Both valves are capable of delivering 100 kW high-frequency energy.

Fig. 4 depicts a group of transmitting triodes equipped with thoriated tungsten heater (TB 2.5/300, TB 3/750 and TB 4/-1250). The first of these delivers 390 W at 2500 V anode potential and the TB 4/1250 gives 1750 W at 4000 V anode voltage. In fig. 5 two tetrodes with this type of heater are shown, viz. the QB 3/300 and the QB 3.5/750, of which the first is rated at 375 W with an anode potential of 3000 V and the second at 1000 W with 4000 V anode voltage.

The highest specific emission is obtained from what are known as oxide cathodes, and these occur in transmitting valves in two different forms, namely directly heated and indirectly heated cathodes. The first-mentioned have the form of a wire stretched in the shape of a zig-zag and consist usually of nickel, tungsten or a combination of both, although other metals or alloys are also sometimes employed. The indirectly heated cathode comprises a nickel tube with a filament mounted inside it, and both types are coated with a layer of barium-strontium carbonate. When such cathodes are heated to incandescence

in vacuo the carbonate is broken down to form, amongst other things, barium oxide, and continued heat treatment ultimately produces free barium at the surface of the layer of oxide. The emission of electrons from a cathode of this type is very high; at a working temperature of about 1060 °K the specific emission is 200 to 300 mA/W, and such cathodes are used in small transmitting valves.

In valves intended to deliver more than 100 W, oxide cathodes are rarely employed, owing to the deposition of barium on parts of the valve where it is not wanted, during the process of heating, pumping and degassing. Local differences in temperature inside the valve during pumping are not so great in smaller valves, and there is then less chance of undesirable deposits.

Fig. 6 illustrates two double tetrodes of the oxide-cathode type, viz. the QQE 06/40 and the QQC 04/15; the first of these has an indirectly

Fig. 3. Triode with thoriated tungsten heater: TBW 6/6000. The anode is water-cooled.

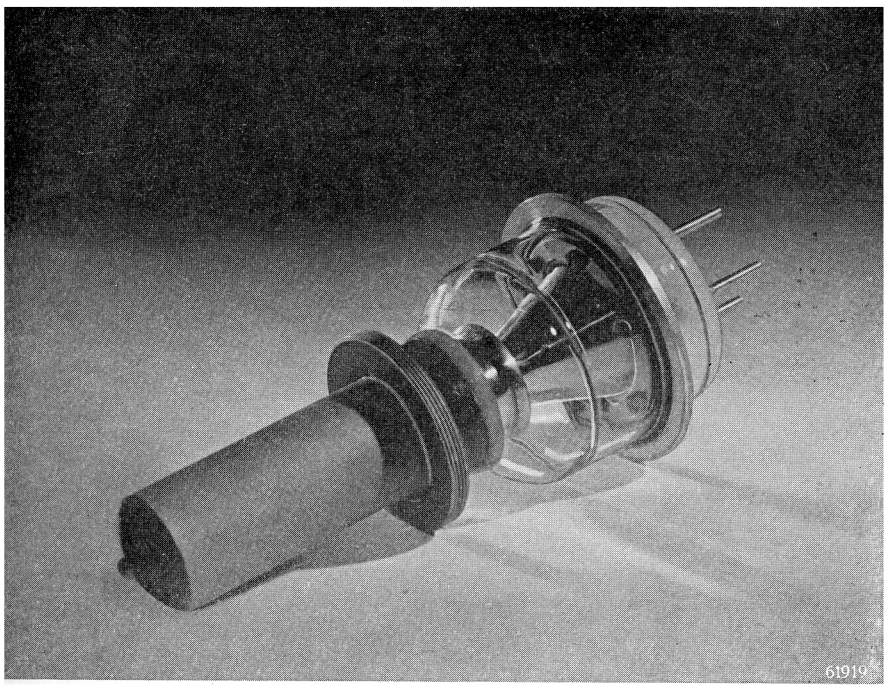

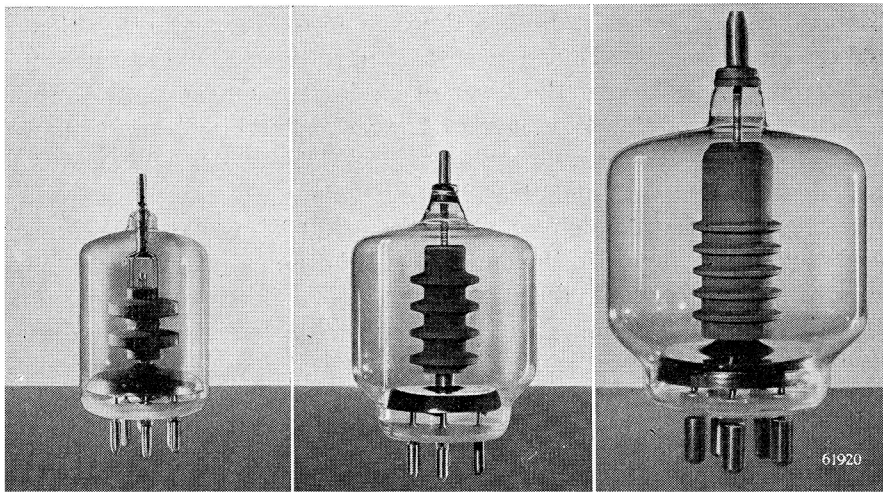

Fig. 4. Triodes with thoriated tungsten heater:
TB 2.5/300, TB 3/750 and TB 4/1250.

heated cathode and delivers 85 W at an anode potential of 600 V, and the other is directly heated, giving 20 W at 400 V anode. Pentodes fitted with oxide cathode are depicted in fig. 7, namely the PE 1/100 and PE 05/25, both of which are indirectly heated. The PE 1/100 delivers 132 W at 1000 V anode voltage and the PE 05/25 33 W at 500 V anode voltage.

§ 2. The anode

The choice of material for the anode is governed by the rating of the transmitting valve, seeing that this is linked with the anode dissipation and, therefore, with the temperature to which the anode is raised, under working conditions. In low-power valves with oxide cathode, the anode is nearly always made of nickel, one reason being that this metal can be very easily worked into almost any desired shape.

The surface of these anodes is generally blackened, since the heat must be dissipated by radiation and this occurs more efficiently at lower temperatures the nearer the surface of the anode approximates that of a black body. If the anode were made of bright nickel, it would run at a higher temperature in comparison with a black anode radiating a given

amount of power. Too high a temperature is undesirable, since nickel volatilizes at relatively low temperatures and also because an increase in anode temperature is accompanied by a corresponding rise in the temperature of the grid, which tends to produce grid emission.

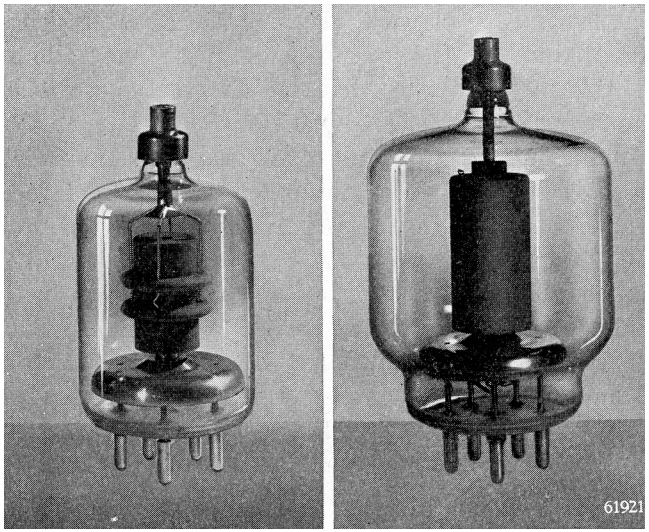

Fig. 5. Tetrodes with thoriated tungsten heater: QB 3/300 and QB 3.5/750.

The anodes of the valves shown in fig. 7 are made of black nickel. Most anodes are provided with cooling fins, to increase their radiating surface.

Another component of the valve is the getter, which usually takes the form of a barium mirror, to be found deposited on the wall of the bulb; this getter serves to absorb any traces of gas that may be liberated when the valve is put into service, and thus maintain a high vacuum. In valves of higher power, such as those fitted with thoriated tungsten heater, the anode is usually of molybdenum or graphite, since the anode dissipation and therefore also the working temperature of the anode, are too high to permit of the use of nickel. It might be argued that the temperature could be reduced by increasing the area of the anode, but internal capacities and self-inductances are also increased with the size of the anode, and this is undesirable, especially at the higher frequencies. The only remedy is to employ a metal that will withstand heavier loads, and molybdenum is admirably suited to this purpose: its melting point is 2600° C, as compared with 1450°C in the case of nickel; so it can be used at higher temperatures than the latter. Moreover, molybdenum is fairly easily processed and in this respect is preferable to tungsten, which is extremely difficult to machine. Tantalum is another metal sometimes used for this purpose.

The latter type of valve also includes a getter, usually zirconium, which is introduced in the form of a fine powder on the anode, an advantage of this method being that the zirconium-coated surface of the anode radiates very well. The QQE 06/40 depicted in fig. 6 is fitted with a molybdenum anode, but, apart from this material, graphite is often employed for valves of this size, the excellent radiating properties of graphite being a distinct advantage. The brittleness of this substance, however, necessitates a much thicker anode wall in comparison with that of the metal anode, but any risk of warp in the anode is thereby eliminated. Furthermore, the distribution of heat in a thick-walled anode is more uniform than in a thin one, apart from the fact that the thermal capacity is greater. Graphite anodes are therefore especially suitable for use in cases where short-lived overloads are liable to occur, as in industrial applications. The valves shown in figs. 4 and 5 are equipped with graphite anodes.

So far, the types of valve described all have anodes which depend upon radiation for the dissipation of their heat, but this system is restricted to valves of fairly low power, i.e. valves with not too high an anode dissipation. The largest triode in this category is the TB 3/2000, the maximum anode dissipation of which is 1100 W.

Fig. 6. Double tetrodes with oxide cathode: QQE 06/40 (indirectly heated) and QQC 04/15 (directly heated).

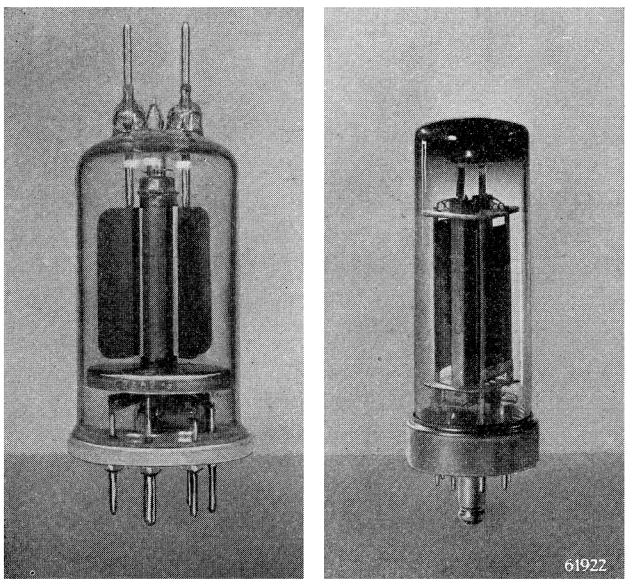

In valves of a higher rating, i.e. higher anode dissipation, special methods of cooling are employed, the most common being water-cooling; the envelope in this case is not the conventional glass bulb as

in the radiating-anode types, but the anode itself, made of copper, functions also as part of the envelope. Grid and heater leads are carried through a glass seal, which not only renders the anode vacuum-tight, but also ensures adequate insulation between the different electrodes.

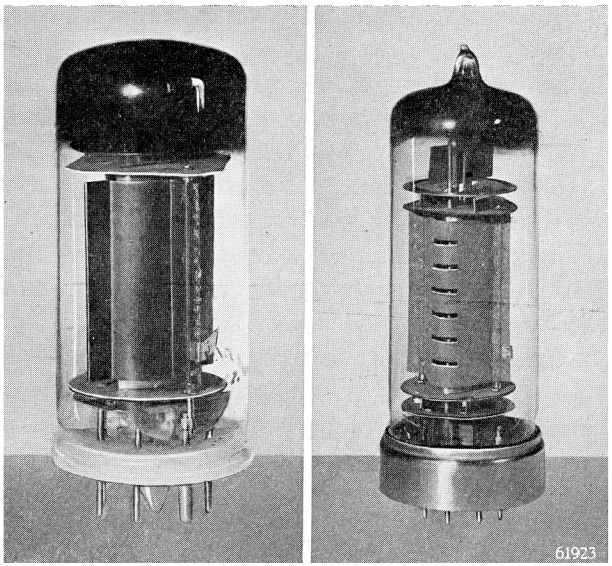

Fig. 7. Pentodes with oxide cathode: PE 1/100 and PE 05/25.

The anode is then encased in a cooling jacket, which in turn may be double-walled, in which case the cooling water enters between the anode and the inner face of the jacket and flows out between the inner- and the outer wall. In valves intended for a high specific anode dissipation, the turbulence of the cooling water (and therefore also the speed at which the heat is conveyed away) is increased by means of a spiral winding soldered at the inner surface of the water jacket. A sketch of the jacket, partially open, is given in fig. 9. From the same sketch follows that the water jacket of the valve TBW 12/100 has an automatically working water seal: the enlarged view in the separate circle in fig. 9 shows how the rubber washer (indicated by hatching from left top to right bottom) is pressed against the anode flange through the working of the water pressure. This construction permits just to turn and take the valve vertically out of the water jacket, without any timetaking unscrewing, after the water pressure has been taken away. Fig. 10 shows the TA 12/35, together with its appropriate cooling jacket. This triode has an output power of 42 kW at an anode potential of 15 kV, the maximum anode dissipation being 18 kW. For comparative purposes it may

be noted that the quantity of cooling water required by this valve is 20 litres/min.

The heater wattage of this valve is 4.44 kW, which is in itself sufficiently high to necessitate water cooling, even if no further power were applied to the valve, and for this reason the water-cooling system must always include a water switch to cut off the heater current in the event of the flow of water falling below a certain pressure.

In view of the high anode voltages involved, the cooling water must be introduced in such a manner that there is sufficient insulation resistance between anode and earth, and this is achieved by feeding and draining away the water through rubber tubes of adequate length, which, in order to save space, are coiled on a drum. Instead of rubber tubing, plastic tubing or porcelain tubes, built up to form a spiral, are nowadays used.

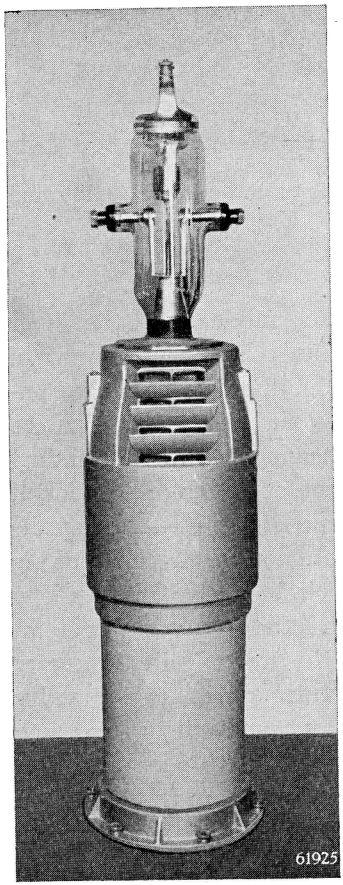

Fig. 8. Triode TAL 12/20 in an air distributor. The air is applied from below, is then separatee into numerous horizontal ducts, one above thd other, and passes along the anode, leaving the distributor by way of similar ducts, of which the outlets are partly visible in the figure.

Air under pressure is also employed for the cooling of the anode. The copper anode is then mounted in the cooler, which consists of a jacket having in it a number of longitudinal baffles.

A thin metal case is placed round this radiator, to the underside of which a stream of air from a blower is applied. The anode is brassed into the radiator, to ensure proper heat transfer between the anode and the cooling fins.

In the case of transmitting valves whose anode dissipation is of the order of 20 kW the system in question is not practicable since the temperature of the air increases continually as the latter passes along the anode, with the result that the part of the

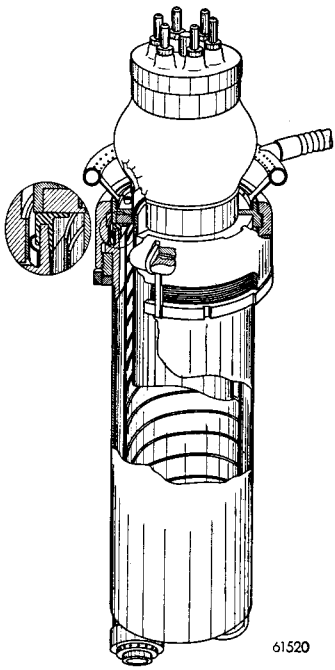

Fig. 9. Sketch of the water jacket for the valve TBW 12/100. The copper spiral winding for increasing the turbulance of the cooling is shown, and in the separate circle the automatic waterseal which enables a quick change-over to new tubes, is depicted.

anode which is the last to receive the air is unable to transfer sufficient of its heat. In a new design this objection is overcome by dividing the stream of air among a number of horizontal ducts, in each of which it has only a short distance to travel; the temperature of the anode, as between one end and the other, thus varies only slightly. Another advantage of this system is to be found in the fact that the loss in air pressure in the short ducts is very small, so that, without losing too much overall pressure, it is possible to employ a large number of cooling fins of small radial dimensions and keep the width of the system at a minimum.

By this means it has

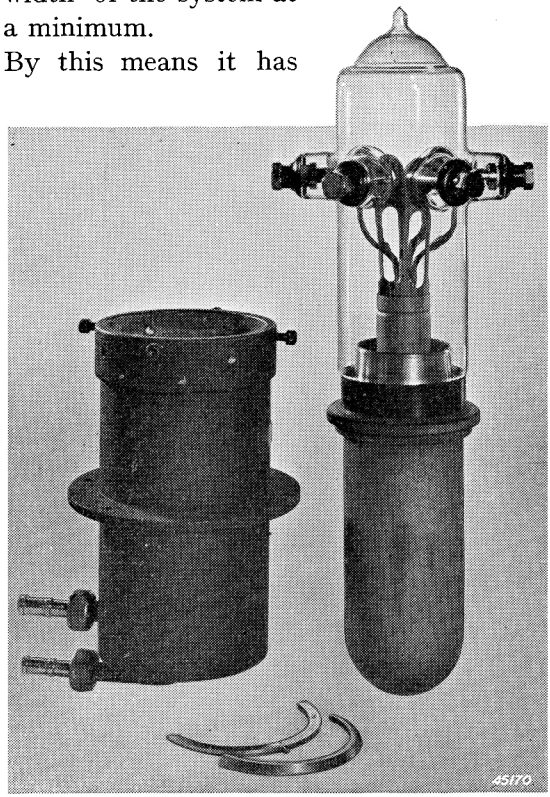

Fig. 10. Water-cooled triode TA 12/35, showing separate cooler. Anode voltage 15 kV. R.F. power 42 kW. Anode diss. 18 kW. Cooling water 20 litres/min.

proved possible to obtain the same anode dissipation from Philips water-cooled valves, using air cooling, as when using the original water system. The advantages of air cooling lie in the absence of insulated water hoses or ceramic cooling spirals, as also in the possibility of employing high-power valves at points where the lack of a fresh-water supply would otherwise necessitate the use of a complicated, closed water system.
Fig. 8 depicts the triode TAL 12/20, of which the anode is cooled in the manner described above. The permissible anode dissipation is 18 kW. The valve is placed in the appropriate air distributor, of which the horizontal baffles can be clearly seen.
Fig. 11 illustrates the triode TBL 6/6000, which is cooled in the first mentioned manner. This valve delivers approximately 6 kW at 6 kV. The maximum permissible anode dissipation amounts to 5 kW.
The quantity of air required to meet this depends upon the temperature of the air entering the cooler and also upon the height above sea level. At sea level and an initial temperature of 25° C, the amount of air required is 9.2 m³/min, whilst at 3000 m above sea level, for the same temperature, 13 m³ would be needed.

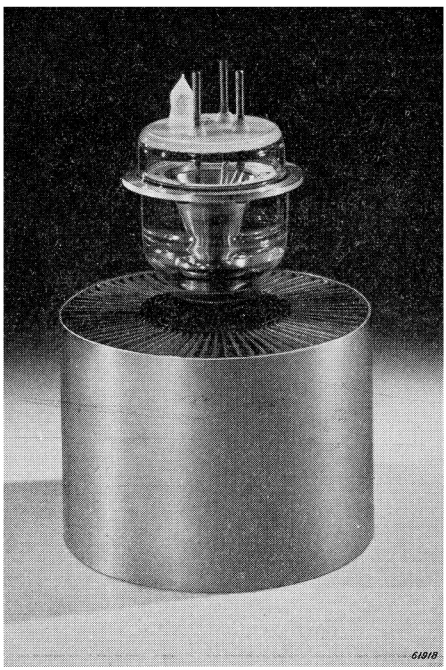

Fig. 11. Triode TBL 6/6000 with air-cooled anode. A cooling jacket with baffles is brazed to the anode and the air passes upwards through the baffles. Anode voltage 6 kV. R.F. output 6 kW. Anode dissipation 5 kW.

§ 3. The grids

The metal employed for the grids is again dependent upon the rating of the valve. As with the anode, it is also important for the grids to be able tot dissipate as quickly as possible the heat developed by them, especially in valves with oxide cathode, since materials that emit readily, such

as barium, evaporate from the cathode and are deposited on the grids, notably the control grid. If the grid temperature is too high, this layer of deposit will in turn emit, and this thermal grid emission, as it is termed, tends to produce some very undesirable effects which will be referred to in detail later.

One method of ensuring a low temperature of the grid wire is to use thick grid supports of a highly conductive metal, and, in order to render the transference of the heat through these supports as effective as possible, blackened cooling fins can be welded to their free ends, to conduct away the heat by radiation.

Another method applied successfully in the construction of the grids of oxide-cathode transmitting valves consists in processing the surface of the grid wire in a manner that reduces the absorption of heat to a minimum, on the principle that the temperature of the control grid is almost wholly governed by the heat radiated by the cathode and other electrodes in the direction of the control grid, whereas the amount of heat generated in the latter itself by electronic bombardment (control-grid current) is only very small. The surfaces of the grid then function effectively as reflectors of the heat, and this is one of the reasons why the control grid of some oxide-cathode valves is coated with gold; moreover, gold will not absorb oxygen from any barium oxide that may be deposited on the grid by evaporation from the cathode, and the grid therefore does not become coated with free barium. In this way secondary emission is avoided. For valves with thoriated tungsten filament, platinum coating of the grid is often used.

If heat is developed within the grid itself, as occurs in the screen grid of a pentode by reason of the electronic bombardment by the screen current, the surface should possess good radiating properties, and this is ensured by coating it with zirconium, to enable it more easily to dispose of the heat. Zirconium has the additional advantage that it binds any traces of residual gas in the valve, especially when the metal is hot.

Owing to the higher excitation voltages applied to the grid of this type of valve, which may attain positive grid potentials of 100 to 200 V, the occurrence of secondary grid emission is fairly common; it is known that when metals are bombarded by electrons they emit secondary electrons in a concentration that depends upon the speed of movement of the primaries, the angle of incidence, the material and the condition of its surface. In certain circumstances then, the

number of secondary electrons liberated from the metal may exceed the number in the primary stream impinging upon the grid. In the case of a transmitting valve, the externally measured grid current, equal to the difference between the primary (arriving) and secondary (departing) electrons, is reversed, because, in view of the higher anode- or screen potential, the greater part of the secondary electrons liberated from the grid do not return thence, but flow away to the anode or screen. The degree to which the grid current becomes lower, or negative, is, for a given valve, dependent on the ratio between the anode- and grid potentials; this is illustrated in fig. 23, which shows the control-grid current plotted against the anode potential at different control-grid voltages of a triode. This valve is equipped with a molybdenum grid. Secondary grid emission brings in its train certain advantages as well as disadvantages and these will form the subject of later discussion. If the secondary emission of the grid is to be suppressed, the wire must be coated with a substance that will give only a low secondary emission, or the configuration of the valve must be such that a potential minimum is formed in the region of the control grid as soon as the primary grid current reaches maximum, thus preventing any secondary electrons from leaving the electrode. In water-cooled valves with tungsten filaments, molybdenum is again used for the grid; only in the largest types, in which the grid is more heavily loaded, tungsten is employed.

§ 4. The envelope

The envelope of small and medium-sized valves consists of a glass bulb, closed at one end by a powder glas- or pressed glass base into which the leading-in wires for the electrodes are mounted.

The heat generated in the various electrodes within the valve is radiated towards the bulb, and part of this heat passes through the glass, the rest being absorbed by it. The temperature of the bulb, therefore, increases to the point where, mainly through convection in the surrounding air, a certain final temperature is reached, and this ultimate value must be kept sufficiently low, to ensure that the glass does not soften or liberate any gases.

Low-power valves (oxide cathode) can be made with ordinary soft glass bulbs, i.e. lime and lead glass, and the latter is employed for the more heavily loaded valves. When the anode temperature is fairly high, as in the thoriated tungsten types, it is better not to use soft glass,

in view of its low softening point; hard, or borosilicate glass, of which the softening point is much higher, is better able to withstand the higher temperatures and is therefore generally used for such valves.
In effect, this means that for a given power, the dimensions of a valve with hard-glass bulb may be smaller than those of an equivalent valve in soft glass, and this is a great advantage at very high frequencies, as will be explained in chapter IX.
As already mentioned, the anode of water-cooled valves is closed by means of a glass seal (see fig. 1), through which the leading-in wires pass to the heater and grids, and, as the working temperature of this class of valve is not very high, soft (lead-) glass is used for the seal, provided the construction of the valve is such that radiation from the heater does not fall upon the glass parts. Valves with external metal anode intended for high frequencies are preferably not made from soft glass. At such frequencies transit-time effects are very liable to occur, which in turn may give rise to electronic bombardment of the glass. Furthermore, dielectric losses in the glass, as well as capacitive currents between the electrodes, are increased at the higher frequencies. These currents increase the amount of heat generated in the leading-in wires, and this heat also raises the temperature of the surrounding glass. For all these reasons valves which are suitable for the higher radio frequencies are usually made from hard glass, of which the softening point is higher than that of ordinary glass. In Philips water-cooled valves of the soft-glass kind, the joint between the glass and the anode takes the form of a chromium-iron ring, to overcome the difficulty arising from the fact that the wide difference between the coefficients of expansion of glass and copper renders it impossible to seal the one to the other without involving very unconventional methods of construction. Chromium-iron is an alloy of which the coefficient of expansion is almost identical with that of glass, and the ring in question can be clearly seen from the illustration of the TA 20/250 in fig. 1. In hard-glass valves use is made of fernico alloy (iron, nickel and cobalt), which is adapted to hard glass in the same way that chromium-iron is adapted to soft glass.
Connection between the heater- and grid leading-in wires and the glass of the Philips water-cooled valves is established by means of chromium-iron or fernico flanges, to the inside and outside of which copper rods are soldered, to ensure sufficient electrical conductivity between the electrodes and the outer circuit.

For use at the higher frequencies, the metal is often coated with a highly conductive material, in order to reduce the amount of heat produced by the R.F. currents.
In the smaller valve types, nowadays often employed for higher radio frequencies, efforts to ensure low capacitances and inductances often result in cramped construction. In such cases the resultant high specific load on the envelope makes the use of a hard glass essential. The material used for the leading-in wires sealed into the sintered glass base as well as in the bulb itself is then molybdenum, whose coefficient of expansion closely matches that of hard glass. Usually the heater- and grid connections are in the base, the anode connection being in the top of the envelope, as in the TB 2.5/300, TB 3/750, TB 4/1250, QB 3/300, QB 3.5/750 and QQE 06/40 (figs. 4, 5 and 6). In the QQC 04/15, PE 05/25 and PE 1/100, however, all the electrode connections are taken through the glass base (see figs. 6 and 7).

§ 5. Construction

Before the different components are assembled in the complete valve, they are first cleaned in one or more baths and are subsequently degassed.

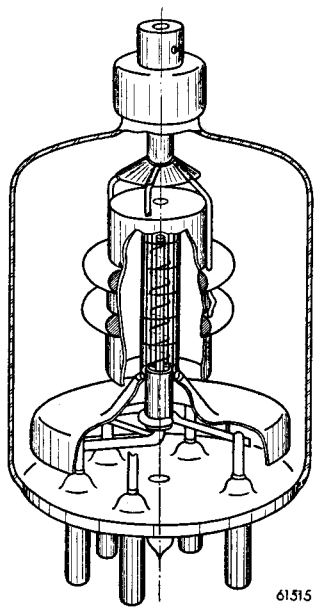

Fig. 12. Sketch showing the construction of the tetrode QB 3/300.

The method of assembly reveals individual peculiarities in each different type of valve, but in both those with pressed glass- and sintered glass base, the heater- and grid assemblies are mounted on those components; in some types the anode is also included, whilst in others it is carried by the bulb. The insulating material employed for holding the various electrodes of the valve in position is usually mica, but, generally speaking, and more especially in the case of high frequency valves, the use of insulating materials is avoided wherever possible because of their dielectric losses. Fig. 12, depicting

the transmitting tetrode QB 3/300, is a typical example of modern assembly methods.
The sintered-glass base carries five molybdenum leading-in pins and also the exhaust stem. Two of these pins are joined to the extremities of the heater and one to the control grid, whilst the two others support the cap to which the screen grid is attached; in this arrangement no additional insulating material is necessary between those parts of the system which carry the R.F. voltages. The cap attached to the screen grid has several functions, the first of which is to prevent capacitive coupling between the anode and the other parts of the system. Secondly, it intercepts heat radiated by the anode and heater and thus prevents the base of the valve from overheating. Finally, it constitutes a non-inductive connection between the leading-in pins and the screen grid itself. The anode is suspended on a molybdenum rod, which also serves for the external connection passing through the envelope.
The grid-heater assembly of a water-cooled valve such as the TA 12/35 (fig. 10) is mounted on the glass closure of the anode.
The heater is supported from a central rod by a spring device which counteracts the changes in the length of the wire due to expansion when hot. The grid is supported by a metal can which is in turn attached to the grid leading-in pins. Returning to the heater, this is wound in such a manner that the heater current of each section is 120° out of phase with its neighbour (when fed with three-phase current); at the same time, diametrically opposite, sections of the heater are connected to the same phase. This arrangement ensures a very low hum level, which is further hardly affected by any possible lack of symmetry.

§ 6. Pumping

Pumping operations are carried out in order to evacuate the valve to an extent that will eliminate any risk of liberation of residual gases when the valve is subsequently put to work. Apart from the degassing of the individual components before they are assembled in the valve, the various electrodes are raised during pumping to a temperature far in excess of that under which they normally function.
Glass valves are heated in an oven, to release any gases that may have been adsorbed (mainly water vapour), which are then removed by the vacuum pump.
Next, the anode is heated to redness by means of R.F. currents, the

latter being supplied by a coil which is placed round the valve; this coil may be regarded as the primary winding of a transformer of which the secondary is the anode itself, functioning, as it were, as a short-circuit winding. When the anode has been sufficiently degassed in this manner, the heater is "formed", by raising it, at a carefully adjusted voltage, to the temperature at which the emitting layer forms.

The grids, and usually also the anode, are then degassed by electronic bombardment, after which the getter is touched off (in oxide-cathode valves and in some thoriated tungsten filament valves). A small metal tray with gauze cover, or possibly a tube, filled with metallic barium is mounted at a convenient point within the valve, and this is heated by means of R.F. current to the temperature at which the barium volatilizes: the latter is thus deposited on the nearby wall of the bulb and serves to absorb any residual gases still within the valve or liberated subsequently, so that a good vacuum is always maintained.

At this stage the valve is sealed and capped. Oxide-cathode valves are then generally left for some time on a slightly higher heater voltage than normal, and a certain cathode current is maintained, to complete the forming process and stabilize the emission.

The pumping operation in the case of small oxide-cathode valves is carried out on a rotary pumping machine, on which the various manipulations described above are completed in their proper sequence and for a certain pre-determined time. Larger valves, such as the more highly powered, thorium, and water-cooled valves, are pumped singly. The pumping method as applicable to thorium valves differs slightly from that employed for oxide valves in that the heater undergoes a different treatment. As previously mentioned, this heater is carbonized and this carbonizing operation is completed before pumping is commenced: further the heater is momentarily raised to a high temperature, before carbonizing, in order to degas it.

It is not possible to heat the anodes of water-cooled valves by the R.F. method; so these are heated in a furnace, after which the heater is degassed at a high temperature, and lastly the grids, by electronic bombardment.

All these operations connected with the various components of the valve have to be repeated a number of times, since the gases liberated by the degassing of the heater and grids are readily deposited on the cold anode.

CHAPTER II

Classification

§ 1. Classification according to number of electrodes

Transmitting valves may be separated into groups according to the number of electrodes they contain, e.g. diodes, triodes, tetrodes, pentodes and dual valves.

a. *Diodes* are employed for voltage rectification in the conversion of alternating mains voltages to the direct current required for feeding transmitting valves. In former years high-vacuum diodes were used, but today preference is usually given to mercury-vapour rectifiers, which have the advantage that their efficiency is very high (as much as 99.5%), thanks to their extremely low internal resistance, which means also that the direct voltage delivered is practically independent of the load. To obtain less temperature dependance, a xenon gas filling is used instead of mercury vapour, for some applications.

b. *Triodes*, in transmission work as well as reception, figured as the original R.F. amplifiers, but the higher power demanded has tended to render them bulky, whilst in some cases special cooling of the anode, by means of air, water or oil, has to be resorted to. Since the transmitting valve, as explained in Chapter III, functions as a converter of energy, the method of its incorporation in the circuit differs from that employed in reception (see § 3 — Applications).

c. *Tetrodes* in comparison with triodes have in transmitting technique the advantage of lower driving power (see Chapter IV). The screen grid also reduces the capacity between anode and control grid, to such an extent that the neutralizing circuit, which is essential to a triode, only becomes necessary at the higher frequencies.

d. *Pentodes* were developed from the tetrode as a natural result of the drawback inherent in the latter in the shape of secondary emission at the anode, which renders the flow of anode current, and therefore also the efficiency, lower than that of an equivalent triode. The provision of a "suppressor" grid between screen and anode remedies this and even makes comparable the efficiency of a pentode and that of a triode, whilst maintaining all the advantages of a tetrode. Due to the presence of the two grids between anode and control grid, the capacity between these electrodes is less than in a corresponding

tetrode. In transmission work, so-called "suppressor-grid modulation" has acquired some importance (see Chapter V, § 6, in view of the fact that this method of amplitude modulation entails only a very small amount of modulation power. At the present time tetrodes are frequently made with "beaming" electrodes, so that the space charge between screen grid and anode constitutes a potential minimum, which assumes the function normally fulfilled by the suppressor grid. Modulation without power consumption is not then possible however.

e. *Dual valves.* Valves of this type embody two identical electrode systems in a common envelope, the special advantage of which, when used at ultra-high frequencies, is that it then becomes possible to construct balanced circuits with only very short leads. This point is referred to again in Chapter IX.

§ 2. Classification according to power

It is also possible to classify valves according to their output power rating, with special reference to the method of cooling the anode.

a. In valves of low or medium power (up to a maximum of about 2 kW) the anode is cooled by *radiation*, the envelope being a glass bulb, and in this category the highest possible anode dissipation obtainable is roughly 1 kW.
   It would not be practicable to handle a higher anode dissipation in this manner, since the proportions of the anode, and consequently also of the bulb, would become too great, making the valve unsuitable for use at ultra-high frequencies.

b. For valves of higher power, *forced cooling* is therefore employed, by means of either air or water, as described in Chapter 1, § 2. In certain cases oil is used for cooling purposes.

§ 3. Classification according to function

a. *Rectifying valves* are used for the conversion of alternating voltage into direct voltage, for feeding transmitting valves. As already mentioned, the valves employed are diodes with mercury vapour or xenon filling and with or without grid control.

b. *R.F. power amplifiers* provide for the conversion of direct currents into R.F. currents, making use of a separately generated alternating voltage for purposes of control, and it is essential to effect this con-

version with the highest possible degree of efficiency: a power amplifier must be regarded more as a converter, in contrast with the R.F. and I.F. amplifiers in a receiver which function as voltage amplifiers. As described more fully in Chapter III, the transmitting valve (triode, tetrode or pentode) must be made to work at a certain setting in order to ensure maximum efficiency, namely the type of setting known as Class C, whereas in reception work, the Class A setting is almost invariably employed (see Chapter III, § 1).
When R.F. power amplifiers serve for the transmission of speech or music, they have to be modulated, and the oldest and most common form of modulation is known as "amplitude modulation". This is referred to again in Chapter V.

c. *Modulator valves* are those which are employed for amplification of the signal supplied by the microphone to the level required for the modulation of the power amplifier. Their uses thus lie within the range of low (audio) frequencies.

d. *Oscillators* serve for generating R.F. oscillations and constitute the first stage of a transmitter, often in conjunction with a crystal, for stabilization of the frequency.
Applications of transmitting valves as oscillators for much higher power ratings are to be found in R.F. heating- and diathermy equipment (see Chapter VI).

e. *Frequency multipliers* are included in transmitters operating at high frequencies, where direct excitation and amplification would present difficulties. One or more such stages are employed between the oscillator and the output stage for purposes of frequency multiplication (usually doubling or trebling), and in this application transmitting valves in the Class C setting are eminently suitable by reason of the fact that the anode current of a Class C amplifier contains components having frequencies which are multiples of the fundamental frequency. Suitable circuits (see Chapter VII) make it possible to separate the desired component and amplify or multiply it.

CHAPTER III

The Triode as R.F. Power Amplifier

Introduction

In this chapter a calculation will be given of the power absorbed and dissipated, and of the efficiency of a triode in a R.F. power amplifier.

A. In §§ 1 to 3, calculations will be found of Class A, B and C triodes in which it is assumed that the slope of the I_a/V_g characteristics is constant, and that the amplitude of the alternating anode voltage is equal to the steady anode voltage. The anode current is not affected by the anode voltage; the I_a/V_g characteristics are straight lines, parallel to the V_a axis and terminating at the I_a axis. The effect of curved I_a/V_g characteristics is also investigated.

B. §§ 4 to 10 furnish calculations in which the I_a/V_g characteristics are again straight and mutually parallel, but not parallel to the V_a axis; they all terminate at a straight line passing through the origin of the I_a/V_g diagram (the so-called limit characteristic; see fig. 25). The maximum and minimum values of the anode current and voltage respectively are determined by this characteristic, i.e. the valve is excited up to its limit characteristic.

Reminding the limitations due to the maximum permissible values for anode dissipation, steady anode current and peak current (§§ 4 to 10), we shall calculate the greatest value of output power that can be attained under these conditions.

In §§ 8 to 10, calculations are also given on the basis of the static characteristics as actually measured from various transmitting valves, from which it will be proved that the schematic method of showing the characteristics, referred to above, is quite suitable for the calculation of output power and efficiency.

§ 11 includes a summary of the conclusions to be drawn from the preceding arguments, whilst §§ 12 to 15 touch upon certain special subjects of interest.

§ 1. Impulse excitation

At the commencement of this work it was stated that impulse excitation is employed in transmitter amplifiers to ensure high efficiency. This is brought about by using the transmitting valve in the so-called Class C

setting, with the negative grid bias and alternating voltage on the control grid so adjusted that anode current does not flow during the whole cycle of the alternating voltage, but only for a part of it. In transmitting work three different settings of the valve can be employed, namely Class A, B or C: in Class A the grid bias and alternating grid voltage (the excitation voltage) are given a value that will cause anode current to flow during the whole cycle of the grid voltage; in Class B the anode current flows during roughly half the grid cycle, whilst in Class C the current period is less than half that of the excitation period.
In order to estimate the effects of these different valve settings on output power and efficiency, let us consider idealized conditions for a transmitting valve in which the I_a/V_a characteristics are straight lines, parallel to the V_a axis, in which case the anode voltage does not influence the magnitude of the anode current.

In practice, the pentode more or less fulfils these conditions, as does also the triode when the amplification factor is sufficiently high. Let the D.C. anode voltage be V_a and the grid-bias voltage V_g (the latter is a negative quantity), with alternating grid voltage $V_{gp} \cos \omega t$. The anode circuit will include an impedance Z_a, which, as explained in § 3, consists of a parallel arrangement of an inductance, capacitance and resistance. The value of the inductance and capacity is such that the resonant frequency of the circuit is equal to the frequency ω of the excitation voltage.

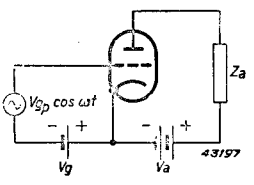

Fig. 13. Circuit of a transmitter amplifier.

From the theory of alternating currents we know that the impedance of this parallel circuit is a real quantity in respect of the frequency ω, and that it reaches its highest value at that point, being very much lower at both higher and lower frequencies. The impedance to direct current is nil. Fig. 14 shows the variation of anode current as a function of time, relating to the Class A setting of the valve derived from the given excitation voltage and static characteristic. It is evident that

$$i_a = I_{ao} + I_{a1} \cos \omega t, \quad \ldots\ldots\ldots\ldots \quad (3.\ 1)$$

in which $I_{a1} = SV_{gp}$, with S as the slope of the characteristic.
The anode current (3. 1) flows through Z_a and produces therein a voltage drop which, by reason of the above-mentioned properties of Z_a, may

be represented by $V_{a1} \cos \omega t = I_{a1} R_a \cos \omega t$, so that the residual anode voltage is:

$$v_a = V_a - V_{a1} \cos \omega t \quad . \quad . \quad . \quad . \quad . \quad . \quad . \quad . \quad (3.2)$$

At time t, the power converted into heat at the anode of the valve is equal to the product of v_a and i_a from (3. 2) and (3. 1); therefore:

$$w_a (t) = v_a i_a = (V_a - V_{a1} \cos \omega t) (I_{ao} + I_{a1} \cos \omega t),$$

or:

$$w_a (t) = V_a I_{ao} + (V_a I_{a1} - V_{a1} I_{ao}) \cos \omega t - V_{a1} I_{a1} \cos^2 \omega t \quad . \quad . \quad (3.3)$$

The power developed in Z_a is then:

$$w_o (t) = V_{a1} \cos \omega t \, i_a = V_{a1} \cos \omega t \, (I_{ao} + I_{a1} \cos \omega t), \quad . \quad . \quad . \quad . \quad (3.4)$$

whilst that supplied by the source of anode voltage is:

$$w_i (t) = V_a i_a = V_a (I_{ao} + I_{a1} \cos \omega t) \quad . \quad . \quad . \quad . \quad . \quad . \quad . \quad . \quad . \quad . \quad (3.5)$$

Naturally, $w_i (t) = w_o (t) + w_a (t)$.

The greatest amplitude that can be attained by the alternating component of the anode current $I_{a1} \cos \omega t$ in the case of Class A, is then apparently $I_{a1} = I_{ao}$; the highest value of the alternating anode voltage V_{a1} is slightly less than the steady voltage V_a, as will be shown later. If we now assume the ideal case whereby $V_{a1} = V_a$, we have:

$$w_a (t) = V_a I_{ao} - V_{ao} I_{ao} \cos^2 \omega t = V_a I_{ao} \sin^2 \omega t \quad . \quad . \quad . \quad . \quad . \quad . \quad . \quad (3.6)$$

$$w_o (t) = V_a \cos \omega t \, (I_{ao} + I_{ao} \cos \omega t) = V_a I_{ao} (\cos \omega t + \cos^2 \omega t) . \quad (3.7)$$

$$w_i (t) = V_a (I_{ao} + I_{ao} \cos \omega t) = V_a I_{ao} (1 + \cos \omega t) \quad . \quad . \quad . \quad . \quad . \quad (3.8)$$

The curves relating to $i_a(t)$, $v_a(t)$, $w_o(t)$, $w_a(t)$ and $w_i(t)$ are shown in fig.14, from which it may be seen that during a single cycle, the anode dissipation passes through two minima, namely when i_a and v_a respectively are zero. At all other values of t, the value of $w_a(t)$ must be other than zero, seeing that neither i_a, nor v_a is zero.

Fig. 14 further shows that the instantaneous power $w_o(t)$ over a certain part of the cycle is negative, and this fact is related to the definition of the power in question, i.e. the product of the alternating anode voltage and the total anode current. In the impedance R_a itself, however, the momentary power is expressed by:

$$V_a \cos \omega t \, . \, I_{a1} \cos \omega t = V_a I_{a1} \cos^2 \omega t,$$

which is therefore always positive. The rest of the anode current, I_{ao},

flows through the virtual circuit, that is, the parallel-connected L and C, and this component contributes towards the instantaneous power the portion:

$$V_a \cos \omega t \, . \, I_{ao},$$

which, being alternately positive and negative, means that the resultant instantaneous power is negative for a part of the cycle. The actual point at issue, however, is not the instantaneous value of the respective powers, but their average value over a single cycle of the excitation voltage. These values, which we term W_a, W_o and W_i (anode dissipation, output- and input power), can be very simply calculated from (3. 3), (3. 4) and (3. 5). We thus find that:

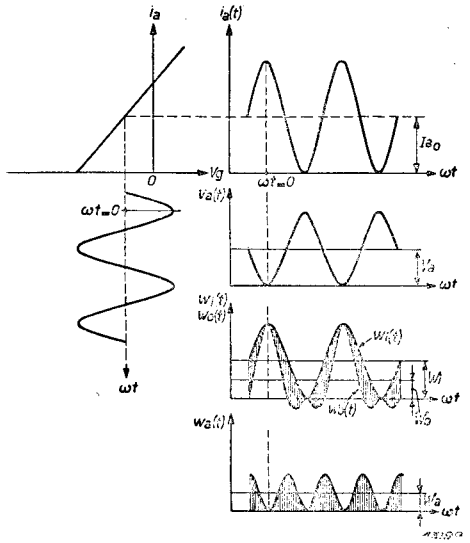

Fig. 14. Construction of the anode current, anode voltage, input power, output power and anode dissipation as function of the time in an R.F. Class A amplifier.

$$W_a = V_a I_{ao} - \tfrac{1}{2} V_{a1} I_{a1} \quad . \quad . \quad . \quad . \quad . \quad . \quad . \quad (3.\ 9)$$

$$W_o = \tfrac{1}{2} V_{a1} I_{a1} \quad . \quad . \quad . \quad . \quad . \quad . \quad . \quad . \quad . \quad . \quad (3.\ 10)$$

$$W_i = V_a I_{ao} \quad . \quad . \quad . \quad . \quad . \quad . \quad . \quad . \quad . \quad . \quad . \quad (3.\ 11)$$

The efficiency η, by which is meant the ratio of output power to input power, is:

$$\eta = \frac{W_o}{W_i} = \tfrac{1}{2} \frac{V_{a1} I_{a1}}{V_a I_{ao}} \quad . \quad . \quad . \quad . \quad . \quad . \quad . \quad . \quad (3.\ 12)$$

In the above instance, under the most favourable conditions with $V_{a1} = V_a$ and $I_{a1} = I_{ao}$, $\eta = 50\%$, that is, $W_o = W_a = \frac{1}{2} W_i$, and it will be clear that an efficiency value of this order would generally be far too low for high-power transmitters.

The reason for the high anode dissipation is clearly demonstrated by fig. 14, for the greatest instantaneous values of $w_a\,(t)$ are the result of the simultaneous occurrence of relatively high values of $v_a\,(t)$ and $i_a\,(t)$. If the efficiency is to be improved, therefore, the valve setting must be so modified that anode current will only flow when the anode voltage

is at fairly low values, and this is achieved in the Class B, and to a still higher degree, in the Class C setting.

Fig. 15 illustrates the Class B arrangement: the anode current, plotted against time, can now no longer be represented by a single formula, such as (3. 1) in the previous example, but must be written thus:

$$i_a = SV_{gp} \cos \omega t \text{ for } \begin{cases} -\pi/2 < \omega t < \pi/2 \\ \dfrac{3\pi}{2} < \omega t < \dfrac{5\pi}{2}, \text{ etc.} \end{cases}$$

and

$$i_a = 0 \text{ for } \begin{cases} \pi/2 < \omega t < \dfrac{3\pi}{2} \\ \dfrac{5\pi}{2} < \omega t < \dfrac{7\pi}{2}, \text{ etc.} \end{cases}$$

In § 2 it will be shown that this pulsating anode current may be broken down into a direct- current component and a number of sinusoidal components of frequencies which are all multiples of the excitation frequency ω. The anode impedance Z_a possesses the same characteristics as in the case of the Class A valve setting, and therefore only the component

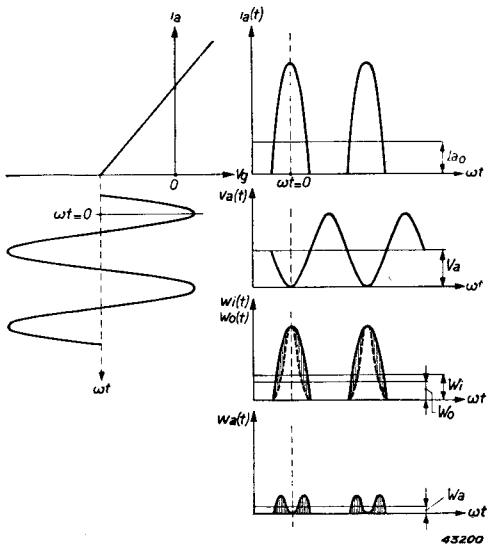

Fig. 15. As fig. 14, but in relation to R.F. Class B.

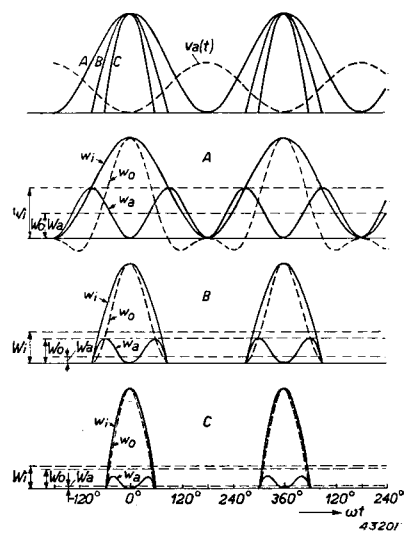

Fig. 16. Comparison of current and power in Class A, B and C R.F. amplifiers.

of which the frequency is ω will produce a voltage drop in the impedance, whilst the form of this voltage drop will naturally be sinusoidal with time.
At any given moment, the anode dissipation is again the product of the anode current passing and the anode voltage, but, due to the fact that the current is zero for a considerable period, just at the time when the voltage is high, the dissipation during that time is also zero, as will be seen from the curve of w_a with t, shown in fig. 15.
The Class C setting differs from Class B in that the negative bias on the control grid has a higher absolute value, which means that the part of the excitation period during which current flows is less than 180°.

From fig. 16 a comparison may be made between the three possible settings of the valve. In the upper figure the anode current is shown for each of the settings as a function of ωt, assuming the same maximum value of the current and the same anode voltage curve, in each case. It will be seen that in the Class A setting, current flows during the whole 360°, in the Class B for 180°, and the Class C setting has been chosen such that current flows only for 120°. Below this figure are shown the w_i, w_o and w_a curves, together with the average values of W_i, W_o and W_a. It is plainly seen from these diagrams that the low anode dissipation in the Class B and C settings is due to the decay of the anode current at those moments when the voltage is high.
This then is all to the good of the optimum efficiency, which in these settings is 78.5 and 89% respectively. It should be added that the efficiency of the Class C arrangement increases as the cycle during which current flows (the current angle) decreases. Calculations will show that the theoretical efficiency attainable is 100% (see § 2).

§ 2. Calculation of the current components

In calculations relating to the Class A setting, the curve of the anode current plotted against time may be deduced direct from the sinusoidal grid voltage and the straight I_a/V_g characteristic. The same holds good for Classes B and C, except that only in the case of Class A it is possible to effect a simple analysis of the anode current, that is into a D.C. component and an A.C. component of frequency ω.
The behaviour of each of these components in respect of the anode impedance Z_a can be ascertained, and from this the anode voltage

curve; in this way the action of the valve can be fully determined. The procedure in respect of Class B and C is similar, although the result of the division into the respective components is slightly more complex. It may be asked why this division into sinusoidal components should be necessary; the answer is that it is only possible in this way to determine the behaviour of the non-sinusoidal anode current in respect of the LCR circuit, by means of the methods of calculation known in the theory of alternating currents.

It is certainly possible to determine by a direct method the action of a series of impulses upon an LCR circuit, but this is not only a more complicated procedure; in the end it is less clear.

The division, or analysis, referred to above results in what is known as a Fourier series. Such a process enables any function which is periodic with time to be divided into a component that does not change with time, as well as a number of components which are sinusoidally dependent upon time. The frequencies of these components are not indefinite, but full multiples of another frequency, known as the fundamental.

Turning once more to the Class B and C settings, the anode impulses follow each other in synchronism with the positive voltage amplitudes of the grid; naturally then the anode current is a cyclic occurrence and can be divided into a Fourier series.

If, in the case of figs. 14, 15 and 16, we place the origin (zero time) at the point where the grid voltage has its positive maximum, the grid voltage may be represented by:

$$v_g(t) = V_g + V_{gp} \cos \omega t \quad . \quad . \quad . \quad . \quad . \quad . \quad (3.\ 13)$$

Then the peak of one of the anode-current impulses coincides with $\omega t = 0$, and the whole series of impulses becomes symmetrical with the line $\omega t = 0$. (It is important to note here that not only the impulses for $t < 0$, but also those for $t < 0$ must be taken into consideration, since the Fourier series applies to the whole range

$$-\infty < t < +\infty,$$

and not to a part of it).

Under these conditions, the anode current at all values of time may be represented by a series of the following type:

$$i_a(t) = I_{ao} + I_{a1} \cos \omega t + I_{a2} \cos 2\omega t + I_{a3} \cos 3\omega t + \ldots \text{ad inf.}, \quad (3.\ 14)$$

of which the various coefficients can be calculated from the following integrals:

$$\left.\begin{aligned} I_{ao} &= \frac{1}{T}\int_o^T i_a\,(t)\,dt \\ I_{a1} &= \frac{2}{T}\int_o^T i_a\,(t)\cos\omega t\,dt \\ I_{a2} &= \frac{2}{T}\int_o^T i_a\,(t)\cos 2\omega t\,dt \\ I_{a3} &= \frac{2}{T}\int_o^T i_a\,(t)\cos 3\omega t\,dt \end{aligned}\right\} \quad \ldots\ldots\ (3.\ 15)$$

and so on. In the above, $T = \frac{2\pi}{\omega}$ is the duration of one cycle of the excitation voltage. Equation (3. 14) demonstrates that the anode current does actually consist of a component I_{ao} which does not vary with t (the D.C. component), a component of which the frequency is ω, that is the frequency of the alternating grid voltage, and, further, of components at frequencies 2ω, 3ω, — etc. The latter are termed the "higher harmonics", whilst the component of which the frequency is ω (the fundamental), is the "first harmonic".

The result of the integrations (3. 15) is naturally dependent upon the form of the anode-current impulses $i_a\,(t)$ which, in turn, are governed by the form of the I_a/V_g characteristic as well as by the magnitude of V_g and V_{gp}.

It is only in the case of tetrodes and pentodes that the I_a/V_g characteristic is referred to as "static" (for a certain screen voltage); with triodes, in which the cathode current is controlled not only by the control grid, but also to a certain extent by the anode, the so-called dynamic I_a/V_g characteristic is employed; this point is referred to again later.

As the reader will be aware, the relation between the cathode current and the control voltage in the case of the ideal triode is given by Langmuir's "space-charge formula":

$$i = cv_g^{3/2} \quad \ldots\ldots\ (3.\ 16)$$

The control voltage is expressed by the following:

$$v_s = \frac{v_g + D_{ag} v_a}{1 + D_{ag} + D_{kg}} , \quad \ldots\ldots\ldots \quad (3.\ 17)$$

in which D_{ag} and D_{kg} represent

$$\left(\frac{\partial V_a}{\partial V_g}\right)_{i_a} = \text{constant} \quad \text{and} \quad \left(\frac{\partial V_k}{\partial V_g}\right)_{i_a} = \text{constant} \quad \text{respectively.}$$

In practice, due to various circumstances, this 3/2-power law will not always be obeyed; further, seeing that we are concerned with a study of the anode current and not of the cathode current, we must bear in mind that the former is obtained from the latter, subtracting the grid current. This factor is all the more significant when, as is the case with transmitting valves, a positive grid voltage occurs simultaneously with a fairly low anode voltage, as a result of which the grid currents are quite high. In assuming the three-halves power law in respect of the I_a/V_g characteristic, therefore, a completely true representation of what happens in practice is not being given.

Although details of the method of plotting the dynamic characteristic for a given instance are shown in a later §, it is necessary to complete the picture by carrying out the Fourier analysis in relation to different idealized types of dynamic characteristic; in due course (§ 5), we shall ascertain in how far these forms agree with the practical results. Fig. 17 shows a dynamic characteristic $i_a = f(v_s)$ in which, in order to suit all cases, the control voltage according to (3. 17) is taken as basis, instead of the grid voltage. This is composed of a direct voltage V_s and an alternating voltage $V_{sp} \cos \omega t$. The amplitude V_{sp} is greater than — V_s, so anode current flows during a part of the cycle which we will term 2Θ, as against the whole cycle, represented by $\omega T = 2\pi$. Class A, B and C settings, as defined above, can now be represented more precisely by means of the current angle: in Class A, $2\Theta = 360°$, in Class B, $2\Theta = 180°$ and in Class C, $2\Theta < 180°$. The calculation is carried out for a characteristic of the following form:

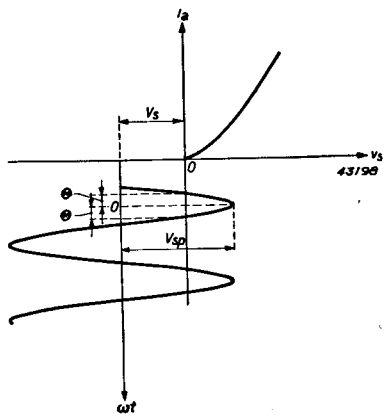

Fig. 17. Anode current of a (high vacuum) valve with control voltage $v_s = V_s + V_{sp} \cos \omega t$.

$$\left.\begin{aligned} i_a &= c v_s^k (v_s > 0) \\ i_a &= 0 \quad (v_s < 0) \end{aligned}\right\}, \quad \ldots\ldots\ldots \quad (3.\ 18)$$

for the three cases where $k = 1$ (straight characteristic); $k = 2$ (parabola) and $k = 3/2$ (space- charge characteristic).
From the figure it will be seen that half the current angle Θ is determined by:

$$\cos \Theta = -\frac{V_s}{V_{sp}} \quad \ldots\ldots\ldots \quad (3.\ 19)$$

For $k = 1$, we then have, in accordance with (3. 15), (3. 18) and (3. 19):

$$I_{a0} = \frac{1}{T}\int_0^T i_a(t)\, dt = \frac{2}{T}\int_0^{\frac{\Theta}{\omega}} c\,(V_s + V_{sp}\cos \omega t)\, dt = \frac{c}{\pi}(V_s\Theta + V_{sp}\sin\Theta);$$

$$I_{a1} = \frac{2}{T}\int_0^T i_a(t)\cos \omega t\, dt = \frac{4}{T}\int_0^{\frac{\Theta}{\omega}} c\,(V_s + V_{sp}\cos\omega t)\,.\cos\omega t\, dt =$$

$$= \frac{2c}{\pi}\left[V_s \sin\Theta + V_{sp}\left(\frac{1}{2}\Theta + \frac{1}{4}\sin 2\Theta\right)\right];$$

$$I_{a2} = \frac{2}{T}\int_0^T i_a(t)\cos 2\omega t\, dt = \frac{4}{T}\int_0^{\frac{\Theta}{\omega}} c\,(V_s + V_{sp}\cos\omega t)\,.\cos 2\omega t\, dt =$$

$$= \frac{c}{\pi}\left[V_s \sin 2\Theta + V_{sp}\left(\sin\Theta + \frac{1}{3}\sin 3\Theta\right)\right];$$

and, in general, for $n \geqq 1$:

$$I_{an} = \frac{2}{T}\int_0^T i_a(t)\cos n\omega t\, dt = \frac{4}{T}\int_0^{\frac{\Theta}{\omega}} c\,(V_s + V_{sp}\cos\omega t)\cos n\omega t\, dt =$$

$$= \frac{2c}{\pi}\left[V_s\frac{\sin n\Theta}{n} + \frac{1}{2}V_{sp}\left\{\frac{\sin(n+1)\Theta}{n+1} + \frac{\sin(n-1)\Theta}{n-1}\right\}\right].$$

These expressions gain in clarity by converting V_s to V_{sp} by means of (3. 19), which gives:

$$\left.\begin{aligned} I_{ao} &= \frac{c}{\pi} V_{sp} (\sin \Theta - \Theta \cos \Theta), \\ I_{a1} &= \frac{c}{\pi} V_{sp} \left(\Theta - \frac{1}{2} \sin 2\Theta\right), \\ I_{a2} &= \frac{c}{2\pi} V_{sp} \left(\sin \Theta - \frac{1}{3} \sin 3\Theta\right), \end{aligned}\right\} \quad \ldots\ldots \quad (3.\ 20)$$

and, in general, for $n \geqq 1$:

$$I_{an} = \frac{c}{n\pi} V_{sp} \left[\frac{\sin (n-1)\,\Theta}{n-1} - \frac{\sin (n+1)\,\Theta}{n+1}\right].$$

Of importance, too, is the maximum value attained by the anode current during the impulse, and this is:

$$I_{ap} = c\,(V_s + V_{sp}) = cV_{sp}\,(1 - \cos \Theta) \ldots\ldots \quad (3.\ 21)$$

In later calculations it will also be useful to know the relation of each of the components to the maximum value of anode current which, from (3. 20) and (3. 21), may be given by:

$$\left.\begin{aligned} \frac{I_{ao}}{I_{ap}} &= f_o(\Theta) = \frac{1}{\pi} \cdot \frac{\sin \Theta - \Theta \cos \Theta}{1 - \cos \Theta} \\ \frac{I_{a1}}{I_{ap}} &= f_1(\Theta) = \frac{1}{\pi} \cdot \frac{\Theta - \frac{1}{2} \sin 2\Theta}{1 - \cos \Theta} \\ \frac{I_{a2}}{I_{ap}} &= f_2(\Theta) = \frac{1}{2\pi} \cdot \frac{\sin \Theta - \frac{1}{3} \sin 3\Theta}{1 - \cos \Theta} \\ \frac{I_{an}}{I_{ap}} &= f_n(\Theta) = \frac{1}{n\pi} \cdot \frac{\frac{\sin (n-1)\,\Theta}{n-1} - \frac{\sin (n+1)\,\Theta}{n+1}}{1 - \cos \Theta} \end{aligned}\right\} \quad (3.\ 22)$$

The calculation for $k = 2$ is carried out in the same manner, and the results are as follows:

$$I_{ao} = \frac{c}{\pi} V_{sp}^2 \left[\Theta \left(1 + \frac{1}{2} \cos 2\Theta\right) - \frac{3}{4} \sin 2\Theta\right];$$

$$I_{a1} = \frac{2c}{\pi} V_{sp}^2 \left(\sin \Theta - \frac{1}{3} \sin^3 \Theta - \Theta \cos \Theta\right);$$

$$I_{a2} = \frac{2c}{\pi} V_{sp}^2 \left[\frac{1}{4} \Theta + \frac{1}{24} \sin 2\Theta\,(-4 + \cos 2\Theta)\right];$$

$$I_{an} = \frac{2c}{\pi} V_{sp}^2 \left[\left\{ \frac{1}{4n} - \frac{1}{2(n-1)} + \frac{1}{4(n-2)} \right\} \sin(n-2)\Theta + \right.$$
$$+ \left\{ \frac{1}{n} - \frac{1}{2(n-1)} - \frac{1}{2(n+1)} \right\} \sin n\Theta$$
$$\left. + \left\{ \frac{1}{4n} - \frac{1}{2(n+1)} + \frac{1}{4(n+2)} \right\} \sin(n+2)\Theta \right];$$
$$I_{ap} = c(V_s + V_{sp})^2 = cV_{sp}^2 (1 - \cos\Theta)^2.$$

From this it follows that:

$$\left.\begin{aligned} f_0(\Theta) &= \frac{1}{\pi} \frac{\Theta\left(1 + \frac{1}{2}\cos 2\Theta\right) - \frac{3}{4}\sin 2\Theta}{(1-\cos\Theta)^2} \\ f_1(\Theta) &= \frac{2}{\pi} \frac{\sin\Theta - \frac{1}{3}\sin^3\Theta - \Theta\cos\Theta}{(1-\cos\Theta)^2} \\ f_2(\Theta) &= \frac{2}{\pi} \frac{\frac{1}{4}\Theta - \frac{1}{24}(4 - \cos 2\Theta)\sin 2\Theta}{(1-\cos\Theta)^2} \end{aligned}\right\} \quad \ldots\ldots \quad (3.\ 23)$$

When $k = 1.5$, integration in finite form is not possible, and the calculation is therefore based on Simpson's law[1].

The results of the above calculations are reproduced in figs. 18,

[1] See Appendix

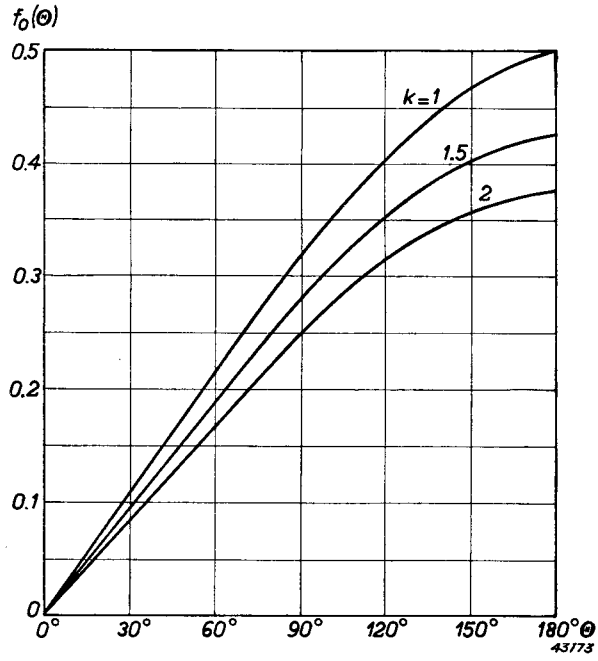

Fig. 18. The relation $I_{a0}/I_{ap} = f_0(\Theta)$ as function of the half currentangle Θ in respect of an i_a/v_s characteristic of the type $i_a = cv_s^k$, at $k = 1$—1.5 and 2.

19 and 20, giving $f_0(\Theta)$, $f_1(\Theta)$ and $f_2(\Theta)$ as a function of Θ, with k as parameter.
It will be seen from these figures that the curves do not vary a great deal at different values of k and, actually, in most cases met with in practice, it is sufficient to assume that $k = 1$ (straight characteristic).

§ 3. The tuned anode circuit

It is stated in the Introduction that the transmitting valve is employed as a converter and as such converts D.C. energy into R.F. energy at the highest possible efficiency. In most instances this R.F. energy is radiated from an aerial, the latter being fed by alternating current of a certain amplitude and frequency, and it is understood in transmission work that the aerial, as a source of energy, behaves in the same way as an ohmic resistance (radiation resistance). In high-frequency furnaces a powerful R.F. current is passed through a coil, in the centre of which the crucible of metal is placed for melting, and, here again, the whole apparatus can be regarded as being replaceable by an equivalent resistance, the square of whose R.F. current, multiplied by the resistance, is equal to the R.F. energy. Dielectric heating equipment makes use of a high-frequency voltage which is applied to a capacitor

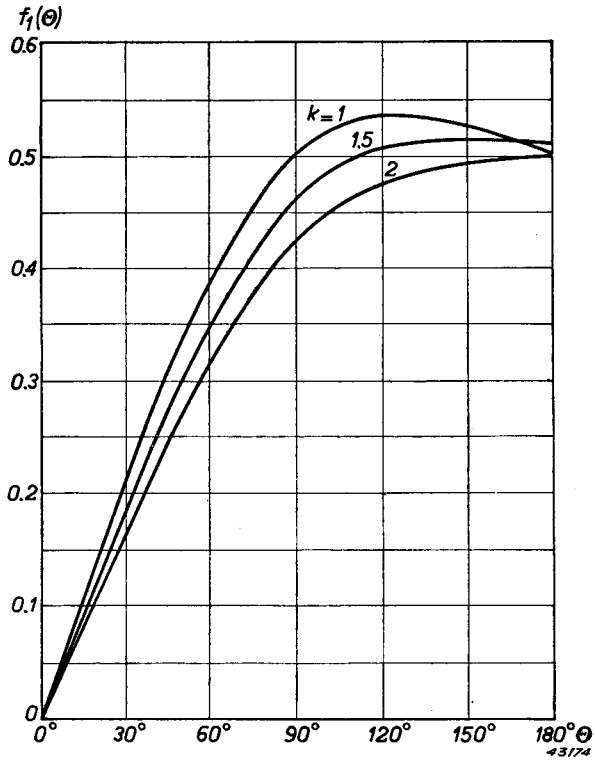

Fig. 19. The relation $I_{a1}/I_{ap} = f_1(\Theta)$ as function of Θ, at the same values of k as in fig. 18.

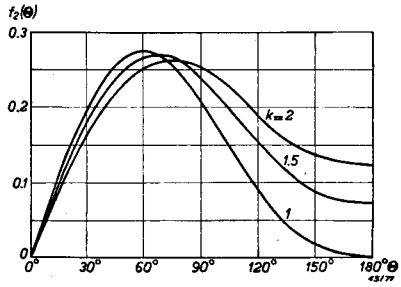

Fig. 20. The relation $I_{a2}/I_{ap} = f_2(\Theta)$ sa function of Θ, for the same values of k as in fig. 18.

into which the material to be heated is introduced. The equivalent resistance is then equal to the square of the R.F. voltage divided by the R.F. power. Large transmitters are often trimmed by means of dummy aerials, consisting in the main of an ohmic resistance which functions in the place of the aerial proper, as a load for the transmitter: the energy dissipated is calculated very simply on the basis of Joule's law. Fig. 21*a* shows the circuit of a transmitting valve working as a converter. The D.C. source, V_a, supplies current to the loading resistance R_a, and the transmitting valve, connected in this circuit, makes and breaks the circuit under the influence of the excitation on the grid. In consequence, a pulsating direct current flows through R_a; the actual form of this current is depicted in fig. 16. This anode current, analyzed by a Fourier expression, comprises not only the D.C. component, but also A.C. components of various frequencies, and only one of these, usually the lowest (that is, the frequency of the alternating grid voltage) is desired in the load resistance. The circuit, therefore, has to be so arranged that only the desired frequency can pass through R_a, while all other components, including the D.C. components, are by-passed.

This is effected by connecting an L–C circuit in parallel with R_a (see fig. 21*b*), and if the circuit is then tuned to the frequency of the desired component (generally the frequency of the excitation voltage), this component of the anode current will encounter high resistance in the L–C circuit (viz. $R_a = L/Cr$, where r is the series-loss resistance of the circuit).

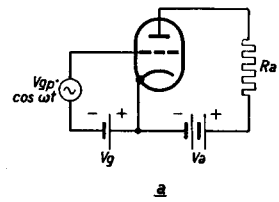

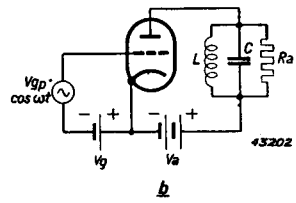

Fig. 21. Circuit of a transmitter amplifier:
a. theoretical, with resistance R_a in the anode circuit;
b. practical, with L—C circuit in parallel with R_a and tuned to the excitation frequency.

All the other components meet with only slight impedance, due to the form of the resonance curve of the circuit. The required component, then, does not follow the circuit, but takes the path through R_a (in practice, L/Cr is of the order of 10^5 to 3.10^5 ohms, with R_a: 10^3 to 10^4 ohms), all the remaining components passing through the circuit.
Naturally, the impedance of the circuit to the higher harmonics is not quite zero; in effect, weak harmonics of the higher order are actually encountered in R_a, and the degree to which this applies is governed, amongst other things, by the magnitude of the circuit impedance to such harmonics, as compared with R_a. From the formula given above for R_a, it is seen that this impedance decreases as the self-inductance of the circuit decreases and its capacitance increases; the anode circuit of the output stage of a transmitter should therefore always be given a sufficiently high capacity. For further details in this connection reference should be made to works on transmission technique.

§ 4. The static characteristics of the triode

The behaviour of the components in the circuit in fig. 21*b* has now been described, but for a deeper study of the conversion process it is necessary to look more closely into the action of the transmitting valve as such.
We have seen from the foregoing that three quantities are of primary importance in the proper working of a transmitting valve, namely the anode voltage V_a, the grid voltage V_g and the anode current i_a; the grid current will be considered later. The relationship between these quantities is demonstrated by the static characteristics. In contrast with reception work, in which the I_a/V_g characteristics play an important part, among other things in connection with the use of the valve as a voltage amplifier, transmission technique demands almost exclusively the use of the I_a/V_a characteristics. This is because the energy conversion actually takes place at the anode and can best be visualized from the curves of i_a and v_a, as plotted against t. In recent years, there has been some tendency to employ the V_a/V_g curves, in view of the fact that they do possess certain advantages over the I_a/V_g curves, but this point will be discussed in the appendix § 4.
For illustration purposes, the I_a/V_a curves of a triode are reproduced in fig. 22. In contrast with conventional reception practice, the curves for positive values of V_g are also given, since, in order to furnish a

sufficiently high output and efficiency, it is necessary to swing the grid right up into the positive zone. It is also necessary to show the I_g/V_a curves, alongside those for I_a/V_a (fig. 23), to be in a position to calculate the energy conversion in the grid circuit.

§ 5. The load line in a tuned anode circuit

As the I_a/V_a characteristics furnish the relationship between the three quantities i_a, v_a and v_g, the curve of i_a, plotted against t, can be derived if that of v_a and v_g is known.

The grid voltage v_g invariably consists of the superposition of the (negative) direct voltage V_g and the R.F. excitation voltage which we represent by $V_{gp} \cos \omega t$; therefore:

$$v_g(t) = V_g + V_{gp} \cos \omega t \quad . \quad . \quad . \quad . \quad . \quad . \quad . \quad (3.\ 24)$$

At any moment, the anode voltage $v_a(t)$ is equal to the difference between the steady anode voltage V_a and the voltage drop that the anode current causes in the combination of load resistance and tuned anode circuit. In § 3 it was mentioned that only one component of the anode current encounters impedance, namely that component of which the frequency is the same as the natural frequency of the L–C circuit. Let us

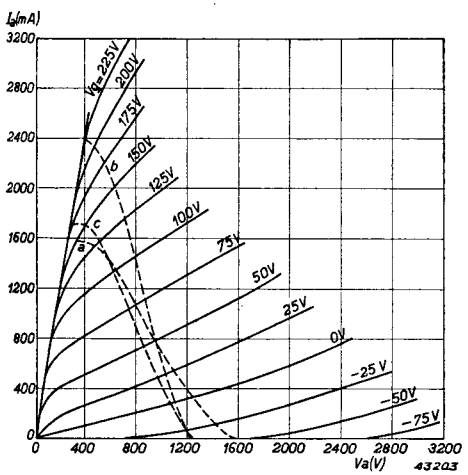

Fig. 22. I_a — V_a characteristics of a triode showing various load lines (*a*, *b* and *c*).

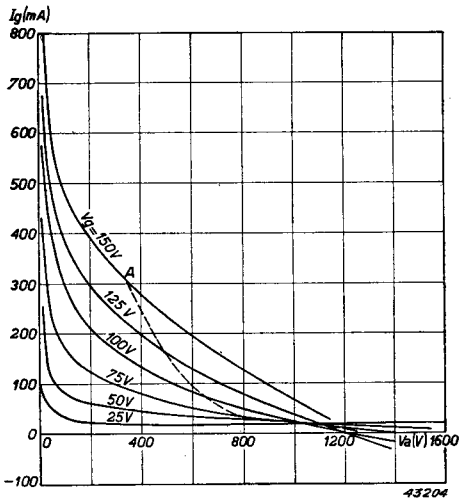

Fig. 23. I_g — V_a characteristics of the triode referred to in fig. 22. The broken line is a load line.

assume that the circuit is tuned to the frequency of the alternating control-grid voltage; the voltage drop in question then, according to (3. 14), takes place at the expense of the first harmonic $I_{a1} \cos \omega t$ of the anode current and is equal to $I_{a1} R_a \cos \omega t = V_{ap} \cos \omega t$. Therefore:

$$v_a (t) = V_a - I_{a1} R_a \cos \omega t$$

or, again:

$$v_a (t) = V_a - V_{ap} \cos \omega t \quad . \quad . \quad . \quad . \quad . \quad . \quad . \quad (3.\ 25)$$

(see also (3. 2) in § 1).

With the aid of (3. 24) and (3. 25), v_g and v_a can now be calculated for any value of t, and, from the I_a/V_a characteristic, we then have the corresponding value of I_a.

In the I_a/V_a diagram, the appropriate values of v_a, v_g and i_a, at any value of t, can be marked with a point (working point), and the chain of working points during the course of one cycle of the R.F. grid voltage is then termed the "working-" or "load" line. By way of illustration, fig. 22 shows the load line (a) drawn on the I_a/V_a characteristics of a triode using the following expressions for v_a and v_g:

$$v_g (t) = -120 + 270 \cos \omega t,$$
$$v_a = 2000 - 1660 \cos \omega t,$$

while the corresponding curve for i_a with respect to t is reproduced in fig. 24 (curve a). From these figures it also follows that the load line for that part of the cycle in which $i_a < 0$ is practically a straight line and that, consequently, the anode current pulses, to a fair approximation, may be regarded as sine-peaks, in respect of which formulae (3. 22) apply. In point of fact, it will be seen at once that the load line is actually a straight line when the static characteristics I_a/V_a are straight; in that case, when $i_a > 0$, we have:

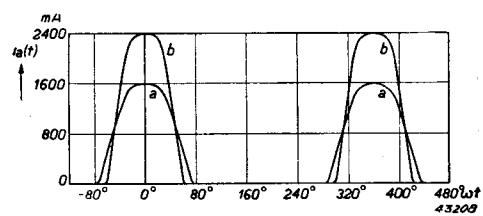

Fig. 24. Anode current impulses in respect of the load lines a and b in fig. 22.

$$i_a = \alpha v_a + \beta v_g,$$

and further, in view of (3. 24) and (3. 25):

$$i_a (t) = \alpha (V_a - V_{ap} \cos \omega t) + \beta (V_g + V_{gp} \cos \omega t),$$

or

$$i_a (t) = \alpha V_a + \beta V_g + (\beta V_{gp} - \alpha V_{ap}) \cos \omega t.$$

Substituting for $\cos \omega t$:

$$\cos \omega t = \frac{V_a - v_a(t)}{V_{ap}} \text{ in accordance with (3. 25),}$$

we have:

$$i_a(t) = \alpha V_a + \beta V_g + (\beta V_{gp} - \alpha V_{ap}) \frac{V_a - v_a(t)}{V_{ap}} = A - B v_a(t),$$

which demonstrates the linear relationship between $i_a(t)$ and $v_a(t)$ when $i_a > 0$.

In the example given in fig. 22, it is evident that the approximation of the static characteristics by means of straight lines is permissible for practical purposes and, for the majority of our calculations, we shall therefore employ this approximation, introducing corrections only in special cases.

§ 6. Input power, output power and efficiency

From the preceding considerations it has been ascertained that the R.F. output power is equal to the power developed by the component $I_{a1} \cos \omega t$ of the anode current in R_a; now, according to Joule's law, this power, averaged over one R.F. cycle, is:

$$W_o = \frac{1}{2} I_{a1}^2 R_a,$$

or, if the alternating anode voltage is introduced by means of the formula:

$$V_{ap} = I_{a1} R_a \; ; \quad \ldots\ldots\ldots \quad (3.\ 26)$$

then:

$$W_o = \frac{1}{2} I_{a1} V_{ap}, \quad \ldots\ldots\ldots \quad (3.\ 27)$$

which expression has already been developed in § 1 (3. 10). Also the input power was found to be (3. 11):

$$W_i = V_a I_{ao}, \quad \ldots\ldots\ldots \quad (3.\ 28)$$

where I_{ao} is the steady component of the anode current. Even in the general case when the anode current is of a pulsating character, the input power is given by (3. 11). It has already been shown in § 1, that the instantaneous value of the input power is equal to the product of the steady anode voltage and the instantaneous value of the anode current; the average input power W_i, which in practice is the only factor of importance, therefore equals the product of the steady anode voltage

and the average anode current. Referring to (3. 14) and (3. 15) the latter is equal to the D.C. anode current I_a. For the efficiency, therefore, the formula (3. 12) from § 1 is still valid:

$$\eta = \frac{W_o}{W_i} = \frac{1}{2}\frac{I_{a1}}{I_{ao}} \cdot \frac{V_{ap}}{V_a} \quad \ldots\ldots\ldots \quad (3.\ 29)$$

The conversion conception demands that endeavours should be made to increase the efficiency as much as possible. Naturally a transmitting valve, or any other type of converter, cannot work at an efficiency of 100%. The difference between the values of the input and the output power remains as a loss in the converter itself, in this case in the form of anode dissipation W_a:

$$W_a = W_i - W_o \quad \ldots\ldots\ldots \quad (3.\ 30)$$

Obviously, if the valve is to work reliably, this anode dissipation must not be allowed to exceed a certain value, and this maximum is actually one of the factors that tend to limit the power to be derived from a given transmitting valve. Another limiting element is the maximum permissible cathode current; either the highest peak value of the pulsating anode current (I_{ap}) is limited by the saturation current of the cathode, as is the case with tungsten heaters, or, in order to guarantee a reasonable "life" of the valve, the manufacturers will prescribe a maximum cathode current, this being the case with oxide- and thoriated tungsten cathodes.

In the following paragraphs we shall first ascertain what value the efficiency is likely to take under given circumstances, ignoring the limitations just mentioned, after which we shall calculate the output power, making due allowance for these limitations, and see the effect upon the efficiency in these circumstances.

§ 7. Factors governing the output power and efficiency

Let us approximate the I_a/V_a characteristic by means of straight lines (fig. 25), as rendered by the expression:

$$i_a = a\,(v_g + b v_a), \quad \ldots\ldots\ldots \quad (3.\ 31)$$

making it a condition that the formula holds good only for values of v_g and v_a, which conform to:

$$i_a > 0 \text{ and } v_a > 0 \quad \ldots\ldots\ldots \quad (3.\ 31a)$$

The quantity b is the previously mentioned "Durchgriff" D_{ag} between

anode and grid, and the reciprocal of b is the amplification factor μ:

$$b = \frac{1}{\mu}.$$

It will be seen from fig. 22 that this approximation may quite well be applied to practical examples, so long as the values of v_a are not too low. At very low values of v_a, that is less than v_g, the anode current drops sharply (while i_g increases), and fig. 22 shows that each one of the family of characteristics terminates on a line, passing through the origin and practically straight, which we shall term the limit characteristic, represented by the expression:

$$i_a = \sigma v_a. \quad \ldots\ldots\ldots\ldots \quad (3.\ 32)$$

As further limitation to the validity of (3. 31), we then have the condition:

$$i_a \leqq \sigma v_a. \quad \ldots\ldots\ldots\ldots \quad (3.\ 32a)$$

From the latter condition and (3. 31) it is now possible to indicate a value of v_g, for every value of v_a, for which formula (3. 31) just holds, viz:

$$i_a = \sigma v_a = a\,(v_g + b v_a),$$

from which it follows that:

$$v_g = \frac{\sigma - ab}{a}\, v_a.$$

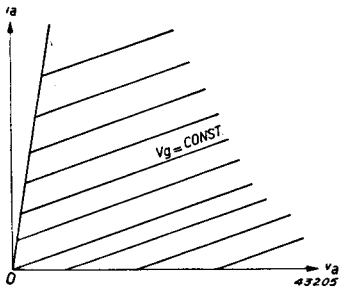

Fig. 25. Approximation of the static characteristics of a triode by means of straight lines: $i_a = a\,(v_g + b v_a)$, valid for $v_a > 0$ and $0 < i_a < \sigma v_a$.

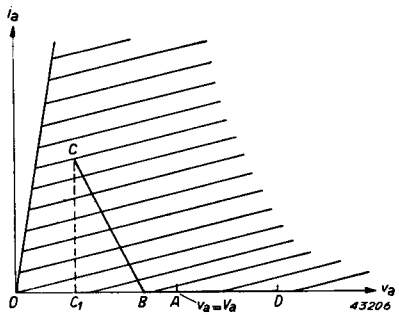

Fig. 26. Working line in the I_a/V_a characteristics diagram of a triode, assuming a tuned L.C. circuit with load resistance in parallel with the anode circuit, under Class C excitation.

The relation between i_a and t then follows directly from (3. 31), by making use of the formulae previously employed:

$$v_g(t) = V_g + V_{gp} \cos \omega t \quad . \quad . \quad . \quad . \quad . \quad . \quad . \quad . \quad . \quad . \quad . \quad . \quad (3.\ 24)$$

$$v_a(t) = V_a - V_{ap} \cos \omega t \quad . \quad . \quad . \quad . \quad . \quad . \quad . \quad . \quad . \quad . \quad . \quad . \quad (3.\ 25)$$

viz:

$$i_a(t) = a\,[V_g + bV_a + (V_{gp} - bV_{ap}) \cos \omega t]. \quad . \quad . \quad . \quad . \quad (3.\ 33)$$

where, in view of (3. 31*a*):

$$-\Theta < \omega t < \Theta;\ 2\pi - \Theta < \omega t < 2\pi + \Theta \text{ etc,}$$

whereas, at other values of ωt, $i_a = 0$; Θ is the halfangle of current flow, as already defined and as represented by the expression:

$$V_g + bV_a + (V_{gp} - bV_{ap}) \cos \Theta = 0,$$

or:

$$\cos \Theta = \frac{-V_g - bV_a}{V_{gp} - bV_{ap}} \quad . \quad . \quad . \quad . \quad . \quad . \quad . \quad . \quad (3.\ 34)$$

In the same manner as in § 5 it can be shown that the load line is a straight line for that part of the cycle during which anode current flows. In fig. 26 this is the line BC, as drawn in for the Class C setting. For the remainder of the cycle the load line coincides with the V_a axis, which, in fig. 26, is BD. A is then the point where the instantaneous potential is equal to V_a (the steady potential). Since the alternating anode voltage is sinusoidal, $AD = AC_1 = V_{ap}$.

The efficiency η, according to (3. 29) is:

$$\eta = \frac{1}{2} \frac{I_{a1}}{I_{ao}} \cdot \frac{V_{ap}}{V_a},$$

so that, in consideration of (3. 22):

$$\eta = \frac{1}{2} \frac{f_1(\Theta)}{f_0(\Theta)} \cdot \frac{V_{ap}}{V_a} = \frac{1}{2} \varphi(\Theta) \cdot \frac{V_{ap}}{V_a} \quad . \quad . \quad . \quad . \quad . \quad . \quad . \quad (3.\ 35)$$

The expression:

$$\frac{f_1(\Theta)}{f_0(\Theta)} = \frac{\Theta - \frac{1}{2} \sin 2\Theta}{\sin \Theta - \Theta \cos \Theta} = \varphi(\Theta) \quad . \quad . \quad . \quad . \quad . \quad . \quad . \quad (3.\ 36)$$

is depicted in fig. 27 as a function of Θ.

The efficiency is therefore dependent upon two factors, i.e. $\varphi(\Theta)$ and V_{ap}/V_a, the first of which is governed only by the (half) current angle Θ and which increases as Θ decreases; the highest value attained by $\varphi(\Theta)$

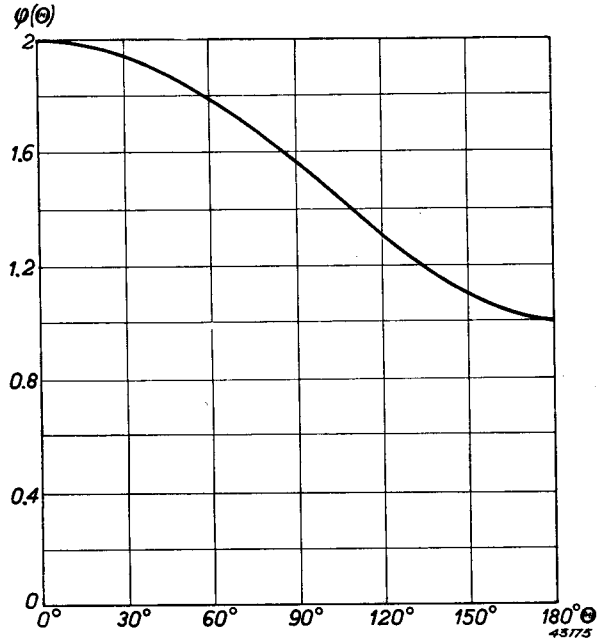

Fig. 27. The quantity $\varphi(\Theta) = f_1(\Theta)/f_0(\Theta)$, plotted against Θ, when $k = 1$, where $f_0(\Theta)$ and $f_1(\Theta)$ are derived from figs. 18 and 19 respectively.

is 2, that is when $(\Theta)=0$. The impulses are then of width zero, and, in order to ensure high efficiency, it is therefore essential that the angle Θ is not taken too large. For the rest, this choice of angle is limited by the condition that the negative grid bias and excitation voltage should preferably not be too high. As shown by (3. 34), Θ becomes smaller and cos Θ accordingly larger as the expression $-V_g - bV_a$ (at given values of V_{gp} and V_{ap}) becomes greater, i.e. when V_g reaches higher negative values, at a given value of V_a. This will at once be obvious from the fact that, in that case, the valve setting tends to

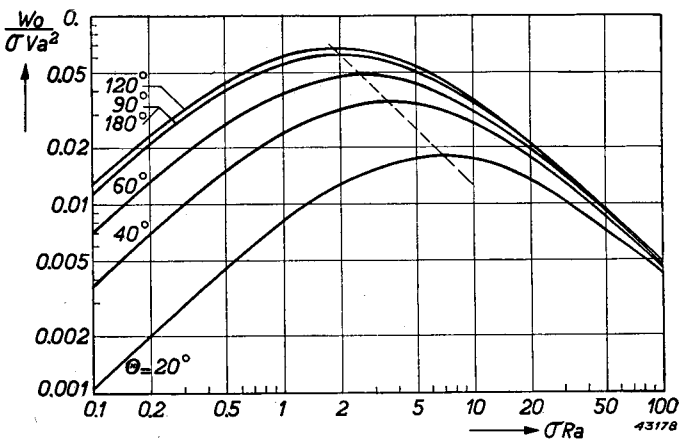

Fig. 28. $W_o/\sigma V_a^2$ as function of σR_a, with Θ as parameter, in the case of a transmitting valve with straight characteristics, and with an excitation voltage that drives the load line to the point of intersection with the limit characteristic (compare fig. 26).

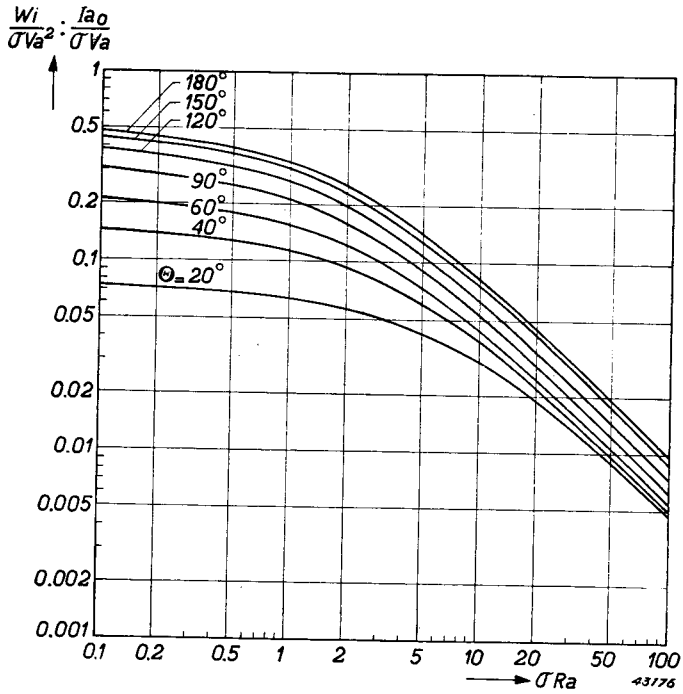

Fig. 29. $W_i/\sigma V_a^2$ (or $I_{a0}/\sigma V_a$) as function of σR_a, with Θ as parameter (compare text, fig. 28).

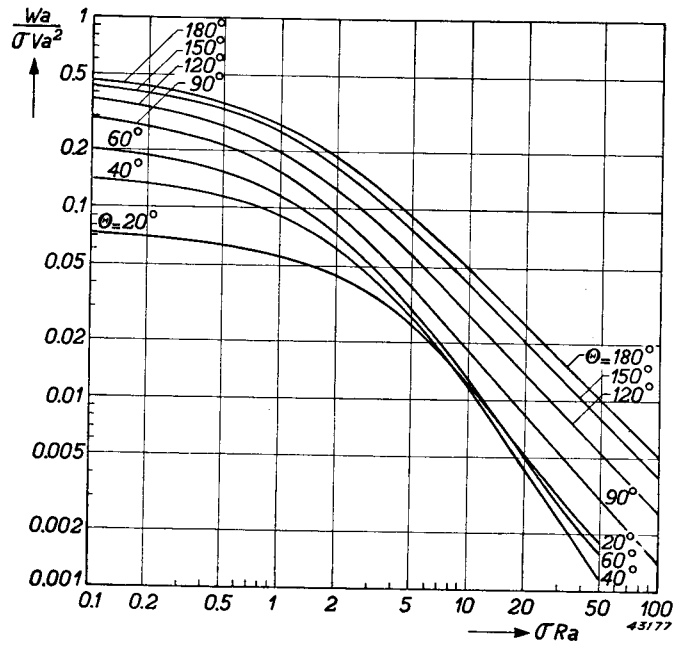

Fig. 30. $W_a/\sigma R_a^2$ as function of σR_a, with Θ as parameter (compare text, fig. 28).

assume more the character of Class C, with consequent smaller impulses of anode current.

The second factor, V_{ap}/V_a, is directly proportional to the alternating anode potential V_{ap}, which in fig. 26 is represented by the distance AC_1.

To ensure high efficiency, therefore, it is important that V_{ap} should be as high as possible, or, in other words, that the end of the working line C be kept as far as possible over to the left of the diagram, and this can be achieved in

two ways, i.e. whilst maintaining a constant V_{gp}, or, in other words, $V_{g\ max}$, to move the point C to the left (that is, along the relevant static characteristic V_g = constant), in order to alter the slope of the load-line (or R_a), or alternatively, to increase the alternating grid voltage at a constant value of R_a.

Let us now see how the efficiency and the input- and output power may be calculated from the characteristics in fig. 26.

The highest value that the alternating anode potential V_{ap} will reach at a given load R_a, with current angle 2Θ, is that at which end C of the load line (Fig. 26) lies on the limit characteristic $i_a = \sigma v_a$[1], under which condition:

$$I_{ap} = \sigma V_{a\ min} \quad . \quad . \quad . \quad . \quad . \quad . \quad . \quad . \quad . \quad . \quad . \quad (3.\ 37)$$

When

$$V_{a\ min} = V_a - V_{ap},$$
$$V_{ap} = I_{a1} R_a$$
$$I_{a1} = f_1(\Theta) \,.\, I_{ap},$$

which means that:

$$I_{ap} = \sigma (V_a - V_{ap}) = \sigma (V_a - I_{a1} R_a) = \sigma [V_a - f_1(\Theta) \,.\, I_{ap} R_a].$$

It then follows that:

$$I_{ap} = \frac{\sigma V_a}{1 + \sigma R_a f_1(\Theta)} \quad . \quad . \quad . \quad . \quad . \quad . \quad . \quad . \quad . \quad . \quad . \quad . \quad (3.\ 38)$$

from which the following may be deduced:

$$I_{ao} = f_o(\Theta) \,.\, I_{ap} = \frac{f_0(\Theta) \,.\, \sigma V_a}{1 + \sigma R_a f_1(\Theta)} \quad . \quad . \quad . \quad . \quad . \quad . \quad . \quad . \quad (3.\ 39)$$

$$I_{a1} = f_1(\Theta) \,.\, I_{ap} = \frac{f_1(\Theta) \,.\, \sigma V_a}{1 + \sigma R_a f_1(\Theta)} \quad . \quad . \quad . \quad . \quad . \quad . \quad . \quad . \quad (3.\ 40)$$

$$V_{ap} = I_{a1} R_a = \frac{f_1(\Theta) \,.\, \sigma V_a R_a}{1 + \sigma R_a f_1(\Theta)} \quad . \quad . \quad . \quad . \quad . \quad . \quad . \quad . \quad . \quad . \quad (3.\ 41)$$

$$W_o = \frac{1}{2} V_{ap} I_{a1} = \frac{1}{2} \cdot \frac{\sigma R_a f_1^2(\Theta)}{[1 + \sigma R_a f_1(\Theta)]^2} \cdot \sigma V_a^2 \quad . \quad . \quad . \quad . \quad (3.\ 42)$$

$$W_i = V_a I_{ao} = \frac{f_o(\Theta)}{1 + \sigma R_a f_1(\Theta)} \cdot \sigma V_a^2 \quad . \quad . \quad . \quad . \quad . \quad . \quad . \quad (3.\ 43)$$

[1] It will be shown later that in the case of over-excitation the alternating anode voltage may increase still more: this arrangement, however, involves certain disadvantages.

$$W_a = W_i - W_o \quad \ldots \ldots \ldots \ldots \ldots \quad (3.\ 44)$$

$$\eta = \frac{W_o}{W_i} = \frac{1}{2} \cdot \frac{\sigma R_a f_1^2(\Theta)}{f_o(\Theta)\,[1 + \sigma R_a f_1(\Theta)]} \quad \ldots \ldots \quad (3.\ 45)$$

The results of these calculations are illustrated in figs. 28 to 32, namely: $W_o/\sigma V_a^2$, $W_i/\sigma V_a^2$ (or $I_{ao}/\sigma V_a$), $W_a/\sigma V_a^2$, η and $I_{ap}/\sigma V_a$, as plotted against σR_a, with Θ as parameter.

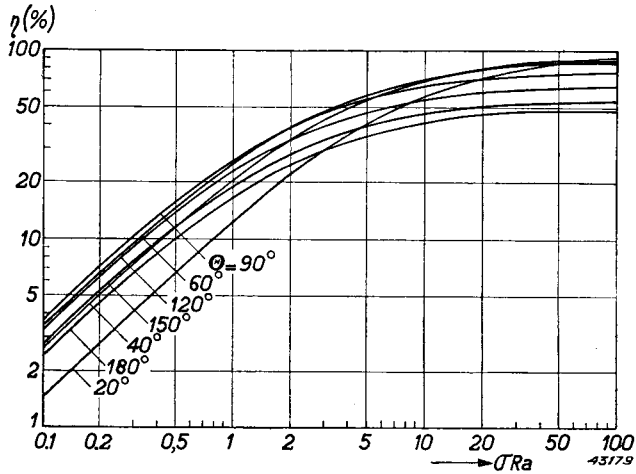

Fig. 31. η as function of σR_a, with Θ as parameter (compare text of fig. 28).

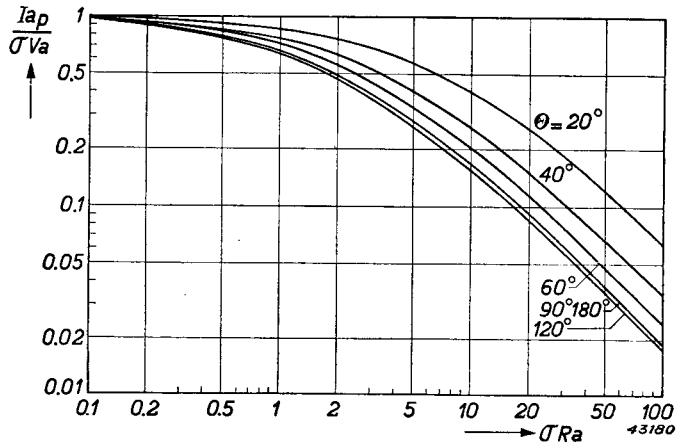

Fig. 32. $I_{ap}/\sigma V_a$ as function of σR_a, with Θ as parameter (compare text of fig. 28).

In the following § we shall demonstrate the method of so adjusting the valve setting that a given maximum anode dissipation is not exceeded.

§ 8. Limitation of the output power by the anode dissipation

By means of fig. 30, the quantity $W_a/\sigma V_a^2$ and, accordingly, for a given value of V_a, the anode dissipation W_a, may be determined for given values of σR_a and Θ. If, however, the anode dissipation is subject to a maximum limit, it is not feasible to employ any arbitrary combination of σR_a and Θ.

If we assume the necessary conditions to ensure a constant value of W_a (for instance the maximum permissible value), then a line $W_a/\sigma V_a^2 =$ constant in fig. 30 will give the appropriate values of σR_a and Θ in conformity with this condition, and this relationship between σR_a and Θ, when $W_a/\sigma V_a^2 = 0.2$, 0.1, 0.05, 0.02, 0.01 and 0.005, is shown by the dotted lines in fig. 33. These curves now enable us to obtain from fig. 28 the corresponding values of $W_a/\sigma V_a^2$, which in turn are reproduced in fig. 33 (full lines), representing $W_a/\sigma V_a^2$ plotted against σR_a, with $W_a =$ constant.

Fig. 34 shows the corresponding efficiency curves, while fig. 33 makes it clear that, for any given anode dissipation, it is always possible to indicate a value for σR_a at which the output power and, therefore, also

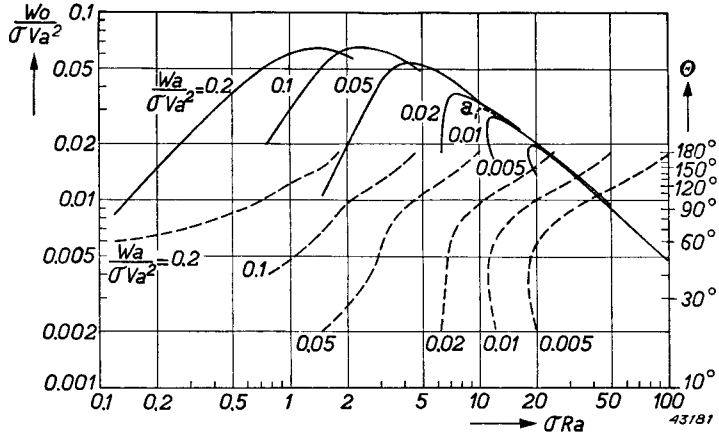

Fig. 33. Full lines: $W_a/\sigma V_a^2$ as function of σR_a, with $W_a/\sigma V_a^2$ as parameter. Dotted lines: the relative values of Θ.

the efficiency, will reach a maximum. The value of σR_a at which W_o attains its maximum for a given value of W_a may be determined in principle from (3. 42), by differentiating this expression with respect to σR_a and equating to zero, making it a condition that W_a = constant (the W_a from (3. 44)). At the same time, the second condition, whilst showing the relationship between Θ and σR_a already mentioned, makes it a very difficult matter to determine the required optimum value of R_a, which prevents us from entering more deeply into the matter here. From fig. 33 it is also seen that, assuming a given value of W_a, certain values can be obtained for W_o at two different values of σR_a. Thus, when $W_a/\sigma V_a^2 = 0.02$, we find that $W_o/\sigma V_a^2 = 0.03$ (i.e. an efficiency of 60%), at $\sigma R_a = 6.5$ and 12. The relative values of Θ are then 30° and 110°, and the anode current pulses are therefore much smaller in the first instance than in the second; as the input power is the same in each case, however, ($W_i/\sigma V_a^2 = 0.05$), the steady anode current must also be the same, so that in the first instance the peak anode current is much the higher of the two.

Fig. 32 shows that, when $\sigma R_a = 6.5$ and $\Theta = 30°$, $I_{ap}/\sigma V_a = 0.4$, whilst, when $\sigma R_a = 12$ and $\Theta = 110°$, $I_{ap}/\sigma V_a = 0.135$. In other words, the peak current in the first case is three times as high as in the second. Even though the two settings are similar from the aspect of anode

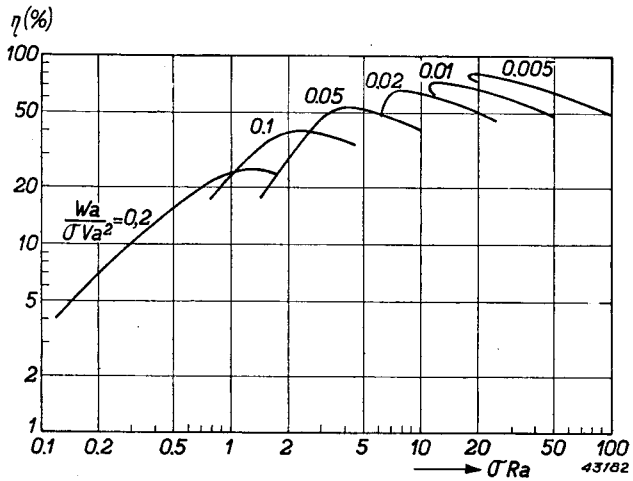

Fig. 34. η as function of σR_a, with $W_a/\sigma V_a^2$ as parameter.

dissipation, the second is preferable to the first in view of the lower cathode load and due to wider current angle, the grid bias and excitation voltage also being lower.

However, in practice, the valve will always be run at its maximum high frequency power, for which only one value of σR_a and Θ applies.

By way of illustration, let us determine the data as applicable to the Class C setting of the triode, of which the characteristics are reproduced in figs. 22 and 23, for $W_a = 300$ W, $V_a = 2000$ V. At a value of $\sigma = 6.10^{-3}$, $W_a/\sigma V_a^2 = 0.0125$. Fig. 30 gives the following combinations of σR_a and Θ, and fig. 28 supplies the appropriate value of $W_o/\sigma V_a^2$.

TABLE I

$\sigma R_a = 9.5$	10	14	22	32	40
$\Theta = 40°$	60°	90°	120°	150°	180°
$W_o/\sigma V_a^1 = 0.0275$	0.031	0.0275	0.0193	0.0137	0 0115

The above values of $W_o/\sigma V_a^2$ will be found in Fig. 33 as indicated by the dotted line a, from which it appears that the output power is at a maximum when $\sigma R_a = 10$, $\Theta = 60°$; $W_o/\sigma V_a^2$ is then equal to 0.031. From this it follows that:

$$W_o = 0.031\ \sigma V_a^2 = 0.031 \cdot 6 \cdot 10^{-3} \cdot (2000)^2 = 744 \text{ W};$$
$$W_i = W_o + W_a = 1044 \text{ W};$$
$$\eta = \frac{W_o}{W_i} = 71.2\%$$
$$I_{ao} = \frac{W_i}{V_a} = 522 \text{ mA}.$$

Further, at $\Theta = 60° : f_o(\Theta) = I_{ao}/I_{ap} = 0.218$, so that $I_{ap} = 522/0.218 = 2400$ mA and $f_1(\Theta) = I_{a1}/I_{ap} = 0.391$; therefore $I_{a1} = 0.391.2440 = 938$ mA. From $W_o = \frac{1}{2} I_{a1} V_{ap}$, we then have: $V_{ap} = 1588$ V, so that, finally:

$$R_a = \frac{V_{ap}}{I_{a1}} = 1690 \text{ ohms}.$$

As a check on the above: $\sigma R_a = 10$, which gives: $R_a = 1670$ ohms, and this is a reasonable result [1].

[1] The difference is due to the fact that the value of σ can only be determined roughly from the $I_a - V_a$ diagram.

An endeavour will now be made to show the method by which the same result may be obtained by graphical means, in order to give some idea of the accuracy of the method used. Let us take from fig. 22 the point $i_a = 2400$ mA: $v_a = 400$ V, as being the end of the load line (curve *b*) and in accordance with the above calculation. Then $v_g = 225$ V and $V_{ap} = 1600$, with V_a at 2000 V.
To ascertain the correct value of the current angle, we take $V_g = -275$ V; then $V_{gp} = 500$ V. The amplification factor μ of this valve is 30, so that, according to (3. 34):

$$\cos \Theta = \frac{275 - \frac{2000}{30}}{500 - \frac{1600}{30}} = 0.466; \quad \Theta = 62°,$$

which is practically the same result as that obtained from the preceding calculation.
Maintaining the values:

$$v_g(t) = -275 + 500 \cos \omega t, \text{ and}$$
$$v_a(t) = 2000 - 1600 \cos \omega t,$$

we can then use these formulae to determine v_g and v_a as function of t and also i_a (fig. 24, curve *b*).
Employing Simpson's law, the anode current is next calculated: $I_{ao} = 573$ mA, with $I_{a1} = 1023$ mA for the first harmonic.
We then have:

$$W_o = \frac{1}{2} \cdot I_{a1} \cdot V_{ap} = 820 \text{ W}$$
$$W_i = V_a I_{ao} = 1146 \text{ W}$$
$$W_a = W_i - W_o = 326 \text{ W}$$
$$\eta = \frac{W_o}{W_i} = 71.5 \%$$
$$R_a = \frac{V_{ap}}{I_{a1}} = 1560 \text{ ohms.}$$

If these figures are compared with the earlier calculations it will be seen that W_o, W_i and W_a are now about 10% higher, whilst R_a is lower and η unchanged, all of which is explained very simply by the form of the load line (fig. 22, curve *b*), which is reasonably straight, except at the upper end, where it bends sharply. This bending is due to the admitted

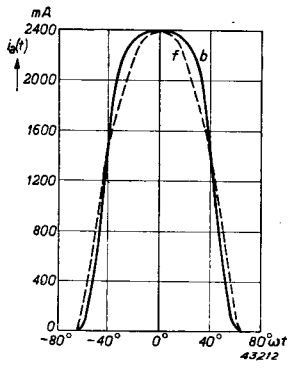

Fig. 35. Anode current impulse of a triode:
b) relating to the load line *b* in fig. 22;
f) calculated on the hypothesis of straight line characteristics.

non-linearity of the static characteristics in the vicinity of the limit line, in consequence of which the anode current impulses (fig. 24, curve *b*) loose their peaked character and assume a more rectangular form. For comparative purposes, fig. 35 shows the actual anode current impulse *b*), together with an impulse of which the peak current is the same (*f*), but which is in the form of the sinusoidal curve underlying the theory of straight characteristics as outlined in the foregoing. The broadening of the impulse results in an increase of I_{ao} and I_{a1}, which explains the increase in W_i and W_o.

§ 9. Limitation of the output power by the steady anode current

It is also possible for the output power to be limited by the cathode current in cases where the latter must not exceed a specified value, and this applies to transmitting valves having oxide or thoriated tungsten cathodes. As is known, the saturation current of this type of cathode is very high, but as it is likely that an excessive current demand would impair the life of the cathode, the maker will always specify a maximum permissible cathode current, of an order that will guarantee a reasonable life, and the effects will now be considered in relation to the output of a transmitting valve of which the steady anode current [1] is kept constant at a certain value which may be the permissible maximum in respect of the valve.

In fig. 29, which shows the relation $I_{ao}/\sigma V_a$ plotted against σR_a and Θ, it is possible to draw lines parallel to the abscissa, to determine values of σR_a and Θ corresponding to certain constant values of I_{ao}. The dotted lines in fig. 36 give such values for σR_a and Θ for $I_{ao}/\sigma V_a$=0.3, 0.2, 0.15, 0.1, 0.06, 0.04, 0.02 and 0.01. Using these curves in conjunction with fig. 28, we obtain the corresponding values of $W_o/\sigma V_a{}^2$ (fig. 36, full lines), whilst fig. 31 furnishes the appropriate efficiency (fig. 37).

[1] Since the cathode current is the sum of the anode current and the current passing to the grid, the maximum permissible value of the anode current is less than that of the cathode.

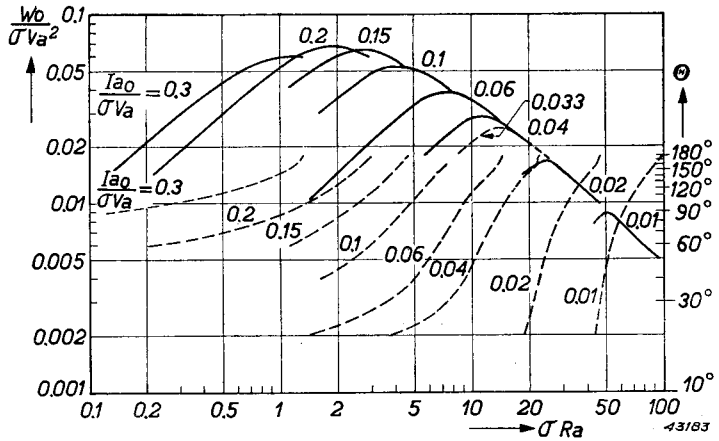

Fig. 36. Full lines: $W_o/\sigma V_a^2$ as function of σR_a, with $I_{ao}/\sigma V_a$ as parameter. Dotted lines: the corresponding values of Θ.

As is also the case with constant anode dissipation, each curve exhibits a maximum in respect of $W_o/\sigma V_a^2$ (and therefore also for η), at a certain value of σR_a, and, here again, assuming a constant direct current at the anode, it is possible to obtain a certain power value at two different values of σR_a, namely at high and low values of Θ. For example (fig. 36), at $I_{ao}/\sigma V_a = 0.02$, we find that $W_o/\sigma V_a^2 = 0.015$ both at $\sigma R_a = 20$ and 29.5. The corresponding values of Θ are 26° and 90° and, at one and the same value of the steady anode current, these angles naturally give rise to widely divergent peak values of the current. For these angles, fig. 32 gives us $I_{ap}/\sigma V_a = 0.20$ and 0.063, or more than three times as much in the first instance than in the second. Needless to say, a

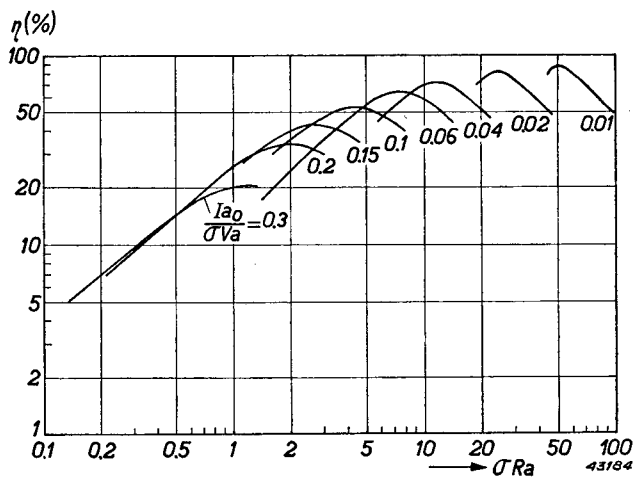

Fig. 37. η as function of σR_a, with $I_{ap}/\sigma V_a$ as parameter.

setting that will result in a wide current angle again has the preference. Otherwise, the same choice of setting will be made here as in the case of the limited anode dissipation, that is, one which will yield the maximum output, which occurs at only one value of σR_a and Θ. Suppose then that it is required to know the setting that will give the highest output in the case of the triode whose characteristics are depicted in figs. 22 and 23, at $V_a = 2000$ V and $I_{ao} = 400$ mA.
Now:

$$\frac{I_{ao}}{\sigma V_a} = \frac{0.04}{6 \,.\, 10^3 \,.\, 2000} = 0.33.$$

From figs. 29. and 28 the following values are found for Θ, σR_a and $W_o/\sigma V_a^2$:

TABLE II

$\sigma R_a = 8.5$	12.5	14.5	17.3	20.7	25.5	28
$W_o/\sigma V_a^2 = 0.018$	0.024	0.025	0.023	0.020	0.017	0.0157
$\theta = 20°$	40°	60°	90°	120°	150°	180°

These values of $W_o/\sigma V_a^2$ are shown by a dotted line in fig. 36 (indicated by the parameter 0.033), and the maximum point on this curve lies at $\sigma R_a = 14.5$, with $\Theta = 60°$; then: $W_o/\sigma V_a^2 = 0.025$, so that $W_o = 0.025$. $V_a^2 = 600$ W. Further, $W_i = 800$ W; $W_a = 200$ W; $\eta = 75\%$. $R_a = 14.5/\sigma = 2420$ ohms, whilst the alternating anode potential V_{ap} follows from:

$$W_o = \frac{V_{ap}^2}{2R_a}; \text{ therefore } V_{ap} = \sqrt{2R_a W_o} = 1705 \text{ V}.$$

The first harmonic of the anode current is: $I_{a1} = V_{ap}/R_a = 705$ mA; so $I_{a1}/I_{ao} = \varphi(\Theta) = 1.76$. From fig. 27 it then appears that this value of $\varphi(\Theta)$ occurs at $\Theta = 65°$. The difference between this and the original result of 60° is explained by fig. 29, in which the line $I_{ao}/\sigma V_a = 0{,}033$ shows that a small variation in σR_a results in quite a large difference in Θ (compare table II, where, at angle $\Theta = 60°$ and 90°, $\sigma R_a = 14.5$ and 17.3). A difference of 5° in Θ is accompanied by only a small change in σR_a and a negligible variation in W_o (fig. 36); in other words, the value of the current angle in relation to the power is not critical.
Assuming then, for the purpose of calculating $\varphi(\Theta)$, that $\Theta = 65°$, fig. 18 gives us: $f_o(\Theta) = I_{ao}/I_{ap} = 0.235$; thus, $I_{ap} = 1700$ mA.
Fig. 22 demonstrated that the calculated values of I_{ap} and V_{ap} are

reached at $v_g = 175$ V. The grid bias, V_g, can then be calculated from (3. 34) in relation to $\Theta = 65°$: this is $V_g = -200$ V, so that $V_{gp} = 375$ V. To verify the theory, let us now work along the lines adopted in the previous paragraph and calculate the actual load line on the basis of the given values of V_g, V_a, V_{gp} and V_{ap}, proceeding from there to the anode current impulse and components. The working line is as shown in fig. 22 (curve *c*) and the result of the calculation is given below: $I_{ao} = 435$ mA; $I_{a1} = 767$ mA; $W_i = 870$ W; $W_o = 653$ W; $W_a = 217$ W; $\eta = 75\%$; $R_a = 2220$ ohms.

Here again, as in the preceding §, W_i, W_o and W_a are about 10% higher than according to the theory based on linear characteristics; R_a is lower and η unchanged. Once more, the reason for this lies in the curving of the load line in the region of the peak anode current which tends to flatten out the anode current impulses.

§ 10. Limitation of the output power by the cathode saturation current

Another form of limitation in the output is met with in transmitting valves fitted with tungsten filaments. Obviously, the peak anode current cannot in any circumstances exceed the saturation current of the cathode and, in cases where the specific saturation current of a tungsten filament valve (by which is meant the saturation current per watt of filament

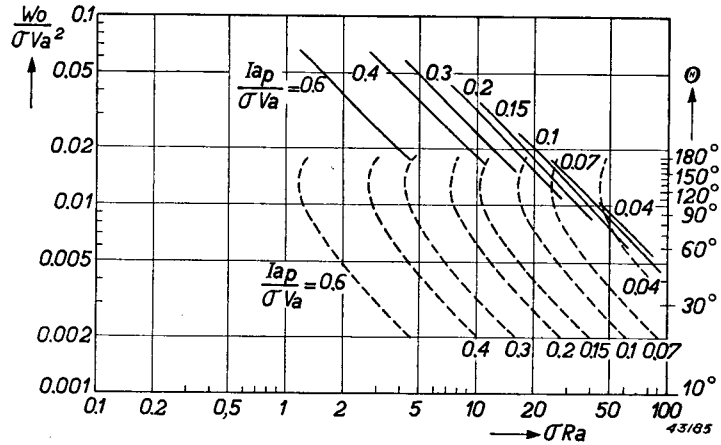

Fig. 38. Full lines: $W_o/\sigma V_a^2$ as function of σR_a, with $I_{ap}/\sigma V_a$ as parameter.
Dotted lines: the relative values of Θ.

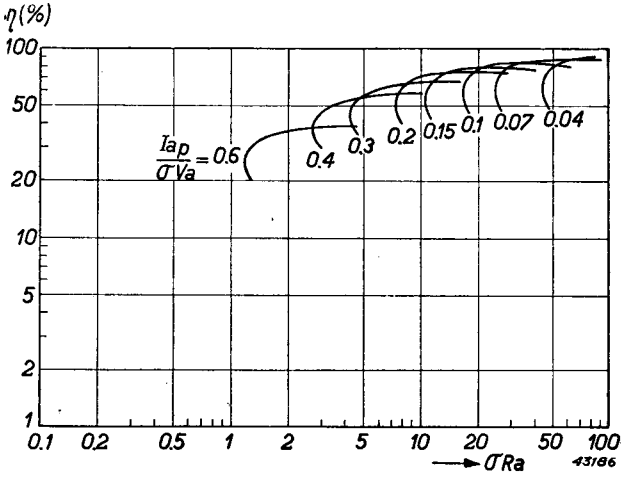

Fig. 39. η as function of σR_a, with $I_{ap}/\sigma V_a$ as parameter.

power) is small in contrast with that of other types of cathode, it is clear that the output power will be limited by this saturation current.

To ascertain the extent of this effect, use is made of fig. 32 to calculate the values of Θ and ΘR_a, at which the peak anode current is constant, and such values are shown by the dotted lines in fig. 38, with $I_{ap}/\sigma V_a$ at 0.6, 0.4, 0.3, 0.2, 0.15, 0.1, 0.07 and 0.04. The corresponding values of $W_o/\sigma V_a^2$ are then again taken from fig. 28, these being shown by the full lines in fig. 38.

In the first place it will be seen that there is one value for σR_a at every value of the expression $I_{ap}/\sigma V_a$, at which the output power reaches a maximum, and that the corresponding value of Θ is about 120° whilst being only very slightly dependent upon $I_{ap}/\sigma V_a$; further, that values of $W_o/\sigma V_a^2$ less than the maximum can occur at two different current angles, provided that these lie between 90° and 180°. Thus, at $I_{ap}/\sigma V_a = 0.6$, we find a value $W_o/\sigma V_a^2$ of 0.06, with $\sigma R_a = 1.3$; this occurs both at $\Theta = 90°$ and 180° (in this case, then, Class B and Class A respectively).

In the first instance the steady anode current is less than in the second, and the efficiency is therefore greater, as can be observed from fig. 39.

§ 11. Conclusions regarding the operating conditions of a triode

From the preceding §§ we are now in a position to formulate the following general rules for the operating conditions of a Class C triode.

Firstly, the efficiency at a given load resistance R_a will reach its optimum value if the valve be run at its limit characteristic. The fact that this condition has been reached in practice may be recognized from the output

and efficiency, which then show no appreciable further increase for a corresponding increase in the excitation voltage; the grid current, on the other hand, rises sharply when the excitation voltage rises above this optimum value. In the second place, at the setting so obtained, neither the steady cathode current (in valves having oxide- or thoriated tungsten cathode), nor the anode dissipation must exceed their maximum permissible values. If they do, the load resistance R_a must be increased in value until the above conditions are complied with.

In tungsten filament valves, as already mentioned, the anode current may be raised to the saturation point of the cathode, and this condition may be verified by making a small variation in the heater voltage, seeing that the saturation current, and also the anode current, rise or fall with the heater voltage. The correct setting of this type of valve is therefore that at which it runs at both limit characteristic and saturation current. It will be easily seen that under these conditions the anode current will drop when the heater voltage is reduced, but will remain constant if this voltage be increased.

Regarding the order of the grid bias for a given anode potential, the following should also be mentioned: at the Class C setting, the absolute value of the bias will necessarily be *at least* equal to V_a/μ, since at that value of the grid potential, the anode current is just zero. The *indicated* value, that is the value at which, under the prescribed limitations, the optimum setting is obtained, can be read from any of the figures 33, 36 or 38, provided that the slope σ of the characteristic is known. If this is not known for the valve in question, it is common practice to employ a grid bias equal to $-2V_a/\mu$; experience has shown that the output and efficiency in the Class C setting do not vary greatly with changes in the grid bias.

§ 12. Grid current and driving power

If we examine the different load lines drawn in fig. 22, it will be seen that they lie to a great extent in the region where the grid potential is positive; this means that grid current is flowing, and it is a simple matter to calculate the amount of current flowing, since, on the one hand fig. 23 gives the grid current i_g plotted against v_a and v_g, whilst on the other hand the curve of v_a and v_g as function of t is known.

Considering the case presented in § 5, in which:

$$v_g(t) = -120 + 270 \cos \omega t,$$
$$v_a(t) = 2000 - 1600 \cos \omega t,$$

$v_g(t)$ and $v_a(t)$, and, from fig. 23, $i_g(t)$, can be calculated for every value of ωt.

The grid current impulse is shown in fig. 40 (dotted line), and, for comparative purposes, also the anode current impulse, as calculated above. Now, due to the fact that grid current flows during part of the total cycle of the excitation voltage, this voltage supplies to the grid circuit a certain amount of power, known as the driving power. Let T designate the length of time of one cycle, then this power is:

$$W_{HF} = \frac{1}{T} \int_0^T V_{gp} \cos \omega t \, . \, i_g(t) \, dt \quad . \quad . \quad . \quad . \quad . \quad . \quad (3.\ 55)$$

The grid current $i_g(t)$ may be imagined as broken down into a Fourier series, viz.:

$$i_g(t) = I_{go} + I_{g1} \cos \omega t + I_{g2} \cos 2\omega t + \ldots \quad . \quad . \quad . \quad (3.\ 56)$$

In the integration of expression (3. 55), it is only the second term of (3. 56) that makes any actual contribution, and the result is therefore:

$$W_{HF} = \frac{1}{2} V_{gp} \, . \, I_{g1} \quad . \quad . \quad . \quad . \quad . \quad . \quad . \quad . \quad . \quad (3.\ 57)$$

The amplitude of the first harmonic of the grid current I_{g1} may be determined from the given impulses by means of Simpson's law, but this method of calculating the control power is too cumbersome for practical purposes and the following method is to be preferred.

When it is considered that grid current commences to flow only when the control grid becomes positive, it follows that the grid current impulses are smaller than those of the anode current, and it may be assumed as a first approximation that the current angle of the impulses is so small that the quantity

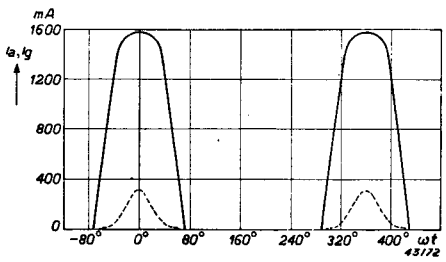

Fig. 40. Anode- and grid current impulses of a triode with Class C excitation on the basis of the load line *a* in fig. 22.

$\varphi(\Theta) = I_{g1}/I_{go}$ from fig. 27[1] is practically equal to 2. In that case, $I_{g1} = 2I_{go}$, so that expression (3. 57) becomes:

$$W_{HF} = V_{gp} \cdot I_{go} \quad \ldots\ldots\ldots \quad (3.\ 58)$$

As V_{gp} and I_{go} can be directly read from measuring instruments, the control power is then immediately known.

The accuracy of this approximation can again be verified in the case of the grid-current impulses shown in fig. 40. For these impulses, Simpson's law gives:

$$I_{go} = 46.7 \text{ mA}: I_{g1} = 86.8 \text{ mA},$$

from which it follows that $\frac{I_{g1}}{I_{go}} = 1.86$; so in this case (3. 57) can be written: $W_{HF} = 0.93\ V_{gp} \cdot I_{go}$.

The numerical factor of this formula can also be arrived at by the following argument:

In view of the fact that grid current only flows at positive values of $v_g(t)$, it follows from:

$$v_g(t) = V_g + V_{gp} \cos \omega t,$$

that the half current angle Θ_g of the grid current impulse can be derived from:

$$0 = V_g + V_{gp} \cos \Theta_g,$$

or

$$\cos \Theta_g = -\frac{V_g}{V_{gp}}.$$

In our example, $V_g = -120$ V; $V_{gp} = 270$ V; therefore $\cos \Theta_g = 0.445$, or $\Theta_g = 63\frac{1}{2}°$.

From fig. 27 we then obtain: $\varphi(\Theta) = \frac{I_{g1}}{I_{go}} = 1.77$, so that:

$$W_{HF} = \frac{1}{2} V_{gp} \cdot I_{g1} = 0.885\ V_{gp} I_{go}.$$

It is to be observed that the latter calculation is based on the assumption that the grid-current impulses are parts of sine waves, whereas in fact, as appears from fig. 40, this is not quite true. The fact, however, that

[1] Fig. 27 is derived from figs. 18 and 19 by dividing $f_1(\theta)$ and $f_0(\theta)$ at $k = 1$. Naturally, at other values of k (which would probably give a better rendering of the static grid-current characteristics), different curves $\varphi(\theta)$ are obtained, for all of which, however, the value of φ is 2 when $\theta = 0$.

the formula for W_{HF} furnishes a factor differing only 5% from that of the more exact calculation, justifies the assumption that, for practical purposes, the control power can be closely approximated by means of the formula:

$$W_{HF} = 0.9\, V_{gp} . I_{go} \quad . \quad . \quad . \quad . \quad . \quad . \quad . \quad . \quad (3.\ 59)$$

for other forms of grid current impulse as well, and this can also be proved mathematically.

The driving power is utilized on the one hand as grid dissipation, and on the other as charging power for the source whence the grid bias is obtained. The grid dissipation is the product of grid voltage and -current, averaged over one cycle:

$$W_g = \frac{1}{T}\int_o^T (V_g + V_{gp} \cos \omega t) . i_g (t)\, dt. \quad . \quad . \quad . \quad . \quad . \quad (3.\ 60)$$

According to (3. 55) and (3. 60), the residual power is:

$$W_{HF} - W_g = \frac{1}{T}\int_o^T - V_g . i_g (t)\, dt,$$

or, in view of (3. 56):

$$W_{HF} - W_g = - V_g I_{go},$$

which is, in fact, the power absorbed by the source of grid bias, or the power developed across the grid leak.

§ 13. Detuning of the anode circuit

In the foregoing §§, all the calculations are based on the assumption that the anode circuit is tuned to the excitation frequency, in fact, that the anode load is real. We shall now see what happens when the anode circuit is slightly detuned with respect to that frequency.

In fig. 21*b*, the anode impedance Z_a is complex, i.e.:

$$\frac{1}{Z_a} = \frac{1}{R_a} + j\omega C + \frac{1}{j\omega L},$$

from which the modulus $|Z_a|$ and the phase angle φ of Z_a can be calculated:

$$\frac{1}{|Z_a|^2} = \frac{1}{R_a^2} + \left(\omega C - \frac{1}{\omega L}\right)^2; \quad \operatorname{tg} \varphi = R_a \left(\frac{1}{\omega L} - \omega C\right). \qquad (3.\ 61)$$

The relationship between $|Z_a|$ and φ is the important factor, and, by eliminating the quantity $1/\omega L - \omega C$ in the expression (3. 61), we have:

$$|Z_a| = R_a \cos \varphi, \quad \ldots\ldots\ldots \quad (3.\ 62)$$

which clearly illustrates the well-known fact that in a detuned circuit in which the phase angle $\varphi = 0$, the modulus of the impedance is at a maximum and equal to R_a.

Let us then ascertain the behaviour of the load line in the I_a/V_a diagram when the anode circuit is detuned. For this purpose, suppose that the anode current may be represented by straight lines parallel to the V_a axis and, further, that the dependence of i_a upon v_a is linear:

$$i_a = s v_g,$$

making it a condition that this formula applies only when $i_a > 0$ and $v_a > 0$. In practice, this means that the anode potential will have no effect upon the anode current, and this is actually a condition that exists more or less in pentodes as well as to a certain extent in triodes of high amplification factor.

The grid voltage is written in the form:

$$v_g = V_g + V_{gp} \cos \omega t;$$

then

$$i_a = s\,(V_g + V_{gp} \cos \omega t) \quad \ldots\ldots\ldots \quad (3.\ 63)$$

is valid for: $\quad -\Theta < \omega t < \Theta$

$2\pi - \Theta < \omega t < 2\pi + \Theta$ and so on,

while

$$\cos \Theta = -\frac{V_g}{V_{gp}}.$$

This again indicates an anode current of the impulse type, at least if $\Theta < 180°$, and development of the Fourier series produces:

$$i_a = I_{ao} + I_{a1} \cos \omega t + I_{a2} \cos 2\omega t + \ldots\ldots$$

The component $I_{a1} \cos \omega t$ flows through the anode impedance across which the alternating anode voltage is developed, viz: $V_{ap} \cos (\omega t + \varphi)$, with

$$V_{ap} = I_{a1} |Z_a|, \quad \ldots\ldots\ldots \quad (3.\ 64)$$

so that the anode potential is:

$$v_a = V_a - V_{ap} \cos (\omega t + \varphi) \quad \ldots\ldots\ldots \quad (3.\ 65)$$

The load line in the I_a/V_a diagram is determined by (3. 63) and (3. 65), together with expressions (3. 62) and (3. 64). Elimination of ωt between (3. 63) and (3. 65) then makes it a simple matter to show that this load line is an ellipse. It follows from (3. 63) that:

$$\cos \omega t = \frac{i_a}{sV_{gp}} - \frac{V_g}{V_{gp}}, \text{ so that:}$$

$$\sin \omega t = \sqrt{1 - \left(\frac{i_a}{sV_{gp}} - \frac{V_g}{V_{gp}}\right)^2}.$$

Expression (3. 65) then becomes: $v_a = V_a - V_{ap} \cos \omega t \cos \varphi + V_{ap} \sin \omega t \sin \varphi =$

$$V_a - V_{ap} \cos \varphi \cdot \left(\frac{i_a}{sV_{gp}} - \frac{V_g}{V_{gp}}\right) + V_{ap} \sin \varphi \cdot \sqrt{1 - \left(\frac{i_a}{sV_{gp}} - \frac{V_g}{V_{gp}}\right)^2}$$

or:

$$\left\{v_a - V_a + V_{ap} \cos \varphi \cdot \left(\frac{i_a}{sV_{gp}} - \frac{V_g}{V_{gp}}\right)\right\}^2 = V_{ap}^2 \sin^2 \varphi \cdot \left\{1 - \left(\frac{i_a}{sV_{gp}} - \frac{V_g}{V_{gp}}\right)^2\right\}.$$

This is a quadratic equation between the co-ordinates i_a and v_a in the i_a/v_a diagram, in other words, the equation in respect of a conic. Further investigation shows this to be an ellipse. An elliptical load line of this type is depicted in fig. 41; the equidistant horizontal lines represent the lines $i_a = f(v_a)$ for v_g = constant.

Two load lines are shown, the first of which (the broken line $DABC$) refers to a tuned anode circuit, whereby the portion BC of the line is straight, as previously demonstrated. The anode current CE, according to (3. 63), is equal to $s(V_g + V_{gp})$, whilst $AE = AD = V_{ap}$.

When the anode circuit is detuned, so that $\varphi \neq 0$ and $|Z_a|$ become

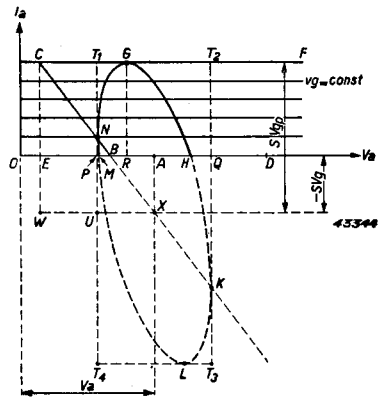

Fig. 41. Effect of detuning of the anode circuit upon the shape of the load line in the i_a/v_a diagram of the hypothetically ideal pentode, Class C.
CBD: anode circuit tuned.
DMGHD: anode circuit detuned; phase angle of the anode impedance = 60°.

$< R_a$, the expression (3. 63) in respect of the anode current remains unchanged, since V_g and V_{gp} do not alter. In effect, then, the peak anode current retains its original value, with the result that in the new load line in fig. 41, the point corresponding to this current must lie on the line CF.

However, if the form of the anode-current impulse does not change, the components also retain their value, namely I_{ao} and I_{a1}. Therefore, when the anode circuit is detuned, the steady anode current remains constant (which is quite conceivable in the case of a valve having horizontal I_a/V_a characteristics) and, further, V_{ap}, according to (3. 64), becomes smaller only because $|Z_a| = R_a \cos \varphi$ and $\cos \varphi$ is < 1.
Fig. 41 shows the conditions when $\varphi = 60°$; then

$$|Z_a| = \frac{1}{2} R_a \text{ and } V_{ap} = \frac{1}{2} I_{a1} R_a = \frac{1}{2} V_{ap\,o},$$

that is, the value of the alternating anode current is equal to one half of what it is when tuned. The load line can be constructed with reference to (3. 63) and (3. 65), and this proves to be the ellipse $GHKLMN$. The centre point X of this ellipse is situated at $i_a = -sV_g$; $v_a = V_a$.
Since (3. 63) is valid only when $i_a > 0$, the only portion of any importance is $MNGH$. The various quantities can now be easily identified, viz:
GR = peak anode current = CE;
$AP = AQ = \frac{1}{2}AE = \frac{1}{2}AD$ = amplitude of the alternating anode potential;
AO = steady anode voltage.
Just as in the case of the tuned circuit, of which the working line consists of a current-carrying portion CB and another portion BD where no current flows, the working line of the untuned circuit also comprises a current portion $MNGH$ and a neutral portion $HQAM$.
The value of ωt at the various points on the load line can also be readily given: according to (3,63), the maximum value of i_a occurs at $\omega t = 0$ (point G), zero at $\omega t = \Theta$ (point H) and at $\omega t = -\Theta$ (point M), i.e. the load line runs in the direction MGH, which is confirmed by (3. 65) since, when $\omega t = 0$ and $\varphi = 60°$,

$$v_a = V_a - V_{ap} \cos 60° = V_a - \frac{1}{2} V_{ap} = OR,$$

whilst for $\omega t = -60°$:

$$v_a = V_a - V_{ap} \cos 0° = V_a - V_{ap} = OP.$$

The point N is then reached at $\omega t = -60°$ and point G at $\omega t = 0°$, which determines the direction of circulation on the line.
At point Q, v_a is at a maximum and, according to (3. 65), $\cos(\omega t + \varphi) = -1$; therefore $\omega t + \varphi = 180°$, or $\omega t = 180° - \varphi° = 120°$. At A, $v_a = V_a$ and $\cos(\omega t + \varphi) = 0$, so that $\omega t + \varphi = 270°$, or $\omega t = 210°$. The following table gives a summary of the values of ωt at the different points.

TABLE III

Point	G	H	Q	A	M	N
$\omega t =$	0	Θ	$180° - \varphi$	$270° - \varphi$	$360° - \varphi$	$360° - \varphi$

Clearly then, the course of the working point is governed by the sign of φ in (3. 65); in the case in point, where a positive value of φ is assumed, this means that the alternating anode voltage leads the alternating anode current, in other words, the anode impedance is inductive.
Conversely, it is easily shown that the working point proceeds to the left when the anode impedance is capacitive.
At other values of φ an ellipse is produced, having the same centre point X and also touching CF; the tangents T_1T_4 and T_2T_3 are therefore removed from X a distance equal to the peak value of the alternating anode voltage in the case under consideration. The latter reaches its highest value in the tuned condition and the load line then straightens out. The point where the anode current reaches its maximum thus moves along the line CF (line of constant v_g, i.e. constant V_{gp}), reaching the point C when the circuit is tuned.

Note. The point N in fig. 41, where the ellipse has a vertical tangent T_1T_4 is, at the same time, the point where the working line CBX of the tuned anode circuit cuts the ellipse. To demonstrate this, we have only to prove that angle CXW = angle NXU. Now, $CW = sV_{gp}$; $WX = V_{apo}$ (= alternating anode voltage in tuned anode circuit) $= I_{a1}R_a$; $UX = V_{ap1}$ (= alternating anode voltage in detuned circuit) $= I_{a1}R_a \cos\varphi$; $NU = sV_{ap} \cos\varphi$ (the latter is obtained as follows: in N, v_a is at a minimum in the detuned circuit, so that, according to (3. 65), $\omega t = -\varphi$; further, according to (3. 63), $i_a = sV_g + sV_{gp} \cos\varphi = NP$, and therefore $NU = NP + PU = sV_{gp} \cos\varphi$). Apparently, then, $CW/WX = NU/UX$, so that angle CXW = angle NXU.

Consider now the case where the anode current is to some extent dependent upon v_a, which condition, as pointed out in § 7, more closely agrees with observation. In accordance with fig. 25 we then write:

$$i_a = a\,(v_g + bv_a) = av, \quad \ldots\ldots\ldots \quad (3.\ 66)$$

in which v_s is the control voltage.
Further:

$$v_g = V_g + V_{gp} \cos \omega t. \quad \ldots\ldots\ldots \quad (3.\ 67)$$

and

$$v_a = V_a - V_{ap} \cos (\omega t + \chi), \quad \ldots\ldots \quad (3.\ 68)$$

in which χ is the phase angle, as yet unknown.
This, then, gives us:

$$v_s = v_g + bv_a = V_g + bV_a + V_{gp} \cos \omega t - bV_{ap} \cos (\omega t + \chi). \quad (3.\ 69)$$

The control voltage therefore consists of direct voltage:

$$V_s = V_g + bV_a$$

and an alternating voltage:

$$V_{gp} \cos \omega t - bV_{ap} \cos (\omega t + \chi).$$

The different alternating voltages with their mutual phase displacements are shown in the vector diagram in fig. 42, where it is seen that the two components of the alternating control voltage combine to form the vector V_{sp} which lags in phase by an angle ψ behind V_{gp}, so that:

$$V_{gp} \cos \omega t - bV_{ap} \cos (\omega t + \chi) = V_{sp} \cos (\omega t - \psi). \quad (3.\ 70)$$

The total control voltage v_s is then, according to (3. 69):

$$v_s = V_s + V_{sp} \cos (\omega t - \psi) \quad \ldots\ldots \quad (3.\ 71)$$

(3. 66) now gives:

$$i_a = aV_s + aV_{sp} \cos (\omega t - \psi), \quad \ldots\ldots \quad (3.\ 72)$$

which applies only to the values of ωt whereby $i_a > 0$, viz:

$$-\Theta + \psi < \omega t < \Theta + \psi$$
$$2\pi - \Theta + \psi < \omega t < 2\pi + \Theta + \psi \text{ etc.},$$

in which

$$\cos \Theta = -\frac{V_s}{V_{sp}} \quad \ldots\ldots\ldots\ldots \quad (3.\ 73)$$

Once more, then, the anode current takes the form of a series of pulses of which the first harmonic may be represented by:

$$i_{a1} = I_{a1} \cos (\omega t - \psi),$$

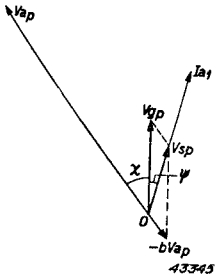

Fig. 42. Vector diagram of the different alternating anode currents of a triode in a detuned circuit.

and this is shown in fig. 42 by a vector of which the direction coincides with V_{sp}, so that the vector I_{a1} lags in respect of V_{ap} by an angle of:

$$\chi + \psi = \varphi.$$

It is evident, that φ is the phase angle of the anode impedance Z_a, whilst the modulus $|Z_a| = R_a \cos\varphi$ of this impedance is again related to V_{ap} and I_{a1}, in accordance with:

$$V_{ap} = I_{a1}\,|Z_a|.$$

The difference between this and the previous instance, in which i_a is not dependent upon v_a, lies in the fact that b was then 0, so that the vector V_{sp} coincided with V_{gp} and angle $\psi = 0$. I_{a1} then also coincided with V_{gp} and angle χ was the same as φ.

That the load line in the previous case is an ellipse can be shown in the same way; to this end the quantities ωt and v_g are eliminated in the equations (3. 66), (3. 67) and (3. 68), leaving a quadratic equation between i_a and v_a.

Fig. 43 shows a load line of this type, i.e. the ellipse $MGHK$, together with the load line CBX for the case of the tuned circuit. Owing to the limited validity of (3. 72), only that part of both curves above the v_a-axis is of interest.

The centre point X of the ellipse is determined by those terms in (3. 68) and (3. 72) which are independent of t, that is by:

$$v_a = V_a \text{ and } i_a = aV_s = a\,(V_g + bV_a).$$

In the case of the tuned circuit, C is the point at which both grid potential and anode current reach their maximum, with the anode voltage at a minimum. CE is then the peak anode current and AE the amplitude of the alternating anode voltage.

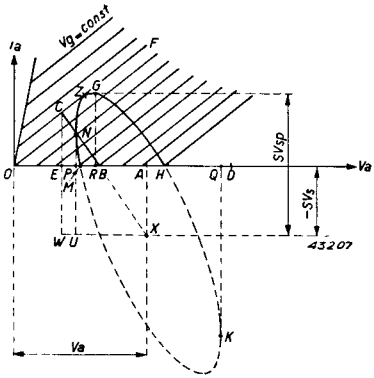

Fig. 43. As fig. 41, but as applicable to a triode.

When the anode circuit is detuned, the excitation voltage remains unchanged, as does also the maximum value of v_g, and the elliptical working line must therefore touch line CF, of which v_g is constant (point Z).

It is also seen from fig. 42 that the first harmonic of the anode current, and therefore also the anode- current impulse, attain their maximum later than the excitation voltage by a phase angle ψ, for which reason the point G in fig. 43, where i_a is at a maximum, does not coincide with Z, but is reached by the working point slightly later, i.e. at a time $\omega t = \psi$, while Z is passed at $\omega t = 0$. Because of the pulsating character of the anode current, the latter becomes zero at angle Θ before, and after, reaching maximum, and in the figure this takes place at the points M $(\omega t = \psi - \Theta)$ and H $(\omega t = \psi + \Theta)$. After reaching H, the load line proceeds along the $v_a$axis to Q, where the anode voltage is maximum: according to (3. 68), ωt is then $\omega t = 180° - \chi$. Subsequently, the working point returns from Q to A $(\omega t = 270° - \chi)$, then to M and along the ellipse, via N $(\omega t = -\chi)$, to Z.

Here again, the ellipse is followed in a clockwise direction, which in fig. 42 corresponds to a lag in I_{a1} with respect to V_{ap}, i.e. with inductive anode circuit. The magnitude of the alternating anode voltage in this case too, as already pointed out, is given by:

$$V_{ap} = I_{a1} R_a \cos \varphi.$$

When the anode circuit is detuned, cos φ decreases, but I_{a1} increases due to the fact that the peak anode current I_{ap} increases (fig. 43: $GR > CE$). In practice, this increase is not so very great, however, since the static characteristics (including CF) are fairly flat, due to the value of the amplification factor, which is generally high. For this reason, the decrease in cos φ in the expression V_{ap} will far exceed the increase in I_{a1}, with a consequent drop in V_{ap}. For this reason, also, the points P and Q, between which v_a fluctuates, lie between E and D.

Note. When the anode circuit is detuned, the current angle Θ is not entirely constant, for, according to (3. 73), cos $\Theta = -V_s/V_{sp}$, in which V_s is constant, whereas, as shown in fig. 42, V_{sp} is dependent on the direction and magnitude of V_{ap}, or, upon the degree to which the circuit is detuned. It is clear that V_{sp} will be at its lowest value in a tuned anode circuit, and at a maximum when the circuit is as far as possible off tune.

In the first instance, the vectors V_{ap} and $-bV_{ap}$ lie on the line of the vector V_{gp}, so that $V_{sp} = V_{gp} - bV_{ap}$. In the last mentioned case, $|Z_a| \approx 0$ and, therefore, so do V_{ap} and $-bV_{ap}$; thus $V_{sp} = V_{gp}$. The difference in the alternating control voltage is therefore bV_{ap}, where V_{ap} is the alternating anode voltage in the case of the tuned circuit. Off the tuning point, then, cos Θ decreases slightly, with an accompanying increase in Θ; $f_1(\Theta) = I_{a1}/I_{ap}$, as in fig. 19, then also becomes slightly higher.

It may be said at once, however, that this increase in $f_1(\Theta)$ is extremely small, not only because Θ varies only very slightly, but because the term bV_{ap} is small compared with V_{gp}, so that, for practical purposess this effect may be ignored.

In the end, the result of detuning the anode circuit is an increase in the steady anode current I_{ao}, since $I_{ao} = f_o(\Theta)$. I_{ap}, and, as already shown, I_{ap} increases according to the amount of detuning, with a corresponding slight increase in $f_o(\Theta)$ as well; in practice, therefore, when the anode circuit is tuned, a minimum value of I_{ao} is obtained.

The fact that the output power is at a maximum when the anode circuit is detuned follows from the formula

$$W_o = \frac{1}{2} I_{a1} \cdot V_{ap} \cos \varphi,$$

which, together with:

$$V_{ap} = I_{a1} R_a \cos \varphi \text{ or } I_{a1} \cos \varphi = \frac{V_{ap}}{R_a},$$

gives us:

$$W_o = \frac{1}{2} \frac{V_{ap}^2}{R_a}.$$

It has been shown that under tuned conditions, V_{ap} reaches its extreme value, and this, then, is also the case with W_o, so that the anode circuit can be tuned also by adjusting W_o to a maximum.

The steady grid current also undergoes a change when the anode circuit is detuned, as will be seen from the disposition of the load line in fig. 23 for the case of the tuned circuit. The end point A of this line indicates the maximum values of v_g and i_g, as well as the minimum value of v_a, and, when the circuit is detuned, the alternating anode voltage, as already seen, decreases whilst $v_{a\,\min}$ increases: but, as $v_{g\,\max}$ remains constant, the point A will move to the right along the line v_g = constant (in this case 150 V), which means that I_{gp} will decrease.

Together with I_{gp}, the steady grid current I_{go} will also drop, since the angle Θ_g of the grid current impulse is constant, so that I_{go} is controlled only by I_{gp}.

It follows, then, that the steady grid current attains a maximum when the anode circuit is tuned. As is the case with the load line in the I_a/V_a diagram, the load line of the I_g/V_a diagram also assumes the form of a loop when the anode circuit is detuned, but the exact form of this curve need not be investigated here.

§ 14. Over-excitation of transmitting valves

In the theory of transmitting triodes discussed in § 7 and onwards, the I_a/V_a characteristics have been represented by straight lines which, at low values of anode potential, terminate on the line $i_a=\sigma v_a$, the so-called limit characteristic. This method was adopted on the evidence of the practical example of a family of I_a/V_a curves as shown in fig. 22; the latter also shows that the load line is more or less straight, having a noticeably sharp bend only at the upper end. This is due to the fact that, at a given value of V_{gp}, that is, $V_{g\,\max}$, $v_{a\,\min}$ reaches very low values, causing the load line to approach more and more towards the limit characteristic. Evidently, such a condition may be brought about either by increasing V_{gp}, or V_{ap}, or both. We now propose to investigate the consequences of this.

Reverting to § 5, in which the load line a (fig. 22) was based on:

$$V_g = -120 \text{ V},\ V_{gp} = 270 \text{ V},\ V_a = 2000 \text{ V},\ V_{ap} = 1660 \text{ V},$$

we shall now construct the load line in the I_a/V_a diagram of the same triode as in fig. 22 under three different conditions, namely at $V_{ap} = 1500$ V, 1900 V and 2200 V.

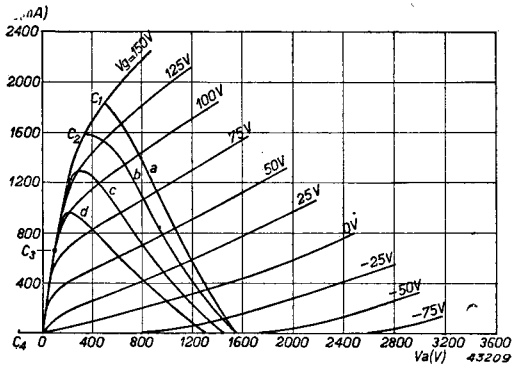

Fig. 44. Load lines in the I_a—V_a characteristic of a triode: *a*) $V_{ap}=1500$ V, *b*) $V_{ap}=1660$ V, *c*) $V_{ap}=1900$ V, *d*) $V_{ap}=2200$ V.

The method of calculation is analogous to that followed in the earlier example; $v_g\,(t)$ and $v_a\,(t)$ are calculated at different values of ωt with the

aid of the above data, and the corresponding value of $i_a\,(t)$ is then obtained from the I_a/V_a diagram. The results are shown in figs. 44 and 45, the first of which indicates the load lines and the second the corresponding anode-current impulses: *a*, *b*, *c* and *d* represent the conditions at $V_{ap} = 1500$, 1660, 1900 and 2200 V respectively.

Fig. 44 reveals the fact that, when V_{gp} is constant, with increasing V_{ap}, the load line bends over more and more towards the top, the end point first curving at $v_g = 150$ V, then making a further dip along the limit-characteristic line and terminating at the negative v_a axis when the alternating anode voltage becomes higher than the steady anode voltage. C_1, C_2, C_3 and C_4 are the terminating points in the four cases mentioned.

The conclusion may then be immediately drawn that in this process the anode current impulses first flatten out (*b*, fig. 45) and then dip in the centre (*c*) to an extent that may eventually reach the zero current axis (*d*). Simpson's law furnishes the components I_{ao} and I_{a1} of the anode current in each of the four instances, after which W_i, W_o, η and R_a are easily determined. The results are tabulated in the following table and are shown graphically in fig. 46:

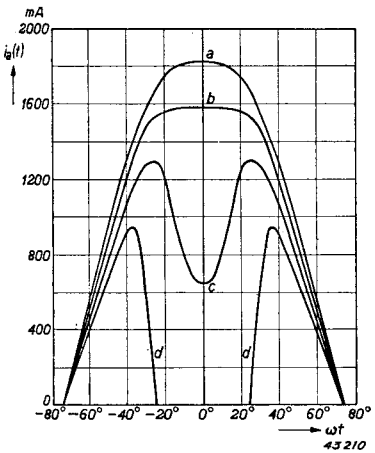

Fig. 45. Anode current impulses in respect of the load lines in fig. 44.

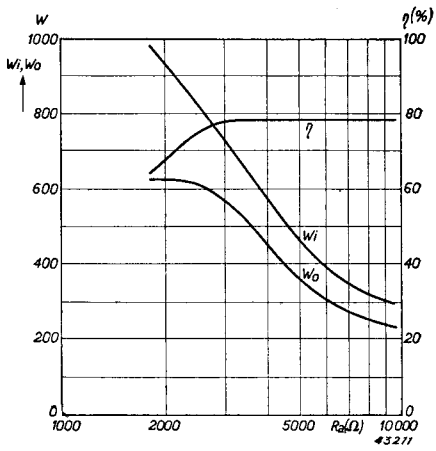

Fig. 46. W_i, W_o and η as function of R_a, calculated for a triode from the load lines in fig. 44.

TABLE IV

Load line	*a*	*b*	*c*	*d*
I_{ao} (mA)	489	447	332	148
I_{a1} (mA)	836	758	547	211
W_i (W)	978	894	664	296
W_o (W)	627	629	520	232
η (%)	64.0	70.3	78.3	78.4
R_a (ohms)	1795	2190	3470	9490
V_{ap} (V)	1500	1660	1900	2200

Apparently, the highest output power is obtained at R_a = approx. 2200 ohms, that is, on the load line *b*. When R_a is increased, W_o drops due to the indentation in the curve of the anode-current impulse, which greatly reduces the component I_{a1}.

It is also a striking fact that the efficiency continues to improve up to a value of R_a = approx. 3500 ohms, after which it becomes constant; the reason for this is that the relation I_{a1}/I_{ao}, which figures in the expression that gives η in the three cases, *a*, *b* and *c*, retains practically the same value and commences to drop only when, as in the case *d*, the dip in the curve extends right down to zero. This happens at $R_a > 3500$ ohms. With $R_a < 3500$ ohms, the increase in efficiency for an increasing value of R_a will be governed by the increase in V_{ap}/V_a, whereas when $R_a > 3500$ ohms, the latter increase is closely compensated by the drop in I_{a1}/I_{ao}, leaving the efficiency constant.

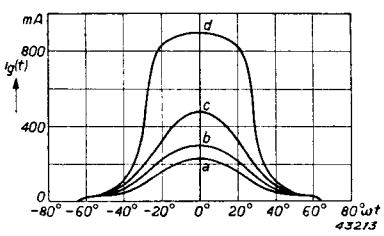

Fig. 47. Grid current impulses corresponding to the load lines *a*, *b*, *c* and *d*, fig. 44.

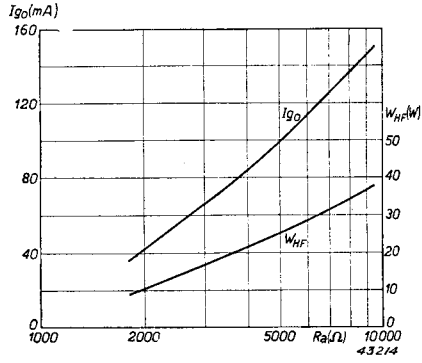

Fig. 48. I_{go} and W_{HF} as function of R_a, calculated from fig. 46.

From this example it is found, then, that the most favourable setting for the valve is the one at which the load line begins to show a downward tendency. The output power is then as high as possible (at a given excitation voltage) and the efficiency is quite reasonable. At higher values of R_a only a very slight increase in efficiency can be obtained, but the output then drops; moreover, the grid current, and therefore also the control power, rise sharply, as demonstrated in fig. 47, in which the grid current impulses are shown, under the different conditions in question. The figure makes it possible to calculate the D.C. component I_{go} and the first harmonic I_{g1} of the grid current, and, from these, the control power.

This gives the following results:

TABLE V

Load line	*a*	*b*	*c*	*d*
I_{go} (mA)	35	48	74	150
I_{g1} (mA)	65	89	139	282
W_{HF}(W)	8.8	12.0	18.8	38.0

In fig. 48, I_{go} and W_{HF} are shown plotted against R_a. The marked increase in driving power in the presence of over-excitation may be attributed to the sharp rise in the I_g/V_a characteristics in the region of the I_g-axis (see fig. 23).

§ 15. Disadvantages of the triode as a transmitter amplifier

It was stated in § 12 that the disposition of the different load lines in the I_a/V_a diagram of a triode is such that most of them lie in the range where v_g is positive. The consequence is that, when a transmitting valve is run at these settings, there is a fairly heavy flow of grid current, necessitating a certain driving power, and this power must come from the stage preceding the valve under consideration. It is naturally an advantage to be able to design a transmitter with the smallest possible number of stages to produce a given output power, and to this end the ratio of the output of each stage to the driving power, or so-called power gain, is made as high — i.e. the driving power itself as low — as possible.

It might be expected that this could be brought about by re-arranging the static I_a/V_a characteristics, so that a large portion of the load line falls in the zone of negative v_g; and, in the case of the triode, attempts should accordingly be made to make the characteristic for $V_g = 0$ as steep as is practicable, in other words, I_a should be increased as much as possible for a given value of V_a and $V_g = 0$.

Obviously, then, the only course to take in the case of a triode is to increase the effect of anode potential upon the magnitude of the anode current, that is, to decrease the amplification factor.

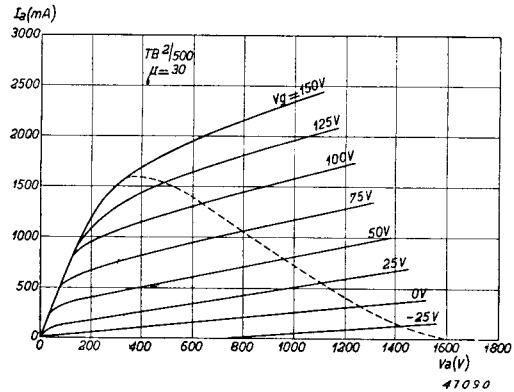

Fig. 49. Characteristics of a triode ($\mu = 30$), with load lines in respect of $V_a = 2000$ V, $I_{ap} = 1600$ mA and $V_{a\,\min} = 340$ V.

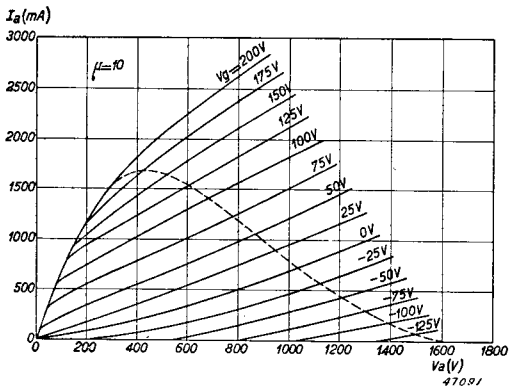

Fig. 50. Characteristics of a similar triode (see fig. 49) but with $\mu = 10$. Data regarding load line as in fig. 49. Owing to the reduction in μ, both V_{gp} and $V_{g\,\max}$ will be seen to have increased.

Figs. 49 and 50 illustrate the significance of this amplification factor with regard to the position of the I_a/V_a curves; the former shows the curves for a triode with $\mu = 30$, whereby $D = 1/\mu = 0.033$, whilst the latter reproduces the same curves as calculated for a similar type of triode, but having an amplification factor $\mu = 10$, i.e. $D = 0.1$. It can be seen that the slope of the characteristic of the last, mentioned valve at $V_g = 0$ is much the steeper of the two.

It might be considered that a low amplification factor is, therefore, desirable from the aspect of a low excitation power, but that this is not so will be seen when the load lines of these two valves are constructed for a Class C set-

ting. Suppose that $V_a = 2000$ V and $I_{ap} = 1600$ mA; further, that $V_{a\,\min}$ = approx. 340 V. In the low μ valve we then have $V_{g\,\max} = 200$ V, whilst the other valve gives $V_{g\,\max} = 150$ V. If in the latter case V_g is taken to be —120 V, then $V_{gp} = 270$ V and $\cos \Theta = 0.248$. To obtain the same value of Θ in the low μ valve, V_g must be —275 V, that is, $V_{gp} = 475$ V. The load line of the two types is therefore obtained from the following equations:

triode ($\mu = 30$)
$$\begin{cases} v_g = -120 + 270 \cos \omega t \\ v_a = 2000 - 1660 \cos \omega t \end{cases}$$

analogous valve ($\mu = 10$)
$$\begin{cases} v_g = -275 + 475 \cos \omega t \\ v_a = 2000 - 1660 \cos \omega t \end{cases}$$

The respective load lines are given in figs. 49 and 50.
It appears that the low μ valve requires, firstly, a higher $V_{g\,\max}$ and, secondly, a much higher V_{gp} than the high μ type, and this may be explained by employing expression (3. 17), giving the control voltage of a triode and which, written in a modified form, is as follows:

$$v_s = \frac{\mu v_g + v_a}{\mu + C} = v_g \frac{\mu + v_a/v_g}{\mu + C}.$$

In this expression, C may be regarded as a constant for valves of similar construction, and in the present instance the value of the constant is 6. The maximum value I_{ap} of i_a, and therefore also of v_s, occurs when v_a is low, and in this case v_a/v_g appears to be $< C$. In order, then, to ensure the same value of v_s at the same value of v_a, v_g must be increased according as μ is decreased, and this explains the higher value of $V_{g\,\max}$ where low values of μ are concerned.
In this case, too, V_{gp} is also greater, due to the fact that, according to the above formula, at the point where $i_a = 0$, i.e. also $v_s = 0$, v_g is inversely proportional to μ. A low amplification factor is therefore accompanied by a more negative value of v_g, and, since the current angles in the equation are assumed to be the same, V_{gp} in the case of the low μ valve must also be considerably higher than in the other type.
The increase in $V_{g\,\max}$ and V_{gp} when μ is reduced, as deduced from the above argument and formulae, now leads to the following conclusion. Due to the increase in $V_{g\,\max}$, the grid current also increases; the effect of this is slightly compensated by the smaller angle of the grid current,

but the effect of the two factors is still that, due to the lower amplification factor, the reduction originally anticipated in the average grid current I_{go} is realized only to a very slight degree, or not at all. Now, as the driving power, according to (3. 59), is proportional to $(I_{go} . V_{gp})$, and as V_{gp} in the low μ valve is so much higher than in the high μ type, it must be concluded that the driving power in this case is greater and that the reduction in μ, in this respect, is more of a disadvantage than otherwise.

In the design of modern triodes there is therefore a definite tendency towards the highest possible amplification factors, and a figure of 50 is by no means uncommon. Even higher factors are obtainable by employing screen-grid valves, and these are the subject of the next chapter.

CHAPTER IV

The Tetrode and Pentode as R.F. Power Amplifier

§ 1. The importance of the screen grid

The screen grid valve, as is generally known, has been evolved from the triode by introducing between the control grid and the anode a second or screengrid which, is maintained at a constant positive potential with respect to the cathode.

That part of the valve which comprises the cathode, control grid and screen grid may be regarded as a triode in which the screen plays the part of the anode, and the amount of current passing in the direction of the screen, under the influence of the control- and screen-grid potentials, is then dependent upon these potentials, as is the anode current in an ordinary triode.

Due to the mesh or spiral structure of the screen grid, the major part of the current passes through this grid to the anode beyond it, whilst only a small part is collected by the screen itself. For this reason the I_a/V_g characteristics (at constant V_a) of a triode become the I_a/V_{g1} characteristics in the case of the screen grid valve, but with the screen-grid voltage as parameter. (The anode is considered to be at a positive potential with respect to the cathode). Just as the location of the I_a/V_g characteristics of the triode is determined by the value of V_a, the curve shifting to the left of the diagram when V_a is increased, the location of the curve in the case of the tetrode is governed by V_{g2}, the characteristic moving towards the left (towards the zone of negative V_{g1}) when V_{g2} is increased. Due to the screening effect of the extra grid, the anode potential has practically no influence on the value of the anode current. (The region of very low anode voltages may be ignored for the moment.)

When a valve of this type is employed as an R.F. power amplifier with alternating grid excitation, to ascertain the anode current from the I_a/V_{g1} characteristics, it is only necessary to take a single curve into consideration, namely that corresponding to the screen-grid potential at which the valve is to work.

This means that the dynamic I_a/V_{g1} characteristic is identical with the static curve, so that, in comparison with a triode, the dynamic characteristic is much the steeper of the two: a given peak anode current can therefore be obtained with less positive potential on the control

grid, i.e. the grid current is lower. This improvement can further be enhanced by increasing V_{g2}, thus moving the curve towards the left, when a required anode current may be obtained at a still lower positive grid voltage.

At the same time, this increase in V_{g2} is not unrestricted, since the screen absorbs a part of the cathode current, and this in turn gives rise to screen-grid dissipation which increases as the screen potential is raised. Practically speaking, then, this increase in V_{g2} is limited to the point of the maximum permissible screen-grid dissipation for a given alternating control-grid voltage.

§ 2. Secondary emission

Due to the screening effect of the second grid, the anode potential (apart from very low values) exercises practically no influence on the cathode current, and, since the anode current is only less than that of the cathode by the small amount of control- and screen-grid currents, the anode current will also be very little affected by the anode voltage.

It might be expected that the I_a/V_a characteristics of a tetrode will run almost parallel with the V_a axis- and, from fig. 51, showing the curves of an older type of tetrode at a screen-grid potential of 500 V, it will be seen that this is fairly well justified in the region where V_a is greater than approx. 500 V. When the anode voltage is equal to, or less than 500 V, the anode current drops suddenly and even becomes negative, reaching zero at $V_a = 0$.

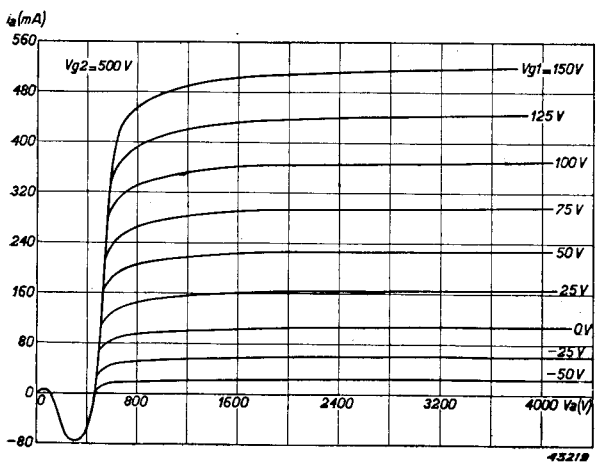

Fig. 51. I_a — V_a characteristics of an older type of tetrode, with V_{g2} = 500 V.

Fig. 52 shows the screen-grid characteristics, with I_{g2} as a function of V_a and V_{g1} as parameter, from which it appears that with V_a greater than 650 V approx, the screen grid current is

negative, but at $V_a = 650$ V it suddenly becomes positive and remains so at lower anode voltages.
These phenomena are due to the liberation of secondary electrons from the cathode- and screen grid, resulting from their bombardment by the cathode current.

When the anode voltage is higher than that of the screen, the field between screen and anode tends to accelerate the passage of electrons in the direction of the latter; the secondary electrons from the screen pass therefore to the anode and contribute to the anode current, whilst reducing the (externally measured) screen current. Since each colliding electron may liberate more than one secondary electron, the current of the emerging electrons may be accordingly greater than that of the primary bombarding electrons, in which case the (external) screen current becomes negative. Secondary electrons liberated from the anode are repelled in their flow by the surrounding field and fall back on the anode; so they play no part in the (externally measured) anode current. The conclusion is then that, when $v_a > V_{g2}$, the (externally measured) anode current is equal to the sum of the primary stream of electrons and the secondaries from the screen, but because the former is by far the greater quantity, the behaviour of the anode current at $v_a > V_{g2}$ will be much the same as though the secondary emission were entirely absent. Hence, the I_a/V_a characteristics in this region will run approximately parallel to the V_a axis.
If, on the other hand, $v_a < V_{g2}$, the secondary anode electrons flow away from the anode, whilst those from the screen are repelled back to the screen; the anode current then consists of the difference between the absorbed primary,

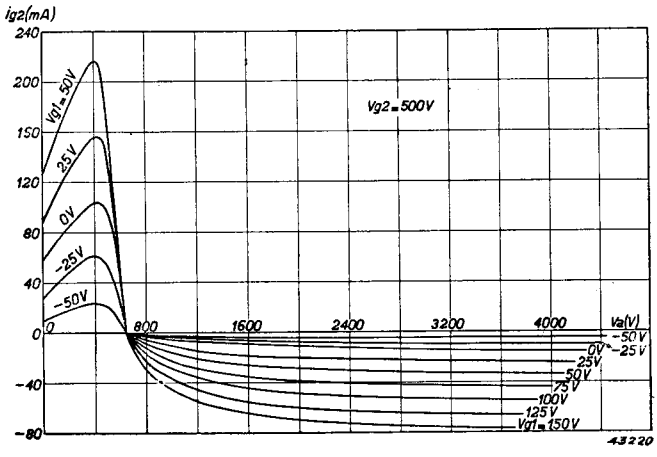

Fig. 52. $I_{g2} - V_a$ characteristics of the tetrode referred to in Fig. 51.

and dispersed secondary, electrons. The latter may exceed the former in number, in which case the externally measured anode current is negative. In contrast, the screen current comprises the collected primary electrons and a large portion of the secondary anode electrons, and this current is highly negative. This, then, is the qualitative explanation of the I_a and I_{g2} curves, plotted against V_a.

Comparison of the I_a/V_a characteristics of a triode (fig. 22) with the tetrode under review shows that in both cases the family of curves is bounded at the left-hand end by a steep envelope; this means that the anode voltage of the tetrode, or of the triode, cannot be increased beyond that line.

Since this envelope is situated roughly at the point where $v_a = V_{g2}$, the alternating anode voltage will be, at the most, equal to the difference between the steady anode- and screen potentials. It follows that the efficiency of a tetrode is relatively low, since the efficiency equation contains the quotient V_{ap}/V_a, which cannot then exceed

$$(V_a - V_{g2})/V_a = 1 - V_{g2}/V_a.$$

Therefore, the higher the screen potential in comparison with that of the anode, the lower the efficiency.

Fig. 53 reproduces the control-grid current curves of the tetrode in question, which have the important feature of running practically parallel with the V_a axis, at any rate in that region where the anode voltage is operative. Due to the screening effect of the extra grid, the control grid current is not dependent upon the alternating anode voltage, as is the case with the triode (compare fig. 23), which implies that the full anode voltage may be utilized without involving excessive excitation power: this is, in effect, the great advantage of the tetrode over the triode.

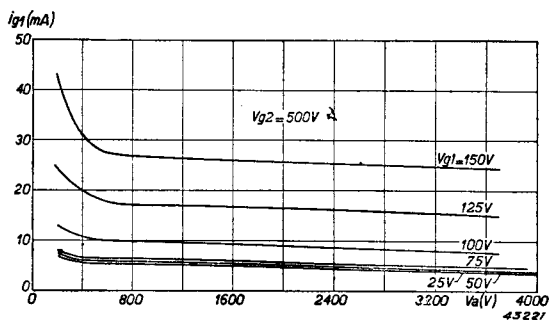

Fig. 53. $I_{g1} - V_a$ characteristics of the tetrode referred to in fig. 51.

There is also another feature in its favour, in that the capacity between anode- and control grid is very low, again due to the effect of the screen

grid: this coupling is of an electrostatic type, and, as it has an adverse effect on the working of the valve, it is all to the good of the ultimate performance that this coupling is so small. By way of illustration it may be noted that the TB 2.5/300 has a $C_{ag} = 5{,}5$ pF, as compared with $C_{ag1} = 0.05$ pF in the QB 3/300.

§ 3. The suppressor grid

Every effort has naturally been made to eliminate the disadvantages inherent in the secondary emission of tetrodes, and one of the most successful steps in this direction has been the introduction of a third grid, kept at cathode potential, between the screen and the anode. This ensures a zone of low potential in the space between the last-named electrodes, and thereby checks the passage of secondary electrons, both from the screen and from the anode; on the other hand, the electrons in the cathode current, when once past the screen grid, are not withheld, since the speed with which they enter the space between g_2 and anode is far greater than that with which the secondary electrons emerge. The effect of this third, or suppressor grid, is, then, that the sharp drop in the anode-current curve, at the point where $v_a \approx V_{g2}$, no longer occurs.

This is demonstrated in fig. 54, in which the characteristics of a pentode are shown for a screen voltage of 300 V. It will be seen that at $v_a = 300$ V the curves reveal no unusual behaviour, but run to their termination through the limit line at low values of v_a. There are two causes for the sharp drop in the anode current at low anode voltages (in other words, the existence of limit line): firstly, due to the presence

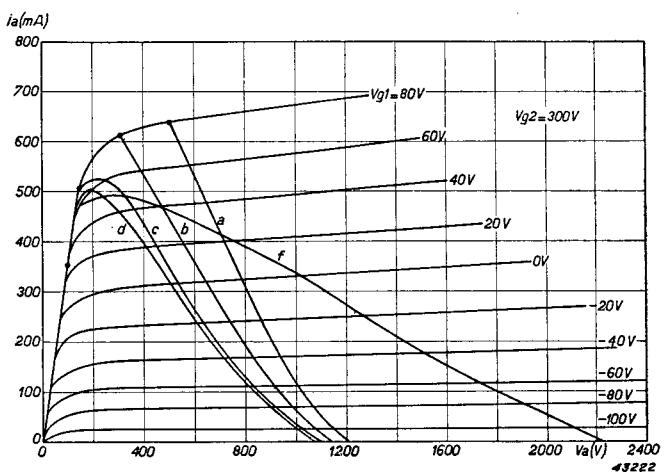

Fig. 54. $I_a - V_a$ characteristics of a pentode, with $V_{g2} = 300$ V, showing load lines *a*, *b*, *c*, *d* and *f*.

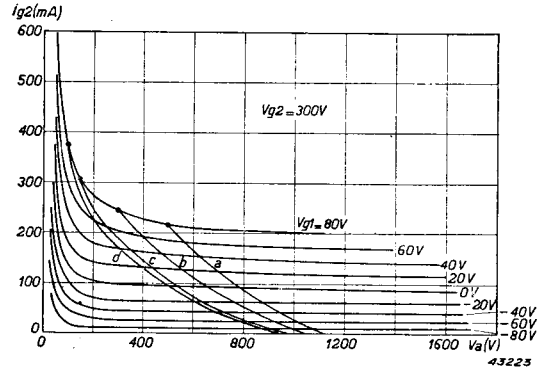

Fig. 55. $I_{g2} - V_a$ characteristics of the pentode referred to in fig. 54 for $V_{g2} = 300$ V, showing load lines *a*, *b*, *c* and *d*.

of the various grids, the electrons are diverted from their original course (perpendicular to the faces of the different electrodes) and a large number can no longer reach the anode when the latter is at a low potential, although they would do so if their movement were unimpeded. These electrons therefore turn back in quantities which become larger as the anode potential is reduced.

Secondly, at higher currents, a not inconsiderable negative space charge occurs in the area between the screen grid and the anode, especially at low anode voltages, and this exercises a retarding effect on those electrons which have passed the screen on their way to the anode. This effect, too, is the more marked when the anode potential is reduced.

The screen-grid current, plotted against anode potential, is shown graphically in fig. 55.

This current appears to follow more or less the same curve as that obtained with the grid of a triode, namely a rise at low anode potentials, and again, as with the triode, an increase in screen current may be expected for very high alternating anode voltages.

The control-grid current of the pentode under review is shown graphically in fig. 56, from which it is evident that, as with tetrodes, the current is almost independent of v_a. This implies that no increase in control-grid current is to be expected at high alternating anode potentials; hence the valve can be run very efficiently on only a low driving power. In

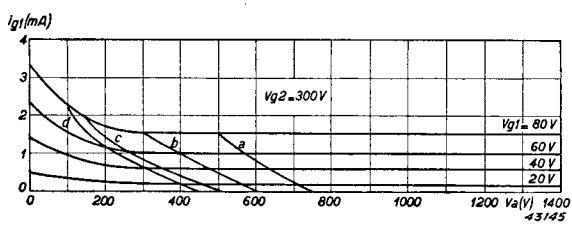

Fig. 56. $I_{g1} - V_a$ characteristics of the pentode referred to in fig. 54 with $V_{g2} = 300$ V, showing load lines *a*, *b*, *c* and *d*.

recent years the pentode has replaced the tetrode at least in those cases where secondary emission has not been rendered innocuous by any other means.

§ 4. Energy conversion in pentodes

Comparison of the static characteristics of a pentode (fig. 54) with those of a triode (fig. 22) shows that these can well approximate in both cases to straight lines, as in fig. 25. Hence the triode theory outlined in Chapter II, § 5 onwards, also holds good for pentodes, so that, when considering possible maxima of output power, with regard to the various limiting factors such as anode dissipation, steady anode current and peak anode current, reference may be made to this chapter. It should be remembered however, when calculating the current angle, that the anode current is also dependent upon the screen-grid voltage, as follows:

$$i_a = a\,(v_{g1} + bv_a + cv_{g2}).$$

Substituting $v_{g1} = V_{g1} + V_{g1p} \cos \omega t$; $v_a = V_a - V_{ap} \cos \omega t$, and, bearing in mind that, when $\omega t = \Theta$, $i_a = 0$, it follows that:

$$\cos \Theta = \frac{-V_{g1} - bV_a - cV_{g2}}{V_{g1p} - bV_{ap}}.$$

For the ideal pentode, in which $b = 0$, the formula becomes:

$$\cos \Theta = \frac{-V_{g1} - cV_{g2}}{V_{g1p}}.$$

Another factor to be reckoned with in pentodes is the screen-grid dissipation, which should not exceed a certain value if the working efficiency of the valve is not to be impaired. In order to obtain some idea of the amount of this dissipation under various working conditions, let us investigate the position in relation to the pentode already referred to. Suppose that:

$V_a = 1500$ V; $V_{g1} = -200$ V; $V_{g2} = 300$ V; $V_{g3} = 0$ V; $V_{g1p} = 280$ V;

and, further, that:

a) $V_{ap} = 1000$ V; *b*) $V_{ap} = 1200$ V; *c*) $V_{ap} = 1350$ V; *d*) $V_{ap} = 1400$ V.

From the formulae:

$$v_g(t) = -200 + 280 \cos \omega t \text{ and}$$
$$v_a(t) = 1500 - V_{ap} \cos \omega t$$

$v_g(t)$ and $v_a(t)$ can be calculated as functions of ωt, and figs. 54, 55

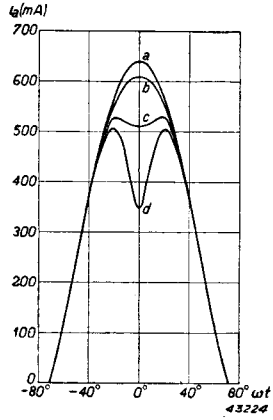

Fig. 57. Anode current impulses corresponding to the load lines in fig. 54.
a) V_{ap} = 1000 V;
b) V_{ap} = 1200 V;
c) V_{ap} = 1350 V;
d) V_{ap} = 1400 V.

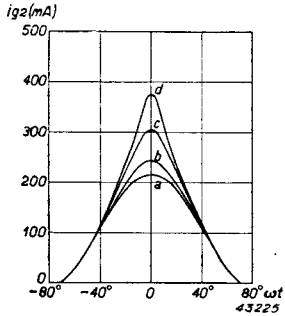

Fig. 58. Screen grid impulses corresponding to the load lines *a*, *b*, *c* and *d* in fig. 55.

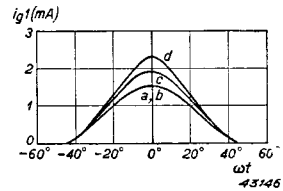

Fig. 59. Control grid impulses corresponding to the load lines *a*, *b*, *c* and *d* in fig. 56.

and 56 then furnish us with i_a, i_{g2} and i_{g1}. The load lines are given in the figures.

Further, figs. 57, 58 and 59 provide the different current impulses for i_a, i_{g2} and i_{g1} respectively, from which I_{ao}, I_{a1}, I_{g2o}, I_{g1o}, W_i, W_o, W_a, W_{g2} and η can be derived, as functions of R_a. These values are reproduced in figs 60 and 61, for four different values of V_{ap}, i.e. for four values of R_a. (The curves in figs. 60 and 61 are an approximation through the calculated points.)

As in the case of the triode (fig. 46), a maximum value of W_o occurs at a certain value of R_a, and from fig. 57 it will be seen that at this point the anode-current pulse just shows the first sign of a dip, or, that (fig. 54) the working line bends over (line *c*) in the direction of the limit line.

At the same time, at this value of R_a the efficiency becomes rather constant. The screen-grid dissipation continuously increases with increasing R_a; this is caused by the increasing amplitude of the screen-current pulses, which in itself, according to fig. 55, is caused by the increase of the I_{g2}/V_a characteristics near the I_{g2} axis.

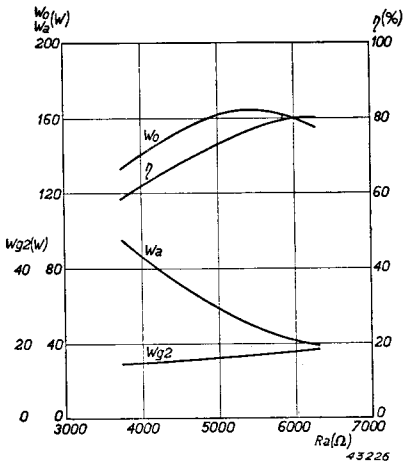

Fig. 60. W_o, W_a, W_{g2} and η as function of R_a, calculated from the load lines in figs. 54 and 55.

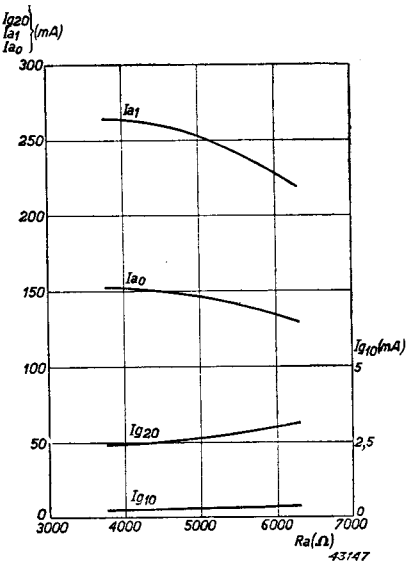

Fig. 61. I_{ao}, I_{a1}, I_{g2o} and I_{g1o} as function of R_a, calculated from the load lines in figs. 54, 55 and 56.

The control-grid current is hardly affected by changes in R_a (see figs. 61, 59 and 56) and contrasts with variations obtained from a triode (fig. 48).

In the example under consideration, $W_{o\,max} = 163$ W for $R_a = 5500$ ohms, at which value $W_a = 49$ W, $W_{g2} = 17$ W, $\eta = 77\%$, $I_{ao} = 141$ mA, $I_{g2o} = 57$ mA, $I_{g1o} = 0.5$ mA; therefore $I_{ko} = 198.5$ mA. The values subject to limitations are: W_a (= max. 85 W), W_{g2} (= max. 25 W) and I_{ko} (=max. 200 mA). Apparently, at this setting, the cathode current just attains its maximum value; the R.F. power is therefore limited by the cathode current and by neither anode- nor screen-grid dissipation.

§ 5. Tetrodes having the characteristics of pentodes

As explained in § 3, a flow of secondary electrons can be prevented by a low-potential field between the screen grid and the anode. In pentodes this field is produced by the suppressor grid, which is at the same potential as the cathode, but in modern tetrodes the area of low potential is formed by artificially producing a dense space charge between screen grid and

anode. This space charge causes a sharp drop to take place in the local potential, so that a potential minimum is formed between the anode and g_2. This blocks the passage of secondary electrons in just the same way as a low-potential suppressor grid.

The concentration of this space charge can be increased in different ways, the first of which is to assemble g_1 and g_2 one behind the other in such a way that a line drawn from the cathode at right angles to the anode simultaneously intersects turns of g_2 and g_1; this arrangement is known as "shadowing", since the turns of g_2 lie as it were in the shadow of those of g_1, when regarding the cathode as a source of light. In this way the electron stream is bunched into the form of a number of parallel beams when the grids are of the ordinary wire-wound type. If the grids consist of a number of rods equally spaced about a circle, the electron stream is broken up into sectors.

Another method of increasing the space-charge density consists in placing the anode as far as is practicable away from the screen grid. Once the electrons have passed g_2 they remain relatively long in the space between g_2 and anode and thus tend to augment the space charge. An example of this is to be found in the QB 3/300, whose I_a/V_a characteristics are depicted in fig. 54*a*, for $V_{g2} = 350$ V. The I_{g2}/V_a curves for this valve are shown in fig. 55*a* for the same screen voltage, and comparison of fig. 54 with fig. 55 will show that the characteristics of the QB 3/300, at high values of the anode current, are similar to those of a pentode. At lower values of I_a (and also of V_a) the current density in the space between the anode and g_2 is too low to create a suitable potential-minimum and the curves then become more characteristic of the tetrode again. As will be seen from the gradient of the load lines, however, this particular zone is not entered when the valve is working on normal loads, and the tetrode does therefore behave like a pentode. With these valves there are of course no facilities for suppressor-grid modulation; moreover, owing to the absence of the screening effect of a suppressor grid, C_{ag1} is rather higher than in an equivalent pentode. All the same at very high frequencies the pentode is often at a disadvantage owing to its high output capacitance (g_3 close to the anode) and also owing to the necessity for tuning not only the g_2 circuit but also that of g_3, in order to keep high frequency voltages off the grids.

§ 6. Comparison of pentodes and tetrodes with triodes

Summarizing briefly the advantages of pentodes and tetrodes as compared with triodes, we have the following:

a) For the same output power, the controlling power required for pentodes and tetrodes is very much less than that needed for triodes, in other words, the energy amplification of the former is much the greater.

b) The capacitance between anode and control grid of the pentode is much smaller than in a triode, so that neutralization is often unnecessary, resulting in a great advantage in transmission work. The double screening effect (screen- and suppressor grids) in most cases gives pentodes the preference over tetrodes.

CHAPTER V

Modulation of an R.F. Power Amplifier

§ 1. Types of modulation

In chapters III and IV, the working of the R.F. power amplifier valve has been discussed step by step, and we have also examined the conditions under which the highest possible R.F. power output and efficiency may be obtained.

The ultimate function of the R.F. power amplifier, however, is the transmission of speech and music, or signals as employed in telegraphy, by the transfer in one manner or another of these low, or audio-frequency signals on the R.F. current generated in the transmitting aerial by the amplifier.

In wireless telegraphy this is a very simple matter, the transmitter merely being switched on and off in the required rythm of the signals, for example by keying a sufficiently high negative voltage to the control grid of the transmitter valve, so as to reduce the anode current to zero. During the period of the actual signal, this potential is reduced to its normal value, namely that which will give the most favourable results for a Class C setting, i.e. high efficiency and output power. This Class C setting has been fully described in Chapter III, and, by reason of its general application in telegraph transmitters, the term R.F. Class C Telegraphy has become common usage.

The transmission of speech and music is a rather more complex problem: in order to demonstrate the difficulties to be overcome, let us suppose that an R.F. oscillation, for instance the current in a transmitter aerial, may be represented by the expression:

$$i = A \sin(\omega t),$$

in which A is the amplitude, ω the (cycle) frequency and t the time. The magnitude ωt represents the phase of the oscillation at any given moment.

If A and ω are constant, the R.F. signal will be of constant amplitude, frequency and phase; a signal of this type is supplied by the Class C amplifier already mentioned. Now, if it is possible to vary either of the quantities A or ωt to the rythm of the A.F. signals to be transmitted, the R.F. signal will embody, as it were, the identical A.F. signals themselves; it is then only necessary to have suitable apparatus at the

receiving end for separating the A.F. signals once again (detection or rectification).

If the amplitude A be varied to the extent of the A.F. signals, the result is an R.F. signal with amplitude modulation, and, taking for our example a sinusoidal variation of the amplitude, the latter may be represented by $A + B \sin pt = A\,(1 + m \sin pt)$, where p is the angular frequency of the A.F. oscillation. The aerial current then becomes:

$$i = A\,(1 + m \sin pt) \sin \omega t.$$

Applying the same process to the phase ωt of the oscillation, the result is a type of modulation, which, along the lines of the above, might be termed phase modulation, but this term is generally taken to apply to a special aspect of this particular method of modulation.

If the phase ωt undergoes sinusoidal A.F. variations, it may be expressed by:

$$\omega t + m \sin pt,$$

and the aerial current is:

$$i = A \sin (\omega t + m \sin pt) \ldots\ldots\ldots \quad (5.\ 1)$$

This current is still regarded as a sinusoidal R.F. signal, but of variable frequency. The magnitude of the frequency at any given moment is found by differentiating the phase with respect to time; in the case of the original unmodulated oscillation, $i = A \sin \omega t$, the result is ω, or the frequency of the unmodulated oscillation. Similarly differentiating the phase of the modulated oscillation, we obtain:

$$\omega + mp \cos pt.$$

Apparently then, the frequency varies in step with the A.F. oscillation, and this general concept may be divided into two categories, viz:

(1) mp independent of p: in other words the amplitude (mp) of the variation in frequency is not governed by p. This is known as frequency modulation;

(2) m independent of p, that is, the amplitude (m) of the variation in the phase ωt is not governed by p. This is termed phase modulation.

From the description of the working of the transmitter amplifier set out in Chapter III, it has been seen that the magnitude of the R.F. power output W_o depends on the setting at which the valve is run: the amplitude

A of the aerial current will also be thus dependent, since, if R_s be the radiation resistance of the aerial, the relation between W_o and A can be expressed by:

$$W_o = \frac{1}{2} A^2 R_s.$$

It follows, then, that amplitude modulation is obtained by arranging matters so that the setting of the valve is affected by the A.F. signal; at the same time, the phase ωt is independent of the valve setting, and other means, e.g. circuit modifications, have to be found to produce frequency- or phase modulation, the valve being employed as a C.W. R.F. amplifier or frequency multiplier. Modulation of this type, therefore, provides no further points for consideration, unlike amplitude modulation, which forms the subject of the following discussion.

§ 2. Amplitude modulation. Modulation characteristic

Recalling that the amplitude A of the aerial current, as stated in § 1, is governed by the setting of the valve, let us take the general case of a pentode, of which the setting is dependent on the factors

$$V_a,\ V_{g1},\ V_{g1p},\ V_{g2},\ V_{g3} \text{ and } R_a.$$

If any of these values is modified, it may be said in general that the R.F. output power, and therefore the aerial current, also undergo a change, and this fact forms the basis of practical amplitude modulation. As far as the direct voltages V_a, V_{g1}, V_{g2} and V_{g3} are concerned, the A.F. signal is introduced in the supply circuit, between the particular source of voltage and the transmitting valve; hence we speak of anode-, control grid-, screen grid- or suppressor grid modulation.

When the amplitude of the excitation voltage V_{g1p} is modified in accordance with the audio frequency (due to the introduction of one of the above methods of amplitude modulation into the stage supplying the excitation voltage), it becomes the work of the transmitting valve to amplify this modulated oscillation (telephony amplification), for a study of which reference may be made to § 7.

Lastly, it is also possible to produce amplitude modulation by varying R_a in step with the audio frequency. Seeing that the magnitude of R_a is determined by the aerial impedance as well as by the type of coupling between aerial and anode circuits, the method in question can be put into effect only by means of special circuits in which the particular form

of coupling is capable of following the A.F. signals. The transmitting valve is capable of doing this, but it is not intended to enter here into details of the special circuits involved.

In every form of amplitude modulation it is essential to ensure a linear relationship between the R.F. aerial current and the particular supply voltage upon which the modulation signal is to be impressed, since only then will the A.F. signal be reproduced in the modulated aerial current in an undistorted condition. This relationship, $I_{ant} = f(V)$, or the so-called modulation characteristic, must then assume the form:

$$I_{ant} = a + \beta V.$$

If the value of the unmodulated supply voltage is V_o, with modulation signal $V_1(t)$ superimposed upon it, then:

$$I_{ant} = a + \beta V_o + \beta V_1(t) \ldots\ldots\ldots \quad (5.2)$$

I_{ant} is here understood to mean the effective value of the R.F. aerial current.

The instantaneous value of the aerial current is related to this effective value by the expression:

$$i_{ant} = I_{ant} \sqrt{2} \cdot \sin \omega t,$$

in which ω is the angular frequency of the R.F. oscillation. Comparing this with the expression for I_{ant}, we then have:

$$i_{ant} = [a + \beta V_o + \beta V_1(t)] \sqrt{2} \sin \omega t.$$

Fig. 62*b* shows an example of an R.F. aerial current modulated with the A.F. signal $V_1(t)$ of fig. 62*a*. In the absence of the modulation

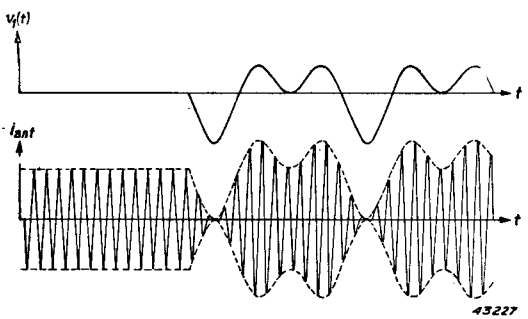

Fig. 62. Top: A.F. signal. Below: R.F. signal modulated with this A.F. signal.

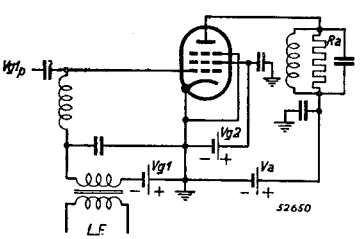

Fig. 63. Circuit of transmitter amplifier with control grid modulation.

signal, the effective value of the aerial current is constant and equal to:

$$I_{ant(o)} = a + \beta V_o, \quad \ldots\ldots\ldots \quad (53)$$

this being known as the value of the aerial current for the (unmodulated) carrier wave, as depicted by the left-hand portion of fig. 62*b*.

§ 3. Control-grid modulation

Control-grid modulation is obtained by applying the A.F. voltage to the control grid in series with the grid bias (see fig. 63). In the running of the valve this means (see fig. 64) that the grid bias, upon which the excitation voltage is impressed, oscillates in step with the audio frequency, with the result that, whereas the excitation voltage remains unchanged, the anode current impulses vary in amplitude and in current angle in the same rythm. In consequence, the first harmonic is changed, and with it, the aerial current.

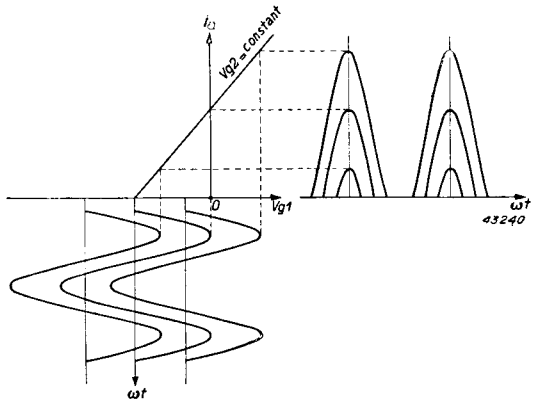

Fig. 64. Excitation of a Class C pentode with variable grid bias.

In making calculations of the modulation characteristic it will simplify matters to proceed from a straight I_a/V_{g1} characteristic which shall be independent of the anode potential (within the voltage range under consideration), that is, the characteristic of a pentode. The anode current is again dependent on v_{g1} and v_{g2}:

$$i_a = a\,(v_{g1} + bV_{g2}).$$

R.F. excitation produces:

$$v_{g1} = V_{g1} + V_{g1p} \cos \omega t, \quad \ldots\ldots\ldots \quad (5.\ 4)$$

that is:

$$i_a = a\,(V_{g1} + bV_{g2} + V_{g1p} \cos \omega t), \quad \ldots\ldots \quad (5.\ 5)$$

this being valid within a current angle of 2Θ as determined by:

$$\cos \Theta = \frac{-V_{g1} - bV_{g2}}{V_{g1p}} \quad \ldots\ldots\ldots \quad (5.\ 6)$$

The peak anode current is then:

$$I_{ap} = a\,(V_{g1} + V_{g1p} + bV_{g2}) \quad . \quad . \quad . \quad . \quad . \quad (5.\ 7)$$

and the first harmonic:

$$I_{a1} = f_1(\Theta)\, I_{ap} = \frac{1}{\pi} \cdot \frac{\Theta - \frac{1}{2}\sin 2\Theta}{1 - \cos\Theta} \cdot I_{ap} \quad . \quad . \quad . \quad . \quad (5.\ 8)$$

These formulae, then, determine the relationship between I_{a1} and V_{g1p}, that is, the modulation characteristic.
To make the matter sufficiently clear, we write: $\cos\Theta = x$; then:

$$V_{g1} = -bV_{g2} - xV_{g1p} \quad . \quad . \quad . \quad . \quad . \quad . \quad . \quad . \quad (5.\ 9)$$
$$I_{ap} = aV_{g1p}\,(1 - x) \quad . \quad . \quad . \quad . \quad . \quad . \quad . \quad . \quad . \quad (5.\ 10)$$

Now $f_1(\Theta)$ can be easily calculated from x, as set out in the following table:

TABLE VI

x	V_{g1}	Θ	$f_1(\Theta)$	$1 - x$	$f_1(\Theta) \cdot (1 - x)$
1	$-bV_{g2} - V_{g1p}$	0°	0	0	0
$^2/_3$	$-bV_{g2} - {}^2/_3 V_{g1p}$	48°	0.33	$^1/_3$	0.110
$^1/_3$	$-bV_{g2} - {}^1/_3 V_{g1p}$	70.5°	0.437	$^2/_3$	0.292
0	$-bV_{g2}$	90°	0.5	1	0.500
$-{}^1/_3$	$-bV_{g2} + {}^1/_3 V_{g1p}$	109.5°	0.53	$1^1/_3$	0.707
$-{}^2/_3$	$-bV_{g2} + {}^2/_3 V_{g1p}$	132°	0.534	$1^2/_3$	0.890
-1	$-bV_{g2} + V_{g1p}$	180°	0.5	2	1.000

The quantity $f_1(\Theta) \cdot (1 - x)$ in the final column is directly proportional to I_{a1}, since, according to (5.8) and (5. 10):

$$\frac{I_{a1}}{aV_{g1p}} = f_1(\Theta) \cdot (1 - x).$$

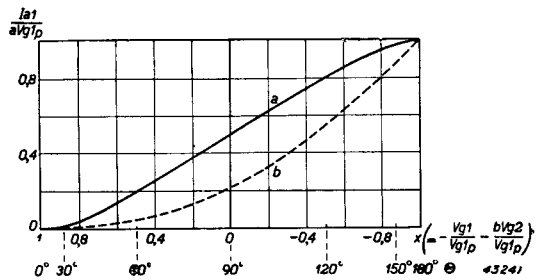

Fig. 65. Control grid modulation characteristic of a pentode having straight I_a–V_{g2} characteristics.

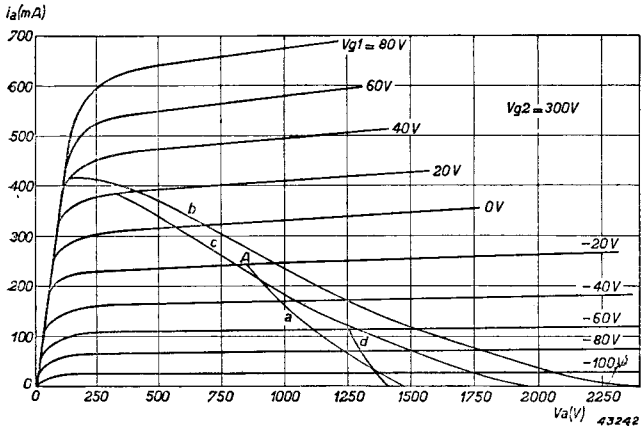

Fig. 66. I_a—V_a characteristics of a pentode, with $V_{g2} = 300$ V, $V_{g1p} = 100$ V; showing load lines for $R_a = 5850\ \Omega$ and V_{g1}
$= -120$ V (*a*)
-60 V (*b*)
-80 V (*c*)
-160 V (*d*)
(control-grid modulation).

Further, in accordance with (5. 9), V_{g1} is proportional to x (apart from the constant $-bV_{g2}$), so that a diagram representing $I_{a1}/aV_{g1p} = \varphi(x)$ also reproduces the modulation characteristic.

This characteristic may be seen in fig. 65 (curve *a*). Below the abscissa, the value of Θ at every point of the curve is shown as well.
The centre part of the characteristic in the figure is reasonably straight; only the ends are curved slightly, and this straight section corresponds to $\Theta = 90°$, or Class B setting. If the grid bias is adjusted to the lower end of the characteristic, therefore, the setting, in the modulated condition, will fluctuate somewhere between Class C and Class A.
Efficiency in this instance is not very high, seeing that during modulation the magnitude of I_{a1}, that is, of V_{ap}, varies. A loading resistance should then be used which, at the modulation peak where the grid bias is as small and the anode current as high as possible, will yield the optimum peak alternating anode voltage, as determined by the steady anode potential and limit characteristic: in the unmodulated condition (carrier wave), this alternating voltage then drops almost to one half, with consequent low carrier wave efficiency.

To illustrate this, data have been calculated in respect of the control grid modulation setting of a pentode, based on I_a/V_a characteristics (Fig. 66) with anode voltage $V_a = 1500$ V and $V_{g2} = 300$ V.
In the light of the above, the grid bias for this carrier wave setting has been placed at $V_{g1} = -120$ V, corresponding to the lower end of the static characteristic of this pentode (fig. 67).

From the position of the limit characteristic (Fig. 66) it may be concluded that, when the valve is run at its optimum output, the alternating anode voltage will be about 1300 V, whilst at the carrier wave setting, whereby the output is about 50% less, this will be approximately 650 V.
Estimating the efficiency at roughly 33% and assuming that the maximum anode dissipation of 85 W is permissible, the output will be about 42.5 W, the power consumed 127.5 W and the steady anode current 85 mA. The peak current, assuming half sinusoidal impulses, will then be $\pi\, 85 = 267$ mA, and this, combined with the alternating anode voltage of 650 V, gives a terminating point for the carrier wave load line as shown at A in fig. 66 on the characteristic for $v_{g1} = -20$ V. An excitation voltage of 100 V is then required.
The load line in respect of this example is now calculated from:

$$v_{g1} = -120 + 100 \cos \omega t$$
$$v_a = 1500 - 650 \cos \omega t,$$

which is curve a in fig. 66. The respective anode current impulse is also indicated at a in fig. 68.

Using Simpson's law, the steady anode current I_{ao} of this impulse (= 68 mA) and the first harmonic I_{a1} (= 111 mA) are then calculated; the alternating anode voltage of 650 V then gives the anode impedance, $R_a = 5850$ ohms.

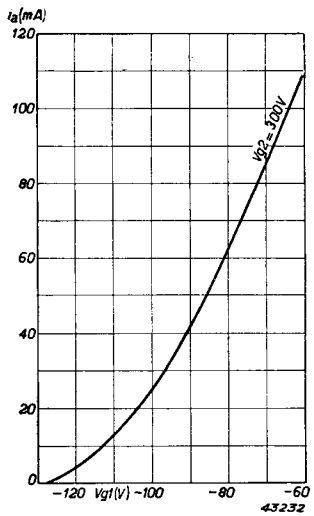

Fig. 67. I_a — V_{g1} characteristic of the pentode referred to in fig. 66, with $V_{g2} = 300$ V, $V_a = 1500$ V.

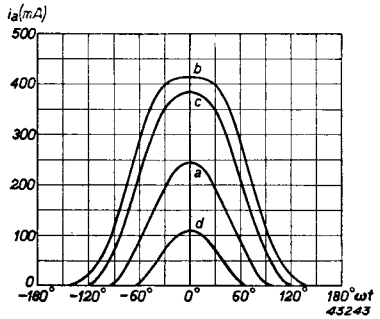

Fig. 68. Anode current impulses in relation to the load lines in fig. 66.

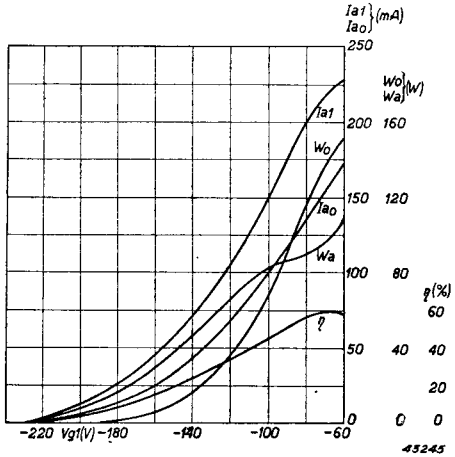

Fig. 69. Characteristics of the pentode referred to in fig. 66, with grid modulation and with $V_a = 1500$ V, $V_{g2} = 300$ V, $V_{g1p} = 100$ V, $R_a = 5850$ Ω.

On the basis of this value of R_a the calculation is now repeated in respect of other values of grid bias, namely $V_{g1} = -60$ V, -80 V and -160 V: the relative load lines are reproduced in Fig. 66 (*b*, *c* and *d*) and the corresponding anode current impulses in Fig. 68, using the same symbols. In these calculations it is necessary to estimate the alternating anode voltage in respect of each new load line, since it is not otherwise possible to construct this line in the I_a/V_a diagram and from it obtain the current impulse, as demonstrated above.

From this the value of I_{a1} immediately follows, and the latter, in combination with V_{ap}, then gives R_a in respect of the particular load line. If it is found that R_a is not actually 5850 ohms, a correction must be made in the value of R_a originally adopted, after which the whole calculation is repeated. The result of the calculations for the load lines in question is shown in the following table and again, graphically, in fig. 69.

TABLE VII

Line	V_{g1}	V_{ap}	I_{a1}	R_a	I_{ao}	W_i	W_o	W_a	η
	V	V	mA	Ω	mA	W	W	W	%
b	— 60	1330	228	5850	172.5	259	151.5	107.5	58.5
c	— 80	1170	200	5850	137	206	117	89	56.8
a	— 120	650	111	5850	68	102	36	66	35.3
d	— 160	249	42.6	5850	24	36	5.3	30.7	14.7

It will be observed that the modulation characteristic $I_{a1} = f(V_{g1})$ is quite curved, with the concave side facing upwards due to the fact that the static I_a/V_{g1} characteristics of the valve are also curved (fig. 67). This becomes all the more apparent when the calculation of the theoretical modulation characteristic (fig. 65, curve *a*) is based not on straight,

but curved I_a/V_{g1} diagrams. The curve b in fig. 65 was plotted in this manner, employing a quadratic relation for the static characteristic (to facilitate comparison between the two curves, the scale of ordinates for b has been so arranged that the terminating points ($x = -1$) coincide) and the modulation characteristic is very definitely curved, as in fig. 69.

Due to the curvature in question, W_o, W_a and W_i, for this carrier wave setting (fig. 69, $V_{g1} = -120$ V) are lower than originally estimated, and the efficiency is slightly higher.
It is noticeable that the top of the modulation characteristic $V_{g1} = -60$V bends over with its concave side facing the abscissa, since the load line is approaching the limit characteristic (see curve b, fig. 66). If the modulation is carried still further, the impulse will tend to reveal the kink already described, thus limiting any further increase in I_{a1}.
Finally, it will be seen that the efficiency at the modulation peak is relatively low, the reason being that the valve setting then practically corresponds to Class A, with unfavourable I_{a1}/I_{ao} ratio. This Class A character is, moreover, clearly manifested by the position of the load line b (fig. 66), since at a direct potential of $V_a = 1500$ V, a standing current of 115 mA occurs.

In modern transmitters, control grid modulation is rarely, if ever met with, not only on account of its low efficiency, but also in view of the curved modulation characteristic which is a cause of distortion of the A.F. signal after subsequent rectification in the receiver.
An exception must be made here for high-power television transmitters; if anode modulation were required, the modulator would have to deliver a great deal of power and this would necessitate a complicated amplifier in view of the width of the modulation frequency band. For this reason grid modulation is employed in the last R.F. stage; the less satisfactory non-linear loading of the modulator (due to the pulsating character of the grid current) is then counteracted by pre-loading the modulator.

§ 4. Screen grid modulation

Whereas in control grid modulation the A.F. variations in the anode current impulses are obtained by varying the grid bias V_{g1} at a constant screen potential, the functions of V_{g1} and V_{g2} are reversed in the case

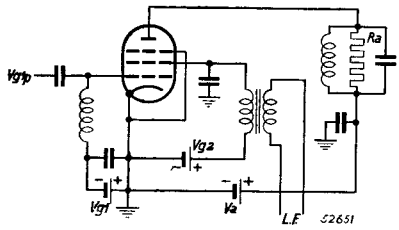

Fig. 70. Circuit of a transmitter amplifier with screen grid modulation.

of screen grid modulation, V_{g1} being kept constant whilst V_{g2} is modified by the A.F. signal (see Fig. 70). The static I_a/V_{g1} characteristics confirm that it is possible to establish modulation in this manner. These characteristics are reproduced diagrammatically in Fig. 71, in respect of three different values of screen potential, together with the excitation voltage: the anode current impulses are given in the right hand portion of the diagram. Due to the fact that the static characteristic is displaced by variations in the screen potential, the amplitude and angle of the impulse current are also changed thereby and, with them, the first harmonic and aerial current.

The shape of the modulation characteristic $I_{a1} = f(V_{g2})$ may be obtained by means of the formula employed in § 3. for control grid modulation, except that V_{g2} is now regarded as an independent variable. Then, with $\cos \Theta = x$, we have

$$I_{a1} = f_1(\Theta) \cdot I_{ap} = f_1(\Theta) \cdot aV_{g1p}(1 - x) \quad . \quad . \quad . \quad . \quad . \quad (5.\ 11)$$

$$bV_{g2} = -V_{g1} - xV_{g1p} \quad . \quad . \quad . \quad . \quad . \quad . \quad . \quad . \quad . \quad . \quad . \quad . \quad . \quad (5.\ 12)$$

Apart from the constant $-V_{g1}$, therefore, V_{g2} is also proportional to x and I_{a1} to $(1 - x) \cdot f_1(\Theta)$; the modulation characteristic is then again curve *a*, Fig. 65. Here, also, the transmitting valve passes during modulation through Class C (no current) and Class A, corresponding to $x = 1$ and -1, while the screen voltage must then change from V_{g2}' to V_{g2}'' as determined by:

$$bV_{g2}' = -V_{g1} - V_{g1p} \text{ and}$$

$$bV_{g2}'' = -V_{g1} + V_{g1p}.$$

Since $-V_{g1}$ is a positive quantity, V_{g2}'' is always positive, and this will be clear when it is recalled that V_{g2}'' corresponds

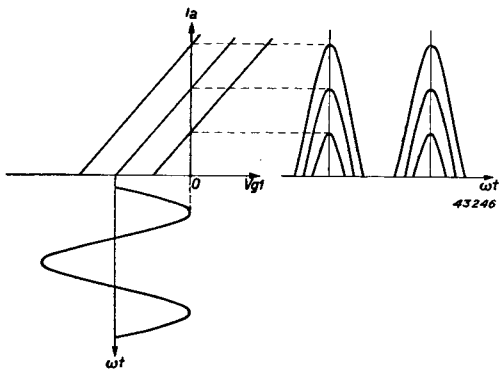

Fig. 71. Excitation of Class C pentode with variable screen-grid voltage.

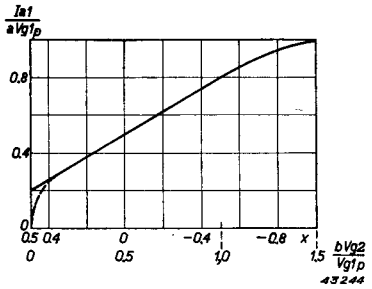

Fig. 72. Screen grid modulation of pentode with straight I_a/V_{g1} characteristics, at $V_{g1p} = 2\ (-\ V_{g1})$.

to the Class A setting referred to above, in which the static I_a/V_{g1} curve is situated as far as possible to the left of the diagram.

V_{g2}' can certainly be negative, namely when V_{g1p} is $> -\ V_{g1}$, that is, when the excitation voltage exceeds the absolute value of the negative grid bias. For negative values of the screen grid voltage, however, the expression employed for the anode current, viz: $i_a = a\,(v_{g1} + bV_{g2})$, no longer applies, seeing that this current drops to zero, or, at any rate, very low values when the screen voltage becomes zero or negative. The theory advanced above is therefore applicable only when $V_{g2} > 0$.

Suppose that $V_{g1p} = 2\,(-V_{g1})$, then curve *a* in Fig. 65 is valid only up to $x = {}^1/_2$, and Fig. 72 illustrates this; below the abscissa, values of the screen voltage are also shown, and it will be seen that, when $-V_{g2} = 0$, the modulation curve bends sharply; I_{a1}/aV_{g1p} drops from 0.2 to 0. In practice, when the screen potential falls to zero, the anode current actually decays more gradually, and in the region of $V_{g2} = 0$ the modulation curve is more or less rounded, as shown by the broken line in Fig. 72.

If the modulation of the screen voltage be increased to an extent where the value of $V_{g2} = 0$ is reached in the trough of the curve, distortion

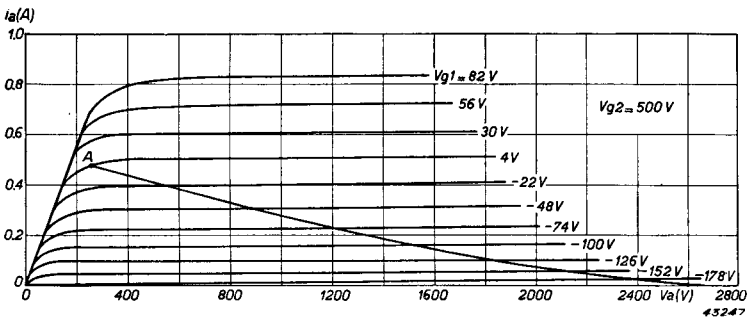

Fig. 73. I_a/V_a characteristic of a pentode, at $V_{g2} = 500$ V, showing load lines for $R_a = 5175$ ohms.

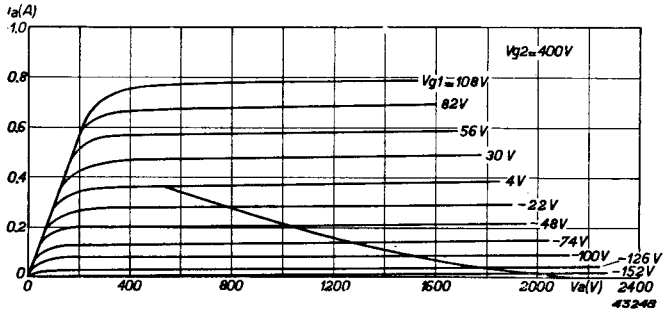

Fig. 74. As fig. 73, but for $V_{g2} = 400$ V.

will occur at that point as a result of the deflection of the curve previously alluded to. It is possible to improve the modulation characteristic by reducing the excitation voltage, for, as indicated by the formula

$$bV_{g2} = -V_{g1} - xV_{g1p},$$

it appears that the point $x = 1$ can be reached at $V_{g2} = 0$ when $V_{g1p} = -V_{g1}$, in other words when the excitation voltage is equal to the absolute value of the D.C. control grid potential. This means that the control grid can never be positive and control grid current will never flow; the modulation characteristic will then once more assume the form of curve a in fig. 65.

If the static characteristics of the valve are not straight, but more or less curved, the modulation characteristic will be similarly affected, so that assuming a quadratic characteristic, the modulation curve will be in accordance with line *b* in fig. 65: this can be improved by utilizing the effect of the excitation voltage in the manner described in relation to fig. 72. Taking as basis the curve *b*, fig. 65, in which $V_{g1p} = -V_{g1}$, we increase V_{g1p}, with the result that the concave shape of the curve is to a certain extent compensated by the convexity of the curve as shown in fig. 72. An example of the calculation in relation to the modulation characteristic of a particular pentode is given in the following figures, of which Nos. 73 to 77 show the I_a/V_a curves for $V_{g2} = 500$, 400, 300, 200 and 100 V. Assuming

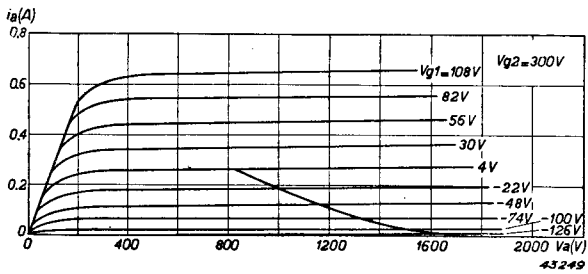

Fig. 75. As fig. 73, but for $V_{g2} = 300$ V.

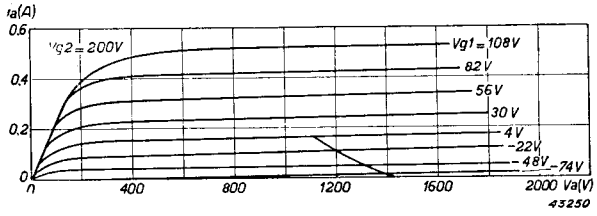

Fig. 76. As Fig. 73, but with $V_{g2} = 200$ V.

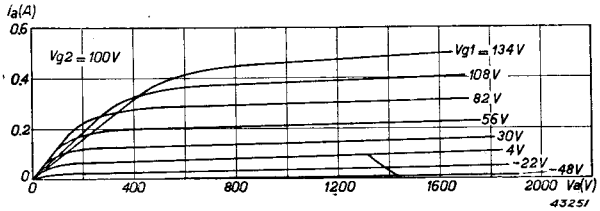

Fig. 77. As Fig. 73, but for $V_{g2} = 100$ V.

a carrier wave setting at V_{g2}=250 V, a modulation depth of 100% will be accompanied by a variation in the screen voltage between 0 and 500 V. At the peak of the modulation, that is, at $V_{g2} =$ 500 V, the alternating anode voltage must be as high as possible, and the end point A on the load line in fig. 73 has therefore been placed at $V_a = 250$ V, i.e. in the neighbourhood of the limit characteristic curve. Taking the steady anode voltage to be $V_a = 1500$ V, the modulation peak is then $V_{ap} = 1250$ V.

The grid bias is fixed at a value that will, at the carrier wave setting with $V_{g2} = 250$ V, place the valve within the class B category: V_{g1} is then —100 V. Excitation voltage should be slightly higher, viz. $V_{g1p} =$ 104 V.

The load line from fig. 73 can then be constructed by means of the formulae:

$$v_{g1} = -100 + 104 \cos \omega t,$$
$$v_a = 1500 - 1250 \cos \omega t,$$

and from this the anode current impulses (*a*, fig. 78).

The first harmonic of the anode current is calculated at $I_{a1} =$ 242 mA, so that with $V_{ap} = 1250$ V, $R_a = 5175$. This value of R_a is subsequently kept constant, and

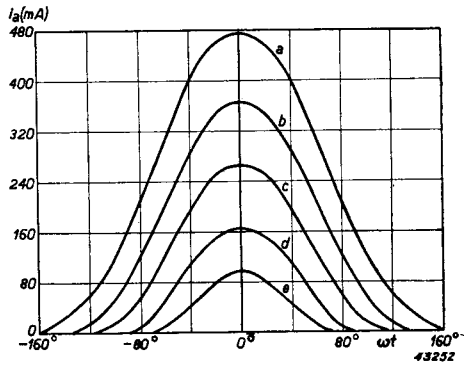

Fig. 78. Anode current impulses of the pentode corcerned in figs. 73–77; with $V_a = 1500$ V; $V_{g1} = -100$ V; $V_{g1p} = 104$ V; $R_a = 5175$ ohms. (screen grid modulation).

the load lines in figs. 74 to 77 are in relation only to this anode impedance: the relative anode current impulses are indicated in fig. 78 by the letters *b*, *c*, *d* and *e*. It is found that the anode current impulses at lower screen potentials have a lower amplitude and smaller angle, the latter changing from $\Theta = 160°$ ($V_{g2} = 500$ V) to $\Theta = 69°$ ($V_{g2} = 100$ V), so that actually the setting of the valve passes from Class A, through Class B, to Class C.

A summary of the various values, as calculated, is given in the following table:

TABLE VIII

Screen grid modulation of a pentode, at $V_a = 1500$ V, $V_{g1} = -100$ V; $V_{g1p} = 104$ V, $R_a = 5175\ \Omega$

V_{g2}	V_{ap}	I_{a1}	I_{ao}	W_i	W_o	W_a	η
(V)	(V)	(mA)	(mA)	(W)	(W)	(W)	(%)
500	1250	242	203	305	151	154	49.5
400	970	188	135	202	91	111	45
300	680	131	86	129	44	85	34
200	390	75	45	67,5	14.5	53	21.5
100	185	36	20	30	3.3	27	11

The modulation curve $-I_{a1} = f(V_{g2})$, together with other relevant data, is given in fig. 79, and the approximation to a straight line will be seen

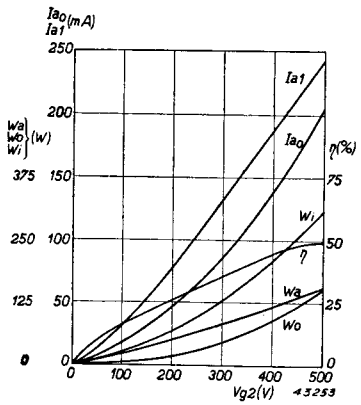

Fig. 79. Screen grid modulation characteristic of a pentode, based on the dates from figs. 73 to 77.

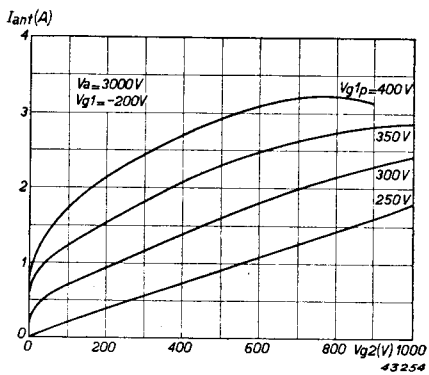

Fig. 80. Effect of the value of the excitation voltage on the form of the screen-grid modulation characteristic, from measurements on a tetrode.

to be fairly good. For the carrier wave setting the following values were selected: $V_{g2} = 250$ V, whereby $I_{ao} = 64$ mA; $W_i = 96$ W; $W_o = 30$ W; $W_a = 66$ W; $\eta = 31\%$.
Efficiency is again on the low side, on account of the low anode potential. Finally, Fig. 80 illustrates the effect of too high an excitation voltage upon the shape of the screen grid modulation curve as applicable to a tetrode $V_a = 3000$ V; $V_{g1} = -200$ V, in the voltage range $V_{g2} = 0 \ldots .$ 1000 V, with excitation voltages of 250, 300, 350 and 400 V.

The straightest characteristic is obtained at $V_{g1p} = 250$ V, the curve becoming more and more pronounced at higher values of V_{g1p}, the concave side facing towards the abscissa, all of which agrees with Fig. 72.

In practice, screen grid modulation is employed when only low modulation power is available, in cases where requirements in respect of distortion and efficiency are not too high. The required modulation power is on the low side, since the screen grid, especially at this particular setting, with low alternating voltages, takes only a small current.

§ 5. Suppressor grid modulation

In this type of modulation use is made of the controlling effect of the suppressor grid upon the anode current when at a negative potential with respect to the cathode. This controlling element finds its origin in the fact that a certain part of the stream of electrons passing the screen grid is thrown back the moment the suppressor grid acquires a negative potential, the proportion increasing as this potential becomes more negative [1].
The major part of these rejected electrons arrives at the screen grid, so that the reduction in the anode current is accompanied by an increase in the screen current; this fact is illustrated in the static characteristics of the pentode with its suppressor grid at a negative potential. Figs. 81 to 85 show the I_a/V_a curves of the pentode PB 3/800 at $V_{g2} = 600$ and $V_{g3} = 0$, —100, —200, —300 and —400 V, whilst figs. 86 to 90 furnish the I_{g2}/V_a characteristics of this valve at the same voltages.

[1] In some types of pentode, electrons are repulsed when the suppressor grid is at zero potential with respect to the cathode; the entire electron stream passes to the anode only when the suppressor is to a certain extent positive.

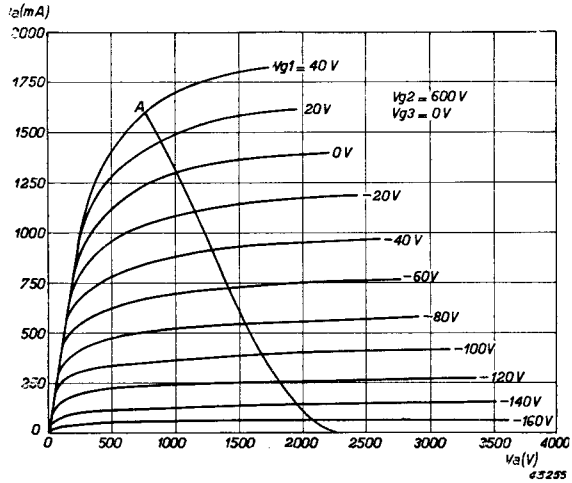

Fig. 81. I_a/V_a characteristics of the pentode PB 3/800 at $V_{g2} = 600$ V; $V_{g3} = 0$ V.

A pentode arranged for class C, R.F. telegraphy, with $V_{g3} = 0$, the load line extending to the limit characteristic and a negative potential applied to the suppressor grid, results in a displacement of the limit line towards the right-hand side in the I_a/V_a diagrams, as revealed by the figures referred to above. Simultaneously, the slope is reduced, the result being that the peak anode current, as well as the alternating anode voltage, are reduced, i.e. output power and efficiency are lower.

In the case of the PB 3/800 this takes place in the voltage range V_{g3} 0 .... to —400 V; if therefore the suppressor grid is given a suitable negative potential, for instance —200 V with A.F. signal superimposed, the aerial current is modulated by this A.F. signal. This method of applying the modulation is shown graphically in fig. 91.

In calculating the data relating to suppressor grid modulation for the pentode in question, let us take as starting point the telegraphysetting at $V_a = 3000$ V, with $V_{g2} =$ 600 V. The anode current, as seen from fig. 81, becomes zero at $V_{g1} =$ —180 V, and for the class C arrangement we therefore take $V_{g1} =$ —300 V, and $V_{g1p} = 340$ V, regarding which latter value more will be said later.

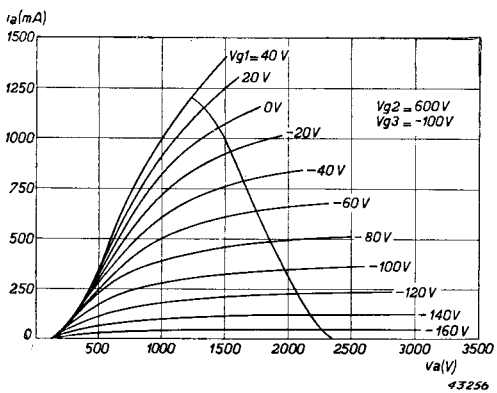

Fig. 82. As fig. 81, but for $V_{g3} =$ —100 V.

Fig. 83. As fig. 81, but at $V_{g3} = -200$ V.

Assuming point A to be the end point of the load line, with $v_a = 760$ V, then $I_{ap} = 1600$ mA and $V_{ap} = 2240$ V.

The anode alternating voltage could certainly be slightly higher, but in that case (for the same excitation voltage), the peak anode current would be lower, in fact considerably so, due to the slope of the I_a/V_a characteristic at that point; the point A is, therefore, probably the best compromise to ensure optimum power. From:

$$v_{g1} = -300 + 340 \cos \omega t$$
$$v_a = 3000 - 2240 \cos \omega t,$$

the load line is then plotted as in fig. 81 and from this the anode current impulse (*a*, fig. 92): from the latter, I_{a1} is calculated to be 657 mA, so that, with $V_{ap} = 2240$ V, $R_a = 3410$ ohms. Further, I_{ao} is calculated very simply, together with W_i, W_o, W_a and η. These calculations are then repeated with

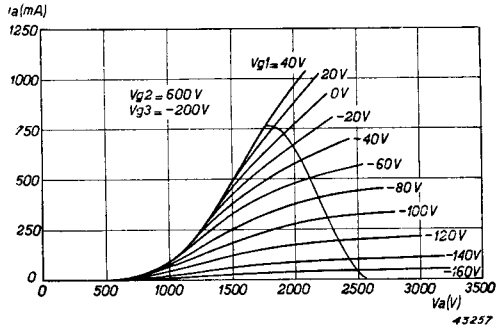

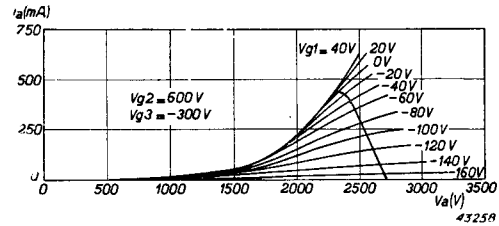

Fig. 84. As fig. 81, but at $V_{g3} = -300$ V.

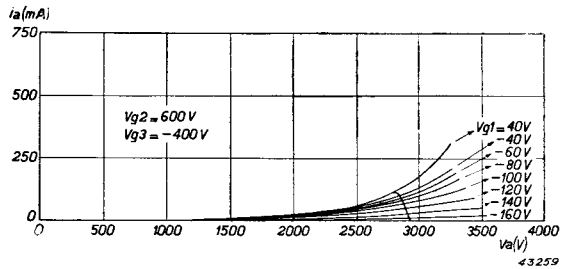

Fig. 85. As fig. 81, but at $V_{g3} = -400$ V.

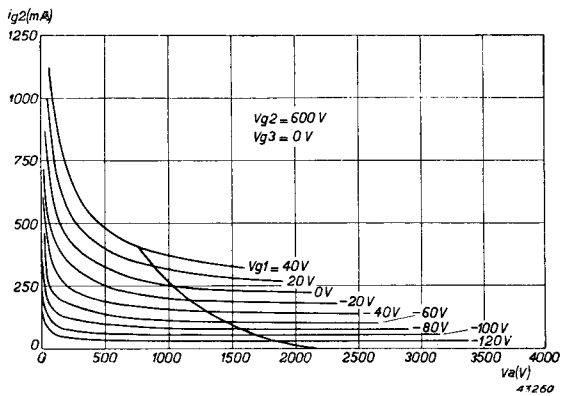

Fig. 86. I_{g2}/V_a characteristics of the pentode PB 3/800 at $V_{g2} = 600$ V; $V_{g3} = 0$ V.

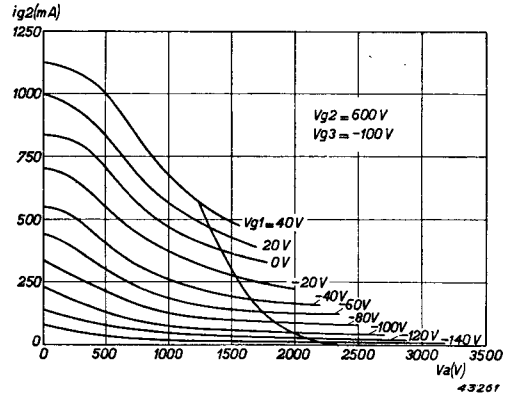

Fig. 87. As fig. 86, but at $V_{g3} = -100$ V.

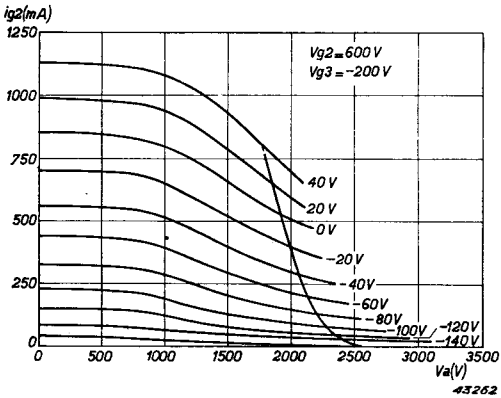

Fig. 88. As fig. 86, but at $V_{g3} = -200$ V.

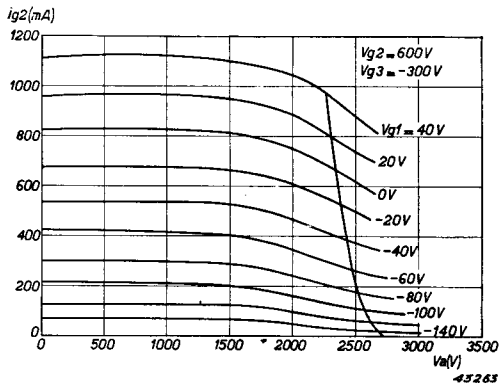

Fig. 89. As fig. 86, but at $V_{g3} = -300$ V.

respect to fig. 82 ($V_{g3} = -100$ V), fig. 83 ($V_{g3} = -200$ V), fig. 84 ($V_{g3} = -300$ V) and fig. 85 ($V_{g3} = -400$ V), all at $R_a = 3410$ ohms. It is not possible to draw a working line for a given value of R_a in the I_a/V_a diagram direct; on the contrary, the method followed is such that a suitable value of V_{ap} is accepted and the load line constructed from the known values of $v_{g1}(t)$ and $v_a(t)$. The anode current impulse thus found provides the first harmonic I_{a1} and this, in conjunction with V_{ap}, provides the appropriate value of R_a. Now, if the value of R_a thus obtained is not equal to, but is greater or less than 3410 ohms, the calculation must be repeated, using a higher, or lower value of V_{ap}, until the load line relating to $R_a = 3410$ ohms is found.

This process yields the load lines shown in figs. 82 to 85, whilst the relative anode current impulses are reproduced in Fig. 92, (*b*, *c*, *d* and *e*). It will be seen at once from the respective I_a/V_a diagrams how far the movement of the limit characteristic towards the righthand side, and the decrease in the slope, tend to reduce the peak anode current as well

as the alternating anode voltage when the suppressor grid is made more negative. The attenuation in the impulses is illustrated in fig. 92.

The direct screen current I_{g2o} occurring at different values of V_{g3} may be calculated from the I_{g2}/V_a diagrams in figs. 86 to 90, by constructing the load line in the same manner as in the I_a/V_a diagram. The resultant screen current impulses are reproduced in fig. 93, in which *a*) refers to $V_{g3} = 0$ V, *e*) to $V_{g3} = -400$ V: the increase in the screen current according as V_{g3} becomes more negative can be clearly seen.
The final result of the calculation is set out in the following table.

TABLE IX

Suppressor-grid modulation PB 3/800. $V_a = 3000$ V; $V_{g2} = 600$ V. $V_{g1} = -300$ V; $V_{g1p} = 340$ V; $R_a = 3410$ ohms

V_{g3}	I_{ao}	I_{a1}	V_{ap}	I_{g2o}	W_i	W_o	W_a	W_{g2}	η
(V)	(mA)	(mA)	(V)	(mA)	(W)	(W)	(W)	(W)	(%)
0	372	657	2240	77	1116	736	380	46	66.0
−100	292	520	1770	106	876	460	416	64	52.5
−200	209	360	1230	151	627	222	405	91	35.4
−300	125	217	740	190	375	80	295	114	21.3
−400	35	58.6	200	220	105	6	99	132	5.7

In fig. 94 the various quantities have been plotted as a function of V_{g3}, and in this figure the modulation characteristic $I_{a1} = f(V_{g3})$ very well approximates a straight line in the voltage range $V_{g3} = 0$ .... to −400 V. As carrier wave setting we therefore select $V_{g3} = -200$ V, superimposing an A.F. signal having an amplitude of at most 200 V; the aerial current will then vary fairly well in proportion to the voltage. The efficiency reaches its highest value of 66% at the peak of the modu-

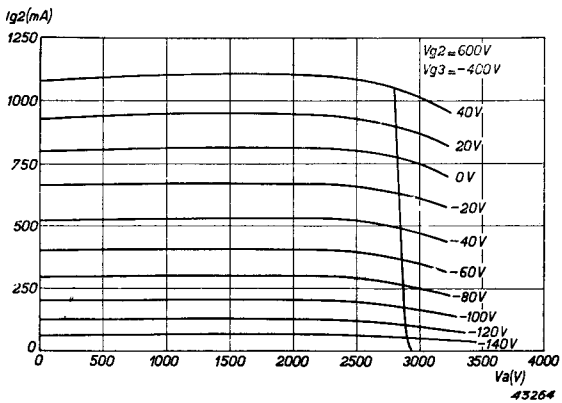

Fig. 90. As fig. 86, but at $V_{g3} = -400$ V.

lation, as is also the case with the other methods of grid modulation. According as the suppressor is made more and more negative, the efficiency decreases more or less in proportion to V_{g3}, giving an efficiency of 35% at the carrier setting. At that point the R.F. output power is 222 W and the dissipation 405 W, which means that the anode is not overloaded, the permissible maximum being 450 W. The steady screen current increases as the suppressor grid becomes more negative; at the setting in question, $I_{g2o} = 151$ mA and the screen-grid dissipation $W_{g2} =$ 91 W: the screen, then, is also within the limit, the maximum being 100 W.

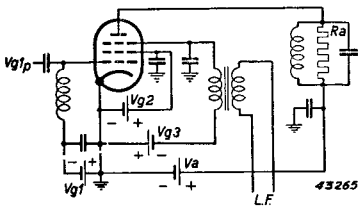

Fig. 91. Circuit of transmitter amplifier with suppressor grid modulation.

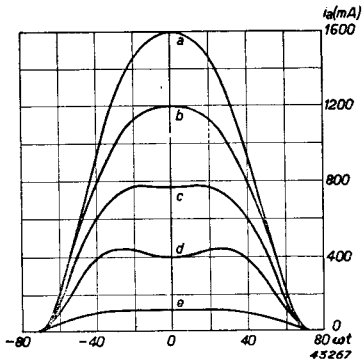

Fig. 92. Anode current impulses in suppressor grid modulation of pentode PB 3/800, based on the load lines in figs. 81 to 85.

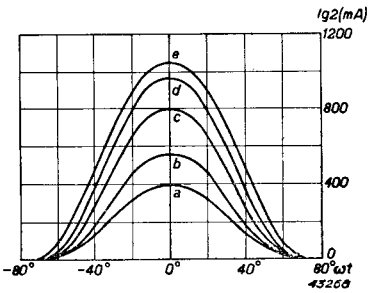

Fig. 93. Screen grid impulses in suppressor grid modulation of the pentode PB 3/800, relating to the load lines shown in figs. 86—90.

Along with the anode dissipation, therefore, the screen-grid dissipation also figures as a limiting factor to the R.F. power, and this must be taken into consideration in the suppressor-grid modulation of pentodes; this is put into effect by fixing a suitable value for the excitation voltage, seeing that the peak screen current is governed by the latter.

Needless to say, the form of the modulation curve is determined entirely by the disposition of the limit characteristic in the I_a/V_a diagram, and fig. 95 shows the limit characteristics at different values of V_{g3}, together with the load line in respect of $R_a = 3410$ ohms. It is a difficult matter to lay down any hard and fast rules for these limit characteristics, on the basis of which to predict the shape of the modulation curve, the more so since the anode current impulses vary not only in

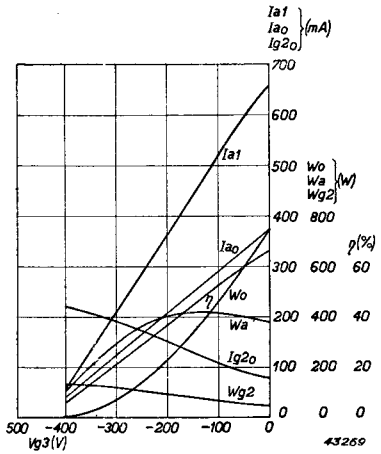

Fig. 94. Suppressor grid modulation characteristics of the pentode PB 3/800 at V_a = 3000 V; V_{g2} = 600 V; V_{g1} = —300 V; V_{g1p} = 340 V; R_a = 3410 ohms.

amplitude, but also in their form, being more or less flattened or even "double-humped" at negative values of V_{g3} (fig. 92). This latter effect depends both on the limit characteristic and the degree to which the I_a/V_a characteristics are bunched together in the vicinity of that limit characteristic (compare figs. 81 to 85).

Some types of pentode reveal a very marked tendency towards curving of the modulation characteristic, the convex side facing the abscissa, and in such cases some improvement may be brought about by applying modulation voltage to the screen grid, producing a sort of combined modulation; this possibility is referred to again in § 8 of the present chapter.

Suppressor-grid modulation is frequently met in small transmitters, in view of the small amount of modulation power required (which drops to zero when the suppressor potential is not positive under modulation); efficiency and distortion do not conform to very high requirements.

§ 6. Anode modulation

All the methods of modulation so far discussed depend upon the controlling action which each of the grids is capable of exercising on the

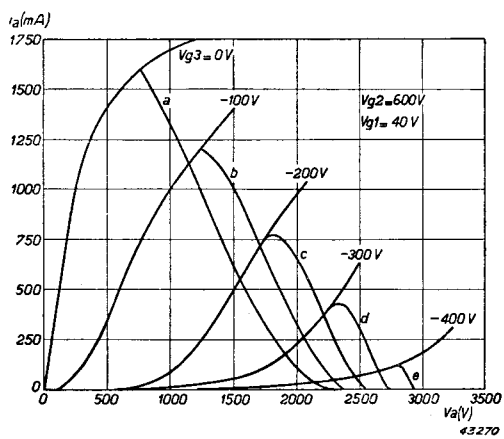

Fig. 95. Load lines in respect of suppressor grid modulation of the pentode PB 3/800, at R_a = 3410 ohms, V_a = 3000 V, V_{g1} = —300 V, V_{g1p} = 340 V, V_{g2} = 600 V, with different values of V_{g3}.

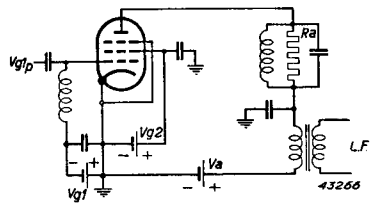

Fig. 96. Circuit of a transmitter amplifier employing anode modulation.

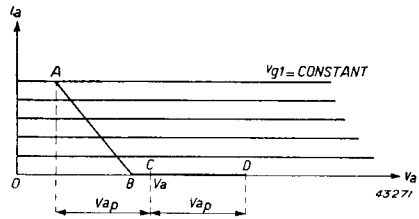

Fig. 97. Ideal I_a/V_a characteristics of a pentode, showing load line for R.F. Class C setting, at $V_{ap} < V_a$.

anode current: the control- and screen grids directly govern the cathode current, whilst the suppressor determines the distribution of current between screen and anode; in other words, out of the total amount of current passing the screen, a greater or smaller portion is allowed to pass to the anode.

In each instance, too, the magnitude of the impulse is modified by the modulation, either in amplitude only, as in suppressor grid modulation, or in amplitude, and angle, as in the case of control- and screen grid modulation. Together with the magnitude of the impulse, the first harmonic I_{a1} of the anode current is also changed and simultaneously the alternating anode voltage $V_{ap} = I_{a1}R_a$. Further, since the steady anode current is fixed at a certain value, the resultant voltage ratio V_{ap}/V_a, and with it the efficiency, are directly affected by the modulation voltage.

This will explain why the efficiency of the carrier-wave setting for any arbitrary method of applying grid modulation is so low, because I_{a1}, and consequently also V_{ap}, are roughly equal to only one half of the full rating, i.e. at the modulation peak.

When anode modulation is employed, that is, when the A.F. modulation signal is applied in series with the steady anode voltage (see fig. 96), the setting of the valve must be arranged so that the anode voltage will influence the magnitude or shape of the anode-current impulses and therefore of the first harmonic I_{a1} also. Just as in the case of grid modulation, a reduction of the appropriate potential, in this instance the steady anode voltage, must be accompanied by a drop in the first harmonic of the anode current and, consequently, in the alternating anode voltage. Seeing that it is the direct voltage which becomes smaller, V_{ap}/V_a shows no appreciable change in value, and the efficiency,

for so far as it depends upon this value, is therefore not impaired. Let us now trace the method whereby the anode voltage may be made to modify the anode current impulses, and see how this renders modulation possible.

Taking the case of the ideal pentode [1], working under class C conditions (fig. 97), excited by means of an R.F. voltage, of amplitude V_{g1p} applied to the control grid, let the anode impedance R_a be such that the alternating anode voltage V_{ap} is less than the steady anode potential V_a.

The R.F. power is determined by the size of V_{ap} and I_{a1}, or, since $V_{ap} = I_{a1} R_a$, by I_{a1}. The latter is obtained from the peak anode current I_{ap} and half the current angle Θ, by means of the expression previously employed, viz.:

$$I_{a1} = f_1(\Theta) \cdot I_{ap} = \frac{I_{ap}}{\pi} \cdot \frac{\Theta - {}^1/_2 \sin 2\Theta}{1 - \cos \Theta},$$

in which Θ is evaluated from:

$$\cos \Theta = \frac{-V_{g1} - bV_{g2}}{V_{g1p}},$$

since the static characteristics are expressed by:

$$i_a = a\,(v_{g1} + bv_{g2}).$$

From the above formulae it is immediately obvious that I_{a1} is not dependent on V_a, seeing that I_{ap} and Θ are independent of it. This implies, in the circumstances, that modulation of the aerial current by means of variations in anode voltage is not possible, which fact is at once corroborated by fig. 97, for, as V_a increases, the working line $ABCD$ moves bodily to the right, without the slightest alteration in the anode current impulse.

As already stated, then, the setting of the valve must be such that variations in the steady anode potential do produce a change in the magnitude or form of the current impulse, and this is effected in the manner shown in fig. 98, where the alternating anode voltage is higher

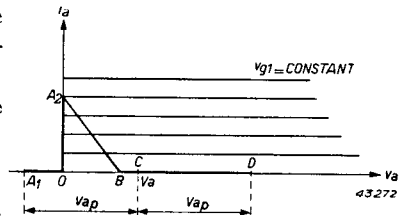

Fig. 98. As fig. 97, but with $V_{ap} > V_a$.

[1] For anode modulation of a triode, see note at the end of this paragraph.

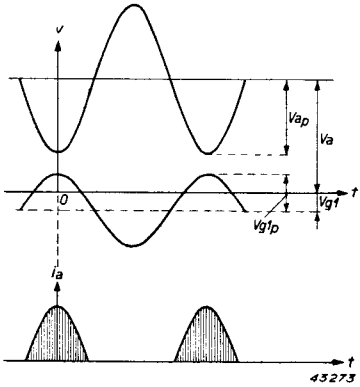

Fig. 99. Anode voltage, grid voltage and anode current, as function of the time, in respect of the load line in fig. 97.

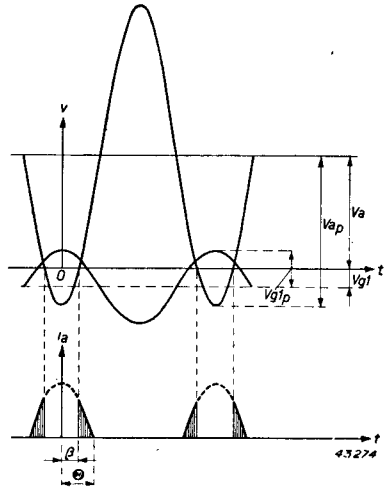

Fig. 100. As fig. 99, but for the load line in fig. 98.

than the direct voltage. The working line then assumes the form A_1OA_2BCD, the anode voltage being negative during the period that the working point is passing through OA_1O, whilst the anode current in the same period is zero. In contrast with the normal arrangement according to fig. 97, in which the anode current reaches its maximum value simultaneously with the minimum value of the anode voltage, the anode current is now zero in the region of the minimum anode voltage, and the impulse of the former therefore shows a depression which reaches right down to the abscissa axis.

Figs. 99 and 100 illustrate the currents and voltages applicable to the conditions shown in figs. 97 and 98: from fig. 100 it will be seen that the part of the anode current impulse where no current flows occurs during the time that the anode voltage is negative.
In practice, matters are rather different, in that the I_a/V_a characteristics (fig. 98) do not extend to the vertical axis, but only as far as the limit characteristic previously referred to, which, in contrast with the axis itself, possesses a finite slope. The dip in the anode current impulse is therefore not really as abrupt as is shown in fig. 100, but is more gradual, which fact will be demonstrated later.

Turning to fig. 98, let us now examine the shape of the modulation characteristic $I_{a1} = f(V_a)$. The I_a/V_a characteristics are again represented by:

$$i_a = a\,(v_{g1} + b v_{g2})\,.\; i_a > 0,\; v_a > 0 \quad . \quad . \quad . \quad . \quad . \quad . \quad (5.\ 13)$$

the control voltage by:

$$v_{g1} = V_{g1} + V_{g1p} \cos \omega t. \quad . \quad . \quad . \quad . \quad . \quad . \quad . \quad . \quad . \quad . \quad (5.\ 14)$$

and the anode voltage by:

$$v_a = V_a - V_{ap} \cos \omega t. \quad . \quad . \quad . \quad . \quad . \quad . \quad . \quad . \quad . \quad . \quad (5.\ 15)$$

As a function of time, the anode current will be:

$$i_a = a\,(V_{g1} + V_{g1p} \cos \omega t + b V_{g2}) \quad . \quad . \quad . \quad . \quad . \quad . \quad (5.\ 16)$$

as applicable to those values of ωt for which $i_a > 0$ and $v_a > 0$. The first of the conditions is usually met by:

$$\omega t < \Theta$$

with

$$\cos \Theta = \frac{-V_{g1} - b V_{g2}}{V_{g1p}} \quad . \quad . \quad . \quad . \quad . \quad . \quad . \quad (5.\ 17)$$

and the second by:

$$\omega t > \beta,$$

where β is determined by

$$\cos \beta = \frac{V_a}{V_{ap}} \quad . \quad . \quad . \quad . \quad . \quad . \quad . \quad . \quad . \quad . \quad (5.\ 18)$$

Angles Θ and β are shown in fig. 100, from which the formula for $\cos \beta$ can also be drawn.

The anode current is then given by:

$$i_a = a\,(V_{g1} + b V_{g2} + V_{g1p} \cos \omega t),\; \beta < \omega t < \Theta,$$

or, if $V_{g1} + b V_{g2}$ is replaced by $-V_{g1p} \cos \Theta$:

$$i_a = a\, V_{g1p}\,(\cos \omega t - \cos \Theta),\; \beta < \omega t < \Theta. \quad . \quad . \quad . \quad . \quad . \quad (5.\ 19)$$

At all other values of ωt, $i_a = 0$.

The D.C. component of the series of impulses thus defined is then:

$$I_{ao} = \frac{1}{\pi} \int_o^{\pi} i_a\,(\omega t)\, d\,(\omega t) = \frac{1}{\pi} \int_{\beta}^{\Theta} a V_{g1p}\,(\cos \omega t - \cos \Theta)\, d\,(\omega t) =$$

$$= \frac{a V_{g1p}}{\pi} \Big[\sin \omega t - \omega t \cos \Theta\Big]_{\beta}^{\Theta} = \frac{a V_{g1p}}{\pi} \Big[\sin \Theta - \sin \beta - (\Theta - \beta) \cos \Theta\Big],$$

which is then written in the form:

$$\frac{\pi I_{ao}}{aV_{g1p}} = \sin\Theta - \sin\beta - (\Theta - \beta)\cos\Theta = g_o(\Theta, \beta). \quad (5\ 20)$$

For the first harmonic we have then:

$$I_{a1} = \frac{2}{\pi}\int_o^{\pi} i_a(\omega t)\cos\omega t\, d(\omega t) = \frac{2}{\pi}\int_{\beta}^{\Theta} aV_{g1p}(\cos\omega t - \cos\Theta)\cos\omega t\, d(\omega t)$$

$$= \frac{2aV_{g1p}}{\pi}\left[{}^1/_2\,\omega t + {}^1/_4\sin 2\omega t - \cos\Theta\sin\omega t\right]_{\beta}^{\Theta} =$$

$$= \frac{aV_{g1p}}{\pi}\left[\Theta - \beta + {}^1/_2(\sin 2\Theta - \sin 2\beta) - 2\cos\Theta(\sin\Theta - \sin\beta)\right],$$

or, in another form:

$$\frac{\pi I_{a1}}{aV_{g1p}} = \Theta - {}^1/_2\sin 2\Theta - \beta - {}^1/_2\sin 2\beta + 2\cos\Theta\sin\beta = g_1(\Theta, \beta). \quad (5.21)$$

The alternating voltage is:

$$V_{ap} = I_{a1}R_a = \frac{aV_{g1p}}{\pi} R_a g_1(\Theta, \beta). \quad (5.\ 22)$$

On the other hand, we find from the formula for $\cos\beta$:

$$V_{ap} = \frac{V_a}{\cos\beta}. \quad (5.\ 23)$$

Equating, we have:

$$\frac{aV_{g1p}}{\pi} R_a g_1(\Theta, \beta) = \frac{V_a}{\cos\beta},$$

or:

$$g_1(\Theta, \beta)\cdot\cos\beta = \frac{\pi V_a}{aV_{g1p}R_a} = C, \quad (5.\ 24)$$

from which latter equation it is possible to evaluate β for a given value of V_a, that is, of C.

When once the relationship between C and β has been established, the modulation characteristic is determined in accordance with (5. 21) and (5. 24), by:

$$\frac{\pi I_{a1}}{aV_{g1p}} = g_1(\Theta, \beta) = f(C) \quad (5.\ 25)$$

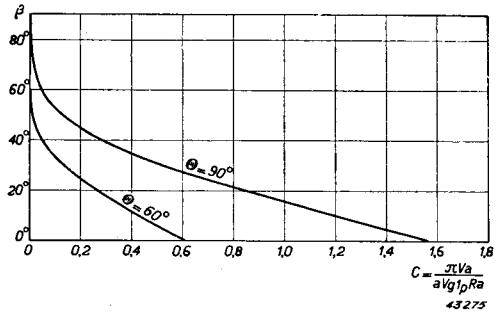

Fig. 101. The relationship between the angle β in Fig. 100 and the quantity $C = \frac{\pi V_a}{a V_{g1p} R_a}$ for a pentode, R.F. class C, with $V_{ap} > V_a$.

Fig. 101 shows the connection (5. 24) between β and C at two values of Θ, and the modulation characteristic (5. 25) will be seen in fig. 102 for the same values of Θ. For the greater part, this latter very closely resembles a straight line, there being a certain amount of convexity only at the lower end, i.e. at low values of C. It is noticeable that the characteristics, at the upper end, terminate at different values of $C = \frac{\pi V_a}{a V_{g1p} R_a}$ and, as will be seen from fig. 101, it is just at those lower values of C that $\beta = 0$. The reason for this is furnished by figs. 97 and 98: if the steady anode potential is increased in the latter figure, leaving all else constant, the kinked load line DBA_2OA_1 will move more and more to the right, although the point A_2 remains on the I_a axis and B, D, O and A_1 on the V_a axis, A_1 moving towards O.

It is now possible to find a value of V_a where A_1 exactly coincides with the zero point; V_{ap} is then equal to V_a and the load line is as shown in fig. 97 (with A on the I_a axis).

At that moment $\beta = 0$, and the kink in the anode current impulse disappears. If V_a now be increased any further, the anode current does not change, nor, there-

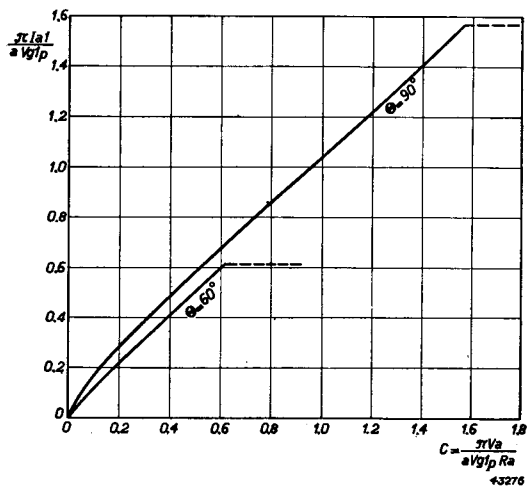

Fig. 102. Anode modulation curve of a pentode of the characteristics shown in fig. 98, at two values of the current angle of the anode current impulses.

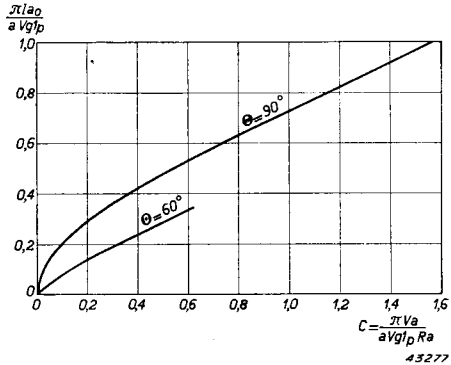

Fig. 103. Steady anode current as a function of the direct anode voltage for an anode-modulated pentode of the characteristics given in fig. 98, at two different angles of anode current impulse.

fore, does I_{a1}, and the modulation curve proceeds horizontally along the broken line shown in fig. 102. The value of C (and therefore of V_a), at which the kink in the modulation curve occurs, is then determined by $\beta = 0$, so that, in relation to (5. 24) and (5. 21):

$$C_{\max} = g_1(\Theta, 0) = \Theta - {}^1/_2 \sin 2\Theta,$$

which value is thus definitely dependent on Θ.
Fig. 103 shows the steady anode current as a function of the voltage at $\Theta = 90°$ and 60°, calculated from (5. 20) and (5. 24). The efficiency, as determined by (5. 20), (5. 21) and (5. 23), is:

$$\eta = {}^1/_2 \frac{I_{a1}}{I_{ao}} \cdot \frac{V_{ap}}{V_a} = {}^1/_2 \frac{g_1(\Theta, \beta)}{g_o(\Theta, \beta)} \cdot \frac{1}{\cos\beta} =$$

$$= \frac{\Theta - {}^1/_2 \sin 2\Theta - \beta - {}^1/_2 \sin 2\beta + 2\cos\Theta \sin\beta}{2\cos\beta\,[\sin\Theta - \sin\beta - (\Theta - \beta)\cos\Theta]}.$$

From the latter, η can be calculated as a function of Θ and β and, since C (i.e. V_a) is also known as function of these factors (5. 24), the relationship between η and C is readily available; this is given in fig. 104 in respect of $\Theta = 60°$ and 90°, and, as anticipated, the efficiency is seen to be only very slightly variable with the steady anode potential. When $C = C_{\max}$, with $\beta = 0$— we have:

$$\eta = \frac{\Theta - {}^1/_2 \sin 2\Theta}{2(\sin\Theta - \Theta\cos\Theta)},$$

which is in agreement with what has been said in Chapter III con-

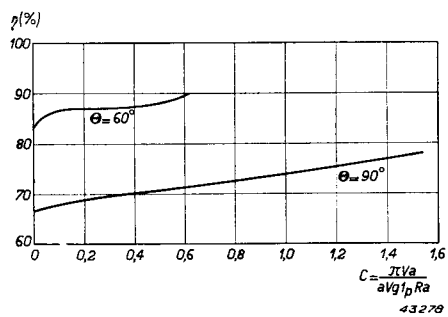

Fig. 104. Efficiency as a function of the steady anode voltage, with anode modulation as in fig. 98.

cerning class C amplification. At $\Theta = 60°$ and 90°, $\eta = 89.5$ and 78.5% respectively.

At $C = 0$ (i.e. $V_a = 0$), $\beta = 0$, and the efficiency is then:

$$\eta = \frac{3 \cos 2\Theta - 1}{6 \cos 2\Theta};$$

from which it follows that, when $\Theta = 60°$ and 90°,

$$\eta = 83.8\% \text{ and } 66.7\% \text{ respectively.}$$

Thus, with $\Theta = 60°$, the efficiency lies between 83.3 and 89.5%, and at $\Theta = 90°$ between 66.7 and 78.5%.

Let us now ascertain how far this theory is borne out in practice, when applied to the static characteristics of the pentode given in fig. 105, proceeding to a calculation of the setting for anode modulation in respect of which the carrier wave shall be based on a steady anode potential of 1500 V. To obtain a reasonable class C setting, V_{g2} will be placed at 300 V, V_{g1} at —200 V, V_{g1p} at 280 V. It is required that a modulation depth of 100% be obtainable, with straight modulation characteristic. The direct anode voltage will therefore attain all values between 0 and 3000 V.

In accordance with the theory outlined above, the anode resistance R_a, at $V_a = 3000$ V and at the specified screen-and control voltages, must be of such value that the alternating anode voltage is just reaching the limit line. For this reason the end point A relative to the load line a in fig. 105 (at $V_a = 3000$ V) is taken to be:

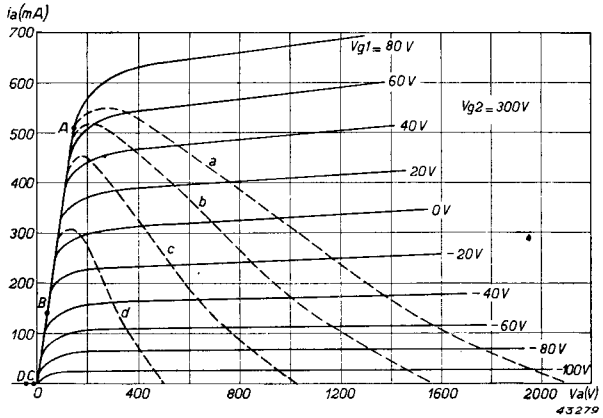

Fig. 105. I_a — V_a characteristics of a pentode, with load lines for anode modulation.

$$V_{a\min} = 150 \text{ V}, \quad I_{ap} = 510 \text{ mA, so that:}$$

$$v_{g1} = -200 + 280 \cos \omega t$$

$$v_a = 3000 - 2850 \cos \omega t.$$

The load line can now be plotted and, from that, the anode current

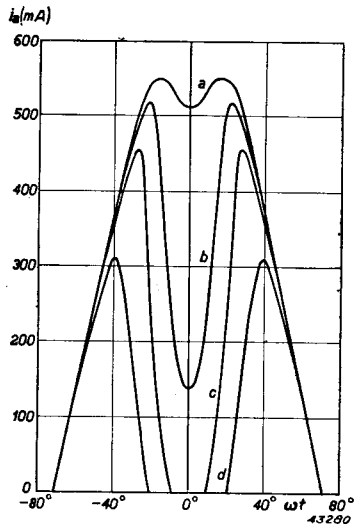

Fig. 106. Anode current impulses in a pentode of the kind whose characteristics are illustrated in fig. 105 and relating to the load lines in that figure.

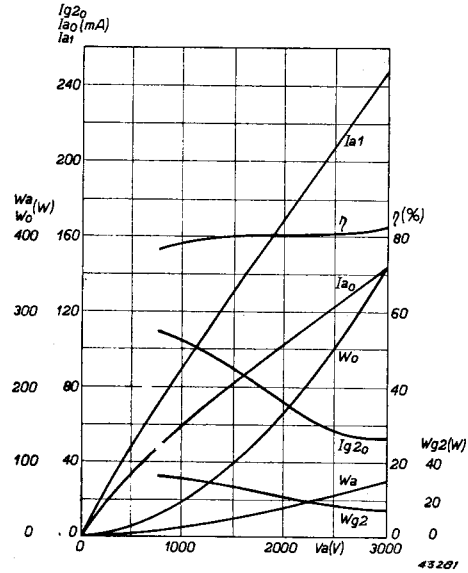

Fig. 107. Anode modulation characteristics of the pentode referred to in fig. 105, with $V_a = 1500$ V, $V_{g1} = -200$ V, $V_{g1p} = 280$ V, $V_{g2} = 300$ V, $R_a = 11{,}500\ \Omega$.

impulse (*a* in fig. 106). In accordance with Simpson's law, the first harmonic is then $I_{a1} = 248$ mA and the loading resistance therefore:

$$R_a = \frac{2850}{0.248} = 11{,}500 \text{ ohms.}$$

Taking this value of R_a, together with the appropriate values of control- and screen voltage, similar settings can be calculated with respect to $V_a = 2250$, 1500 and 750 V.

The corresponding load lines are reproduced in figs. 105, *b*, *c* and *d*, whilst the impulses are shown in fig. 106.

These impulses do certainly show a dip which becomes the more marked according as V_a is reduced, but, since the slope of the limit line in fig. 105 is finite, the development of this dip is more gradual, reaching the abscissa axis only at the lower values of V_a (compare impulse *c*, at $V_a = 1500$ V).

Various data derived from the impulses are grouped together in the following table and are further shown graphically in fig. 107.

TABLE X

Anode modulation of the pentode of fig. 105. $V_a = 1500$ V; $V_{g1} = -200$ V; $V_{g1p} = 280$ V; $V_{g2} = 300$ V; $R_a = 11{,}500$ ohms

V_a	V_{ap}	I_{a1}	I_{ao}	W_i	W_o	W_a	η	I_{g2o}	W_{g2}
(V)	(V)	(mA)	(mA)	(W)	(W)	(W)	(%)	(mA)	(W)
3000	2850	248	143	429	354	75	82.4	54	16
2250	2180	189	114	257	205	52	80	64	19
1500	1510	131	82	123	99	24	80.3	90	27
750	795	69	48	36	27	9	75.0	109	33

Fig. 107 demonstrates clearly that the modulation curve $I_{a1} = f(V_a)$ is quite a fair approach to a straight line, except for the lower end, where a slight curvature is to be seen, as was the case in fig. 102. The figure also proves the efficiency to be quite high and almost independent of the steady anode voltage. Included in the figure are, further, the direct screen current I_{g2o} and screen dissipation W_{g2}, both of which increase when the steady anode voltage is raised. The explanation of this is to be found in fig. 108, giving the screen-grid characteristics of this pentode and the load lines in respect of $V_a = 3000$, 2250, 1500 and 750 V.

The current impulses will be seen from fig. 109; these assume a higher and wider form with decreasing direct voltage on the anode, due to the fact that the minimum anode voltage becomes lower and lower. For instance, at $V_a = 3000$ V, $v_{a\min} = V_a - V_{ap} =$ 150 V at $V_a = 750$ V, $v_{a\min} = -45$ V, and the lower $v_{a\min}$ becomes, the higher the value of I_{g2p} (compare the terminating points of the relative load lines A, B, C and

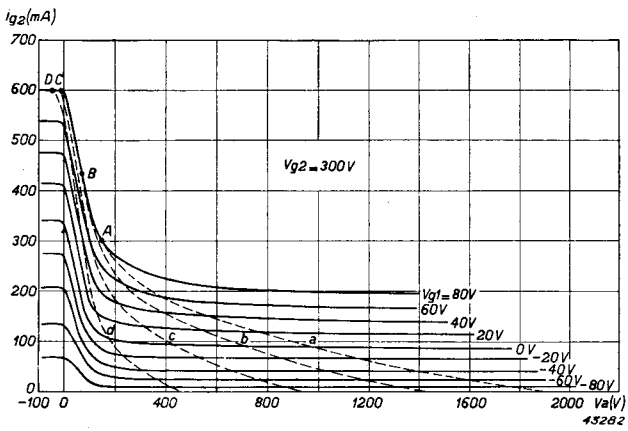

Fig. 108. I_{g2}—V_a characteristics of the pentode of fig. 105, showing load lines for anode modulation.

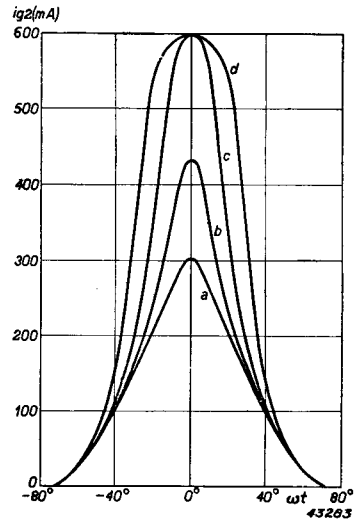

Fig. 109. Screen grid current impulses with anode modulation, in accordance with the load lines shown in fig. 108.

D in fig. 108). The carrier-wave setting for anode modulation of this pentode will therefore be taken at $V_a = 1500$ V and then makes possible a modulation depth of 100%, with practically straight modulation characteristic. Owing to the high efficiency of 80%, the anode dissipation is well below the permissible maximum, W_a being 24 W. The screen-grid dissipation, on the other hand, does reach the maximum, namely at 27 W, which is even in excess of the specified 25 W [1]. In fact, the high screen dissipation is invariably a drawback to the anode modulation of pentodes. Nevertheless, to ensure a straight modulation characteristic, the setting must be so arranged that at the modulation peak, that is, at twice the steady anode voltage, the optimum alternating voltage is obtained. This peak-setting is then nothing more than the class C telegraphy setting, and it has already been seen (Chapter IV) that the screen dissipation is likely to be fairly high.

If the anode potential be reduced, whilst retaining the previously fixed values of V_{g1}, V_{g1p}, V_{g2} and R_a, over-excitation occurs, with consequent increase in screen current and dissipation. Hence, the setting of a pentode for anode modulation is usually limited by the maximum permissible screen dissipation, and the following paragraphs are devoted to an investigation into possible methods of circumventing this.

In principle, there is no difference between anode modulation in a triode and in a pentode; the modulation is established by the fact that the alternating anode voltage is, as it were, checked by the limit characteristic, thus producing a dip in the anode-current impulse, but since the

[1] As already pointed out, the value of 27 W for W_{g2} is that in respect of the unmodulated carrier wave ($V_a = 1500$ V). During modulation, the anode voltage fluctuates around the 1500 V, so that the instantaneous screen dissipation actually swings above and below the 27 W, the average being therefore taken as criterion. Simple calculation will show that this average dissipation does not deviate very far from 27 W on account of the roughly linear W_{g2} line.

I_a/V_a characteristics of a triode do not run horizontally, as in fig. 97, but subtend a certain angle with the V_a axis, the flowing part of the modulation line also does not lie horizontally (as in fig. 102), but obliquely upwards. In practice, then, this is the "bend" in the modulation characteristic.

This type of modulation is of special value in cases where high quality and efficiency of modulation are required, but as disadvantage may be cited the very high modulation power required, namely one half of the direct-current anode input, for a modulation depth of 100% (see § 9). High-power transmitters therefore involve the use of very powerful modulation amplifiers.

§ 7. Telephony amplification (R.F., Class B)

It has already been stated in § 2 that telephony amplification is understood to imply that the transmitting valve is excited by means of an audio-frequency modulated excitation voltage.

Fig. 110 reproduces the circuit employed, this example being based on a pentode of which the control grid is excited by an A.F. modulated alternating voltage V_{g1p}.

In this case the excitation voltage is supplied by a triode, of which the anode is modulated by the A.F. signal.

Making use once more of the hypothetical ideal characteristics of the transmitting valve, it will now be interesting to ascertain in general the behaviour of the class C amplifier on a variable excitation voltage, again as applicable to a pentode.

As a near approximation, the anode current of the pentode may be represented by the expression:

$$i_a = a\,(v_{g1} + b v_{g2});$$

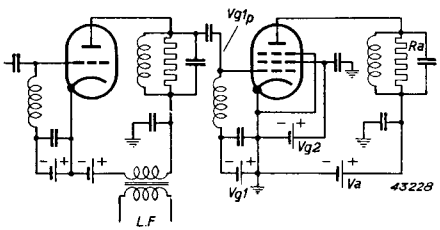

Fig. 110. Circuit of transmitter amplifier with R.F. class B modulation.

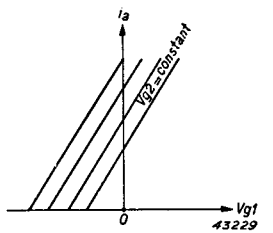

Fig. 111. Diagrammatic I_a/V_{g1} characteristics of a pentode.

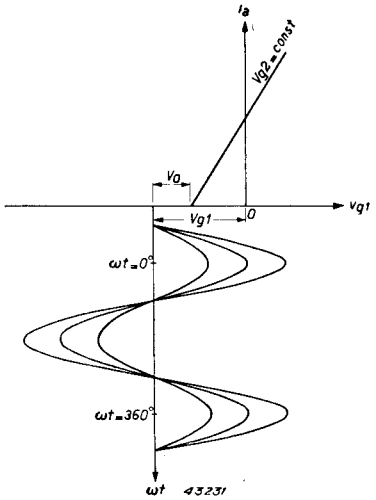

Fig. 112. Excitation of a pentode in class C, at different excitation voltages.

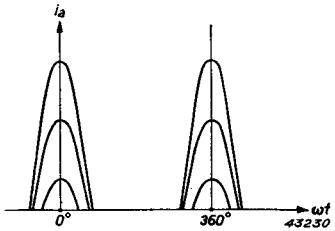

Fig. 113. Anode current impulses relating to the excitation voltages shown in fig. 112.

in other words, the anode current has a linear dependence upon v_{g1} and v_{g2}, but is not dependent on v_a. This formula, however, applies only for as far as it yields values of i_a above 0 and, further, only when $v_a = 0$; the I_a/V_{g1} diagram then has the appearance of fig. 111. Fig. 112 reproduces one of these characteristics in conjunction with three different values of the excitation voltage, superimposed on the grid bias V_{g1}. The anode-current curve i_a as a function of ωt is easily derived from this figure and is shown in fig. 113, from which it is seen that the changes in excitation voltage modify both the amplitude and the angle of the current impulses.

For any value V_{g1p} of the excitation voltage, half this angle Θ of the impulses shown in fig. 112 may be calculated from:

$$\cos \Theta = \frac{-V_{g1} - bV_{g2}}{V_{g1p}}, \quad (5.\ 26)$$

provided that:

$$V_{g1p} > -V_{g1} - bV_{g2},$$

whilst the peak current is represented by:

$$I_{ap} = a\,(V_{g1} + V_{g1p} + bV_{g2}) \quad . \quad . \quad . \quad . \quad . \quad (5.\ 27)$$

The peak value of the 1st harmonic of the anode current is:

$$I_{a1} = f_1(\Theta)\,.\,I_{ap} = \frac{1}{\pi}\,.\,\frac{\Theta - {}^1/_2 \sin 2\Theta}{1 - \cos \Theta}\,.\,I_{ap}, \quad . \quad (5.\ 28)$$

the alternating voltage is:

$$V_{ap} = I_{a1} R_a, \quad . \quad . \quad . \quad . \quad . \quad . \quad . \quad . \quad . \quad (5.\ 29)$$

and the R.F. output power:

$$W_o = {}^1/_2\, I_{a1}\, V_{ap} = {}^1/_2\, I_{a1}{}^2\, R_a \quad . \quad . \quad . \quad . \quad . \quad (5.\ 30)$$

This output is absorbed by the aerial [1], part of it being radiated into space as electro-magnetic energy; the rest is dissipated as loss in the resistance of the aerial. Let R_{ant} be the aerial resistance (comprising radiation and loss resistance), and I_{ant} the effective value of the R.F. aerial current; then:

$$W_o = I_{ant}^2 R_{ant} \quad \ldots\ldots\ldots\ldots \quad (5.\ 31)$$

Expressions (5.30) and (5.31) give the relation between I_{a1} and I_{ant}, viz:

$$I_{ant} = I_{a1} \sqrt{\frac{R_a}{2 R_{ant}}}, \quad \ldots\ldots\ldots \quad (5.32)$$

which means that I_{ant} is proportional to I_{a1}, seeing that the term within the root sign is constant. Equations (5. 28), (5. 27) and (5. 26) then establish the connection between I_{ant} and V_{g1p}.
For convenience let us assume that:

$$-V_{g1} - bV_{g2} = V_o,$$

where V_o is the absolute value of the difference between the negative bias and the voltage relating to the foot of the I_a/V_{g1} characteristic (see fig. 112); then I_{a1} and V_{g1p} can be derived from the above by means of:

$$\frac{\pi I_{a1}}{aV_o} = \frac{\Theta - {}^1/_2 \sin 2\Theta}{\cos \Theta}$$

$$\frac{V_{g1p}}{V_o} = \frac{1}{\cos \Theta}.$$

This makes it possible to calculate the relation between I_{a1} and V_{g1p} at a constant value of V_o, and this is illustrated in fig. 114, where $\pi I_{a1}/aV_o$ is shown plotted against V_{g1p}/V_o. The figure shows that I_{a1}, and therefore I_{ant}, reach values other than zero only when $V_{g1p}/V_o > 1$, which will easily be understood on referring to fig. 112, since it is only then that the anode impulse is generated. Changes in V_{g1p}, in the region where $V_{g1p} < V_o$, therefore have no effect on the aerial current.
It follows then that, when the amplitude V_{g1p} during modulation becomes less than V_o, that is, at the trough of the modulation curve, the aerial current no longer follows these variations in V_{g1p}; it is therefore obvious that true reproduction of the A.F. variations in V_{g1p} is

[1] Apart from circuit losses, see Chapter VIII. § 4.

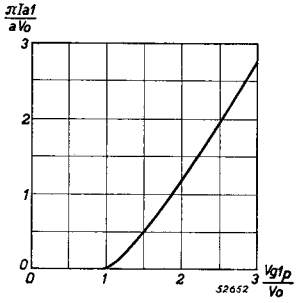

Fig. 114. Modulation curve of class C amplifier with modulated excitation voltage.

not possible; it is essential to have a linear relation between the aerial current and the excitation voltage, which means an expression of the form $I_{ant} = \text{constant}\ V_{g1p}$ or, again, $I_{a1} = \text{constant}\ V_{g1p}$. This is the equation for a straight line passing through the origin of the ordinates, and, as evidenced by fig. 114, this condition can never be realized in class C amplification.

On the contrary, it is essential that anode current commences to flow as soon as $V_{g1p} > 0$, and this is possible only when $V_o = 0$, in other words, in class B.

In a class B setting, in accordance with (5. 26) and (5. 27):

$$V_{g1} = -bV_{g2} \text{ or } V_o = 0.$$

The negative bias is then adjusted to the foot of the I_a/V_{g1} curve, with $\cos \Theta = 0$, so that the condition $\Theta = 90°$ is not affected by the value of the excitation voltage.

Further, we have:

$$I_{ap} = aV_{g1p},$$

and

$$I_{a1} = f_1(\Theta) \,.\, I_{ap} = {}^1/_2\, aV_{g1p},$$

which is the required linear relation between I_{a1} and V_{g1p}.

This result owes its existence to the fact that the static characteristic is straight with the neutral point at the base, implying that the excitation generates anode-current impulses of half-sine form.

It is assumed thereby that the anode current is solely dependent on v_{g1} and v_{g2}, i.e. not on v_a, but this is actually realized only when the excitation voltage does not reach the limit characteristic: if the excitation voltage is increased until this point is reached, the anode current impulse becomes kinked and the first harmonic is reduced accordingly. Consequently, the anode current does not continue to rise; the modulation curve follows a horizontal course, and this effect is now illustrated in the case of a pentode in R.F. class B.

Fig. 67 shows the I_a/V_{g1} curve of this pentode and fig. 115 the I_a/V_a characteristics, in both instances at $V_{g2} = 300$ V. Let it be assumed that a class B setting is required that will ensure the closest approxi-

mation to a straight line in representing the relation between I_{a1} and V_{g1p}, which we shall term the amplifier characteristic, and further that the maximum permissible anode dissipation of 85 W shall not be exceeded at any point. The steady anode potential V_a is to be 1500 V.

To meet the first condition it is necessary that the absolute value of the negative bias on the control grid, at the particular screen voltage of $V_{g2} = 300$ V, is slightly less than that which is obtained at the base of the characteristic. In fig. 67 this point lies at $V_{g1} = -128$ V, and this should then really be the neutral point of the class B setting. In that case, however, the amplifier characteristic would be curved at the lower end, due to the bend in the static characteristic, as will be demonstrated later. The zero signal point is therefore placed at $V_{g1} = -100$ V, at which value there will naturally be a certain standing current, in this case 25 mA.

The second condition, concerning the anode dissipation, can only be considered in the light of the amplifier characteristics, that is, the behaviour of currents and voltages, and also power, plotted against the excitation voltage, and, for the purpose of a provisional calculation, the maximum excitation voltage will be taken to be 140 V (the most positive value of v_{g1} is then + 40 V), with a corresponding alternating anode voltage of 1250 V. The following expressions then give the values of $v_{g1}(t)$ and $v_a(t)$:

$$v_{g1}(t) = -100 + 140 \cos \omega t$$
$$v_a(t) = 1500 - 1250 \cos \omega t,$$

from which the load line is constructed (*a*, in fig. 115) and from the latter the anode current impulse (*a*, fig. 116).

The anode current I_{ao} and peak value of the 1st harmonic I_{a1} are then obtained in the manner already described, and these in turn give $R_a = 5680$ ohms,

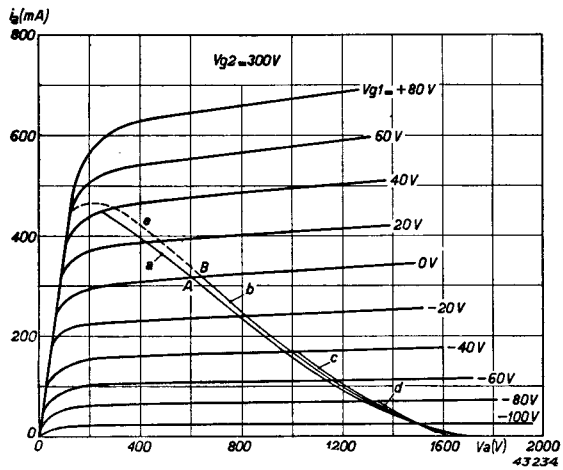

Fig. 115. $I_a - V_a$ characteristics of a pentode, with $V_{g2} = 300$ V, showing load lines for R.F. Class B, at $R_a = 5680\ \Omega$.
a) $V_{g1p} = 140$ V; *b*) $V_{g1p} = 100$ V; *c*) $V_{g1p} = 60$ V; *d*) $V_{g1p} = 20$ V; *e*) $V_{g1p} = 160$ V.

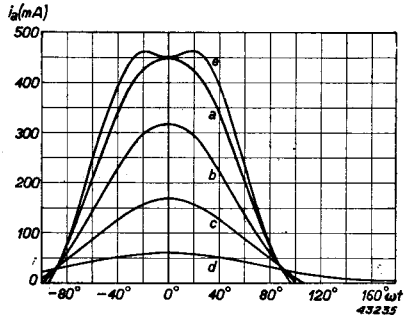

Fig. 116. Anode current impulses relating to the load lines in fig. 115.

together with W_i, W_o, W_a and η. Once the value of R_a is known, the whole calculation, with the same value of R_a, is then repeated on the basis of some other values of the excitation voltage; in this case $V_{g1p} = 100$, 60 and 20 V, corresponding to the lines *b*, *c* and *d* in figs. 115 and 116, have been selected. It should be noted that the various load lines in fig. 115 do not coincide, as would be the case if the characteristics of the valve were straight in the first instance. The load line *b* is obtained by first calculating the anode-current impulse and I_{a1} for the line *a*, with V_{g1p} at a voltage of up to 100 V (point *A*); from this and the alternating anode voltage of 895 V, R_a is then found to be 5930 ohms, which is rather too high. This is then corrected by taking point *B* to be the end of the load line, corresponding to an alternating anode voltage of 5680 . 985/5930 = 857 V (this minor alteration in the load line has practically no effect on the anode current impulse).

The result of the calculation is shown in fig. 117. Line I_{a1} is now the required gain characteristic, since the aerial current is proportional to I_{a1}; it will be seen that the line is reasonably straight, with a tendency to bend at the upper end. To give some idea of what actually takes place, a further calculation is made, for $V_{g1p} = 160$ V, still on the basis of 5680 ohms, which shows us that the load line bends at the limit line (*e*, in fig. 115), resulting in a dip in the anode-current impulse (*e*, in fig. 116). The increase in I_{a1}, W_o

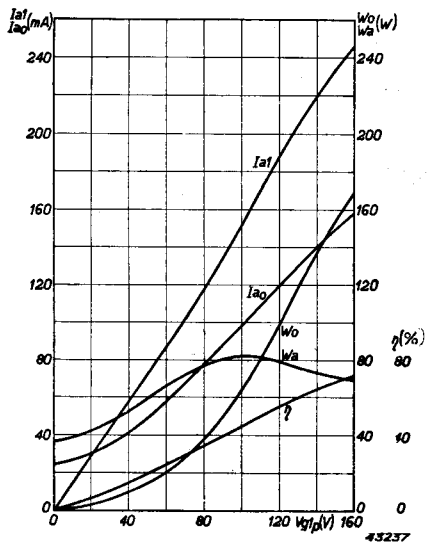

Fig. 117. R.F. Class B amplification curves of the pentode referred to in the text, with $V_a = 1500$ V, $V_{g1} = -100$ V, $V_{g2} = 300$ V, $R_a = 5680\ \Omega$.

and I_{ao} in fig. 117 is then not so sharp, and this effect becomes the more marked as the excitation voltage is raised still further and the dip in the impulse increases in size: it is at that point in the excitation voltage that the straight part of the amplifier characteristic is limited. Conversely, it may be said that the variations in V_{g1p}, produced by the modulation voltage from the preceding stage, may lie only between 0 and 160 V if distortion, for all practical purposes, is to be avoided.
As the variations in a positive sense are just as great as those that may be regarded as negative, however, the carrier wave setting of the telephony amplifier should be based on an excitation voltage of 80 V.

An objection to this method of amplification then comes to light, viz. the low efficiency. From fig. 117 it will be seen that the efficiency is roughly proportional to V_{g1p} and reaches a maximum of 72% at $V_{g1p} =$ 160 V; the fact that these two factors are approximately proportional is evident from the load lines in fig. 115. The alternating anode voltage in respect of these lines falls for practical purposes, proportionally to V_{g1p}, and the efficiency is in turn proportional to the alternating anode voltage. The maximum value of this voltage, that is, of the efficiency, occurs at $V_{g1p} = 160$ V, in which case $\eta = 72\%$; at $V_{g1p} = 80$ V (carrier wave) the efficiency is reduced by about one half, in this instance 33%. This also explains why the anode dissipation for the carrier wave is about twice the R.F. power, whereby $W_a = 77$ W, $W_o = 38$ W. Due to this low efficiency, then, the optimum amount of power is limited by the maximum value specified for the anode dissipation.
In accordance with the choice of the operating point at $I_{ao} = 25$ mA, the line I_{ao} in fig. 117 does not pass through the origin, but commences at 25 mA; the anode dissipation curve (W_a) begins at $V_{g1p} = 0$, with a value of 37.5 W. Let us now follow up the trend of the amplifier characteristic at another operating point than $V_{g1p} = -100$ V. By means of fig. 67, the quantities I_{a1} and I_{ao} as function of V_{g1p} are

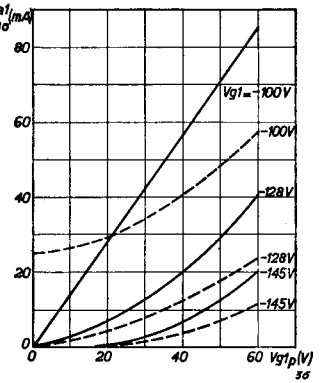

Fig. 118. Effect of negative bias on the form of the amplification curve at the R.F. Class B setting:
Full lines: $I_{a1} = f(V_{g1p})$-amplifier characteristic.
Dotted lines: $I_{ao} = f(V_{g1p})$.

then calculated in respect of $V_{g1} = -128$ V (base of the characteristic), and $V_{g1} = -145$ V. The results of these calculations are set out in fig. 118, which also includes the case of $V_{g1} = -100$ V from fig. 117. The full lines represent I_{a1}, plotted against V_{g1p}, with $V_{g1} = -100$, -128 and -145 V, and it will be seen that, when the base of the static characteristic is employed, that is $V_{g1} = -128$ V, the amplifier characteristic is curved, with its hollow side facing upwards, presumably after the similar trend evidenced by the static characteristic.

When the bias is increased to -145 V, that is into the Class C setting, the amplification characteristic remains curved and even approaches the abscissa axis, at a value of $V_{g1p} = 17$ V, which apparently represents the difference between the working point and the base of the curve, this being in agreement with what has been seen from fig. 114.
On the other hand, a reduction of the bias to -100 V produces the desired straight line, although this is accompanied by a standing current greater than zero; in any case, generally speaking, the direct anode current will be higher and this has an adverse effect on the efficiency. It is therefore important that the curvature of the static characteristics should be as slight as possible.

§ 8. Combined modulation methods

The high screen-grid current of a pentode working under anode modulation is due to the fact that the direct anode voltage, at the trough of the modulation curve, drops below the screen voltage, so that a large part of the cathode current passes to the grid. If this high screen current is to be avoided, matters must be so arranged that the screen voltage changes simultaneously with the anode voltage, and this can be achieved by modulating the screen grid as well.
The fact that it is then still possible to maintain a straight modulation characteristic will be seen from the following: it was stated in § 6 that the valve setting for anode modulation must be so contrived that the anode voltage has a controlling effect on the anode current.
To this end, the alternating anode voltage is increased as much as possible, to produce a dip in the anode-current impulse, and the more so, according as the direct anode voltage becomes less. The indentation in the impulse curve reduces the first harmonic of the anode current, which is, in effect, just what is expected. The high efficiency is accounted

for by the fact that a reduction in V_{ap} ($= I_{a1}R_a$) is accompanied by a drop in V_a; the relation V_{ap}/V_a, however, remains nearly constant. Needless to say, it is not necessary, in order to achieve this, for the reduction in I_{a1} to be brought about by the dip in the impulse; any other method of changing the size of the anode-current impulse and, therefore, also of I_{a1}, may be employed. It is essential only that the reduction in I_{a1}, that is, of $V_{ap} = I_{a1}R_a$, should keep in step with the decrease in V_{ap}; in this way a straight modulation characteristic $I_{a1} = f(V_a)$ is ensured on the one hand, whilst maintaining constant efficiency on the other. In principle, it is even possible to obtain better modulation characteristics by this method than by means of anode modulation alone.

Taking the case of a transmitting valve in class B, used for the amplification of a modulated oscillation, it should be recalled that, as stated in § 7, the valve setting must be such that the optimum alternating anode voltage is obtained at the peak of the modulation, where the value of the excitation voltage is twice that at the carrier wave. A suitable choice of control-grid bias makes it possible to obtain a very straight amplifier characteristic, whereby the first harmonic of the anode current I_{a1} and, therefore, V_{ap}, decreases in proportion when the excitation voltage is reduced. At the same time, if the direct anode voltage V_a is permitted to decrease as well, the efficiency will remain constant, since V_{ap}/V_a does not vary. If the alternating anode voltage is, say, 90% of the direct anode voltage at the commencement, this proportion is maintained throughout the whole range of the modulation characteristic, in other words, the anode voltage will never be negative as in the case of simple anode modulation, and there will be no question of a dip in the anode-current impulse. Consequently, the screen-grid current cannot rise to the extreme levels reached under conditions of simple modulation, where the limit characteristic is passed.

This may also be placed in a more general light in the following manner. In a pentode, the cathode current is controlled only by the control- and screen grids; the suppressor grid and anode merely influence the distribution of the cathode current between screen grid and anode. In both suppressor and anode modulation therefore a decrease in anode current means an increase in screen-grid current, with all the disadvantages of high screen dissipation.

To remedy matters — and this applies both to suppressor- and anode

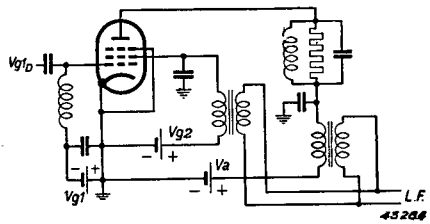

Fig. 119. Circuit of a transmitter amplifier with anode- and screen-grid modulation.

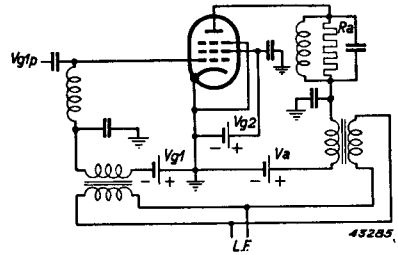

Fig. 120. Circuit of a transmitter amplifier with anode- and control-grid modulation

modulation — the modulation voltage must also be made to govern the cathode current, either through the control grid or the screen, or both, in such a manner that a decrease in anode current (i.e. aerial current) is accompanied by a drop in cathode current.
The following table provides a survey of the possible combinations together with the numbers of the figures showing the relative circuits.

Strictly speaking, figs. 121 and 124 are not true examples of combined modulation, seeing that one source of modulation is in each case in the master oscillator; these two methods are shown, nevertheless, because in connection with the other methods, their object is the improvement of the simple modulation method.

TABLE XI

Combined methods of modulation

V_a/V_{g2}	Fig. 119
V_a/V_{g1}	Fig. 120
V_a/V_{g1p}	Fig. 121
V_{g3}/V_{g2}	Fig. 122
V_{g3}/V_{g1}	Fig. 123
V_{g3}/V_{g1p}	Fig. 124

In figs. 119, 120, 122 and 123 the modulation voltage is applied to one of the electrodes by means of a modulation transformer of which the secondary winding is connected in series with the supply voltage of that electrode, the primary side being fed from an A.F. amplifier.
If use is made of a modulated excitation voltage, it is then obviously

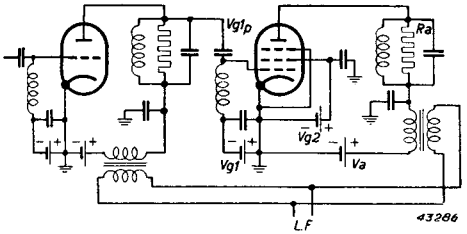

Fig. 121. Circuit of a transmitter amplifier with anode modulation, in R.F. class B.

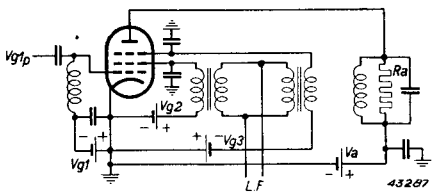

Fig. 122. Circuit of a transmitter amplifier with suppressor- and screen-grid modulation.

necessary to apply the modulation to the master oscillator supplying this voltage (figs. 121 and 124), and these examples show a triode being used as master oscillator with anode modulation.
One objection to the combined modulation method illustrated in figs. 119 to 124 is the necessity for two modulation transformers, of which the ratio of the secondary voltages must be constant at all the lower frequencies concerned, whilst the phasing of these voltages must be equal. This introduces special requirements in connection with the design of the transformers, but details of these will not be given here.

A simple arrangement, employed particularly in connection with small transmitting valves, consists in the application of the auxiliary modulation through a resistance in the supply lead to the electrode concerned. For example, if the modulation transformer for the screen in fig. 119 is replaced by a series resistance (fig. 125), modulation at the anode will be accompanied by a modulation voltage on the screen grid, and in the correct phase.

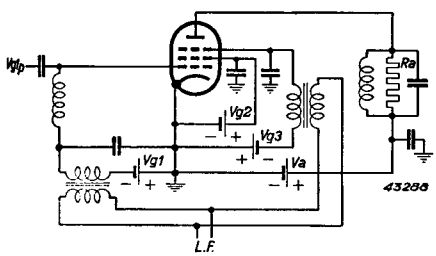

Fig. 123. Circuit of a transmitter amplifier with suppressor- and control-grid modulation.

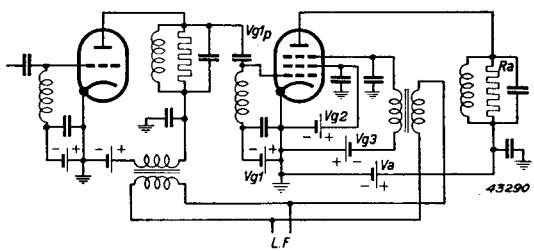

Fig. 124. Circuit of a transmitter amplifier with suppressor-grid modulation, in R.F. class B.

In this connection, it will be seen from fig. 107 that the screen current rises on a decreasing anode voltage, and, since the screen voltage in fig. 125 is determined by:

$$V_{g2} = V_b - I_{g2o} \cdot R_{g2},$$

there is a simultaneous decrease in the screen voltage.

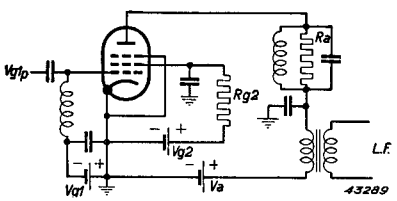

Fig.125. Circuit of a transmitter amplifier with anode-screen grid modulation and resistance R_{g2} in the screen-grid circuit.

The amount of this decrease is of course governed by the form of the curve $I_{g2o} = f(V_a)$, so the resultant screen voltage follows the form of the A.F. anode voltage only when this expression is linear. Usually, this linearity is non-existent (e.g. fig. 107) and the alternating screen voltage is then more or less distorted with respect to the A.F. voltage on the anode, but practical experience has shown that this does not normally prove an obstacle.

In the other types of combined modulation, the second modulation transformer can also be replaced by a suitable resistance, e.g. in suppressor-grid modulation, where the resistance is inserted in the screen circuit, or in anode modulation, when the resistance is connected in series with the control grid.

It is a simple matter to ascertain in each case that the secondary modulation is correctly phased and that the load on the particular electrode has been suitably reduced.

§ 9. Modulation power

In each of the modulation methods described above, the modulation voltage is applied to one or more of the electrodes of the transmitting valve in series with the supply voltage, modulation being obtained by reason of the fact that either the amount of cathode current, or its distribution between anode and screen, is modified by the modulation voltage. Broadly speaking, the currents flowing through all the other electrodes are also altered in this process, especially the current passing to the electrode to which the modulation voltage is applied. This means that, apart from the direct current component, an A.F. current also flows to the modulated electrode, in other words, that the source of modulation voltage must be capable of supplying a certain amount of power.

This quantity of power in the case of anode modulation is of an order of size different entirely from that concerned in grid modulation, because the current and voltage of the anode are so much higher than in any of the grids. The case of suppressor-grid modulation is unusual, in so far that the modulation characteristic lies wholly within the range of negative suppressor voltage, and, since this grid takes no current, the modulation power is nil.

The value of the modulation power can generally be calculated directly, once the direct current on the modulated electrode, as function of the direct voltage on that electrode, is known, given the form of the modulation voltage itself. These calculations will now be carried out with respect to the case of anode modulation (fig. 107, showing the steady anode current I_{ao}, plotted against the voltage V_a).

If the modulation voltage is sinusoidal and the modulation depth 100%, then the relation between V_a and t at a carrier-wave setting of 1500 V is represented by:

$$V_a = 1500 + 1500 \cos pt,$$

where p is the angular frequency of the modulation voltage. V_a can be calculated at any arbitrary value of pt; I_{ao} then follows from fig. 107, thus making available the relation between I_{ao} and pt. Fig. 126 shows V_a and I_{ao} plotted against pt.

The power W_i consumed by the transmitter valve is then a function of pt, viz.:

$$W_i = V_a(pt) \,.\, I_{ao}(pt) = \\ = (1500 + 1500 \cos pt)\, I_{ao}(pt).$$

Fig. 126 also shows this connection between W_i and pt, and, as in the example of the unmodulated amplifier, only the average power consumed is of any interest, this being shown in fig. 126 as $\overline{W_i}$.

In addition, W_o, as function of pt, can be

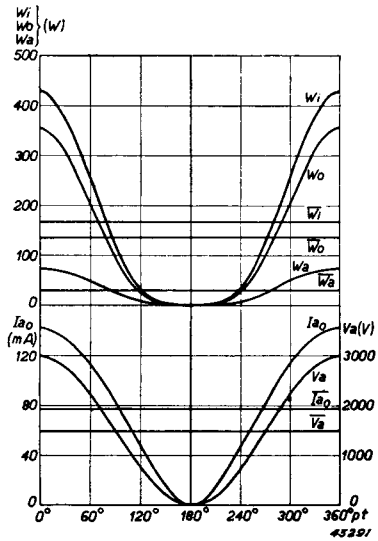

Fig. 126. Anode voltage V_a, anode current I_{ao}, input power W_i, R.F. output W_o and anode dissipation W_a as function of the time in an anode-modulated pentode, on the basis of the modulation characteristic in fig. 107 and for a modulation depth of 100%.

determined from fig. 107, and from this, in turn, the value $\overline{W_o}$ as an average over the cycle of the A.F. oscillation (fig. 126).
The average values of the various quantities, at 100% modulation, with sinusoidal modulation voltage, are then as follows:

$\overline{V_a}$	$\overline{I_{ao}}$	$\overline{W_i}$	$\overline{W_o}$	$\overline{W_a}$	η
1500 V	78 mA	168 W	137 W	31 W	81.5%

Comparison of the figures with the corresponding values for the unmodulated carrier wave, viz:

V_a	I_{ao}	W_i	W_o	W_a	η
1500 V	82 mA	123 W	99 W	24 W	80.3%

shows that the direct anode current and efficiency are hardly affected by the modulation: input and output power, and anode dissipation rise, all more or less in the same proportion, on account of the constant efficiency.
The power supplied by the source of steady anode voltage at the modulation setting is:

$$\overline{W_{io}} = \overline{V_a} \cdot \overline{I_{ao}} = 1500.78.10^{-3} = 117 \text{ W}.$$

Since the total power consumed is 168 W, the difference of 51 W must be supplied by the source of the modulation voltage.
The relation between the different power values can also be very simply demonstrated when the modulation characteristic is a straight line: thus, if the connection between I_{a1} and V_a in fig. 107 is linear and, assuming this also applies to I_{ao} and V_a at a modulation depth m, the modulation voltage being sinusoidal, the anode voltage is found from:

$$V_a = V_{ao}(1 + m \cos pt),$$

the first harmonic from:

$$I_{a1} = I_{a10}(1 + m \cos pt)$$

and the direct current from:

$$I_{ao} = I_{aoo}(1 + m \cos pt).$$

The power consumed is then:

$$W_i = V_a I_{ao} = V_{ao} I_{aoo}(1 + m \cos pt)^2,$$

and the output power:

$$W_o = {}^1/_2 I_{a1}^2 R_a = {}^1/_2 I_{a10}^2 R_a (1 + m \cos pt)^2.$$

Averaged over one cycle of the modulation voltage:

$$\overline{I_{ao}} = I_{aoo}$$

$$\overline{W_i} = V_a I_{aoo} \left(1 + \frac{m^2}{2}\right)$$

$$\overline{W_o} = {}^1/_2 \, I_{a10}{}^2 \, R_a \left(1 + \frac{m^2}{2}\right),$$

whilst the corresponding values in respect of the unmodulated carrier wave are:

$$I_{aoo}, \; V_a I_{aoo} \text{ and } {}^1/_2 \, I_{a10}{}^2 \, R_a.$$

It appears, then, that the direct anode voltage is not altered by modulation, but that the input- and output power both increase by a factor $(1 + m^2/2)$; the anode dissipation is thus increased by a similar factor and the efficiency remains the same.

Seeing that the direct anode current does not change, the source of current continues to deliver the same amount of power $V_a I_{aoo}$, and the extra power consumed, $V_a I_{aoo} \cdot m^2/2$, must be supplied by the modulator.

At a modulation depth of 100% ($m = 1$), $\overline{W_i}$, $\overline{W_o}$ and $\overline{W_a}$ are therefore $1^1/_2$ times as high as in the unmodulated condition, which means that out of the total power consumed, 2/3rds is supplied by the source of direct anode voltage and 1/3rd by the modulator.

Obviously, then, the modulator employed for anode modulation must be capable of delivering a considerable amount of power, for which reason it is usual to employ valves of the same rating as the valves to be modulated. A transmitter having anode-modulated output therefore has the disadvantage that it necessitates a very large modulation amplifier, which must, further, be capable of uniform amplification over a wide range of frequencies (e.g. 30—10.000 c/s). The advantages of this method of modulation are the high quality of the modulation and the high efficiency.

CHAPTER VI

The Transmitting Valve as Oscillator

§ 1. Principle. Circuits

In chapters III and IV the working of the R.F. power amplifier has been discussed in detail, and it has also been shown how, by means of a tuned circuit in parallel with a load resistance in the anode circuit of the valve, the power supplied by the source of the anode d.c. voltage can be converted into R.F. power in the resistance in question. To ensure high efficiency, the valve is run at class C setting, the amplitude of the excitation alternating voltage on the control grid being such that the value of the anode a.c. voltage will be only slightly less than that of the d.c. voltage.

In this process, one of the prominent factors is the gain in power, or ratio between the R.F. power developed in the resistance and the power supplied to the control grid. Now, since this gain, as we have already seen, is many times greater than unity and, since the anode a.c. voltage is moreover very much higher than the excitation voltage, it is possible to draw the required control power from the anode circuit, thus dispensing with the separate source of excitation voltage. The transmitting valve then functions as self-maintained oscillator. It is only necessary in feeding this excitation voltage from the anode circuit back to the grid, to ensure that the grid- and anode a.c. voltages are of opposite phase.

In principle, there are two methods of producing the feed-back, namely by means of a transformer, or by a potentiometer network. The transformer method, more commonly known as "inductive feedback", is depicted in fig. 127: the primary winding of the transformer is formed by the anode circuit coil L, the secondary side being the feed-back coil Lg.

Adjustment of the mutual inductance between L and Lg controls the amount of feed-back, or the ratio between the grid and anode a.c. voltages. The correct phasing of the grid voltage with respect to the anode voltage is dependent on the direction of the windings of the coils Lg and L.

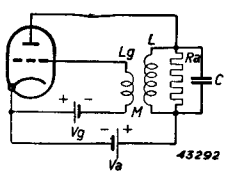

Fig. 127. Oscillator with inductive (transformer) feed-back.

In reception work, oscillators incorporating inductive feed-back are constructed with the grid in the tuned circuit and the feed-back coil in the anode circuit, but this is quite unsuitable for transmitters in so far as the oscillators serve as converters of energy, since this arrangement does not yield sufficient a.c. voltage at the anode, and this is just the important factor for efficient energy conversion. In the potentiometer method of obtaining feed-back, the obvious course is to employ the anode circuit itself as potential divider: when the inductive tapping of the anode circuit is used, we have what is known as the "Hartley" circuit (fig. 128), and, in order to ensure the required reversal of phase, the grid- and cathode connections to the anode circuit must be crossed over, so that anode and grid are taken to the extremities and the cathode to the tapping K. The amount of feed-back is controlled by the location of K; the greater L_2 is made (and therefore the smaller L_1), the stronger the feedback.

If a capacitive tapping is employed, the result is known as "Colpitt's circuit" (fig. 129). Here again, the connections from grid and cathode are "crossed", and the amount of feed-back is governed by the ratio of the capacitances of C_2 and C_1.
Oscillator circuits of the inductive or capacitive potentiometer type may also take the form shown in figs. 130 and 131 respectively, separate feed-back tappings L_p and C_p being provided; these types of circuit are employed in transmitters.

Fig. 132 shows a feed-back circuit in which the potential divider comprises a capacitance C_1 and inductance L_1 in series: because the same alternating current flows through both, the voltage on C_1 is opposite in phase to that in L_1, and by carefully adjusting the impedance of C_1, it is possible to produce an a.c. voltage in both these components together, i.e. the anode a.c. voltage, of which the phase is reversed in

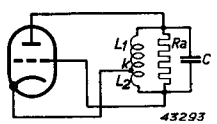

Fig. 128. Hartley circuit.

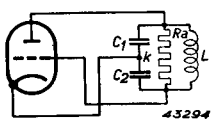

Fig. 129. Colpitts circuit.

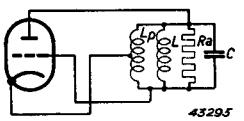

Fig. 130. Hartley oscillator with separate inductive feed-back tapping.

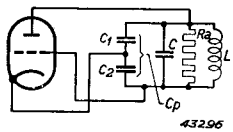

Fig. 131. Colpitts oscillator with separate capacitive feed-back tapping.

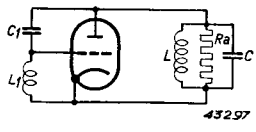

Fig. 132. Oscillator with capacitive feed-back and untuned grid circuit.

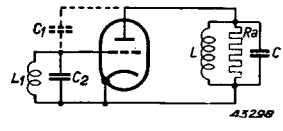

Fig. 133. As fig. 132, but with tuned grid circuit. Feed-back is established by the anode-to-grid capacitance of the valve (tuned plate – tuned grid oscillator).

relation to that of the voltage on L_1, and the excitation voltage thus meeting the requirements for maintained oscillation. The amount of feed-back is again determined by the size of C_1 and L_1; the higher the values of these, the greater the degree of feed-back.

A variation of the circuit in fig. 132 is shown in fig. 133, where the capacitance C_2 is connected in parallel with L_1. The value of C_2 and L_1 is such that the impedance of the resultant grid circuit is inductive at the working frequency; so the circuit behaves in exactly the same manner as that of fig. 132.
The capacitance C_1 in fig. 132, in parallel with the anode-to-grid capacitance C_{ag} of the transmitting valve, is usually omitted in the circuit shown in fig. 133, since the capacitance of the valve itself is in most cases sufficiently high to ensure adequate feed-back. The amount of feed-back is further controlled by the capacitance C_2, seeing that the latter influences the impedance of the grid circuit.

The various circuits of figs. 127 to 133 show, in each case, a triode, but with the exception of fig. 133, they can be applied equally well to a tetrode or pentode. This does not apply to fig. 133, because the capacitance between anode- and control grid of the latter types of valve is too low to produce the required amount of feed-back. This circuit can be employed with a pentode only when it includes an extra feed-back capacitance C_1.
The circuits depicted in the above diagrams include only the R.F. section, but it should be noted that the various supply voltages (anode, grid and heater) must be applied in such a manner that the working of the R.F. part of the circuit cannot in any way be upset and that no short-circuits can occur between the different sources of voltage.

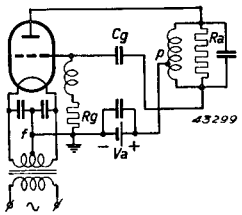

Fig. 134. Hartley oscillator complete with power supply.

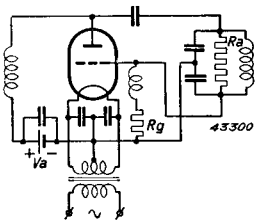

Fig. 135. Colpitts oscillator complete with power supply.

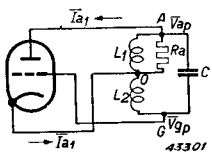

Fig. 136. Hartley oscillator with load (R_a) only across the anode section of the coil (L_1).

Fig. 134 shows the Hartley circuit complete with its power supply, as applicable to a directly heated valve, the filament voltage being derived from a transformer. To eliminate ripple, the cathode current is taken from a centre tap in the secondary winding of the heater transformer, across which two capacitances are connected to filter the R.F. components from the cathode current.

The anode voltage is introduced between filament- and anode circuits, hence the term "series-feed". The source of anode voltage is decoupled by a capacitance to by-pass R.F. currents and to prevent losses in this circuit.

A coupling condenser C_g of negligible impedance to R.F. currents, is included in the feed-back connection to the grid, to prevent the anode d.c. voltage from reaching the latter.

The grid leak R_g resistance is connected between grid and filament, direct current flowing through it to the grid and thus producing the required negative bias; a choke is included in series with R_g, to prevent R.F. currents from passing.

Fig. 135 shows the Colpitts oscillator circuit from fig. 192, complete with details of the power supply, and the difference between this and the circuit in fig. 134 lies in the anode-supply, which is obtained not through the anode circuit itself, but by parallel feed.

A choke is placed in the anode-supply line to eliminate R.F. currents from the source of anode supply, and the anode circuit again includes a coupling condenser to isolate the grid from the anode d.c. voltage.

§ 2. Calculation of frequency and amplitude. Stability and instability

Proceeding to the calculation of amplitude and frequency of the oscillation produced by the Hartley oscillator, it is necessary to modify to

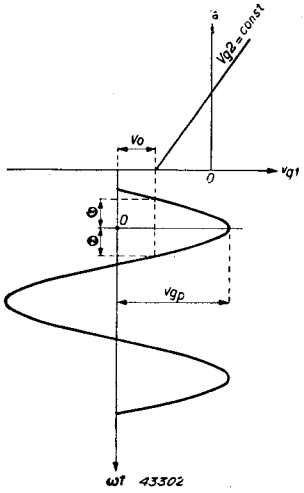

Fig. 137. Ideal i_a–v_{g1} characteristics for class C excitation.

a certain extent the circuit shown in fig. 128, to produce the arrangement depicted in fig. 136. The load resistance R_a is transferred to that part (L_1) of the total circuit inductance which occurs between the anode and the cathode, whilst the mutual inductance between L_1 and L_2 is not taken into account. This simplifies the calculation without departing from actual principles.

It will be assumed, further, that the valve is working in class C and that the static I_a/V_a characteristics are straight lines; to clarify the picture, moreover, these lines are taken to be parallel to the V_a axis. It amounts to this — that we are considering the case of the ideal pentode, although a high-gain triode would also provide a close approximation.

As indicated in Chapter IV, the anode current under the above conditions is represented by (fig. 137):

$$\left.\begin{aligned} i_a &= a\,(V_{g1} + V_{g1p}\cos\omega t + bV_{g2}), \\ &\text{for } -\Theta < \omega t < \Theta \\ \text{and } i_a &= 0 \quad \text{for} \quad \Theta < \omega t < 2\pi - \Theta \end{aligned}\right\} \quad . \; . \; . \qquad (6.\,1)$$

In this, the half-current angle Θ is given by:

$$\cos\Theta = \frac{-V_{g1} - bV_{g2}}{V_{gp}} = \frac{V_o}{V_{gp}} \quad . \; . \; . \; . \; . \qquad (6.\,2)$$

The first harmonic of this impulse-type of anode current is:

$$I_{a1} = f_1(\Theta)\,.\,I_{ap}, \quad . \; . \; . \; . \; . \; . \; . \; . \; . \qquad (6.\,3)$$

with

$$f_1(\Theta) = \frac{1}{\pi}\cdot\frac{\Theta - {}^1\!/_2 \sin 2\Theta}{1 - \cos\Theta}, \quad . \; . \; . \; . \; . \; . \qquad (6.\,4)$$

while the peak anode current is:

$$I_{ap} = a\,(V_{g1} + bV_{g2} + V_{gp}) = a\,(V_o + V_{gp}),$$

or, in view of (6. 2):

$$I_{ap} = aV_{gp}\,(1 - \cos\Theta)\,. \; . \; . \; . \; . \; . \; . \; . \; . \qquad (6.\,5)$$

From (6. 3) and (6. 5) it follows that:

$$I_{a1} = \frac{aV_{gp}}{\pi}(\Theta - {}^1/_2 \sin 2\Theta), \quad \ldots \ldots \quad (6.\ 6)$$

which latter expression, in conjunction with (6. 2), furnishes the relationship between V_{gp} and I_{a1}, as determined by the characteristic of the valve. This we term the "internal relationship".

Since the first harmonic I_{a1} flows in the anode circuit, the alternating anode voltage V_{ap} is developed in this circuit, and from the latter, by means of the feed-back, the excitation voltage V_{gp}. The anode- and feed-back circuits therefore also establish a connection between I_{a1} and V_{gp}, which we shall call the "external relationship", and this may be easily derived by means of the conventional theory of alternating currents. In order to include in the calculation the differences in phase between the various quantities, $\overline{I_{a1}}$, $\overline{V_{ap}}$ and $\overline{V_{gp}}$ will be regarded as complex quantities (see fig. 136).

Kirchhoff's first law furnishes in respect of points A and G the following expressions:

$$-\overline{V_{ap}}\left(\frac{1}{R_a} + \frac{1}{j\omega L_1}\right) + (\overline{V_{gp}} - \overline{V_{ap}})\, j\omega C = \overline{I_{a1}}$$

$$(\overline{V_{ap}} - \overline{V_{gp}})\, j\omega C - \overline{V_{gp}} \cdot \frac{1}{j\omega L_2} = 0,$$

or, when re-arranged:

$$\left.\begin{aligned} \overline{V_{gp}} j\omega C - \overline{V_{ap}}\left(\frac{1}{R_a} + \frac{1}{j\omega L_1} + j\omega C\right) &= \overline{I_{a1}} \\ -\overline{V_{gp}}\left(j\omega C + \frac{1}{j\omega L_2}\right) + \overline{V_{ap}}\, j\omega C &= 0 \end{aligned}\right\} \quad \ldots \quad (6.\ 7)$$

The effect of the grid current on the distribution of voltage in the circuit is thereby ignored.

Elimination of $\overline{V_{ap}}$ from (6. 7) yields:

$$\overline{V_{gp}}\left[j\omega C - \left(1 - \frac{1}{\omega^2 L_2 C}\right)\left(\frac{1}{R_a} + \frac{1}{j\omega L_1} + j\omega C\right)\right] = \overline{I_{a1}},$$

so that:

$$\frac{\overline{I_{a1}}}{\overline{V_{gp}}} = \left(\frac{1}{\omega^2 L_2 C} - 1\right)\frac{1}{R_a} + \frac{j}{\omega^3 L_1 L_2 C}\left[\omega^2 (L_1 + L_2) C - 1\right], \quad (6.\ 8)$$

which is the desired relation between I_{a1} and V_{gp}.

Needless to say, expressions (6. 6) and (6. 8) must yield the same result

for the ratio I_{a1}/V_{gp}. Now, in (6. 6), this ratio is real; therefore the non-real part of the right-hand term of (6. 8) must be nil [1], and this imposes the condition:

$$\omega^2 (L_1 + L_2) C - 1 = 0.$$

Also, since L_1, L_2 and C are known quantities, this means that ω must be of a value that will satisfy the above equation.
For the frequency we then have:

$$\omega = \frac{1}{\sqrt{(L_1 + L_2) C}}, \quad \ldots\ldots\ldots \quad (6.\ 9)$$

which is apparently the resonant frequency of the anode circuit. Equation (6. 8) then becomes:

$$\frac{I_{a1}}{V_{gp}} = \left(\frac{1}{\omega^2 L_2 C} - 1\right) \cdot \frac{1}{R_a},$$

or, in view of (6. 9):

$$\frac{I_{a1}}{V_{gp}} = \frac{L_1}{L_2} \cdot \frac{1}{R_a} \cdot \ldots\ldots\ldots\ldots \quad (6.\ 10)$$

Now, expressions (6. 6) and (6. 10) are to yield the same result for the ratio I_{a1}/V_{gp}; so, in order to illustrate the significance of this, both expressions have been combined in a $I_{a1} - V_{gp}$ diagram. For expression (6. 6) the values of Θ relating to different values of V_o in accordance with (6. 2) are first ascertained for a given value of V_o, after which the appropriate value of I_{a1} is obtained from (6. 6) at each value of V_{gp}. The outcome is reproduced in fig. 138, which is not limited to a single value of V_o, but covers values of from -5 to $+5$; $V_o = 0$ then relates to class B excitation, whereas positive values of V_o refer to class C and negative values to class AB. The units of current and voltage are arbitrary.
From fig. 138 it will be noticed that the relation between V_{a1} and V_{gp} as obtained from (6. 6) is represented by a curved line, only the $V_o = 0$

[1] The fact that the right-hand term of the external relation (6.8) is complex simply means, in the light of the theory of alternating currents, that there is a difference in phase between I_{a1} and V_{gp}. The internal relation (6.2) demands that the phase displacement between these two quantities shall be nil, and, in (6.8), this is met by equating to zero the hypothetical part of the right-hand term. For this reason it is said of an oscillator that the frequency is determined from the phasing.

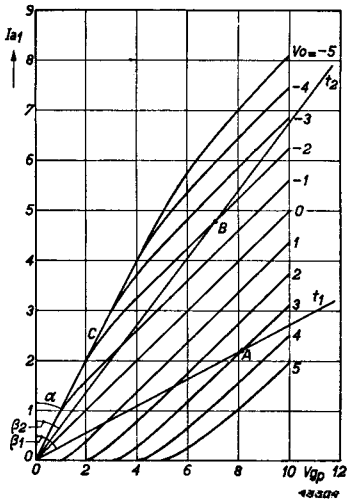

Fig. 138. Excitation characteristics giving $I_{a1} = f(V_{gp})$, with V_o as parameter, under the conditions obtaining in fig. 137.

characteristic being straight. These diagrams will henceforward be referred to as the excitation characteristics.

In contrast, expression (6. 10), giving the external relation between I_{a1} and V_{gp}, is the straight line t in the I_{a1}/V_{gp} diagram, subtending an angle β with the ordinate (fig. 138), as determined by:

$$\cot \beta = \frac{L_1}{L_2 R_a} \quad . \; . \quad (6.\ 11)$$

The angle β becomes wider and the slope of t therefore so much the more gradual as the ratio L_2/L_1 increases and, as shown by fig. 136, as this ratio determines the feed-back, t is known as the feed-back line. Fig. 138 shows two such lines: t_1 in respect of high, and t_2 for low feed-back.

Considering for a moment both the internal and external relations between I_{a1} and V_{gp} for a given instance, viz. firstly, the curve in respect of $V_o = 3$ and, secondly, the line t_1 (see fig. 138), the values of I_{a1} and V_{gp} which satisfy both equations will be represented by the point of intersection A. This is an instance of high feed-back of a valve in class C. Another example is the point B, which is the intersecting point of the feed-back line t_2 and the excitation characteristic for $V_o = -2$; this typifies a class AB setting, with weaker feed-back. It is true that in these examples the points A and B give the only possible values of I_{a1} and V_{gp}, but the point of equilibrium B is still stable, whereas A is unstable. Accordingly, when the oscillator is working at point A, i.e. at amplitudes of I_{a1} and V_{gp}, as determined by the point in question, any small disturbance, say of V_{gp}, will be enough to produce a build-up, or alternatively a decrease in amplitude, according to the nature of such disturbance. At setting B, however, a disturbance in either one direction or the other can produce no increase or decrease in amplitude, since equilibrium is soon restored. This can be explained in the following way.

Fig. 139 gives the excitation characteristic (k) of a valve working in class C, with t as feed-back line. At the point of equilibrium A, the value of V_{gp} is V; that of I_{a1} is I. Now, suppose that for one reason or another the excitation voltage increases from V to VI: according to the excitation curve k, the valve will then produce a first harmonic II, relative to point P. This harmonic generates a certain alternating voltage in the anode circuit, and, by way of the feed-back, an excitation voltage which, according to line t in fig. 139, has a value of VII, this being higher than VI. The augmented excitation VII in turn yields another first harmonic III greater than II, and it will be clear that both excitation- and anode current will in this way increase infinitely.
On the other hand, if the stable excitation V is reduced through some disturbance to $VIII$, the valve produces a first harmonic $IIII$; an excitation voltage VIV which is less than $VIII$ is then returned to the grid through the feed-back, reducing the amplitude more and more until it reaches zero. This demonstrates the instability of the point of equilibrium A.

The stability of point B in fig. 138 may be visualized with the aid of fig. 140. If the excitation voltage increases from V to VI, the valve makes a first harmonic II, of which the magnitude can be found from the excitation characteristic k. By way of the feed-back, II returns an excitation voltage VII which is less than VI, and the original deviation from the point of equilibrium is reduced.
Should the disturbance reduce the excitation voltage to $VIII$, the valve would yield a first harmonic $IIII$, feeding a voltage VIV back to the grid

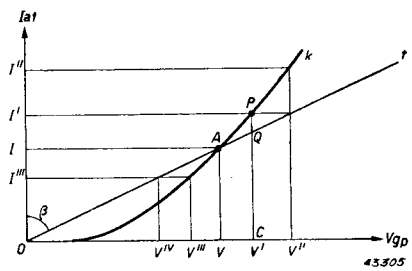

Fig. 139. Excitation characteristic (k) and feed-back line (t) of an oscillator in class C. The point A is a point of unstable equilibrium.

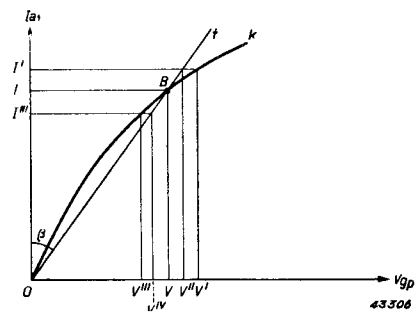

Fig. 140. The same as fig. 139, but for class AB working. The point B is a point of stable equilibrium.

which would be greater than $VIII$, again counter-balancing the effect of the disturbance.

From this it follows that an oscillator is stable when working under the conditions obtaining at point B, the distinguishing feature being that the slope of the excitation characteristic at the point of intersection with the feed-back line is less than that of the latter itself.

On the strength of fig. 138 it might be considered that the valve should always be in class AB, that is, with relatively low efficiency, but this is not necessary; an oscillator in class C can also be quite stable, provided steps are taken to change the instability of point A to one of stability, and we shall now see how this can be done.

§ 3. Stabilization of the amplitude. Intermittent oscillation

The instability at point A in fig. 139 is occasioned by the fact that when the amplitude V under equilibrium is increased, due to some disturbance, to VI, the valve gives a first harmonic PC, whereas only the first harmonic QC is necessary to maintain the proper excitation voltage VI. It must therefore be possible to stabilize the point A by coupling the valve in such a manner that it will produce a first harmonic, at the point VI, which is less than QC, and the method of achieving this is shown in fig. 141. Steps must be taken to ensure that, when the excitation voltage increases from V to VI, the valve will change over to a new excitation characteristic k_1, lying to the right of the original characteristic k, so that, at voltage VI, a first harmonic RC which is lower than QC will occur.

Conversely, if the voltage drops to VII, the valve adopts the characteristic k_2, to the left of k, so that UD is greater than TD; from the point of view of the equilibrium of A, this means that the characteristic k need no longer be taken into consideration, but the "dynamic" excitation characteristic 1,

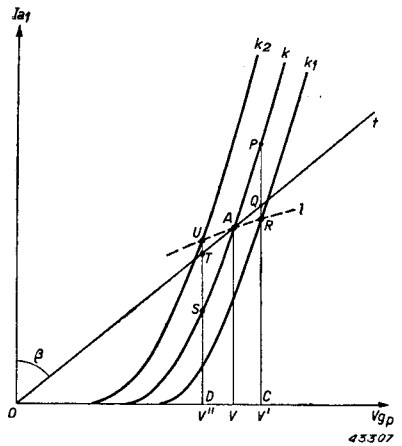

Fig. 141. The conditions shown in fig. 139 stabilized by means of a grid leak and condenser, to produce the dynamic excitation characteristic *l*.

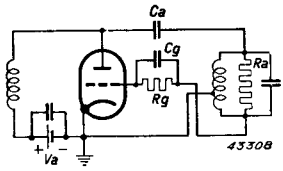

Fig. 142. Practical application of stabilization method, employing grid leak and condenser.

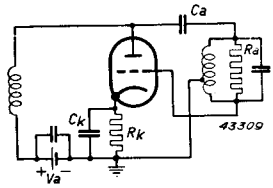

Fig. 143. Stabilization by means of cathode resistance and condenser.

of which the slope at A is not so great as at t. In this way, the conditions obtaining at point B in fig. 140 are simulated.
The displacement of k to the left or right is obtained, as shown in fig. 138, at a higher or lower value of the parameter V_o, that is, according to (6. 2), at higher or lower values of the bias on the control grid: in effect, when the excitation voltage is increased, the bias must also increase.
This is easily brought about by means of the grid leak R_g (fig. 142) and the decoupling condenser in the grid circuit. The grid current flowing through R_g from the cathode to the grid then produces the negative grid bias $V_g = -I_{go}R_g$; the R.F. components of the grid currents pass through C_g. If now the excitation voltage temporarily increases, the direct grid current also rises and, with it, the grid bias, transferring the working point of the valve from the excitation characteristic k (fig. 141) to k_1, which lies more to the right: provided this shifting effect is sufficiently pronounced, the stabilized condition described above is then reached.

Instead of a grid leak, a cathode resistance R_k, with condenser C_k, may be used (fig. 143) for stabilization purposes, in view of the fact that increased excitation is accompanied by an increase in the cathode current. Utilizing this voltage drop in the cathode resistance for biasing purposes, we then again have the situation shown in fig. 141) [1].
The foregoing considerations are based partly on the form and position of the excitation characteristic as reproduced in fig. 138, and in plotting

[1] On the strength of the expression $V_o = -V_{g1} - bV_{g2}$, not only V_{g1}, but also V_{g2} can be employed as stabilizing voltage in the sense that V_{g2} must decrease when V_{gp} rises. This is effected by placing a resistance in series with the screen grid. Since V_{g2} is multiplied by b (i.e. the conductance of g_2 through g_1) and this is rather less than 1, the stabilizing effect of V_{g2} is not particularly marked. In the case of triodes, V_a should be read for V_{g2}.

these characteristics it has been assumed that the anode-current impulses in each case have the form of sine peaks.

This is correct, however, only so far as the anode current does not bring the setting of the valve up to the limit characteristic; if the latter is intersected, an inflexion in the curve occurs which has a limiting effect on the magnitude of the first harmonic of the anode current.
To ascertain the actual effect of this inflexion upon the form of the excitation characteristic, let us now assume that the static characteristics and load line are as shown in figs. 98 and 100.
The value of the first harmonic at a given excitation voltage has already been developed in chapter V (equation 5. 21), viz:

$$\frac{\pi I_{a1}}{aV_{gp}} = \Theta - {}^1/_2 \sin 2\Theta - \beta - {}^1/_2 \sin 2\beta + 2 \cos \Theta \sin \beta = g_1 (\Theta, \beta), \quad (6.12)$$

in which

$$\cos \beta = \frac{-V_{g1} - bV_{g2}}{V_{gp}} \quad . \quad . \quad . \quad . \quad . \quad . \quad . \quad . \quad (6.\ 13)$$

and

$$\cos \beta = \frac{V_a}{V_{ap}} = \frac{V_a}{I_{a1} R_a} \quad . \quad . \quad . \quad . \quad . \quad . \quad . \quad . \quad (6.\ 14)$$

It will suffice here to consider only the case of class B excitation, where $\Theta = \pi/2$ and

$$\frac{\pi I_{a1}}{aV_{gp}} = \frac{\pi}{2} - \beta - {}^1/_2 \sin 2\beta \quad , \quad . \quad . \quad . \quad . \quad . \quad . \quad (6.\ 15)$$

from which I_{a1} can be calculated as function of β.
On the other hand, it follows from (6. 14) that:

$$I_{a1} = \frac{V_a}{R_a \,.\, \cos \beta} \quad . \quad . \quad . \quad . \quad . \quad . \quad . \quad . \quad . \quad (6.\ 16)$$

From (6. 15) and (6. 16), elimination of I_{a1} yields:

$$\frac{V_a}{R_a \,.\, \cos \beta} = \frac{aV_{gp}}{\pi} (\pi/2 - \beta - {}^1/_2 \sin 2\beta) \quad , \quad . \quad . \quad . \quad (6.\ 17)$$

in which β is calculable for any value of V_{gp}, given V_a and R_a. Once β is known, I_{a1} as function of V_{gp} can be obtained from (6. 15). These formulae apply only so far as the anode current impulses are inflected so that $\beta > 0$, and this is naturally only the case when the excitation voltage is high enough.
On decreasing the excitation voltage a point is reached where $\beta = 0$, and

the voltage at this point will be termed V_{gpo}, with first harmonic I_{a1o}. From (6. 15) the values of this voltage and first her monic are found to be as follows:

$$\frac{\pi I_{a1o}}{aV_{gpo}} = \frac{\pi}{2}, \quad \ldots\ldots\ldots \quad (6.\ 18)$$

and from (6. 17):

$$\frac{V_a}{R_a} = \frac{aV_{gpo}}{\pi} \cdot \frac{\pi}{2} = \frac{a}{2} V_{gpo} \quad \ldots\ldots\ldots \quad (6.\ 19)$$

out of (6. 17) and (6. 19) we have:

$$\frac{1}{\cos\beta} = \frac{V_{gp}}{V_{gpo}} \cdot \frac{2}{\pi}\left(\frac{\pi}{2} - \beta - {}^1/_2 \sin 2\beta\right) \quad \ldots\ldots \quad (6.\ 20)$$

and from (6. 15) and (6. 18):

$$\frac{I_{a1}}{I_{a1o}} \cdot \frac{V_{gpo}}{V_{gp}} = \frac{\pi/2 - \beta - {}^1/_2 \sin 2\beta}{\pi/2} \quad \ldots\ldots\ldots \quad (6.\ 21)$$

Elimination of V_{gp}/V_{gpo} from (6. 20) and (6. 21) finally gives:

$$\frac{I_{a1}}{I_{a1o}} = \sec\beta \ldots\ldots\ldots \quad (6.\ 22)$$

In fig. 144, I_{a1}/I_{a1o} and β are plotted against V_{gp}/V_{gpo}, β being calculated from (6. 20) and I_{a1}/I_{a1o} from (6. 22).

From the latter figure it will be seen that the excitation characteristic is the normal straight line relevant to the class B setting, as long as the limit characteristic is not reached ($V_{gp}/V_{gpo} < 1$), whereas beyond that point a marked limiting effect sets in. Qualitatively, the above calculations relating to class B apply equally well to class C, and the latter case is presented in fig. 145, curve k. The intersecting point A on the line k with the feed-back line t corresponds to point A in fig. 138, but as a result of the above mentioned limitation, k and t now have a second common point B, where the slope is less than that of the feed-back line; this point, then, is stable. It therefore follows that in class C, too, a valve having fixed grid bias can also produce a stable oscillation.

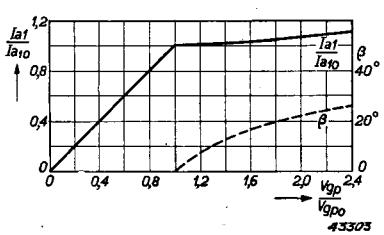

Fig. 144. Excitation characteristic for class B excitation, with over-excitation.

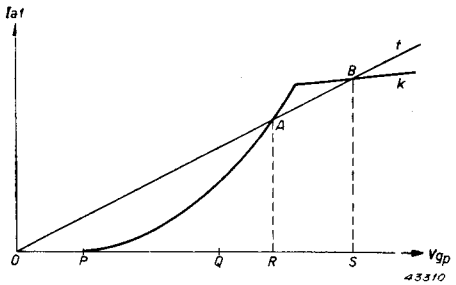

Fig. 145. Excitation characteristic for class C setting, showing limitation imposed by the alternating anode voltage.

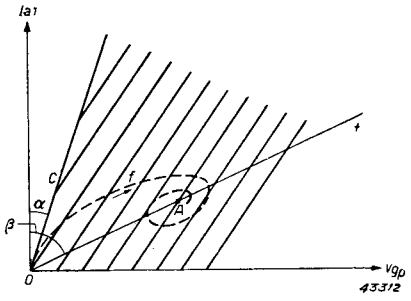

Fig. 146. Gain in the oscillation as shown by the line *f* when grid leak and condenser are used.

It should be noted, however, that, in order to establish these conditions, the valve must be given, in one way or another, an excitation voltage which is greater than OR. The point A, as already pointed out, represents a state of unstable equilibrium; an excitation voltage less than OR therefore becomes smaller and smaller until it reaches zero, whereas a voltage greater then OR increases until the stable value OS is reached at point B.

As a corollary of the foregoing it may be said that a valve in class C, with fixed grid bias, cannot adjust its own setting to the point B, but from fig. 145 it does follow that the first harmonic of the anode current disappears as soon as the excitation voltage drops below OP. The excitation characteristic k may therefore be imagined as extended along the abscissa from P to O. At O, t is again steeper than k and O is therefore a point of stable equilibrium, which fact is self-explanatory, since in class C the standing anode current is zero.

This brings to light a further advantage in the use of a grid leak, namely the effect whereby the oscillation, starting from zero, gains in strength from the moment the anode voltage is applied. At that precise moment the excitation voltage is still zero, and there is therefore no grid current or bias, which means that the valve is in class A. The slope of the relevant characteristic c (fig. 146) is then at a maximum, and, if angle β between t and the ordinate axis is greater than α, between c and the same axis, O will be a point of unstable equilibrium. The slightest disturbance, such as the impulse imparted by switching on the voltage, is then sufficient to produce a build-up of the oscillation. When the excitation voltage is increased, the control-grid current also rises, together with

the grid voltage; the point representing the setting of the valve at any given moment from the relevant values of I_{a1} and V_{gp}, moves therefore along the curve c, towards characteristics relating to more negative values of grid voltage. Fig. 146 shows the path accordingly followed by this point in the I_{a1}/V_{gp} diagram, this being the line f. Theoretically, the line f usually follows a spiral course, approaching the point A on line t asymmetrically: once this point is reached, conditions of equilibrium are established, as at the equivalent point in fig. 141. Line 1, which has been described as a dynamic characteristic, is, in effect, only a special variation of the line f in fig. 146, but in the above comments on fig. 141 it has nevertheless been assumed that the grid bias increases considerably when the excitation voltage is increased, namely until the characteristic k and point R are reached.

In practice, however, it is just this instantaneous response that does not take place, due to the presence of the grid condenser C_g (see fig. 142). With any change in the excitation voltage, the grid current increases by a certain amount and the additional current flows partly through R_g and through C_g, charging the latter to a higher voltage. It is only after C_g has been fully charged and no further charging current is necessary, that the whole of the increased grid current passes through R_g, and only then will the grid voltage have reached its definite value.

It would appear, then, that the direct grid voltage lags behind the variations in the excitation voltage, and this explains why the working point in fig. 146 describes a spiral path around A. The conclusion can be immediately drawn that the delay exhibited by the direct grid voltage with respect to the excitation voltage is so much the greater when the values of C_g and R_g are increased, since, the larger C_g becomes, the longer it takes to charge it, whilst the higher the value of R_g, the smaller will be the portion flowing through it when the grid current is varied; in other words, the longer it will take for equilibrium to be restored.

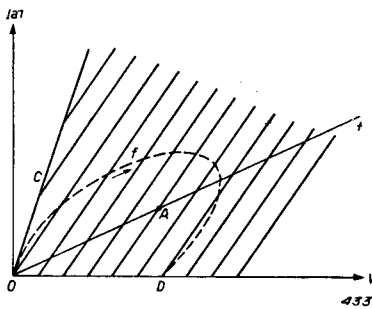

Fig. 147. Change in oscillation amplitude under conditions of intermittent oscillation.

In such cases, the working point of the valve, starting at O, will describe a line f of which the slope is greater than the normal (see fig. 147), whereby the characteristics at higher values of V_g are by no means so quickly reached, whilst in the return branch as well, the excitation characteristics are cut at small angles. The working point then shows a tendency to describe a much wider arc round A.

The result of this may well be — as illustrated in fig. 147 — that the return path of the line f will cut the abscissa at a point D. At that point and further at the relative excitation voltage, the grid bias is so high that the anode current, and with it the first harmonic, decay away to nothing. Consequently, the feed-back voltage also becomes non-existent and the excitation voltage drops from OD to zero. Grid current also ceases to flow, and the grid condenser discharges through the grid leak, so that the grid bias slowly decreases in value. When the latter has decreased so far that, at the given anode voltage, a class A setting is again reached, oscillation recommences and the whole process is repeated. Oscillation is therefore intermittent and the frequency at which the interruption occurs is lower as C_g and R_g are increased in value.

Apart from high values of grid condenser and leak, intermittent oscillation can also be produced by a strong feed-back combined with a low slope of the control-grid current characteristic: the first method means that the angle between t and the V_{gp}-axis (see fig. 146) is reduced, so that the point A appears lower down in the diagram. In otherwise similar circumstances, therefore, the return path of f intersects the abscissa.

If the slope of the grid-current characteristic is small, the grid current and also the bias will gradually increase as the excitation voltage becomes greater; the path of f (fig. 147) starting from O then cuts the successive excitation characteristics at a small angle, so that f describes a wide arc round A, the chances being very great that it cuts the abscissa on its return. The particular case of the characteristic 1 in fig. 141 is then approximated as soon as conditions are such that the grid bias will rapidly follow any variation in grid current, that is, of the excitation voltage. This means that the value of C_g must be such as to ensure that the charging current passing through C_g when the grid voltage is changed, is small with respect to the variation in current in R_g: this is achieved to an increasing degree according as C_g and R_g are made lower in value.

§ 4. Applications

a) *Transmitter driving stage*

The oscillator plays an important part in all transmitters inasmuch as it is the means of initiating the frequency of the power to be radiated by the transmitting aerial, one or more amplification stages being interposed between the oscillator and the aerial to increase the power. The working of these amplifiers has been described in Chapters III and IV.
In certain circumstances it may be desirable that the oscillator does not directly generate at the frequency of transmission, but at another which is an integral fraction lower, the transmission frequency then being obtained by means of frequency multipliers (see Chapter VII).
The indicated procedure is then to employ for the oscillator one of the circuits described in the preceding chapter, but there is an objection to this, namely that the frequency of such oscillator circuits is not very constant unless special precautions are taken. From the calculation in § 2 it might be concluded that the frequency generated is determined solely by the values of the inductance and capacitance of the anode circuit, but in these calculations a number of factors have been ignored, of which the more important are the inter-electrode capacitances of the valve and the control-grid current. The valve capacitances are in any case in parallel with the anode circuit, that is, the whole of C_{ag}, as well as C_{ak} and C_{kg} in series with each other. Naturally these capacitances, being part of the anode circuit, also have a share in determining the frequency, and any variation such as a change in temperature, space charges etc, will in practice produce a corresponding change in the oscillator frequency, this change being much the more marked when the valve capacitances form a considerable part of the total circuit capacitance, especially at the higher frequencies.
In the oscillator circuit, the control-grid current behaves as a resistance in parallel with the feed-back impedance, e.g. in the circuit, fig. 136, in parallel with L_2, and as such the grid current influences not only the amount of the voltage fed back, but also its phase with respect to the first harmonic I_{a1}, and therefore the frequency also, as seen in § 2. Every variation in the grid current thus affects the frequency, and as main causes of such changes in grid current it is only necessary to mention variations in the direct anode voltage and in the emission of the cathode. Closer investigation into the frequency of an oscillator proves that these

disturbing influences have a less marked effect according to the amount of improvement that can be made in the quality of the anode circuit, that is, according as the resonance curve is sharpened.
To this end use is made of quartz crystals in conjunction with the oscillator in a transmitter, in view of their low losses and very sharp resonance curve, but for the special circuits to be used with crystals, as well as for the properties of the latter, reference should be made to works on transmitting techniques.

b) *R.F. melting furnaces*

When a piece of metal is placed within an alternating magnetic field, eddy currents are generated in the metal, which, due to the finite resistance of the latter, develop heat. Using an oscillator equipped with transmitting valves it is thus possible in a very simple manner to generate

Fig. 148. R.F. oscillator for metal smelting, equipped with transmitting valve TA 20/250 (and one spare valve), capable of producing a power of 250 kW at an anode voltage of 20 kV.

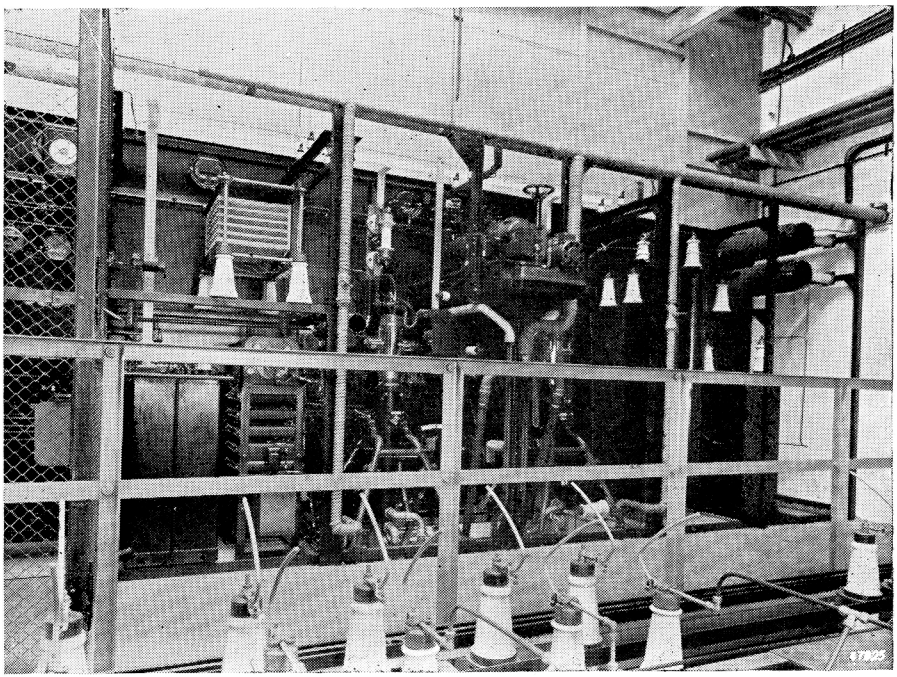

an alternating magnetic field of high frequency and sufficient strength.

The circuit for an R.F. smelting furnace does not differ in principle from that of any other type of oscillator, but, as the crucible of metal is placed in the magnetic field of the anode-circuit coil, it is essential for the current in that part of the circuit which includes the crucible to be extremely high, in order to ensure a sufficiently strong field. For this reason the anode circuit is frequently built up from a number of different windings working together after the manner of a transformer, to provide a very high current in the work coil, which then has to be water-cooled. Fig. 148 depicts the equipment employed for R.F. metal smelting equipped with a transmitting valve TA 20/250 and a spare valve, producing 250 kW at 20 kV anode voltage.

Fig. 149 illustrates the anode-circuit coil and condenser employed in

Fig. 149. Anode circuit coil and condenser used in the equipment shown in fig. 148.

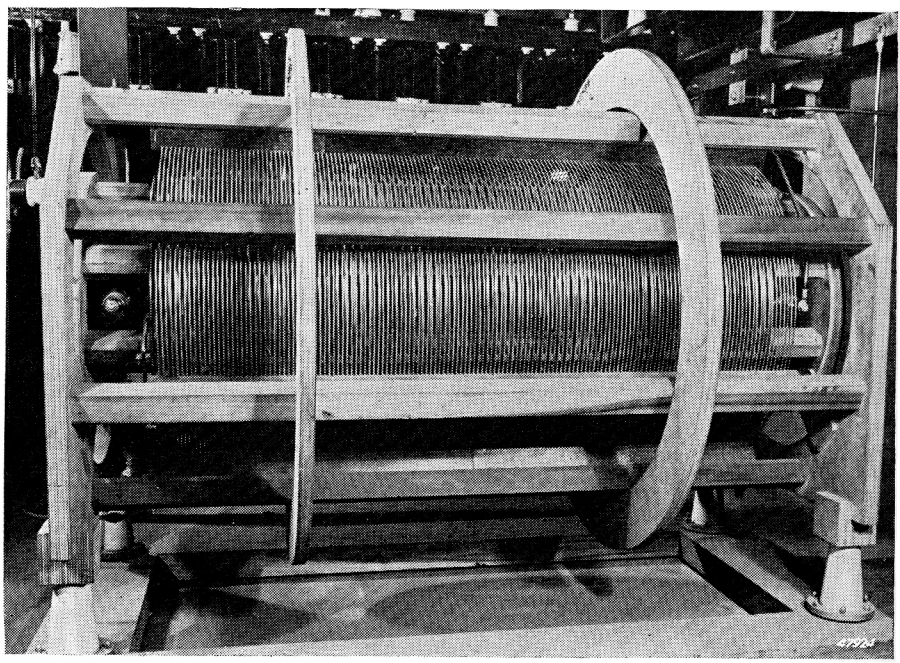

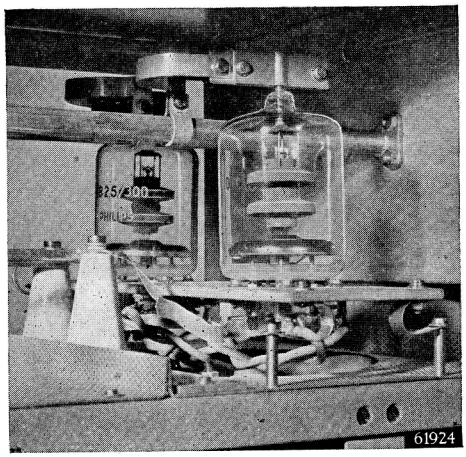

Fig. 150. Equipment for pre-heating synthetic resin by the dielectric method, employing two valves type TB 2.5/300.

this unit, which is capable of smelting about 100 kg of metal in a quarter of an hour.

c) *Dielectric heating*

In dielectric heating use is made of the heat generated in a material in consequence of the dielectric losses occurring when the material is placed in a high-frequency electric field.

The heating effect per cubic centimetre of material is proportional to the square of the field strength, to the dielectric constant, the angle of loss (tan δ) and the frequency. Because of this dependence on frequency, the frequencies employed for dielectric heating are of a high order, being between 10 and 30 Mc/s, or higher. The material or work to be heated is usually inserted between one or more metal plates which constitute the electrodes of a capacitor; for safety reasons, amongst others, these do not form part of any circuit carrying a direct current with earth return. At the same time, the absence of a direct voltage means a somewhat smaller potential difference between the electrodes of the capacitor, with less risk of flash-over to the work placed between them.

Fig. 150 shows a practical type of H.F. pre-heating unit for heating compressed synthetic-resin bonded material, equipped with two Philips transmitting valves Type TB 2.5/300 which are capable of delivering 300 W at 1800 V anode voltage. To give some idea of the capacity of this unit it may be said that about 100 grammes of synthetic resin can thus be raised to the required temperature in about 40 seconds.

d) *Diathermy*

In diathermy, use is made of the heating effects set up by R.F. currents when passed through the human body. The frequency of the current is of the order of 20—40 Mc/s and the method adopted may be one of two

alternatives, viz. treatment either in an electrical field or in a magnetic field. In the first instance the limb is placed between two electrodes carrying the R.F. voltage, when the capacitive current from the condenser thus formed passes as a conducted current through the limb and produces the required heat. In the second method the limb is placed in the magnetic field of a coil and the heat is produced by the eddy currents generated in the limb.

The short-wave therapy apparatus developed by Philips works on the balanced-stage principle; fig. 151 shows the circuit of this type of oscillator. The cathodes of the valves T_1 and T_2 are shorted; the anode circuit lies between the two anodes and the grid circuit between the grids. Direct voltage is supplied to both anode- and grid circuits at the centre tappings of the coils, at *a* and *g* respectively.

This type of oscillator may be regarded virtually as comprising two oscillators having tuned anode and grid, and feed-back derived from the anode-to-grid capacitance of the valve as depicted in fig. 133. Fig. 152 shows the two oscillators separately; they can work individually, but this makes no difference if common sources of voltage are used.

The circuit in fig. 151 differs only in so far that both anode- and grid circuits have been combined, which does not materially alter the situation, except that, due to the coupling between the two halves of the anode- and grid circuits, the alternating anode voltages of the two valves are reversed in phase; the same holds good for the grid voltages. Further, since the amplitudes of the valves are the same, the centre points *a* and *g* of the two coils are at zero point of the R.F. voltage, and the obvious step is therefore to apply the power at those points.

According as the frequency at which the oscillator is to work is increased,

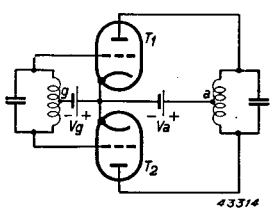

Fig. 151. Balanced oscillator with feedback across the anode-grid capacity.

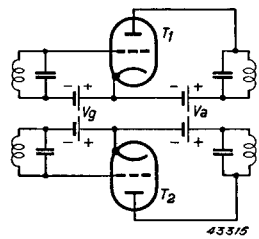

Fig. 152. Balanced oscillator represented as two oscillators as in fig 133, working separately.

the self-inductance and capacitance of the two circuits must be decreased until finally the point is reached where the capacitances of the valves themselves establish the minimum limit. This minimum limit is seldom used, since the circuit capacitance then consists solely of the valve capacitance (and stray capacitance of the coil and wiring); this means that the change in frequency due to warming-up of the equipment after the switch is closed must be fairly considerable. This drawback can be eliminated by employing a crystal-controlled oscillator, followed by a number of amplification stages after the manner of a telegraph transmitter. In practical types of non-controlled diathermy sets, the anode voltage can be either A.C. derived direct from a transformer, or rectified A.C. (full wave), usually without smoothing filter, in order to save space and weight. The latter method has the advantage that the valve receives positive anode voltage with each half cycle of the mains frequency and thus delivers power, whereas, when unrectified A.C. is used, positive and negative half cycles are applied to the anode in succession and the output power is only one half of what is delivered with full-wave rectification of the alternating current.

A circuit incorporating the TB 2.5/300 transmitting valve as fed by means of two rectifiers type DCG 4/1000 is shown in fig. 153. This is a Hartley circuit in which the anode is choke-fed to prevent any radio frequencies from the oscillator from passing back to the rectifier. The circuit coil consists of a single winding to which the load is coupled inductively; the coupling is sub-critical and is made variable as a means of control on the output.

The patient is connected to the oscillator through a tuned circuit

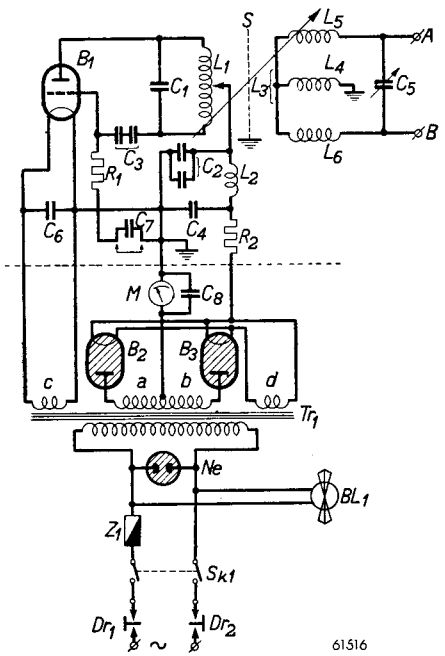

Fig. 153. Circuit of diathermy equipment employing one TB 2.5/300 and two rectifiers type DCG 4/1000.

by means of flexible cables attached to electrodes, between which the affected limb is placed.

e) *Supersonic vibrations*

Supersonic oscillations are vibrations of which the frequency lies above the range of human audibility, of about 20,000 c/s. Oscillations of this type are generated nowadays preferably by means of oscillators incorporating transmitting valves, and there are two main types of oscillator: the magnetostrictive and the piezo-electric.

The principle of the former is based on the peculiarity exhibited by ferro-magnetic metals, notably nickel, that they undergo a change in volume under the influence of a magnetic field. The sign of this change in volume depends upon the direction of the magnetic field; a nickel rod placed within a magnetic field always decreases in length, to an increasing degree as the field strength is raised, although the relation between the two quantities is not linear. Thus, if the rod is placed inside a coil through which an alternating current is flowing, the rod will vibrate at twice the frequency of that current. Should it be required that the rod vibrates at the same frequency as that of the current, it must be premagnetized to such a degree that the direction of the resultant field will always be the same.

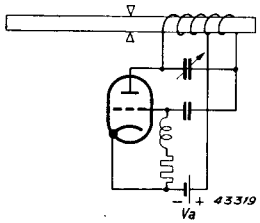

Fig. 154. Magnetostrictive oscillator, with Hartley feed-back circuit.

The amplitude of the vibrating rod reaches a maximum when its own mechanical frequency is the same as that of the magnetic field; in other words the rod is then in resonance with the field.

Fig. 154 is a diagram of the magnetostrictive oscillator circuit, the electrical portion being a Hartley oscillator. The variable condenser in the anode circuit makes it possible to tune the frequency so that the rod resonates; the rod is fixed at the centre and the two ends vibrate longitudinally.

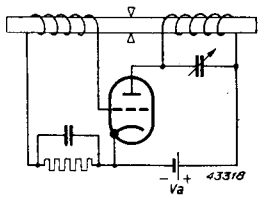

Fig. 155. Magnetostrictive oscillator, with feed-back coil mounted in the vibrating rod.

In fig. 155 the feedback takes place via the rod. Here use is made of the reversed magnetostriction effect consisting in the periodical change of magnetization due to the vibration of the rod, thereby inducing in the feedback

coil wound round the rod an alternating voltage which is applied to the grid and thus sustains the oscillation of the valve.

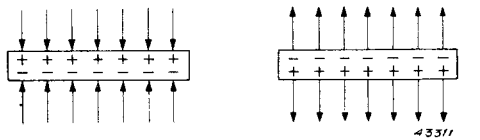

Fig. 156. Relation between the direction of mechanical force and sign of the charge in a quartz crystal.

In the piezo-electric oscillator use is made of the properties of a quartz crystal. When this is compressed in the direction of the so-called electrical axis (see fig. 156) charges of opposed sign arise at the two ends; when the direction of the mechanical force is reversed, also the sign of the charges is reversed. This is the direct piezo-electric effect. The reverse effect also exists: when the crystal is placed in the electric field of a capacitor it contracts or expands according to the direction of the field.

Fig. 157 shows the principle of an ultra-acoustic oscillator with quartz crystal. The crystal K has metal electrodes and is connected in parallel to the anode circuit of a Hartley oscillator. This can be used for small powers in cases where the efficiency of the installation is of minor importance. For larger powers, say of 1 kW, where efficiency is more important, the anode alternating voltage is not large enough to cause the crystal to yield this acoustic energy; the alternating voltage on the crystal has then to be of the order of 20,000 V. This is related to the very high electric impedance of the crystal, which is of the order of 1 megohm. Since a valve of such power has a matching impedance of some thousands of ohms, a transformer T (see fig. 158) has to be connected between the anode circuit and the crystal. This is mostly a Tesla transformer, which has the property of stepping up the anode alternating voltage very high.

For these applications the quartz crystal is placed in oil, because in air the amplitude would be too great and the crystal would become

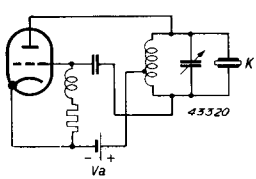

Fig. 157. Circuit of supersonic oscillator with quartz crystal, suitable for very low power.

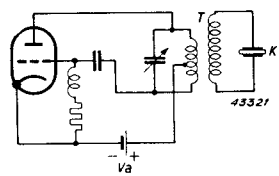

Fig. 158. Supersonic oscillator with quartz crystal, for high power. *T* is the Tesla transformer.

defective. At the same time the oil forms a good insulation for the high tension between the electrodes and serves as a medium for transmitting the acoustic energy.

Among the purposes for which ultra-acoustic generators are employed may be mentioned echo-sounding for determining the depth of navigable fairways and the proximity of other vessels, and the manufacture of fine-grained photographic emulsions and of explosives.

CHAPTER VII

The Transmitting Valve as Frequency Multiplier

§ 1. Principle

In Chapter III, §§ 1 and 2, an explanation is given of the method of analyzing the anode current impulses to form Fourier progressions consisting of a D.C. term and a number of other terms which are dependent sinusoidally upon t and of which the frequencies are multiples of the excitation frequency ω. We can write:

$$i_a(t) = I_{ao} + I_{a1} \cos \omega t + I_{a2} \cos 2\omega t + \ldots\ldots$$

In the subsequent §§ of the same chapter the working of the transmitting valve was investigated in the case of an anode resistance R_a and parallel L–C circuit, tuned to ω.

When this circuit is tuned to a higher harmonic, for instance to 2ω, the latter encounters high impedance in the parallel circuit of L and C, and this component consequently takes the path through the resistance R_a. This means that the power developed in R_a is of twice the excitation frequency, in other words, the valve functions as a frequency doubler.

Tuning to any other frequency component is equally possible and the valve then works, in general, as a frequency multiplier, but, as in practice frequency doubling is the most widely used, this only will form the subject of the following discussion.

The working of the valve as a frequency doubler, as in the case of the ordinary amplifier, is best considered in relation to the load line in the I_a/V_a diagram. The construction of this line is based on the fact that the alternating grid- and anode voltages are sinusoidal functions of time, the first at a frequency ω, the second at frequency 2ω, and, further, that the relation between the alternating anode voltage and the 2nd harmonic of the anode current is given, by Ohm's law, as:

$$V_{ap} \cos 2\omega t = I_{a2} R_a \cos 2\omega t.$$

Therefore:

$$v_g(t) = V_g + V_{gp} \cos \omega t \quad \ldots\ldots\ldots \quad (7.\ 1)$$

$$v_a(t) = V_a - V_{ap} \cos 2\omega t \quad \ldots\ldots\ldots \quad (7.\ 2)$$

Given V_g, V_{gp}, V_a and V_{ap}, the quantities $v_g(t)$ and $v_a(t)$ are obtained from these formulae as functions of t, after which the appropriate value of $i_a(t)$ is found from the I_a/V_a diagram.

In order to obtain some idea of the different possibilities, let us again consider the case of a triode of which the anode-current characteristics are straight lines, of the form:

$$i_a = a\,(v_g + bv_a), \quad \ldots\ldots\ldots \quad (7.\ 3)$$

to hold good only when $v_a < 0$ and $0 < i_a \leqq \sigma v_a$.
The relation between i_a and t is found by substituting (7. 1) and (7. 2) in (7. 3):

$$i_a = a\,[V_g + bV_a + V_{gp}\cos\omega t - bV_{ap}\cos 2\omega t], \quad \ldots \quad (7.\ 4)$$

which expression, in view of the restricted validity of (7. 3), can be used only for values of ωt which will yield $i_a \geqq 0$. From the practical point of view this means that the valve is excited in class C and the anode current is of the impulse type.
The half current angle Θ is therefore given by:

$$0 = a\,[V_g + bV_a + V_{gp}\cos\Theta - bV_{ap}\cos 2\Theta].$$

Employing $\cos 2\Theta = 2\cos^2\Theta - 1$, we derive a quadratic equation for $\cos\Theta$, viz:

$$2bV_{ap}\cos^2\Theta - V_{gp}\cos\Theta - \{V_g + b\,(V_a + V_{ap})\} = 0.$$

From this it follows that:

$$\cos\Theta = \frac{V_{gp} - \sqrt{V_{gp}^2 + 8bV_{ap}\{V_g + b\,(V_a + V_{ap})\}}}{4bV_{ap}}.$$

(The negative root only is of importance in calculating the width of the impulse.)
In the case of a pentode, a further term cV_{g2} must be included in the expression for i_a (7. 3) (see Chapter IV, § 4).
Expression (7. 4) then gives us:

$$i_a = a\,[V_{g1} + bV_a + cV_{g2} + V_{g1p}\cos\omega t - bV_{ap}\cos 2\omega t],$$

and Θ is then calculated from:

$$0 = V_{g1} + bV_a + cV_{g2} + V_{g1p}\cos\Theta - bV_{ap}\cos 2\Theta.$$

From the latter it follows that:

$$\cos\Theta = \frac{V_{g1p} - \sqrt{V_{g1}{}_p^2 + 8bV_{ap}\{V_{g1} + cV_{g2} + b\,(V_a + V_{ap})\}}}{4bV_{ap}}. \quad (7.\ 4a)$$

In the ideal pentode, $b = 0$, so that:

$$\cos \Theta = \frac{-V_{g1} - cV_{g2}}{V_{g1p}} \quad \ldots\ldots\ldots \quad (7.\ 4b)$$

The quantity c is the reciprocal of the amplification factor between the 2nd and 1st grids.

The shape of the load line in the I_a/V_a diagram is found by eliminating ωt between (7. 1) and (7. 2) and substituting the value of v_g thus found in (7. 3). From (7. 2) it follows that:

$$x = v_a(t) = V_a - V_{ap} \cos 2\omega t = V_a - V_{ap}(2\cos^2 \omega t - 1);$$

then:

$$\cos \omega t = \sqrt{\frac{1}{2}\left(1 + \frac{V_a - x}{V_{ap}}\right)}.$$

Expression (7. 1) then becomes:

$$v_g(t) = V_g + V_{gp} \cos \omega t = V_g + V_{gp} \sqrt{\frac{1}{2}\left(1 + \frac{V_a - x}{V_{ap}}\right)},$$

and (7. 3) gives:

$$y = i_a = a\left[V_g + V_{gp} \sqrt{\frac{1}{2}\left(1 + \frac{V_a - x}{V_{ap}}\right)} + bx\right],$$

which is a quadratic equation between $i_a\,(= y)$ and $v_a\,(= x)$, and can also be written thus:

$$\left(\frac{y}{a} - bx - V_g\right)^2 = \frac{1}{2} V_{gp}^2 \left(1 + \frac{V_a - x}{V_{ap}}\right) \quad \ldots\ldots \quad (7.\ 5)$$

Further investigation shows that this is a parabola.

Fig. 159 depicts the curves for v_g, v_a and i_a plotted against ωt, as set out in the equations (7. 1), (7. 2) and (7. 4). Further, fig. 160 shows the I_a/V_a diagram together with the parabolic working line (schematic). Due to the class C setting of the valve, only that part of the working line is of importance which lies above the v_a axis. The path of the working point along the load line during one cycle can be deduced from fig. 159. In the two figures the points concerned are represented by the same letter; thus A refers to the point where v_g and i_a are at a maximum and v_a at a minimum. At B, v_a passes the value of the steady anode voltage V_a; at C, i_a is zero, whilst at D, v_a reaches its maximum.

If the load line lay wholly above the v_a axis, the path of the working point would pass through $ABCD_1E_1F_1$ during a half-cycle of v_g, i.e.

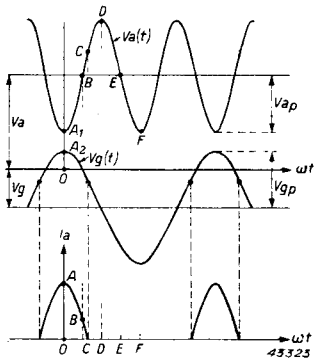

Fig. 159. Anode voltage, grid voltage and anode current plotted against time in a frequency doubler.

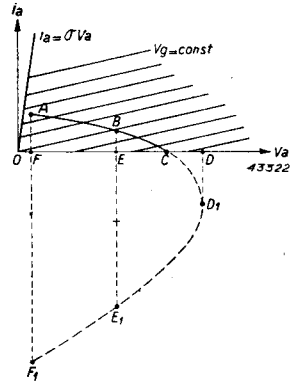

Fig. 160. Load line in the i_a–v_a diagram of a triode working as frequency doubler.

one cycle of v_a, but, because the v_a axis is reached at C whilst i_a cannot be less than zero, the working point, after passing C, first moves towards D and then back via E to F. It then travels in the opposite direction from F, through E to D, back to C and then via B to A. As in the case of the ordinary amplifier, the output power and efficiency for a given load line reach their maximum when the end of the line (point A) lies on the limit characteristic, since the alternating anode voltage also reaches its highest level at that point.

The following §§ are therefore devoted to a discussion of the best location of the load line to yield the optimum power when the valves are running at their limit characteristics, and we shall see what limitations are imposed by the maximum permissible steady anode current, peak current and anode dissipation.

§ 2. Output power and efficiency

When the valve is working up to the limit characteristic, the following applies, in addition to (7. 1) and (7. 2):

$$I_{ap} = \sigma V_{a\min} = \sigma (V_a - V_{ap}) \quad . \quad . \quad . \quad . \quad . \quad (7.\ 6)$$

Further:

$$V_{ap} = I_{a2} R_a,$$
$$I_{a2} = f_2(\Theta) \cdot I_{ap}$$
$$I_{ao} = f_o(\Theta)\, I_{ap}$$

The expressions for $f_2(\Theta)$ and $f_o(\Theta)$ as derived in Chapter III, § 2 are not universally applicable in this instance, seeing that the control voltage v_s can no longer be written in the form:

$$v_s = V_s + V_{sp} \cos \omega t,$$

because the frequency of that part of V_{sp} which derives from the anode is $2\,\omega t$.

In order to simplify the calculation, let us confine ourselves to the idealized tetrode or pentode, used as tripler, in which case the effect of the alternating anode voltage upon the anode current may be ignored. We may then once more write:

$$f_2(\Theta) = \frac{2 \sin^3 \Theta}{3\pi (1 - \cos \Theta)}$$

and

$$f_o(\Theta) = \frac{\sin \Theta - \Theta \cos \Theta}{\pi (1 - \cos \Theta)}.$$

From the latter it follows that:

$$I_{ap} = \frac{\sigma V_a}{1 + \sigma R_a f_2(\Theta)} \quad \ldots\ldots\ldots\ldots \quad (7.\ 7)$$

$$I_{ao} = \frac{\sigma V_a f_o(\Theta)}{1 + \sigma R_a f_2(\Theta)} \quad \ldots\ldots\ldots\ldots \quad (7.\ 8)$$

$$W_i = V_a I_{ao} = \frac{\sigma V_a^2 f_o(\Theta)}{1 + \sigma R_a f_2(\Theta)} \quad \ldots\ldots\ldots \quad (7.\ 9)$$

$$W_o = \frac{1}{2} I_{a2}^2 R_a = \frac{1}{2} \{f_2(\Theta) \cdot I_{ap}\}^2 R_a = \frac{1}{2} \frac{\{\sigma V_a f_2(\Theta)\}^2 R_a}{\{1 + \sigma R_a f_2(\Theta)\}^2} \quad \ldots \quad (7.\ 10)$$

Finally,

$$W_a = W_i - W_o \quad \ldots\ldots\ldots\ldots \quad (7.\ 11)$$

and

$$\eta = \frac{W_o}{W_i}. \quad \ldots\ldots\ldots\ldots \quad (7.\ 12)$$

The results of these equations are given in figs. 161 to 165, which thus give:

$$\frac{W_o}{\sigma V_a^2}, \quad \frac{W_i}{\sigma V_a^2} = \frac{I_{ao}}{\sigma V_a}, \quad \frac{W_a}{\sigma V_a^2} \text{ and } \frac{I_{ap}}{\sigma V_a},$$

all as functions of σR_a with Θ as parameter and also η as a function of Θ with σR_a as parameter.

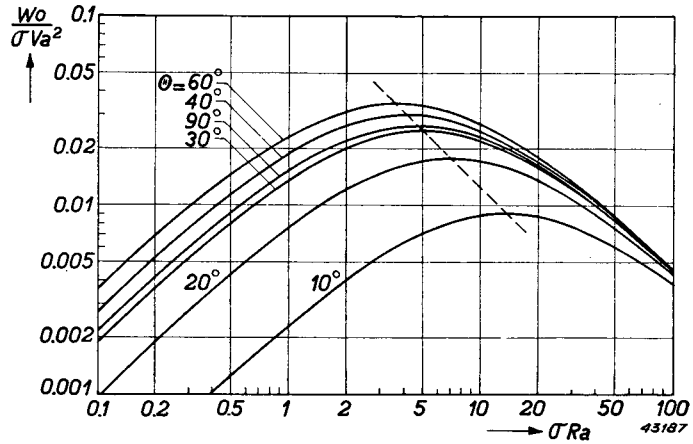

Fig. 161. Output power as function of the loading resistance of an "ideal" tetrode or pentode working as frequency doubler.

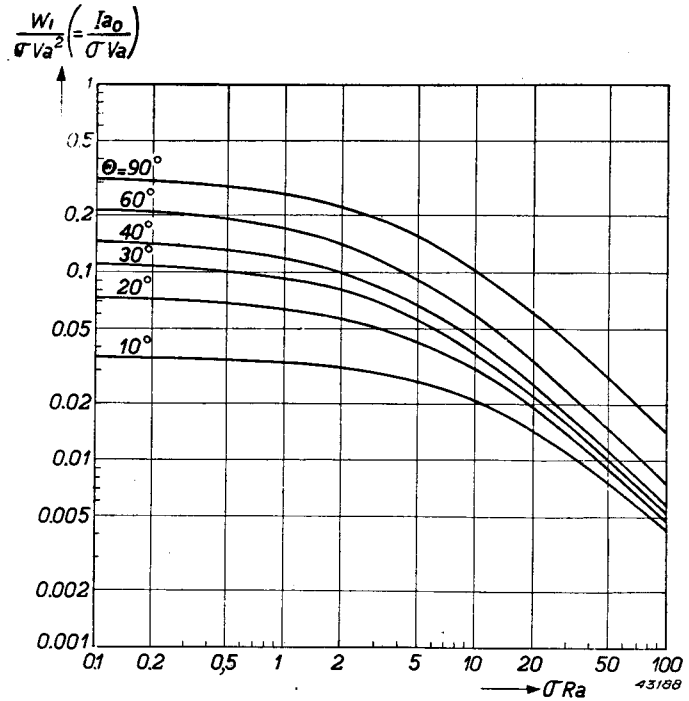

Fig. 162. Input power and steady anode current as function of the loading resistance of an ideal tetrode or pentode working as frequency doubler.

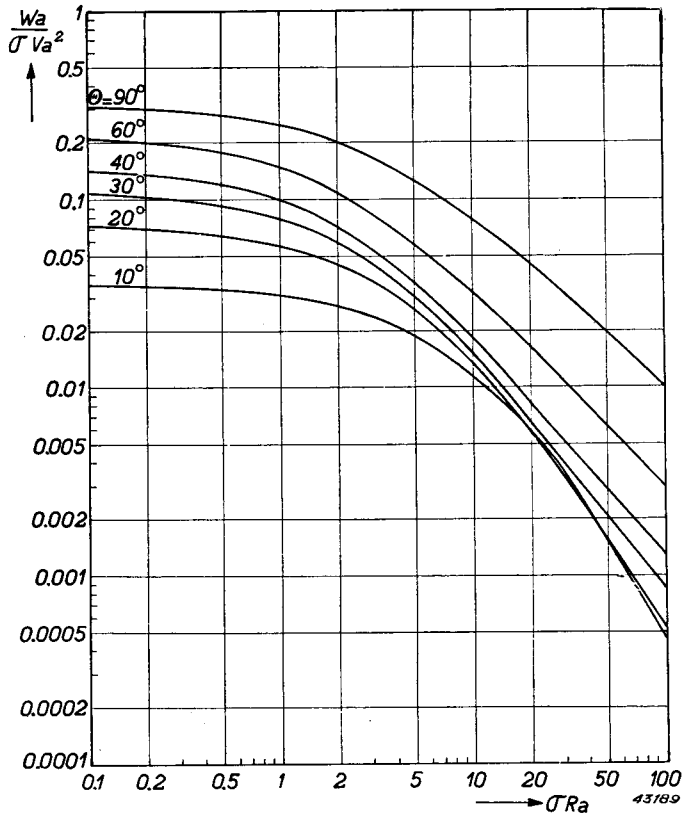

Fig. 163. Anode dissipation as function of the load resistance of an ideal tetrode or pentode used as frequency doubler.

In the same way as for the ordinary amplifier, the output power of the frequency doubler, as a function of σR_a also reveals a maximum (fig.161), which is, moreover, dependent on Θ.

In practice, as for the amplifier, those settings are chosen that will yield high efficiencies, i.e. the anode load resistance is increased beyond the optimum value, care being taken that the anode dissipation, steady anode current and peak anode current do not exceed their maximum allowable values.

The curves of $W_o/\sigma V_a^2$, plotted against σR_a with W_a; I_{ao} or I_{ap} constant, are then constructed from figs. 161 to 164, as reproduced in figs. 166 to 168. In each figure the dotted line represents the relative values of Θ.

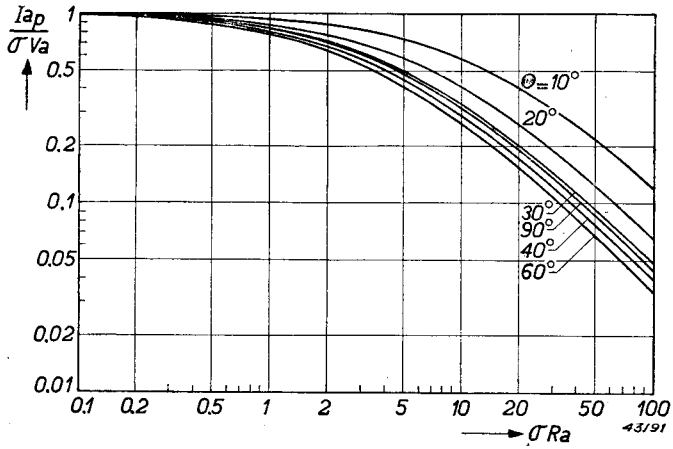

Fig. 164. Peak anode current as function of the load resistance of an ideal tetrode or pentode as frequency doubler.

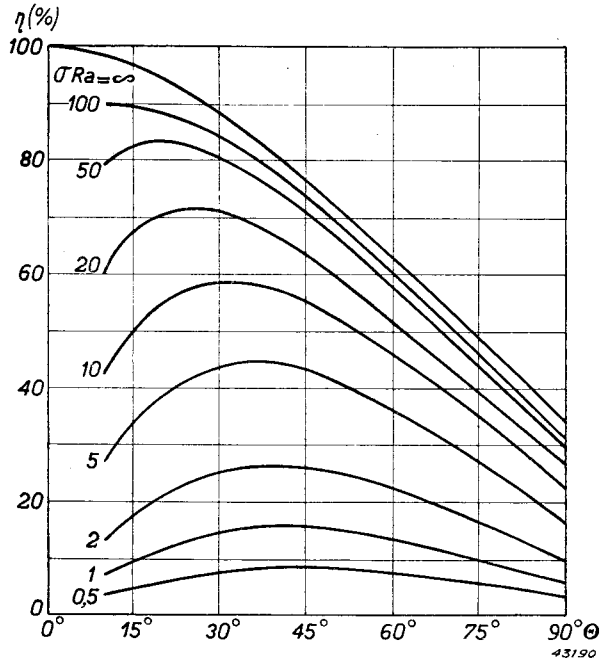

Fig. 165. Efficiency as function of the half-angle of the anode current impulses, with load resistance as parameter, for an ideal tetrode or pentode used as frequency doubler.

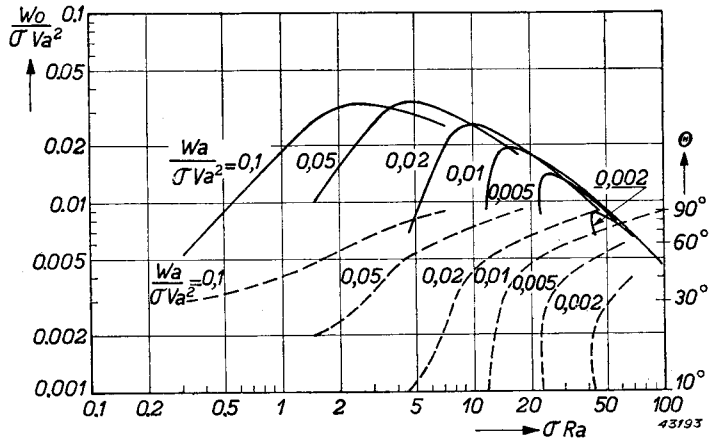

Fig. 166. Full lines: Output power of a frequency doubler as function of the load resistance at constant anode dissipation.
Dotted lines: Relative values of the half angle of the anode current impulses.

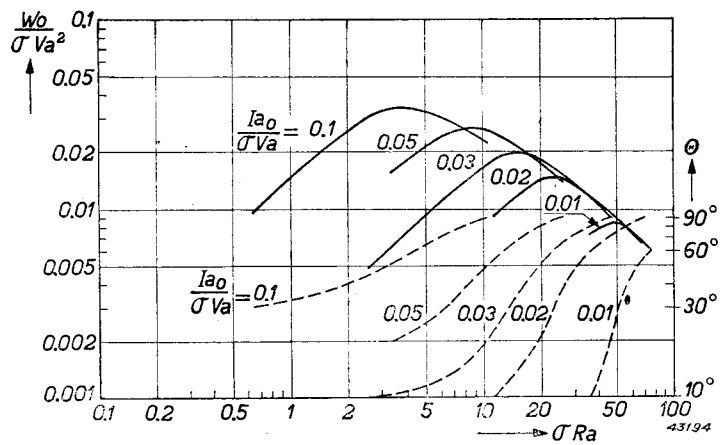

Fig. 167. Full lines: Output power of frequency doubler plotted against the loading resistance at constant anode current.
Dotted lines: Relative values of the half current angle Θ.

Qualitatively, these figures reveal the same shapes as those shown in Chapter III in relation to the amplifier; in just the same way there is a particular value of σR_a at which the output power reaches a maximum. To illustrate this, a calculation is given of the maximum output of the pentode, of which the I_a — V_a characteristics are reproduced in fig. 54, working as frequency doubler at an anode voltage of 1500 V, and with a peak anode current of 525 mA.

From fig. 54 it will be seen that $\sigma = 3.5$ mA/V, so that $I_{ap}/\sigma V_a = 0.1$. Further, from fig. 168, we know that the maximum value of $W_o/\sigma V_a{}^2 = 0.0125$ and that this value is reached at $\sigma R_a = 33$ and $\Theta = 60°$. Therefore:

$$W_o = 98.5 \text{ W}; \quad R_a = \frac{33}{3.5.10^{-3}} = 9430 \text{ ohms}.$$

Further, according to fig. 162:

$$\frac{W_i}{\sigma V_a{}^2} = \frac{I_{ao}}{\sigma V_a} = 0.0220, \text{ and therefore } \frac{W_a}{\sigma V_a{}^2} = \frac{W_i}{\sigma V_a{}^2} - \frac{W_o}{\sigma V_a{}^2} = 0.0095,$$

which is also found in fig. 163.

It then follows that: $W_i = 173$ W; $W_a = 74.5$ W; $\eta = 57\%$.

Finally, V_{ap} is calculated from:

$$I_{ap} = \sigma (V_a - V_{ap});$$

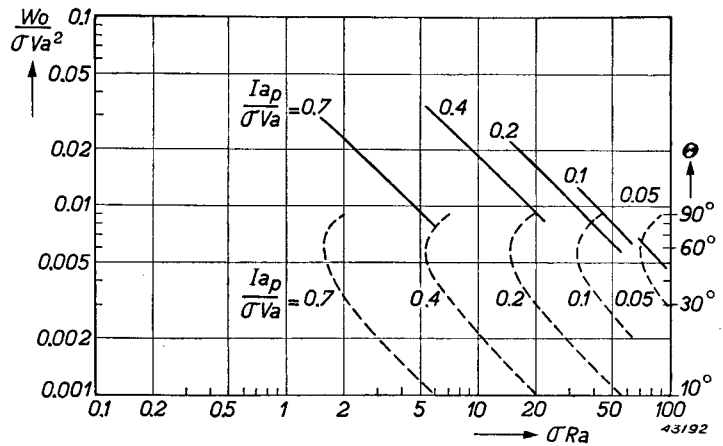

Fig. 168. Full lines: Output power of frequency doubler plotted against load resistance at constant peak anode current.
Dotted lines: Relative values of the half current angle.

so:

$$V_{ap} = V_a - \frac{I_{ap}}{\sigma} = 1350 \text{ V}.$$

These values may be checked against the data supplied by the actual static characteristics in fig. 54. Excitation voltage and grid bias are then taken to be such that the half current angle will be 60°, the alternating anode voltage 1350 V and peak anode current approximately 525 mA. Fig. 54 shows that the grid voltage should run to + 60 V. The grid bias V_{g1} is calculated by means of (7. 4b), where

$$V_{g2} = 300 \text{ V}: \; c = 1/\mu_{g1g2} = 1/2.7.$$

Taking $V_{g1p} = -V_{g1} + 60$, we then have:

$$V_{g1} = -280 \text{ V}, \text{ so that } V_{g1p} = 340 \text{ V}.$$

It is then possible to write:

$$v_{g1}(t) = -280 + 340 \cos \omega t,$$
$$v_a(t) = 1500 - 1350 \cos 2\omega t,$$

and, by means of these expressions, to construct the load line in the i_a/v_a diagram (fig. 54, curve *f*), as well as the anode-current impulse (fig. 169). This shows that the half-current angle is actually 60° and, further, that the anode current impulse is slightly indented, so that the peak anode current will remain below the required level of 525 mA;

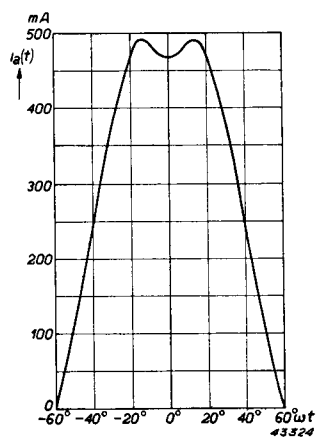

Fig. 169. Anode current impulse of a pentode working as frequency doubler, relating to the load line *f*, fig. 54.

finally, that the curve is not of the parabolic type met with in theory (fig. 160), but approximates more nearly to a straight line. This latter fact may be explained by the increase in the slope at higher anode currents, due to which the i_a/v_a curves are no longer equidistant, but diverge as anode current increases.

From fig. 169 the following is then obtained:
$I_{ao} = 108$ mA; $I_{a2} = 140.5$ mA; therefore $W_i = 162$ W and, with $V_{ap} = 1350$ V: $W_o = 95$ W; $W_a = 67$ W; $\eta = 58.6\%$. Finally $R_a = V_{ap}/I_{a2} = 9600$ ohms.

Comparison of these values with those obtained from the theory of linear characteristics will be found to give very satisfactory results.

CHAPTER VIII

Some Special Items

§ 1. Grid emission

The term "grid emission" refers to the tendency of a grid to emit electrons, and this can be further characterized, according to its origin, as thermal (primary) or secondary emission.

Thermal emission, as with the cathode, depends upon the condition of the surface of the grid and the temperature. Now the temperature of the grid of a transmitting valve under working conditions never reaches the point where the pure metal of which the grid is made commences to emit electrons to any marked degree. It has already been stated in Chapter I, § 3 that it is essential to keep the grid temperature as low as possible, or alternatively, to employ a material that will not easily volatilize, and under such conditions thermal emission is usually below the level where it would produce any troublesome effects.

In valves having an oxide cathode, emitting substances are unavoidably evaporated from the cathode (barium or its oxide) and deposited on the grids, more especially the control grid. It is found in practice that the control-grid temperature, especially in the larger oxide-cathode valves, may reach a level where the thermal emission from this deposited layer does actually become noticeable.

Due to the presence of this emission current from the control grid, the grid current, measured outside the valve, is lower than if the emission were absent. Because the next grid in sequence carries a higher potential (the anode in triodes, screen grid in tetrodes and pentodes), some of the electrons emitted from the control grid pass to the anode or screen grid, as the case may be. The control-grid current, measured externally, is therefore the difference between the number of electrons falling upon this grid by reason of the cathode current, and the number emitted by the grid. In given circumstances the resultant grid current may thus be zero or even negative and, in certain circuits this may produce disastrous results. For example, in the oscillator circuit shown in fig. 134, grid bias is obtained by passing the grid current through the grid leak, so that, when control grid current drops, the bias also decreases, changing the setting of the valve gradually from class C to class B or A. The efficiency is thereby reduced and anode

dissipation increases, with consequent increase in anode temperature and, therefore, also in grid temperature. This increases the grid emission in turn, and the whole condition becomes worse, so that in a very short time the anode dissipation reaches the point where the valve becomes defective.

This detrimental effect of grid emission may be counteracted by arranging matters so that the negative bias is not entirely dependent on the control-grid current, for instance by employing a cathode resistance, as shown in fig. 170. In this case the cathode current determines the bias and, since the control-grid current represents only a small part of the cathode current, the effect of grid emission on the setting of the valve is almost negligible. Otherwise, especially in the case of oscillators, the use of a fixed grid voltage or cathode resistance is not without its drawbacks, as the flexibility with which the oscillation is generated is then curtailed (compare Chapter VI, § 3), and efforts are therefore always made to suppress grid emission as much as possible; the most successful method consists in ensuring a low working temperature of the grid, for which purpose thick grid supports or "backbones" of highly conductive metal are employed, blackened cooling-fins often being fixed to the ends of these backbones. The grid winding-wire is sometimes subjected also to a special surface treatment, to ensure only slight absorption of heat from surrounding electrodes or, again, to produce a surface upon which deposits of barium oxide or strontium oxide from the cathode are not easily reduced to their respective metals, which emit so much the more readily. One such method is to plate the grid wire with gold or platinum, although in valves with thoriated tungsten filaments a layer of zirconium is often applied, as this metal is a very effective thermal radiator.

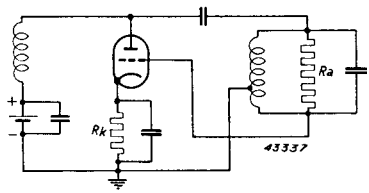

Fig. 170. Use of cathode resistance in a Hartley circuit to ensure a grid bias that will be less dependent on grid emission.

Any thermal emission of the screen grid of a pentode will not usually detract from the performance of the valve; the potential of the screen is higher than that of its neighbouring electrodes, and, since the electrons emitted drift comparatively slowly, they fall back upon the screen and their effect is not apparent in the screen-grid current as measured outside the valve itself.

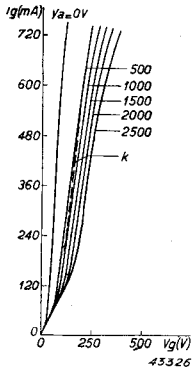

Fig. 171. Grid-current characteristics of a triode with very low secondary emission.

Secondary emission of a grid, as its name implies, refers to the emission of secondary electrons arising from the impact of the electrons in the cathode current (primary electrons) upon the grid. The degree to which these secondary electrons are liberated is governed by the speed at which the primary electrons bombard the grid, the angle of incidence, the material of which the grid is made and the condition of its surface.

Now, since the velocity of the electrons in the direction of the grid is determined by the grid potential, the coefficient of secondary emission (i.e. the number of secondary electrons liberated per primary electron on perpendicular impact) therefore depends also on the grid voltage. With most metals this coefficient is greater than unity in a certain velocity range of the primary electrons, and this zone is, roughly, above 100 V.

Considering for a moment the control grid in particular, the secondary electrons liberated from this grid do not all leave the grid, any more than they do in the case of thermal emission, although the number of electrons actually leaving the grid is naturally greater according as the adjacent electrode (screen of pentode, anode in a triode) is at a higher potential. The control-grid current, measured externally, is therefore less in the presence of secondary emission than when the latter does not occur, and it is moreover to a very great extent dependent on the control-grid voltage and screen- (or anode-) voltage. It is even possible for the resultant control-grid current to be zero or negative, as demonstrated by figs. 171 and 172, where the control-grid current of a triode is shown as function of the grid voltage, with anode voltage as parameter.

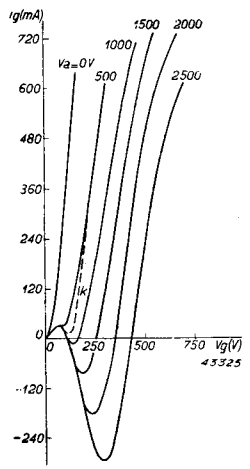

Fig. 172. Grid-current characteristics of a triode with secondary emission.

Fig. 171 refers to a triode having only very slight secondary emission, and fig. 172 gives the position in the case of high grid emission.
The effect of secondary grid emission on the performance of a given circuit is quite different from that of primary emission, seeing that the former depends on grid voltage, whereas the latter, nearly enough, does not.

Taking the case of a transmitting valve having grid-current characteristics as shown in fig. 171 or 172 and excited in R.F. class C, the control power is calculated in the manner described in Chapter III. If V_{g1}, V_{g1p}, V_a and V_{ap} are known, the instantaneous values of the grid- and the anode voltage can be ascertained, whilst fig. 171 or 172 gives the relative grid-current. In the I_g/V_g diagram the grid current is given as a function of grid voltage, under excitation conditions, by the so-called dynamic grid-current characteristic which in figs. 171 and 172 is the line k. The grid-current impulse is easily derived from this, since the grid voltage as function of time is known. Figs. 173 and 174 reproduce the impulses relating to k in figs. 171 and 172.
The excitation power is found by calculating the first harmonic and multiplying this by half the peak value of the excitation voltage. It will thus be found that the excitation power in the presence of secondary grid emission is very much less than otherwise; the reason for this must be sought in the fact that the grid-current impulses with secondary emission are lower and smaller in form, due to the peculiar curve of the dynamic characteristic, which is fairly horizontal over a large portion of the v_g range and rises sharply only in the region of the excitation peak.

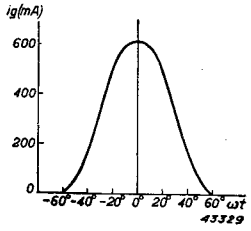

Fig. 173. Grid-current impulse relating to the dynamic characteristic k, fig. 171.

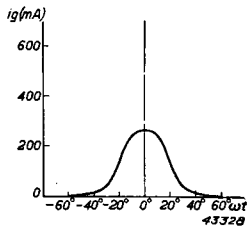

Fig. 174. Grid-current impulse relating to the dynamic characteristic k in fig. 172.

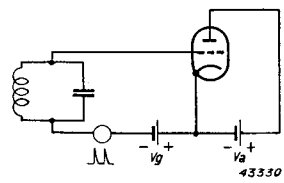

Fig. 175. Circuit in which instability will occur due to secondary grid emission.

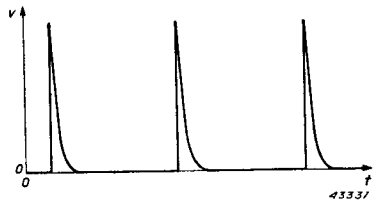

Fig. 176. Impulse type of voltage used in the circuit in fig. 175 to run the grid into the region of positive voltage.

This in turn is a result of the particular form of the static grid-current characteristic, that is, of the secondary grid emission.

In the larger types of transmitting valve especially, secondary emission is sometimes expressly employed to reduce the excitation power. Thus, the driving power of a triode having an effective rating of 1200 W may be reduced from 67 W to 33 W. At the same time the valve manufacturers must be on the watch to ensure that the secondary emission does not become so high that instability of the grid circuit occurs. This instability will manifest itself in various ways: fig. 175 depicts a circuit comprising a triode with its anode connected to a source of voltage, an L.C. circuit on the grid, a source of bias and an alternator generating a sinusoidal pulsating voltage of the type shown in fig. 176.

The amplitude of these impulses is considerably greater than the grid bias, and grid current therefore flows. The grid current as function of the voltage can be rendered visible on the cathode-ray oscilloscope, and fig. 177 illustrates a number of such current characteristics at different anode voltages. It is apparent that there is a high degree of secondary emission; the slope of part of the characteristics is negative, and this seems

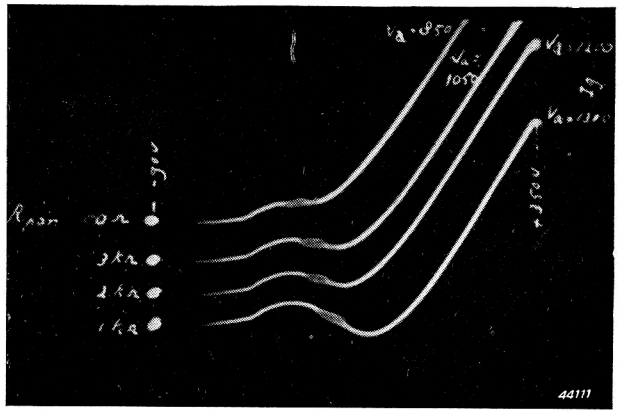

Fig. 177. Oscillogram of grid current as function of impulse voltage in the circuit shown in fig. 175 at different values of anode voltage. The latter increases from top to bottom. Damping of the circuit is so increased that oscillation just sets in at the point on the characteristic where slope is greatest.

to cause instability: the grid circuit starts oscillating, causing thickening of the trace on the oscilloscope.
The oscillation is so much the stronger according as the slope of the characteristic increases; the explanation of this will be found in the negative slope in a certain part of the grid-current characteristic, indicating that the grid-to-cathode space, as seen by the external circuit, is acting as a negative resistance.

This negative resistance is in parallel with the grid circuit, which has its own losses, that may be regarded as a positive resistance in parallel. Now, if the absolute value of the negative resistance of the cathode space is less than the positive resistance in the circuit, the resultant resistance is negative, and any oscillation present will increase in amplitude up to a certain value.
In the curves shown in fig. 177, the point of inflexion in the i_g/v_g characteristic is that where the negative slope is greatest, i.e. where the negative resistance is lowest. If now the anode voltage be raised, the slope of the centre part of the characteristics increases more and more until at a certain voltage the negative resistance at the starting point is equal to the positive resistance in the grid circuit.

At that point the grid circuit is able to oscillate, but not above it. At higher anode voltages there is a zone round the bending point in the characteristic where the negative resistance is equal to, or less than, the circuit resistance, and oscillation then occurs in the whole of that zone. In actual fact, the measurements shown in fig. 177 were carried out in such a way that at the higher anode voltages, that is, a greater negative slope, the damping of the circuit was increased in proportion, so as to leave just a trace of oscillation: fig. 177 then shows clearly that the positive damping resistance required to do this is much less when the anode voltage is increased.
Apart from producing this "dynatron instability", secondary emission is also likely to cause instability of another type, which will now be discussed by reference to an example.

It has been shown in connection with suppressor-grid modulation (chapter V, fig. 100) that the suppressor receives a negative biasing voltage as well as an A.F. voltage, of which the amplitude does not exceed the absolute value of the bias. Since the suppressor grid is thus

always negative, suppressor current, and therefore modulation power also, is nil, whilst distortion is avoided. If measurement of the suppressor-grid modulation characteristic is continued in the region of positive suppressor voltage, suppressor current flows, and this is often affected by secondary emission, which, in view of the proximity of the highly positive anode, is not surprising. Fig. 178 shows an I_{g3}/V_{g3} characteristic of this type. Suppose that the suppressor circuit comprises an ohmic resistance R (fig. 179); the relation between i_{g3} and v_{g3} is then determined in part by the circuit itself, viz:

$$v_{g3} = V_{g3} + V_{g3p} \sin \omega t - i_{g3}R = e - i_{g3}R.$$

This expression is reproduced graphically in fig. 178 by the line b, which cuts the abscissa at A, at the point where $v_{g3} = e$. The values of i_{g3} and v_{g3} that may occur are given by the points of intersection of a and b; in this case these are p, q and r. Of these, p and r are stable; q is unstable, as can be shown by an argument analogous to that put forward in Chapter VI in connection with figs. 139 and 140. Which of the two stable conditions of equilibrium p and r will actually appear depends on the manner in which the variable voltage e attains its relevant value.

In fig. 180, the line b from fig. 178 is reproduced for 7 different values of e, corresponding to the points of intersection A_1 to A_7 on the V_{g3} axis.

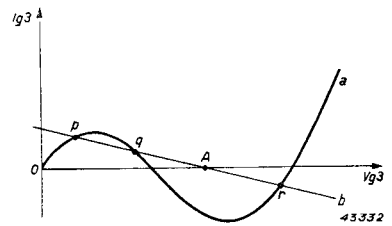

Fig. 178. Suppressor-grid current as function of the (positive) suppressor voltage of a pentode with secondary emission at that grid (curve a). Curve b: load line with respect to the resistance R in fig. 179.

In cases 1 and 2, the current I_{g3} is nil, but in instances 3, 4, 5 and 6 it reaches values corresponding to the points of intersection p_3, p_4, p_5 and p_6. At setting 6, the line b touches curve a. If the voltage e then rises above OA_6, the only remaining intersecting point is r, or, in this case, r_6: the grid current, then, drops in stages and the grid voltage rises in stages. When e is increased still further, it ultimately reaches r_7.

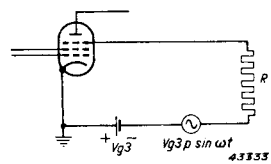

Fig. 179. Suppressor-grid modulation circuit of a pentode with resistance R.

Similarly, when voltage e decreases, the point of intersection passes successively through r_7, r_6 .... r_3, ultimately jumping back to the p-branch (p_3, p_2, p_1). Now, e indicates the course followed by the modulation voltage, whereas the abscissae of p and r represent the suppressor-grid voltage: due to the previously mentioned rise and fall in stages, there can be no question of the suppressor-grid voltage v_{g3} following the modulation voltage e uniformly; on the contrary, serious distortion occurs.

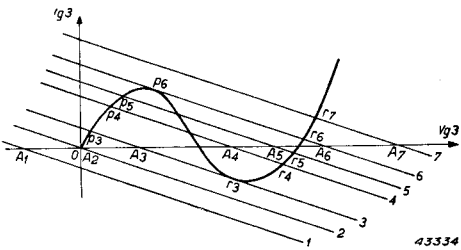

Fig. 180. Due to the alternating voltage V_{g3p} sin ωt (see fig. 179), the load line b in fig. 178 moves to and from parallel to its original position. When three points of intersection in the grid-current characteristic merge into a single point, both current and voltage show a sudden increase.

Some improvement can be obtained by making the resistance R sufficiently small, and, as will be seen from fig. 181, the points of intersection a and b are then always stable.

Similar effects are also likely to occur in control-grid circuits when the secondary emission of this grid is sufficiently high and there is an adequate amount of resistance in the circuit (grid leak).

It may be concluded, then, that too much secondary emission at the grids is undesirable, and valve manufacturers therefore always take steps to minimize this effect, when it occurs, by suitably treating the surfaces of the grids. Regarding secondary emission in tetrodes, enough has been said in chapter IV, to which reference may be made for details.

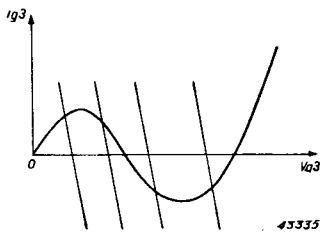

Fig. 181. When the resistance R in fig. 179 is sufficiently small, there is only one point of intersection with the grid-current characteristic and there are no sudden jumps.

§ 2. Discharges in transmitting valves

The vacuum in the modern transmitting valve is of the order of 10^{-7} to 10^{-8} mm mercury, this high degree of vacuum being essential not only for the maintenance of proper emission, but also to provide adequate insulation between the different electrodes.

Especially in high-powered valves such as the TA 20/250, an inferior vacuum would very soon give rise to ionization of gas molecules to an extent that would neutralize the space charge between the electrodes; the result would be a gas discharge instead of an electronic discharge, and proper working of the valve as an R.F. amplifier would be made impossible.

In spite of the high vacuum employed, it sometimes happens however that the insulation between anode and other electrodes suddenly breaks down, with consequent flash-over inside the valve. This is not attributable to a gradual deterioration of the vacuum, since no increase in the ion current to the control grid can be measured, either before or after the occurrence[1]: it may on the contrary be visualized thus, that, arising from one cause or another, a small quantity of gas is liberated from one of the electrodes while the valve is working. Ionization of this gas causes a discharge and the gas then immediately disappears, presumably due to absorption or action of the getter.

In current literature, this phenomenon is generally referred to as "Rocky-Point effect", after the American transmitting station where it was first observed.

Rocky-Point effect occurs in valves of low power working on a low anode voltage, as well as in higher-power valves; in the smaller types, the effect has no damaging consequences, doubtless on account of the limited power of the source of anode-voltage supply. Larger valves, however, especially those of the water-cooled types, are fed by rectifiers with a high capacitance condenser as final smoothing element, charged to a high voltage (fig. 182). If discharge occurs in the valve, this condenser discharges through the latter and, since at that moment the valve forms a virtual short-circuit, the discharge current is liable to become very high.

Although it does not necessarily follow, this heavy current is liable to damage the interior of the valve; the filament poles will show distinctive markings, or the filament itself may show signs of the discharge, in the

[1] It is possible to check the vacuum by passing a certain current through the valve, with negative grid bias and positive anode. The gas molecules are then ionized by the stream of electrons; the positive ions move towards the negative grid and establish an external current from grid to cathode which is a measure of the vacuum.

form of small globules of molten metal, whilst in extreme cases it may be burnt out.

In some instances, again, two "legs" of the filament may be found bent inwards towards each other by the discharge; in fact, in a transmitting valve of which the filament consisted of two parallel sections, each of 4 wires, in the form of a cylinder, this was actually found to have taken place. Fig. 183*a* is a sketch of the assembly, and in fig. 183*b* the development of the filament is shown. The grid in every case appears to be unharmed, probably owing to the fact that it is connected through a relatively high impedance to earth, in contrast with the heater which is earthed direct. A discharge will therefore prefer to flow to earth through the latter, and this path is provided by the wires AP and BP in fig. 183*b*, so that, the discharge being divided between the two wires, the components flow in the same direction towards P. The wires are accordingly drawn towards each other, and if the charge is sufficiently high, permanent deformation takes place.

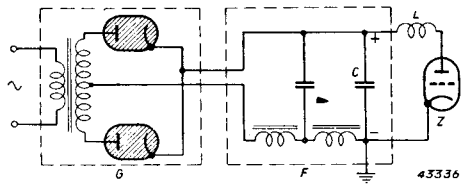

Fig. 182. Transmitter valve Z supplied by rectifier G, with smoothing filter F and choke L. In the event of a discharge, condenser C discharges a heavy current through the valve.

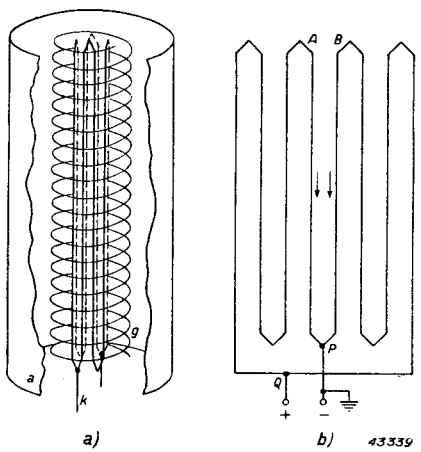

Fig. 183. a. Sketch of the assembly of the filament (*k*), grid (*g*) and anode (*a*) in a water-cooled transmitter valve. *b.* One of the possible circuitings of the filament.

This has been borne out many times in practice and tests have shown that discharge currents of the order occurring in large transmitting valves definitely produce permanent deformation in the manner described. For these tests a filament of the type shown in fig. 183*b* was mounted in a bulb in such a manner that it was possible to apply current to each member separately, either in the same direction, or in the opposite directions through adjacent

members in the two branches (fig. 184). The circuit employed for the test was as shown in fig. 185, a condenser C of 540 μF being charged to 1000 V and subsequently discharged by means of a mercury switch I through the filament. The latter was first raised to the working temperature by rectifier G_2. After a number of discharges had been produced, the deformation was clearly visible, as shown in fig. 186. The arrangement of the filament was as given in fig. 184*a*, and after this experiment it was found possible, by means of the arrangement shown in fig. 184*b*, to repel the wires, so as to restore them to their original form.

Damage to a valve due to Rocky-Point effect may be prevented by ensuring that the discharge current is confined within reasonable limits, namely by including a resistance of some 20 or 50 ohms in the anode circuit. The power developed in this resistance in continuous use is not inconsiderable, however, where the larger types of valve are concerned.

In connection with this problem of discharges, it is useful to note that a certain circuit can be adopted which makes it possible to utilize the heavy discharge current as a means of quenching the rectifier supplying the anode voltage during one cycle of the mains voltage. In this case the rectifier is equipped with grid-controlled mercury-vapour valves. The advantage of this method is that the circuit is broken much more quickly than is possible with a relay, and possible damage due to a discharge current is thus reduced to a minimum. This device, however, only interrupts the control current of the rectifier valve in the event of a discharge; the discharge from the smoothing condenser still passes through the transmitting valve. At the same time, since the rectifier valves are quenched, the charging on the condenser is not continued, and any discharge in

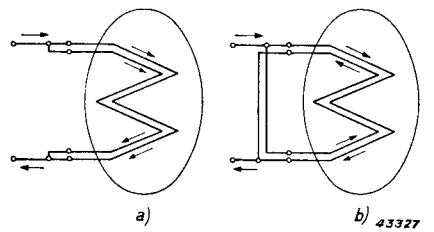

Fig. 184. Alternative circuitings of a filament in a test assembly according to the model of fig. 185:
a. with the parallel wires of the two branches in the same direction of flow;
b. in opposite directions.

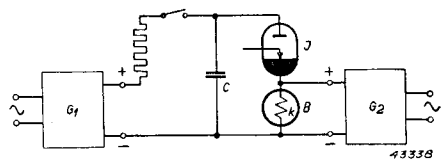

Fig. 185. Circuit to provide powerful current impulses in the heater system depicted in fig. 184.

the transmitting valve must therefore decay within a very short time.

§ 3. A.C. filament supply. Hum. Polyphase connection

The heaters of transmitting valves are usually fed with alternating current and, for various reasons, the anode current in such cases fluctuates in accordance with the frequency of the heater voltage applied. These fluctuations manifest themselves in a transmitter as a modulation of the R.F. signal transmitted, which is heard in the receiver as a hum-

being directly dependent on the temperature, fluctuates at the same frequency, and the anode current flowing through the valve can only be affected by this source of emission for as far as its magnitude is dependent on that emission. In oxide- and in thoriated tungsten-type cathode valves, emission of the heater is so high that the peak anode current is always far below that value, that is to say, the anode current is determined by space charge only and is independent of the emission. It is only in tungsten-cathode types of valve that the anode current can rise to the saturation level of the filament, and in this case ripple in the emission current leads to ripple in the anode current. However, the thermal capacity of transmitting valve tungsten filaments is so high that the anode-current ripple thus produced is negligible when compared with ripple arising from other causes.

Another cause of anode-current ripple is to be found in the fact that filaments fed with alternating current do not present a surface of uniform potential: the potential difference between grid and heater is not the same at all points on the wire, which implies that the control voltage varies along the length of the wire in the heater. It also means that, even though the filament be fed with direct voltage, the I_a/V_g characteristics of the valve are slightly different from those in the case of an equipotential cathode, and further that, in A.C. feeding, the different parts of the filament carry an alternating voltage with respect to the grid and give rise to an alternating anode voltage of the same frequency as the filament voltage. Here we speak of voltage hum, since the ripple is produced by the controlling action of the filament voltage on the anode current.

In receiving valves and also in small transmitting valves, this voltage ripple is avoided by using an indirectly heated cathode, the filament serving only as a heating element, whilst the emitting surface of the cathode provides an area of uniform potential.

In larger transmitting valves this ripple is for the main part eliminated by employing a centre-tapped filament transformer, or even a centre tap in the filament itself. Or again, use may be made of a centre-tapped resistance in

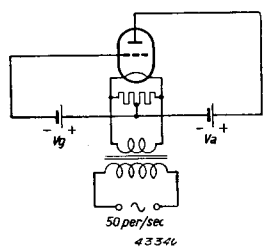

Fig. 187. Centre-tapped resistance in parallel with the heater of a transmitting valve, to reduce hum.

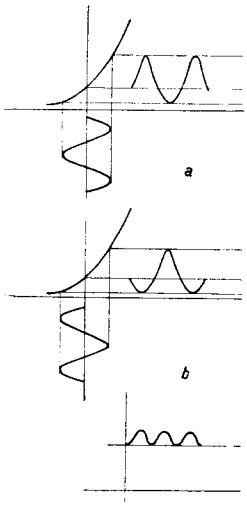

Fig. 188. Explanation of the compensation for ripple with respect to fig. 187:
a) Diagram of the anode current caused by the voltage on one half of the heater;
b) the same, but for the other half of the heater;
c) the residual alternating anode current is at twice the frequency of the heater voltage.

parallel with the secondary winding of the filament transformer (fig. 187). In this way, the filament is virtually divided into two parts, of which the centre point carries a constant potential with respect to the control grid, the voltage of the two half-members, with respect to the grid, being opposed in phase; the increase in anode current in one half of the valve is then compensated by an equally large decrease in the other half, although strictly speaking this compensation is not absolute, as demonstrated in the following example.

In fig. 188 the I_a/V_g characteristics of the two halves into which the valve is divided by the centre-tap (fig. 187) are shown, and these, as is known, are more or less curved. Now, it has just been stated that in the control of anode current the filament voltage is of equal effect as the grid voltage [1]; it may therefore be said of the extremity of the heater, then, that between this point and the grid there is an alternating control voltage whose amplitude is equal to that of half the heater voltage. For those parts of the wire which are nearer to the centre, however, this control voltage is proportionately less than, but in phase with, that at the extremity.

For one half of the filament, therefore, the effect of its voltage on the anode current may be described as that of an alternating voltage in the I_a/V_g diagram (fig. 188*a*): a similar argument may be applied to the other half of the heater, except that the phase of the alternating control voltage is opposed to that of the first half (fig. 188*b*). The relative

[1] Apart from a small correction to be made in the static characteristic, to allow for the fact that the filament is not an equipotential body and that the controlling effect of the filament voltage is consequently not of the same order at every point on the heater.

anode current as function of time is shown in both diagrams and, in consequence of the curvature of the static characteristic, the result is not fully sinusoidal, but in the main may be resolved into a D.C. component, a component whose frequency is the same as that of the filament voltage, and a third component of twice the frequency. When the anode currents of both halves are added together, those components at the filament-voltage frequency counterbalance each other, whereas the double-frequency components are in phase and additive (fig. 188*c*). This proves that complete compensation for ripple is not possible.

Yet a third cause of hum lies in the magnetic field of the heater current, which tends to deflect electrons from their original straight path from cathode to anode. The respective directions of the heater current proper and the deflected electron stream will be seen from fig. 189. The stronger the magnetic field, the greater the deflection, and the effect is therefore all the greater in large transmitting valves with tungsten filaments.

The consequence of this electronic deflection is this, that the space charge established by the electrons between the heater and the grid is greater than if the electrons followed a straight path; the anode current, therefore, is so much the lower according as the magnetic field is greater. In an alternating magnetic field these variations in the space charge are independent of the sign of the field, so that in the case of alternating current feeding, the anode current varies at twice the frequency of the filament current, being thus at a maximum when the filament current is zero and at a minimum when the latter is passing through its maximum.

This so-called magnetic ripple in the anode current, which is present as such even in a diode, is greatly magnified in the presence of one or more grids. Due to the surging to and fro of the "beams" of cathode current, the surface of the grid is in any case bombarded periodically at other angles than the normal; the current passing to the grid is therefore similarly variable, as is also the anode current which is the difference between cathode and grid currents. The presence of other grids (as in pentodes), however, need

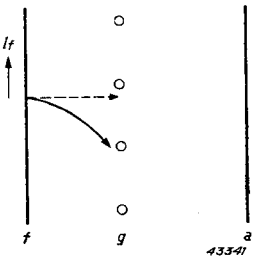

Fig. 189. Deflection of the electrons in a triode, due to the magnetic field of the heater.

not necessarily accentuate the anode ripple on account of the division of the current.

Attenuation of the ripple in water-cooled transmitter valves is ensured by suitable construction of the filament. It has already been pointed out that this wire is mounted in zig-zag fashion in the form of a cylinder in the valve (see fig. 9) and, by ensuring that adjacent wires for as far as possible carry current in opposite directions, the magnetic field of each one is largely counteracted by that of its neighbouring wire. The filament may also be divided into different branches, each of which carries part of the current, so that the magnetic field of any one of the wires is less than if the whole heater current were passed through an otherwise thicker filament. A filament of this type has already been illustrated in fig. 183.

However, experience has proved that anode-current ripple cannot be reduced in this manner to an extent that will satisfy the requirements imposed in modern broadcast transmitters, and another method consists in the use of a filament built up in sections and fed with polyphase A.C. The improvement thus obtained may be demonstrated by calculating the anode current of a valve equipped with the type of heater shown in fig. 183, but fed with alternating current in such a manner that there is a phase difference of 90° between the branches or sections. The relative circuit is reproduced in fig. 190, whereby the phase difference in question is established by means of the well-known Scott circuit. It has already been pointed out that the variation in anode current depends solely on the strength of the magnetic field and not upon its direction. Theoretically speaking, this variation in the anode current may be represented by a series of terms, all of which are powers of the square of the magnetic field, i.e. of the filament current. The anode current is then expressed as:

$$i_a = I_o + a_1 i_f^2 + a_1 i_f^4 + , \ldots . \quad (8.\ 1)$$

where I_o is the anode current in the absence of a magnetic field, i_f is the instantaneous value of the current in one of the branches of the filament and

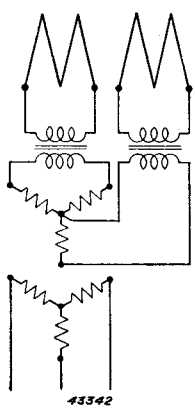

Fig. 190. Reduction of magnetic ripple when using a filament consisting of 2 sections, fed by currents differing in phase by 90°.

a_1, a_2 .... are constants determined by the construction of the valve.

Representing the filament current in one of the sections by:

$$i_f = I_f \sin pt \ , \quad . \ . \ . \ . \ . \ . \ . \ . \ . \quad (8.\ 2)$$

it follows from (8. 1):

$$i_a = I_o + a_1 I_f^2 \sin^2 pt + a_2 I_f^4 \sin^4 pt + , \ . \ . \ .$$

or, employing the goniometric formulae:

$\sin^2 pt = {}^1/_2 (1 - \cos 2\,pt)$: $\sin^4 pt = {}^1/_8 (3 - 4 \cos 2\,pt + \cos 4\,pt)$:

$$i_a = (I_o + {}^1/_2\, a_1 I_f^2 + {}^3/_8\, a_2 I_f^4) - ({}^1/_2\, a_1 I_f^2 + {}^1/_2\, a_2 I_f^4) \cos 2\,pt + {}^1/_8\, a_2 I_f^4 \cos 4\,pt \ , \quad . \ . \ . \ . \ . \ . \ . \ . \quad (8.\ 3)$$

ignoring the terms a_3, a_4, etc.

Apart from the D.C. component, the anode current, according to (8. 3) also contains a term of frequency $2p$, i.e. twice the frequency of the filament current and having an amplitude of $-({}^1/_2\, a_1 I_f^2 + {}^1/_2\, a_2 I_f^4)$, as well as a term of frequency $4p$ and amplitude ${}^1/_8\, a_2 I_f^4$. Of the A.C. components, the first-mentioned is by far the largest.

When the second branch of the filament, which is identical with the first, is fed with A.C. which is 90° out of phase with the current in the other branch, formula (8. 1) also applies to the anode current in this second branch, but the heater current is now:

$$i_f = I_f \cos pt \ . \ . \ . \ . \ . \ . \ . \ . \ . \quad (8.\ 4)$$

For this branch we then have:

$$i_a = I_o + a_1 I_f^2 \cos^2 pt + a_2 I_f^4 \cos^4 pt,$$

or, with

$\cos^2 pt = {}^1/_2 (1 + \cos 2\,pt)$; $\cos^4 pt = {}^1/_8 (3 + 4 \cos 2\,pt + \cos 4\,pt)$:

$$i_a = (I_o + {}^1/_2\, a_1 I_f^2 + {}^3/_8\, a_2 I_f^4) + ({}^1/_2\, a_1 I_f^2 + {}^1/_2\, a_2 I_f^4) \cos 2\,pt + {}^1/_8\, a_2 I_f^4 \cos 4\,pt \ . \ . \ . \ . \ . \ . \ . \ . \ . \ . \quad (8.\ 5)$$

This is identical with (8. 3), except that the term containing $\cos 2\,pt$ is of the opposite sign. The total anode current of the valve is then the sum of (8. 3) and (8. 5), viz:

$$i_a = 2\,(I_o + {}^1/_2\, a_1 I_f^2 + {}^3/_8\, a_2 I_f^4) + {}^1/_4\, a_2 I_f^4 \cos 4\,pt \ , \ . \ . \quad (8.\ 6)$$

from which it will be seen that the component having a frequency of $2p$ has disappeared. Only a component of which the frequency is $4p$

remains, but its amplitude is smaller than that of the original $2p$ component by one order of size. However, in order to ensure effective compensation, it is essential that both sections of the heater shall be identical in every respect; any want of symmetry in the assembly will mean that the coefficients of the anode current a_1, a_2 .... of the one section in expression (8. 1) will differ slightly from corresponding values in respect of the other section. In expression (8. 6), representing the sum of the anode currents, a term cos 2 pt remains, of which the amplitude is certainly smaller than would be the case if no compensation were present, but which, on the other hand, can be a dominating factor in the total ripple current.

Needless to say, hum compensation can also be achieved in a filament working on a current of more than two phases, and a three-phase heater is the obvious answer. It can be shown by means of calculations similar to the above that not only the component cos 2 pt, but also cos 4 pt is eliminated, provided of course that the three branches of the filament are equal in every respect. The term containing cos 6 pt, on the other hand, does not disappear, but the amplitude of this term is only very small.

A further improvement is obtained by constructing the filament in such a manner that the sections in which the phase of the current is the same are arranged symmetrically about the axis of the cylindrical figure which they describe. Slight eccentricity does certainly result in an increase in anode current in the neighbourhood of that part of the filament which then lies nearest to the anode, but this is compensated by a corresponding decrease in the region of the diametrically opposite part of the filament, carrying current of the same phase: the ripple current due to eccentricity is therefore very small. An example of a valve fitted with one of these filaments is the Philips transmitting valve TA 12/35; the arrangement of the filament is such that it can also be fed with direct current if required.

Apart from the considerable decrease in ripple brought about by the special filament arrangement, this ripple is also much reduced by the use of thoriated tungsten wire, which, consuming much less current (and giving less ripple in ratio of the square of the heater current), nevertheless provides adequate emission.

§ 4. Circuit losses

In the calculations in Chapter III it has been assumed that the power developed in the loading resistance R_a is fully available, but in practice

losses always occur in the anode circuit, owing partly to the fact that the anode coil, through which the circuit current flows, offers a by no means negligible resistance, and partly because ohmic losses occur in the plates, and dielectric losses in the insulation, of the condensers in the circuit. Due to the presence of these losses, the impedance of the anode circuit, when tuned to the first harmonic of the anode current, is not infinite; its value is practically equal to $R_k = L/C\,(r_L + r_C)$, where L and C are respectively the self inductance and capacitance of the anode circuit and r_L, r_C represent the loss resistances in the inductive and capacitive branches.

The value of R_k varies a great deal between one case and another, and is, moreover, dependent on the wavelength.

The finite value of the circuit resistance means that of the power delivered by the transmitting valve and designated as W_o in chapter III, only a part, W_n, is developed in the effective loading resistance R_n, the remainder, W_k, being lost in the circuit.

Since R_n and R_k are in parallel with the alternating anode voltage, the following expressions apply:

$$\frac{1}{R_a} = \frac{1}{R_n} + \frac{1}{R_k} \quad \ldots\ldots\ldots \quad (8.\ 7)$$

and

$$W_n = \frac{V_{ap}^2}{2\,R_n};\ W_k = \frac{V_{ap}^2}{2\,R_k};\ W_o = W_n + W_k \quad \ldots \quad (8.\ 8)$$

From this it follows that:

$$\frac{W_k}{W_o} = \frac{1}{1 + \dfrac{R_k}{R_n}};$$

$$R_a = \frac{R_k}{1 + \dfrac{R_k}{R_n}}.$$

Making use of the same expressions as in chapter III, these may be written:

$$\frac{W_k}{W_o} = \frac{1}{1 + \dfrac{\sigma R_k}{\sigma R_n}} \quad \ldots\ldots\ldots \quad (8.\ 9)$$

and

$$\sigma R_a = \frac{\sigma R_k}{1 + \frac{\sigma R_k}{\sigma R_n}} \quad \ldots\ldots\ldots \quad (8.\ 10)$$

Fig. 191 is a graphical representation of (8. 9) in which the relation W_k/W_o is expressed as a percentage, as function of σR_n, with σR_k as parameter. Fig. 192 shows σR_a plotted against σR_n, again with σR_k as parameter.
By means of these graphs it is possible to introduce a correction into the calculations in chapter III to allow for circuit losses. Fig. 192 gives the values of σR_a relative to given values of σR_n and σR_k, and the graphs in chapter III (figs. 28, 33 and 38) then yield the value $W_o/\sigma V_a^2$, that is, the total R.F. output power. Fig. 191 then provides W_k/W_o and both W_k and W_n can then also be calculated.

If necessary the above formulae can also be employed to calculate the effective power W_n as a function of the effective load resistance R_n, in the same way as was done for W_o in relation to R_a in fig. 28. Apart from the fact that this produces a figure with 2 parameters, viz Θ and σR_k, this procedure yields results of interest (as regards maximum effective

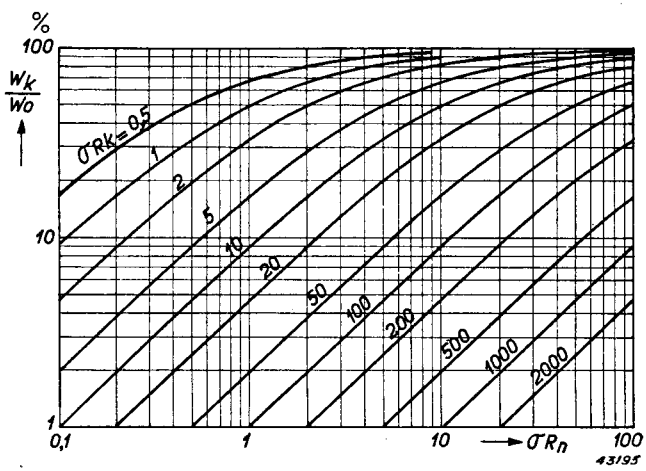

Fig. 191. Circuit losses W_k as percentage of the R.F. output power W_o of an R.F. class C amplifier at different values of effective load resistance R_n and circuit resistance R_k.

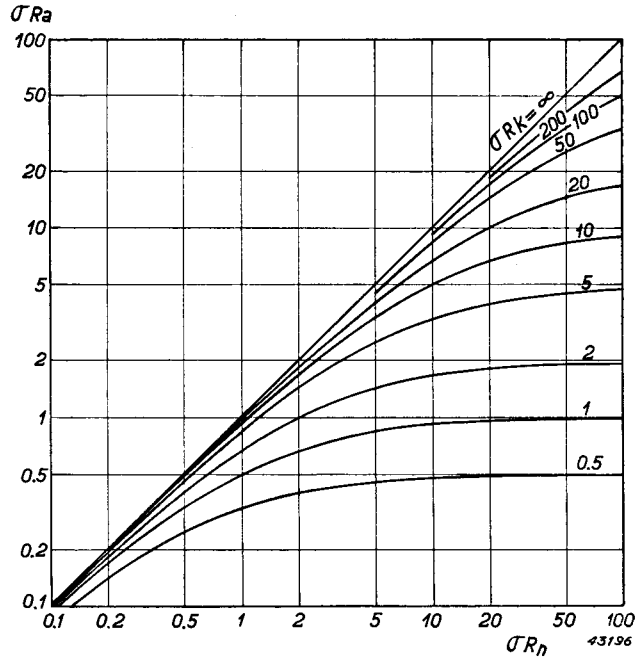

Fig. 192. The relation between R_a, R_n and R_k in accordance with the expression $1/R_a = 1/R_n + 1/R_k$.

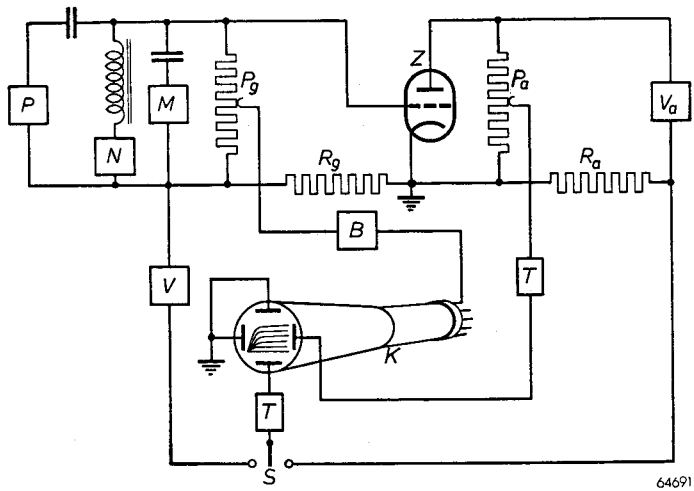

Fig. 193. Circuit of equipment used for measuring static characteristics of transmitting valves in the range of positive control-grid voltage.

power, optimum effective resistance etc,) only when the circuit resistance is of the same order of magnitude as the effective resistance. In practice, at any rate for wavelenghts of more than about 3 m, this condition is usually not fulfilled; the circuit losses generally constitute only a small percentage (5 to 10%) of the total power, for which reason it is better to employ the calculations given in chapter III with corrections on the basis of figures 191 and 192.

§ 5. Measurement of static characteristics of transmitting valves

The families of static characteristics, of which frequent use has been made in the foregoing chapters for the calculation of the current and power of a transmitting valve, whereby anode- or grid current is plotted against anode voltage with control grid voltage as parameter, do not lend themselves to static measurement. For instance, should it be required in the case of the triode, whose I_a/V_a characteristic is shown in fig. 22, to measure the point corresponding to the end of the load line, then v_g at that point is + 150 V, $v_a = 340$ V, $i_a = 1600$ mA. The power then developed as anode dissipation is $340 \cdot 1.600 = 544$ W, but, since a continuous load of only 300 W is permitted, measurement at the point in question must be effected as quickly as possible, so that the overload does not cause the anode to heat up beyond the normal working temperature. It is, however, physically impossible to effect measurement as quickly as this by means of ordinary indicating instruments, and the static characteristics of transmitting valves are therefore always determined with the aid of the cathode-ray oscillograph.

Many methods have been developed in recent years, but it will suffice to describe briefly the equipment employed in the Philips factories. Fig. 193 shows the circuit of this equipment. The grid of the triode whose characteristics are to be measured is excited with pulsating voltages covering within a short space of time all the positive voltages normally occurring on the grid of the valve. These impulses follow each other at comparatively long intervals compared to the duration of the impulses themselves. The best arrangement is one in which the impulse occurs exactly at the moment when the heater current passes through zero; in this way the effects of current and voltage ripple are eliminated. The impulse generator P is connected in parallel with the source of negative voltage N, to ensure that the valve to be measured will be biased to cut-

off in the intervals between impulses. M is a meter for measuring the peak voltage.

To the anode is applied an automatically variable D.C. voltage V_a that will cover all the values to be included in the characteristic. Now, when the horizontal deflection of a cathode-ray tube K (see fig. 193) is proportional to the anode potential and the vertical deflection to the anode current (potentiometer P_a and resistor R_a), completion of each cycle of the anode voltage will mean that every point on the screen of the tube, lying between the horizontal axis and the I_a–V_a curve for the most positive value of V_g will have been traversed. To obtain individual characteristics, care must be taken to see that the cathode-ray tube becomes conductive only when the values of V_g fall within the required I_a–V_a curves, that is, in fig. 22, at 150, 125, 100, 75 V and so on. This is achieved by quenching the cathode-ray tube trace by means of a negative voltage, applied to the grid (Wehnelt cylinder) and capable of being reduced to the necessary value for ordinary operation of the tube at those moments when V_g assumes the desired value.

A number of circuits can be suggested for this purpose, e.g. the grid voltage impulse of the valve to be measured can be made to operate a series of gas-discharge tubes to which successive grid bias voltages of 0, 25, 50, 75 V etc. are applied. The anode-voltage impulse from these tubes then counteracts the bias on the grid of the C.R. tube. Another method is illustrated in fig. 193, in which use is made of a so-called blocking oscillator (B, fig. 193). In this case the grid-voltage impulse of the valve to be measured is applied simultaneously to a second valve which then oscillates at a working point just above the cut-off, but which on completion of a cycle is in itself quenched until, after a period of time, the voltage of the impulse on its grid (and therefore also on the grid of the valve on test) has increased by a certain voltage; a single oscillation cycle then again follows. The anode-current impulse of the blocking oscillator can also be employed to render conductive the C.R. tube used for reproducing the characteristics. The intervals between the excitation impulses are then adjusted to the required value by means of appropriate equipment.

In order that the whole area of the fluorescent screen of the C.R. tube may be utilized, the zero point ($I_a = V_a = 0$) of the characteristics is adjusted to the bottom left corner by means of the transformers T, whose primaries are synchronized with the heater voltage in the same

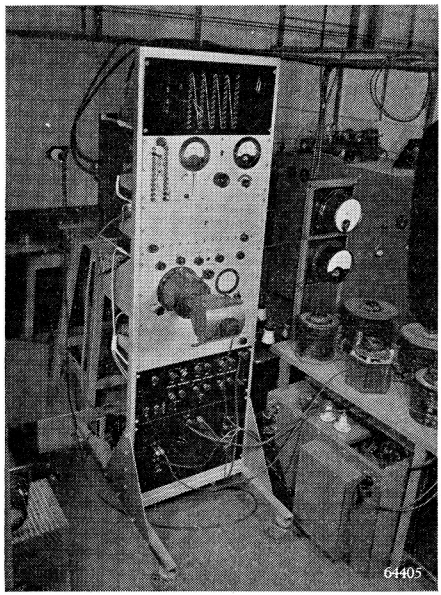

Fig. 193a. Photograph of the curve tracer, for tracing I_a–V_a characteristics at positive values of V_g.

way as the grid impulse. As the duration of the impulse on the grid of the valve on test is only about 1/100th of the interval between impulses, the position of the origin of the curves is sufficiently constant during the impulse time.

By reversing switch S it is possible to measure I_g–V_a as well as I_a–V_a curves.

In order to maintain within the proper limits any discrepancies in the calibrated differences in grid potential due to voltage drop caused by grid current passing through the potentiometer P_g, this potentiometer should be of low resistance, in consequence of which it becomes necessary to employ an amplifier V to ensure sufficient voltage for vertical deflection of the cathode-ray tube trace.

Using equipment of this kind, it is possible to inspect a whole family of I_a–V_a or I_g–V_a characteristics without overloading the transmitting valve, since, although the impulses are applied at high values of current and voltage, they are of extremely short duration.

Another feature, of some importance in measurements on large transmitting valves, is that the measuring equipment described is not too cumbersome. The source of voltage V_a, for example, need supply only a few hundredths of the power needed for dynamic measurement. Fig. 193*a* depicts a photograph of the equipment.

CHAPTER IX

Transmitting Valves for High Frequencies

GENERATION AT HIGH FREQUENCIES BY MEANS OF FEED-BACK CIRCUITS

§ 1. Use of feed-back circuits for long waves in the high-frequency range

Various feed-back circuits have already been described and illustrated by figs. 127 to 133 in chapter VI. In transmission work the circuits most commonly employed are the Hartley (fig. 128) and the tuned plate, tuned grid (fig. 133); the remaining circuits do not find such wide application because they are more complex. For instance, in the Colpitts oscillator (fig. 129), the anode circuit condenser must consist of two parts, otherwise a separate feed-back tapping has to be provided (fig. 131), whilst circuits incorporating inductive feed-back necessitate separate feed-back coils.

It is known (chapter VI, § 2) that the frequency generated by the Hartley oscillator is approximately the same as the resonant frequency of the anode circuit:

$$\omega = \frac{1}{\sqrt{LC}},$$

where L is the self-inductance and C the total capacitance of the oscillatory circuit. From this formula it follows that the frequency generated increases as the product of L and C is reduced.

A reduction in L means that the number of turns, the axial length and diameter of the coil concerned will be smaller, until ultimately the self-inductance will consist of only one single turn. The circuit capacitance C comprises the capacitance of the tuning condenser, with one or more of the valve capacitances in parallel with it.

Turning again to the above-mentioned Hartley- and tuned plate, tuned grid circuits (figs. 194 and 195), it will be seen that in the former, the capacitance C_{ag} between anode and grid is directly in parallel with the external capacitance C_u, whilst the grid-to-filament capacitance C_{gf} and anode-to-filament capacitance C_{af} lie in parallel with the lower and upper portions of the self-inductance L, respectively.

In the tuned plate, tuned grid oscillator, C_{of} is in parallel with C_2 in the

anode circuit, C_{gf} in parallel with C_1 in the grid circuit, and C_{ag} takes care of the feed-back. Clearly, if, to increase the oscillator frequency, the circuit capacitance is reduced, the limit value of this capacitance will be that of the valve capacitances themselves. In the extreme case already alluded to, where the circuit self-inductance consists of only one or two turns, the circuit capacitance being formed by the valve capacitances themselves, the circuits in figs. 194 and 195 assume the forms of figs. 196 and 197. The point p in fig. 196 corresponds to the same point in fig. 194. The amount of feed-back is controlled by shifting the position of the cathode tap p, and the same might be expected in relation to fig. 196, but it is found in practice that the location of this point p does not exclusively determine the amount of feed-back: this will be referred to later.

In fig. 196, as may be anticipated, the wavelength of the oscillator is governed mainly by L_a and C_{ag}; if, then, in fig. 197, L_g and L_a are taken to be the self-inductances of the grid- and anode circuits respectively, the frequency can be approximated by:

$$\omega = \frac{1}{\sqrt{(L_a + L_g)\, C_{ag}}},$$

which virtually means that we are concerned only with a single circuit of which the self-inductance comprises L_a and L_g in series, this self-inductance being tuned by the capacitance C_{ag}; this agrees with the Hartley circuit in fig. 196. Comparison between figs. 196 and 197 shows, moreover, that the two circuits are identical, point k in fig. 197 corresponding to point p in fig. 196 and L_a and L_g in the former to L_2 and L_1 in the latter. In the following paragraphs, therefore, we shall refer only to fig. 196.

There are certain difficulties in connection with the voltage feeds in an oscillator of the type shown in fig. 196, and these will now be discussed

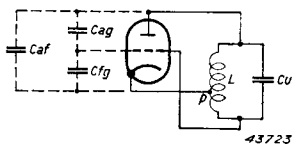

Fig. 194. Hartley oscillator.

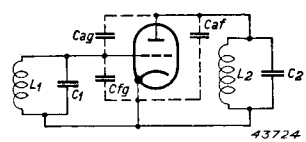

Fig. 195. Tuned plate-tuned grid oscillator.

in reference to a similar circuit for long waves. The feed in a Hartley circuit has already been illustrated in fig. 134: the direct voltage for the anode is applied in the feed-back line *pf* and is decoupled by a sufficiently high capacitance, to ensure that both *p* and *f* are at the same potential under conditions of high frequency. The heater is also connected to point *f* through two condensers of equal capacitance, so that the point *p* will be at the same H.F. potential as the heater. The lower end of the anode circuit is connected to the grid through an isolating condenser C_g whose impedance to H.F. currents is negligible. Direct current is applied to the grid by means of a choke and grid leak R_g.

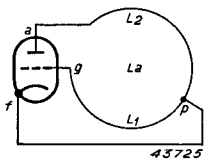

Fig. 196. As fig. 194, but for ultra-short waves.

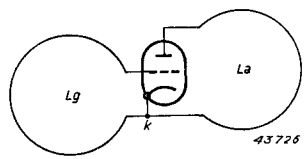

Fig. 197. As fig. 195, but for ultra-short waves.

If this feed system were applied to the circuit in fig. 196, the following difficulties would be encountered:

a) Usually, the heater cannot be earthed, for the heater must be regarded as being the actual emissive part of the filament system; the latter is attached to the connecting terminals by means of comparatively long leads or strips, according to the particular type of construction of the valve. The self-inductance of these strips is small enough, but at the higher frequencies now under consideration their impedance cannot be neglected. When H.F. currents are passed through this impedance, a potential difference occurs between the emissive part of the heaters and the connecting terminals on the glass envelope of the valve, and, when these terminals are earthed, the heater proper is actually not earthed at all.

b) If the grid condenser and leak are mounted at the point *g* (fig. 196), that is, close to the grid, the input impedance of the valve is increased by the self capacitance of the choke as well as by the earth capacitances of both choke and grid condenser. This means that the wavelength of the oscillator will be longer than if these elements

were not incorporated, or else that the working of the valve, to produce a certain desired wavelength, will not be so satisfactory, seeing that the input capacitance of the valve tends to short-circuit the excitation voltage, the more so the greater the capacitance is.

c) The object of the connection *pf* in the Hartley circuit (fig. 196) is to give the point *p* the same potential as the heater, so that the feed-back shall be determined by the relation L_1/L_2. Now, as has been seen, it is not possible by earthing the heater terminals to have the heater itself at earth potential, owing to self inductance of the internal heater leads, and the same actually applies to the point *p* in relation to point *f*; the self-inductance of the lead *pf* cannot be disregarded, since the point *p* is always at some distance from *f*. It follows, therefore, that these two points can never be at the same H.F. potential, and this in turn means that the feed-back by way of *pf* is not fully effective.

d) Whereas in the long-wave circuit in fig. 134 the position of the point *p* in the anode coil is a measure of the H.F. potential of the grid in relation to the heater, the grid potential in the short-wave circuit in fig. 196 is also strongly affected by the capacitances of the valve. The circuit in fig. 196 is reproduced again in fig. 198 with the valve capacitances C_{ag}, C_{af} and C_{fg} added, but omitting the feed-back coil *pf*, comparison of this circuit with fig. 131 shows that this is a Colpitts circuit. C_1 and C_2 in the last-mentioned circuit correspond to C_{af} and C_{fg} in fig. 198, and C in the former to C_{ag} in the latter.

Owing to the high frequency, the impedance produced by these valve capacitances is relatively low and the capacitive currents which they carry are fairly high: consequently, the H.F. grid potential depends to a high degree on the value of the valve capacitances C_{af} and C_{fg}, even when the extra feedback path *pf* is provided. For these reasons, when frequencies over about 100 Mc/s are involved (3 metres wavelength), the circuits are such that the feeds can be easily derived from a part of the network that does not carry H.F. voltages, and the next paragraph deals with the suitability of a balanced oscillator, amongst others, for this purpose.

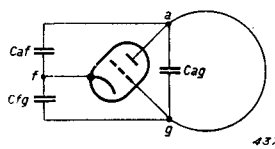

Fig. 198. As fig. 196, but including the valve capacitances.

§ 2. The balanced oscillator. The Lecher system

In chapter VI, § 4*c* something has already been said regarding the balanced oscillator, and figs. 199 and 200 represent two circuits based on this system, the former being one in which the feed-back is derived from the anode-to-grid capacitances of the valves, whilst in fig. 200 the grid of each valve is for this purpose connected through a condenser to the anode of the other.

In fig. 199 the feed-back is naturally always present, as also in fig. 200, but in the latter it is surpassed by the effect obtained from the tapping in the anode circuit. This can best be visualized by substituting for condensers C in fig. 200, of which the impedance is very small, condensers whose capacitances are equal to those of the anode-to-grid capacitances of the valves. In effect, this is the well-known neutralizing circuit in which each grid receives two voltages, namely one from its own anode by reason of C_{ag} and one from the anode of the other valve, through the neutralizing condenser. Since the alternating anode voltages are of the same amplitude, but of opposite phase, no voltage is fed back to the control grids. On the other hand, if the capacitances C are omitted, as in fig. 199, or if they are greater than C_{ag} as in fig. 200, feed-back does occur. At the same time, it is essential for oscillation purposes that the alternating grid voltage feed-back is in each valve in counter-phase with the individual anode voltage, and in fig. 199, where the feed-back is derived from the anode of the valve concerned, the grid circuit must therefore be inductive; in fig. 200, on the other hand, it is capacitive, since the other anode is used as source.

The advantage of the circuit in fig. 200 is that the feed-back can be varied by means of the capacitances C, although that in fig. 199 is

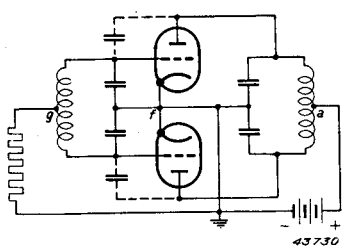

Fig. 199. Balanced oscillator with feed-back through C_{ag}.

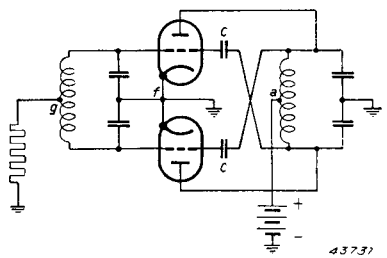

Fig. 200. Balanced oscillator with feed-back obtained from a tapping in the anode circuit.

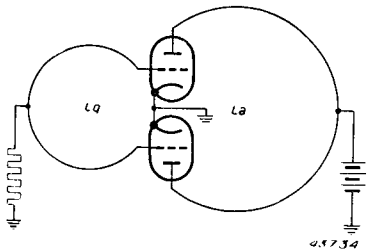

Fig. 201. Circuit as in fig. 199. but for very short waves.

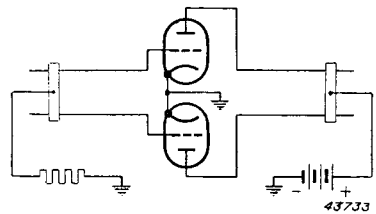

Fig. 202. Circuit as in fig. 201, equipped with Lecher wires.

simpler from the constructional point of view, and the frequencies generated are slightly higher than in fig. 200, under otherwise similar conditions.

In order to produce increasingly higher frequencies, both the self inductance and capacitance of the two circuits may be reduced until ultimately the grid circuit consists of only one turn of wire, having in parallel with it the series-coupled grid-to-filament capacitances of the two valves, and the same applies to the anode side, where the anode-to-filament capacitances in series with each other constitute the circuit capacitance (fig. 201).

Again, it is necessary, to ensure efficient working of the oscillator, for the resonant frequencies of the grid- and anode circuits to be as nearly as possible equal, this being very easily accomplished on long waves by means of the variable tuning condenser. In fig. 201, however, this is no longer possible; only L_a and L_g can be varied, but there is a fairly simple method of overcoming this, by making L_g and L_a in the form of two connections running parallel, with a short-circuiting bridge across them (fig.202). The self-inductance can then be varied at will by sliding the bridge across the two connections. Since the two bridges lie in the axis of symmetry of the circuit and therefore at points of zero H.F. potential, the anodes and grids can be fed from these points. This system of parallel leads, known as a Lecher system, must, however, not be regarded as a pure self-inductance at all frequencies, since the space between the leads is small and their mutual capacitance therefore fairly high. The H.F. current entering the one lead does not follow the whole length of the conductor at full strength, returning by way of the bridge and the other conductor, but, owing to the potential

difference developed between two opposite points in the conductors, a capacitive current passes directly from one conductor to the other.

The magnitude of this capacitive current at any given point in the system is then naturally proportional to the potential difference between conductors at that point, whilst this potential difference is in turn dependent on the loss of potential which the current undergoes in the preceding components of the system. Further, since the current in these components is partly determined by the degree to which capacitive current flows between the conductors, it follows that the current strength cannot be the same at every cross section of the conductors, but must vary between one point and another along the length of the wires: the same naturally holds good with respect to the potential difference between the conductors.

It is possible therefore, to speak of both current- and voltage distribution throughout the whole Lecher system, these being determined, in accordance with the theory of alternating currents, from the so-called telegraphy equations. This point will not be investigated further here, but it is of interest to mention those results which will be of service.
If a pair of Lecher wires, of length l and shorted at one end (fig. 203), is fed at the other end with an alternating voltage represented in its most complete form by:

$$v = V_o e^{j\omega t},$$

then the current at that point is represented by:

$$i = I_o e^{j\omega t},$$

and the relation between the complex amplitudes V_o and I_o by:

$$\frac{V_o}{I_o} = j\zeta \operatorname{tg} \frac{2\pi l}{\lambda} \quad \ldots\ldots\ldots \quad (9.\ 1)$$

In this, ζ is the so-called characteristic impedance of the Lecher system, as calculated from:

$$\zeta = \sqrt{\frac{L^{(1)}}{C^{(1)}}},$$

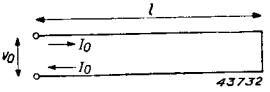

Fig. 203. Double-wire Lecher system of length l, shorted at one end.

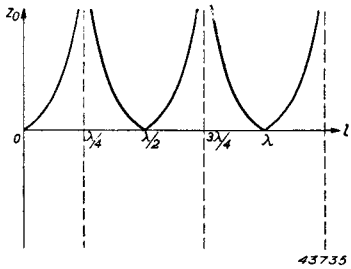

Fig. 204. Input impedance Z_0 of the system shown in fig. 203 as a function of l.

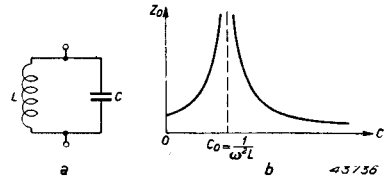

Fig. 205. a) LC circuit. *b)* Parallel impedance Z_0 of this circuit as a function of C.

where $L^{(1)}$ and $C^{(1)}$ are the self-inductance and capacitance of the system per unit of length: the relation between the wavelength λ (in metres) and the angular frequency is given by:

$$\lambda = \frac{2\pi c}{\omega}, \quad c = 3.10^8 \text{ m/sec.}$$

The input impedance thus appears to be reactive, and the modulus of this impedance is set out in fig. 204 as a function of the length of the wire, l. From this figure it follows that, at a given value of λ, that is ω, the input impedance is infinitely great [1] at certain lengths of the system, e.g. at $l = \lambda/4, 3\lambda/4, 5\lambda/4$, etc. On the other hand, when $l = \lambda/2$, λ, $3\lambda/2$ etc., the input impedance is zero.

To left and right of each of the points in question, the sign of the tangential function is reversed, which means, in view of (9. 1), that the input impedance changes from inductive to capacitive and vice-versa. The behaviour of this impedance in the vicinity, say, of $l = \lambda/4$ very closely resembles that of a parallel circuit very near to the resonance frequency, for a circuit of which type (see fig. 205*a*):

$$Z = \frac{j\omega L \cdot \frac{1}{j\omega C}}{j\omega L + \frac{1}{j\omega C}} = \frac{j\omega L}{1 - \omega^2 LC}.$$

This impedance is, then, inductive or capacitive according to whether $1 - \omega^2 LC \gtrless 0$, that is, $\omega \gtrless 1/\sqrt{LC}$, whilst at $\omega = 1/\sqrt{LC}$, it is infinitely great [1]. The curve in fig. 205 represents the impedance as

[1] Assuming no losses occur.

a function of the capacitance C. The similarity between the behaviour of the LC circuit and the Lecher system means that, in a circuit of the type shown in fig. 199, the former can safely be replaced by the latter, and this gives us the arrangement depicted in fig. 202. One difference between the circuit and the Lecher system, however, is that the latter, according to fig. 204, has apparently a large number of resonance points: at a given wavelength, the input impedance is infinitely great at $l = \lambda/4, 3\lambda/4, 5\lambda/4$ etc., and at very short wavelengths it is possible to make good use of this characteristic.

When a balanced oscillator circuit of the kind illustrated in fig. 202 is constructed on the Lecher principle in both anode- and grid circuits, the lengths of these systems will for two reasons be smaller than $\lambda/4$, when λ is the wavelength of the oscillation generated. In the first place, the theory of oscillators on long waves teaches us that a circuit incorporating capacitive feed-back can only oscillate when the anode- and grid circuits are inductive at the working frequency, and, according to fig. 204, this condition obtains when $l < \lambda/4$. Secondly, there exists between the input terminals of the two systems in fig. 202 the capacitance of the transmitting valves, these being $^1/_2\, C_{fg}$ at the grid end and $^1/_2\, C_{af}$ at the anode end, and the effect of these capacitances is to bring the circuits into resonance at a length $l < \lambda/4$: l is so much the smaller according as the input capacitance is increased. The impedance between the points A and B in fig. 206 is that of the Lecher system $j\zeta \tan 2\pi l/\lambda$, in parallel with that of the capacitance $1/j\omega C$, or:

$$Z = \frac{j\zeta \operatorname{tg} \frac{2\pi l}{\lambda} \cdot \frac{1}{j\omega C}}{j\zeta \operatorname{tg} \frac{2\pi l}{\lambda} + \frac{1}{j\omega C}} = \frac{j\zeta \operatorname{tg} \frac{2\pi l}{\lambda}}{1 - \omega C \operatorname{tg} \frac{2\pi l}{\lambda}}.$$

Resonance occurs when:

$$1 - \omega C \zeta \tan \frac{2\pi l}{\lambda} = 0,$$

that is, when:

$$\tan \frac{2\pi l}{\lambda} = \frac{1}{\omega C \zeta} \quad \ldots\ldots\ldots \quad (9.\ 2)$$

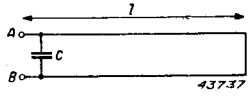

Fig. 206. Lecher system as in fig. 208, but loaded with a capacitance C.

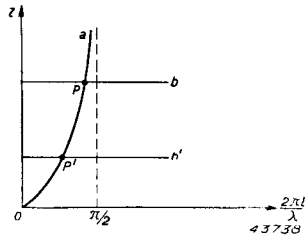

Fig. 207. Determination of the tuning length l of the system shown in fig. 211.

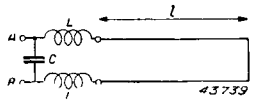

Fig. 208. Lecher system in accordance with fig. 211, connected to feed through two self-inductances L.

In the case of $C = 0$, $\tan 2\pi l/\lambda$ is actually ∞, so that $2\pi l/\lambda = \pi/2$, or $l = \lambda/4$; on the other hand, if $C > 0$, the tangential function is finite and $2\pi l/\lambda < \pi/2$, so that $l < \lambda/4$. This result is also obtained from fig. 207, where the quantity $2\pi l/\lambda$ is plotted as abscissa, λ being regarded as constant, with l as variable. As a function of this quantity, the left-hand term of (9. 2) (curve a) is shown, as well as the right-hand term which is independent of l and which is therefore represented by a straight horizontal line. The point of intersection P, of a and b, gives the value $2\pi l/\lambda$, or that of l, conforming to (9. 2).

Now, the straight line b lies closer to the abscissa according as the product $C\zeta$ becomes greater (b'); the relative value of $2\pi l/\lambda$ then becomes smaller and smaller. In a circuit such as fig. 202, therefore, it is seen that, for a given wavelength, the requisite length of the Lecher system becomes shorter according as the capacitances of the transmitting valves are greater, and, when the required wavelength is very small, this fact gives rise to difficulties in that the system becomes too short.

In many cases there is also a third reason why the length of the system can be less than $\lambda/4$; the ends A and B of the lines in fig. 206 cannot generally be connected direct to the relative electrodes, seeing that the latter are inside the valve and are connected to their terminals by wires or strips. As already explained, the impedance of these leads at the frequencies under consideration must not be overlooked. The circuit in fig. 206 then becomes that of fig. 208 in which the self-inductances of these leads are represented by L. The impedance Z between A and B is then:

$$Z = \frac{j\left(2\omega L + \zeta \operatorname{tg} \frac{2\pi l}{\lambda}\right)}{1 - \omega C\left(\zeta \operatorname{tg} \frac{2\pi l}{\lambda} + 2\omega L\right)},$$

and resonance occurs when:

$$1 - \omega C \left(\zeta \operatorname{tg} \frac{2\pi l}{\lambda} + 2\omega L \right) = 0,$$

that is, at:

$$\operatorname{tg} \frac{2\pi l}{\lambda} = \frac{1}{\omega C \zeta} - \frac{2\omega L}{\zeta} \quad \ldots\ldots\ldots \quad (9.\ 3)$$

Comparison of this expression with (9. 2) shows that the right-hand term has become smaller to the extent of $2\omega L/\zeta$, and the result of this is a further reduction in $\tan 2\pi l/\lambda$, i.e. of l.

The above reasons for the decrease in the resonance length of the Lecher system have resulted in a tendency to produce transmitting valves, for use at high frequency in smaller dimensions, but carrying high specific loads, both the capacitance and the length of the leads being smaller than in earlier types of transmitting valve. This point will be referred to in § 3.

Finally it may be said that, even in cases where the circuits are not balanced, it is advantageous to employ a form of tuned line circuit which then comprises a co-axial system, the transmitting valve being placed within the inner conductor. This method is particularly suitable for valves made with what is known as the "disc-seal". If the disc-seal be attached to a metal plate which divides the outer cylinder into two compartments, with the anode connected to an inner cylinder in one of the compartments and the cathode to the same cylinder in the other compartment, we then have two circuits, each tunable by means of a plunger, the first of these circuits being the anode-grid and the second the grid-cathode circuit. It is not necessary for the plungers to make metallic contact with the outer cylinder, which is preferably earthed.

The capacitance of the plunger with respect to the inner wall of the outer cylinder then forms a sufficiently low reactance to function as a short circuit, whilst the D.C. voltages can be applied direct to the inner conductors. If the valve is to be used as an oscillator, the C_{af} of the valve can be made to serve for the feed-back, although this value is in many cases so low that extra coupling between the compartments has to be provided. Feed-back of the correct phase and intensity is ensured by carefully adjusting both the length of the feed-back lead and the output capacitance.

The advantages of this type of circuit are as follows:

1) Feed-back is by means of the valve capacitance C_{af} and the feed-back lead only, so that parasitic coupling is avoided.
2) The use of a single circuit instead of the balanced type eliminates the risk of parallel oscillation.
3) Since the outer member of the system completely shields all the H.F. components of the circuit, radiation from the valve and associated parts is very slight.
4) In view of the large area of the inner and outer conductors, $\zeta = \sqrt{\frac{L^{(1)}}{C^{(1)}}}$ can be kept quite low. The product $C\zeta$ mentioned in § 2 may thus retain the same value for a higher value of C (or acquire a lower value with constant C), which means that higher valve capacitances can be employed for a certain length l of the circuit (or the length can be increased for a certain value of C).

By this method it is possible to tune valves which are otherwise not tunable when a circuit consisting of two parallel conductors is used.

§ 3. H.F. amplification

The foregoing considerations are applicable mainly to triodes, as this is the most obvious type of valve to use in an oscillator circuit; when high-vacuum valves are employed as controlled amplifiers, however, the generally accepted practice as in long wave technique is also followed in respect of short waves, tetrodes or pentodes being used, the great advantage of these being that they require neutralizing only at the higher frequencies, whilst their control power, owing to the presence of the screen and suppressor grid, which carry on H.F. potential with respect to the cathode, compares very favourably with that of the triode.

When the screen-grid valve (tetrode or pentode) is used on very short waves the situation is not, however, quite the same as with long waves. The screen- and suppressor grids in the more common types of screen-grid valve are also connected within the envelope to their respective terminals by means of more or less long leads. The capacitive currents flowing through the valve as a result of the H.F. alternating voltages on grid and anode pass along these leads to the cathode in sofar as terminals are connected to the cathode in the usual way, through these sufficiently large condensers.

In consequence of the finite impedance of these leads, a H.F. potential is developed across the grids and their respective terminals, the magnitude

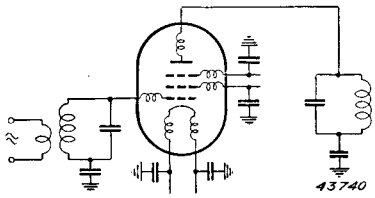

Fig. 209. Circuit of a pentode amplifier for U.S.W., showing the self-inductances of the internal eads of the valve.

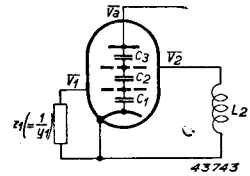

Fig. 210. Tetrode with self-inductance L_2 in the screen-grid lead, showing capacitances C_1, C_2 and C_3.

of which potential depends on the capacitance of the valve, the self-inductance of the leads in question and also on the alternating anode and control-grid voltages. The screen- and suppressor grids are therefore not at zero H.F. potential with respect to the cathode and the specific action of these grids, as obtaining under long wave conditions, namely screening between anode and control grid, is rendered void.

The circuit of an H.F. pentode amplifier thus takes the form shown in fig. 209, which includes the self-inductances of the other electrodes as well as those of the internal screen- and suppressor-grid leads.
The calculation of the alternating voltages on the screen- and suppressor grids in respect of known valve capacitances, self- and mutual inductances of the leads and at given anode- and control-grid potentials is very complicated, and the result is not clearly defined; the followingis therefore restricted to the simple instance of a tetrode (fig. 210), taking into consideration only the capacitances between adjacent electrodes and the self inductance L_2 of the screen-grid circuit. The control grid is regarded as being externally connected to the cathode through the impedance Z_1 (grid circuit).
In respect of a given alternating anode voltage $\overline{V_a}$, the calculation yields the alternating voltages $\overline{V_2}$ and $\overline{V_1}$ produced in the screen- and control grid; the following expressions therefore apply:

$$\frac{\overline{V_2}}{j\omega L_2} + (\overline{V_2} - \overline{V_a})\, j\omega C_3 + (\overline{V_2} - \overline{V_1})\, j\omega C_2 = 0 \quad . \quad . \qquad (9.\ 4)$$

$$\overline{V_1} Y_1 + (\overline{V_1} - \overline{V_2})\, j\omega C_2 + \overline{V_1} j\omega C_1 = 0 \ , \ . \ . \ . \ . \qquad (9.\ 5)$$

or, in re-arranged form:

$$-\overline{V_1}j\omega C_2 + \overline{V_2}\left\{j\omega(C_2 + C_3) + \frac{1}{j\omega L_2}\right\} = \overline{V_a}j\omega C_3 \quad (9.\ 6)$$

$$\overline{V_1}\{Y_1 + j\omega(C_1 + C_2)\} - \overline{V_2}j\omega C_2 = 0 \quad (9.\ 7)$$

From this it follows that:

$$\overline{V_1} = \frac{\omega^2 C_2 C_3}{\Delta}\overline{V_a} \quad (9.\ 8)$$

$$\overline{V_2} = \frac{-j\omega C_3\{Y_1 + j\omega(C_1 + C_2)\}}{\Delta}\overline{V_a}, \quad (9.\ 9)$$

where:

$$\Delta = \omega^2(C_1C_2 + C_1C_3 + C_2C_3) - \frac{C_1 + C_2}{L_2} - Y_1\left\{j\omega(C_2 + C_3) + \frac{1}{j\omega L_2}\right\} \quad (9.\ 10)$$

The admittance Y_1 of the grid circuit will usually be complex, but let us say that:

$$Y_1 = G_1 + jB_1 \quad (9.\ 11)$$

Substitution in (9. 10) then gives:

$$\Delta = \omega^2(C_1C_2 + C_1C_3 + C_2C_3) - \frac{C_1 + C_2}{L_2} + B_1\left\{\omega(C_2 + C_3) - \frac{1}{\omega L_2}\right\} -$$

$$-jG_1\left\{\omega(C_2 + C_3) - \frac{1}{\omega L_2}\right\} = \Delta_1 + j\Delta_2 \quad (9.\ 12)$$

By means of the above, $\overline{V_1}$ and $\overline{V_2}$ can be calculated, but, in order to simplify the outcome, it will be assumed that the self-inductance is so small that in the expression of Δ it is only necessary to take into account those terms in which L_2 occurs in the denominator. Then:

$$\Delta \approx -\frac{C_1 + C_2}{L_2} - \frac{B_1}{\omega L_2} + \frac{jG_1}{\omega L_2}.$$

What we are interested in is the highest value that can be reached by $\overline{V_1}$ in the given circumstances; this value is apparently dependent on the impedance of the grid circuit, $\overline{V_1}$ attaining its maximum value when the real element is eliminated from the expression of Δ. B_1 is the case taken to be such that:

$$-\frac{C_1 + C_2}{L_2} - \frac{B_1}{\omega L_2} = 0,$$

in which $B_1 = -\omega(C_1 + C_2)$. This latter simply means that the

grid circuit is in parallel resonance with C_1 and C_2, under which conditions:

$$\Delta = \frac{jG_1}{\omega L_2};$$

$$Y_1 = G_1 - j\omega (C_1 + C_2),$$

and therefore:

$$\overline{V_1} = \frac{\omega^3 L_2 C_2 C_3}{jG_1} \overline{V_a}. \quad \ldots\ldots\ldots \quad (9.13)$$

and

$$\overline{V_2} = -\omega^2 L_2 C_3 \overline{V_a} \quad \ldots\ldots\ldots \quad (9.14)$$

$\overline{V_1}$ and $\overline{V_2}$ then disappear when $L_2 = 0$, which is as it should be.
Taking the most practical values for the different elements to be as follows:

$$\begin{aligned} \lambda &= 5 \text{ m, i.e. } \omega = 3.77.\ 10^8, \\ L_2 &= 50 \text{ cm} = 5.10^{-8}\ H, \\ C_2 &= 10 \text{ pF} = 10^{-11}\ F, \\ C_3 &= 5 \text{ pF} = 5.10^{-12}\ F, \\ G_1 &= \frac{1}{10^4 \text{ ohm}}, \end{aligned}$$

then:

$$\begin{aligned} \overline{V_1} &= -j\ .\ 1.34\ \overline{V_a} \\ \overline{V_2} &= -0.0355\ \overline{V_a}. \end{aligned}$$

The voltage fed back to the grid in this case is even greater than the anode voltage, and this is, of course, partly due to the fact that the control-grid circuit is in tune and its impedance therefore high. The above value of L_2 is already reached when the connecting lead between the screen grid and its corresponding terminal is about 7 cm long, a length that is sometimes encountered in conventional valves.

It should be noted that from the aspect of the retroaction on the control grid, a pentode is better than a tetrode, in view of the double screening between anode and control grid. In a tetrode, the alternating voltage on the screen is in any case produced direct by capacitive coupling with the anode, which carries a high alternating voltage; in pentodes, on the other hand, the screen is coupled capacitively to the suppressor grid, at which the alternating voltage is usually much lower.

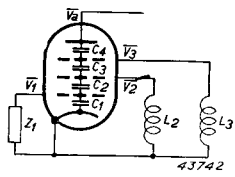

Fig. 211. Pentode with self-inductances L_2 and L_3 in the screen- and suppressor circuits, showing capacitances C_1, C_2, C_3 and C_4.

If we now calculate in terms of fig. 211 the alternating voltages on the various grids, given:

$$\lambda = 5 \text{ m}$$
$$L_2 = L_3 = 50 \text{ cm}$$
$$C_1 = C_2 = C_3 = 10 \text{ pF}$$
$$C_4 = 5 \text{ pF}$$
$$G_1 = \frac{1}{10^4 \text{ ohm}},$$

and assuming the reactive part of the grid circuit to be so adjusted as to give a maximum voltage on the control grid, we have:

$$|V_1| = 9.5 \cdot 10^{-2}|V_a|;\ |V_2| = 0.721 \cdot 10^{-2}|V_a|;\ |V_3| = 3.56 \cdot 10^{-2}|V_a|,$$

in which case the alternating voltage on the control grid is definitely much lower.

For the rest, when tetrodes are used for high frequencies, it is usually necessary to counteract the detrimental effect of the screen and suppressor leads by series-tuning these self-inductances with condensers. Applying this to the original balanced circuit, the arrangement depicted in fig. 212 is obtained, series tuning being also included between the cathodes for the sake of completeness. This series tuning eliminates the impedance between the respective electrodes of the two valves, and, from the point of view of symmetry, it follows that they will assume zero H.F. potential. In these circumstances the valves will function in the same way as for longer wavelengths, apart from the inertia of the electrons, the effect of which becomes more and more marked at higher frequencies.

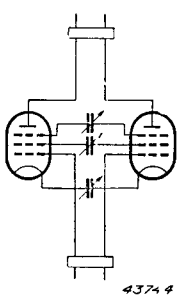

Although good results are obtained from the series-tuning method, it should be remembered that, strictly speaking, the resultant impedance between the electrodes concerned in the balanced circuit disappears at

Fig. 212. Circuit of balanced pentode oscillator for ultra-short waves, employing series tuning on g_3, g_2 and k.

one frequency only, viz. the working frequency and not at all other frequencies. It is therefore quite possible for a balanced oscillator that is stable at a certain short wavelength to be unstable at other wavelengths: for the measures to be taken to counteract such instability, reference should be made to standard works on the subject.

Needless to say, triodes are also employed as transmitting valves in balanced oscillators, although, naturally, neutralizing circuits must be employed to eliminate coupling between the anode and grid of each valve, arising from the inter-electrode capacitance C_{ag}. A neutralizing circuit of this kind has already been discussed in § 2 (fig. 200). If this circuit is drawn after the fashion of fig. 213 it is possible to see how the valve capacitances C_{ag} with the neutralizing condensers C_n together form a Wheatstone bridge which is balanced when $C_n = C_{ag}$, an alternating voltage in the grid circuit being then unable to set up a corresponding voltage in the anode circuit and vice-versa. Furthermore, an alternating voltage in the anode circuit cannot produce a voltage between the filament and grid of each of the valves. This may be expressed otherwise, that feed-through and undesired feed-back are suppressed, leaving only the effect of the inter-electrode and neutralizing capacitances on the tuned circuits.

The advantage of the circuit reproduced in fig. 213 is that the balance of the bridge is not dependent on frequency, the elements of the bridge being purely capacitive. On short waves, however, the situation is not so stable, especially when large transmitting valves are involved.

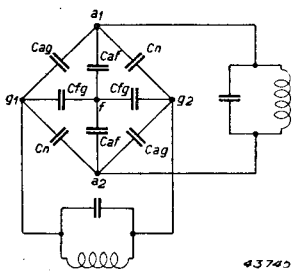

Fig. 213. Circuit of neutralized balanced oscillator, employing triodes, on long waves.

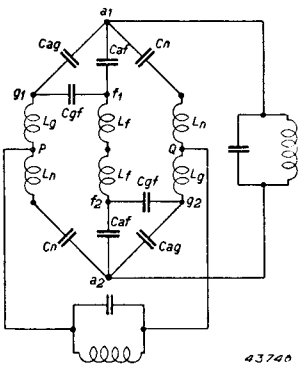

Fig. 214. Circuit of neutralized balanced oscillator comprising two triodes TA 20/250, on a wavelength of 15 metres.

The leads connecting the neutralizing condensers to the different electrodes, as well as the internal connections to the heater and grid, are relatively long, and it is found that the self-inductances of these leads on short waves of, say, about 15 metres, cannot be ignored. The simple bridge circuit shown in fig. 213 then takes the form of that in fig. 214, where L_n, L_g and L_f represent the self-inductances of the neutralizing connections, the grid leads and heater connections.

In the more complicated circuit it is also quite possible to employ a value of C_n that will balance the bridge, producing a condition where complete decoupling exists between the anode- and grid circuits, but this in itself is not sufficient to ensure stability of the amplifier. To this end it is essential (see fig. 214) that an alternating voltage between a_1 and a_2 shall not set up any alternating voltage across g_1 and f_1, and across g_2 and f_2. To meet these requirements various methods have been evolved at the Philips Works.

According to one of these methods, the self inductances of the grid- and heater leads are tuned with series condensers, to remove the impedance, the heater and grid being thus, as it were, taken out of the valve and the circuits and neutralizing condensers connected at those points.
Another, simpler, method meets both the above-mentioned requirements and consists in a careful selection of the position of the points P and Q in fig. 214, at which the grid circuit is coupled to the main circuit. In one example with the Philips valve, type TA 20/250, use is made of the circumstance that the valve has two external grid terminals (see fig. 1), of which one serves for connection of the grid circuit and the other for the neutralizing condenser.
In this way it has been found possible to arrange two of these valves for anode modulation on a wavelength of 15 metres, giving a carrier-wave power of a good 100 kW on 12 kV anode potential. For further particulars in regard to this, reference may be made to existing literature.

§ 4. Valves for high frequencies

In the foregoing, two factors have been mentioned that will give rise to difficulties on short waves when standard "long-wave" transmitting valves are used, viz. the capacitances between the various electrodes and the self-inductances of the leads taken from these electrodes to the

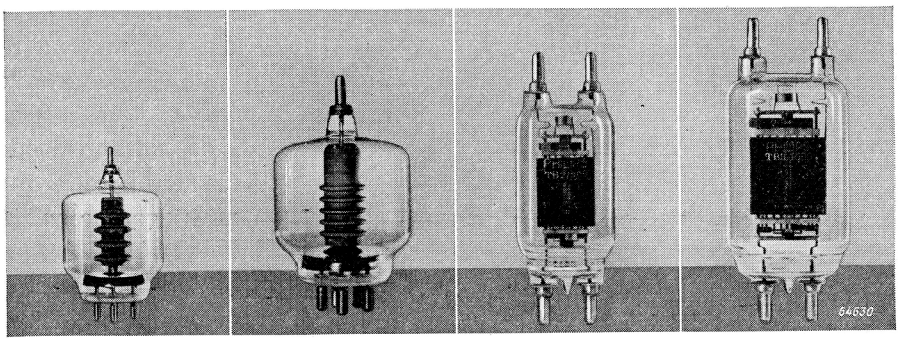

Fig. 215. Triodes TB 3/750, TB 4/1250, TB 2/500 and TB 3/1000 shown together for comparison. The first two of these have the pressed glass base and no further insulating material between the electrodes, their maximum output being 840 and 1450 W at frequencies of 100 Mc/s. The two large valves have the moulded glass base and insulating plates and rods between electrodes; they deliver a maximum of 550 and 1200 W at 20 Mc/s.

outside of the envelope. On short waves, the capacitances, together with the self-inductances, constitute a considerable part of the grid- and anode circuits, so that the external portion of the circuit at a given wavelength must be very much smaller than if the elements in question were not present. This means that there is not only a limit to the extent to which high frequencies can be attained, but also that connection of the load resistance to the anode circuit, and the excitation voltage to the grid circuit, are accompanied by many more difficulties than otherwise, and frequently they cannot be adjusted to their optimum values at all.

Mention should also be made of the dielectric losses in the glass, which constitute loading in the circuits and, at the shorter wavelengths, will even give rise to the destruction of the glass; the anode and control-grid connections are therefore often located at widely spaced points on the envelope, as in the TB 2.5/300, TB 3/750 and TB 4/1250 (cf. fig. 4). A fourth reason why the wave range of a transmitting valve is limited towards the shorter waves is to be found in the inertia of the electrons. In recent years Philips have designed a number of transmitting valves with a view to reducing the effect in question to a minimum, and they have been successful in extending the short-wave range to well below 3 metres.

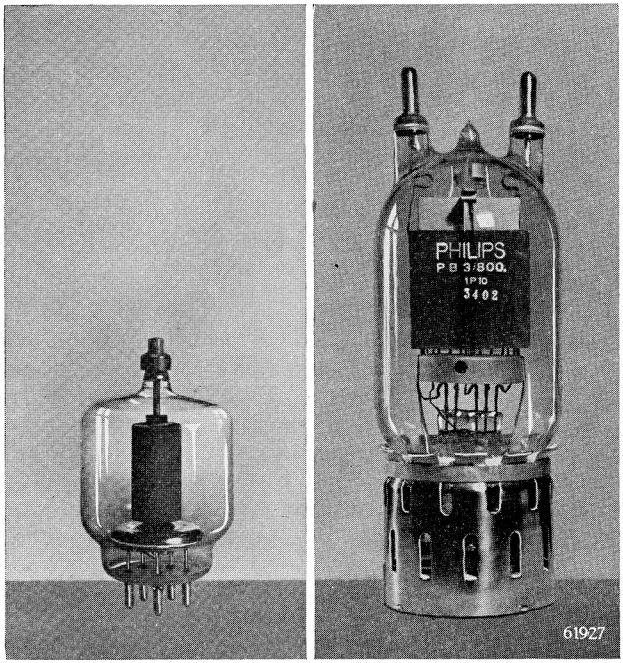

Fig. 216. Tetrode QB 5/750 in comparison with the pentode PB 3/800. The first has a pressed glass base, no other insulating material between electrodes, and delivers 1000 W at 75 Mc/s. The pentode is fitted with moulded glass base and contains insulating plates and rods; the maximum output is 1200 W at 10 Mc/s.

In surmounting the main drawback inherent in long-wave valves, that is, the high inter-electrode capacitances, the only course open is to reduce the area of the electrodes. It might be considered that increasing the distance between one electrode and another would help matters, but sooner or later this involves the fourth objection mentioned above, the inertia of the electrodes.

Any reduction in the area of the electrodes, however, is accompanied by a corresponding reduction in the permissible anode dissipation and cathode current, i.e. the H.F. output power, unless it is possible also to increase the specific load of the various components. In valves with oxide cathodes, such as the QQC 04/15, the emission is 2 to 3 A/cm^2 at a working temperature of the heater of about 1000 °K, but the specific anode dissipation (1 or 2 W/cm^2) must not be so high that radiant back heating of the filament occurs.

In valves with thoriated tungsten filaments, the working temperature is however about 2000 °K and the specific emission about 2 A/cm^2, the higher temperature making it possible for the specific anode dissipation also to be so much the higher (about 5 W/cm^2). In this type of valve, therefore, the nickel normally used for the anode and grids of oxide-

cathode valves is replaced by molybdenum or graphite. The moulded glass base has been superseded by a base of sintered powder glass. These bases are made in cheap graphite moulds; they are not dish-shaped, but flat, and the leads between the contact pins and the electrodes are therefore shorter than otherwise (less self-inductance). Thick metal bushes are mounted on the external extremities of the contact pins, to ensure, proper contact with other parts of the circuit.

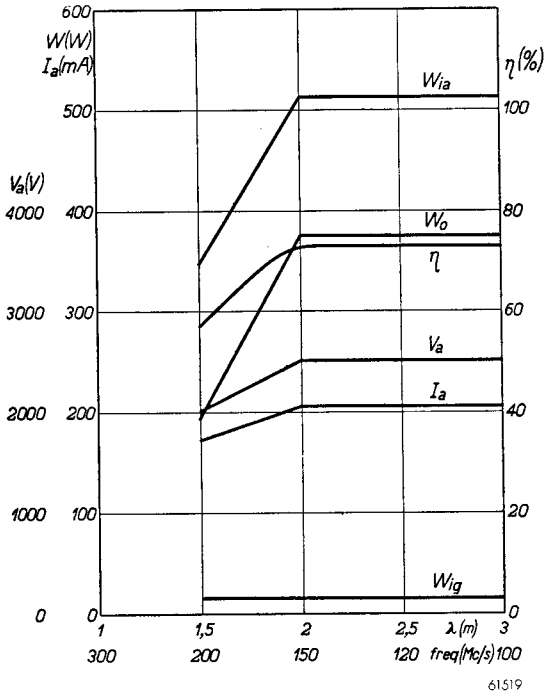

Fig. 217. Efficiency curves of the TB 2.5/300, together with the H.F. power W_o and anode current I_a as function of the wavelength. The values refer to two valves working as balanced oscillator. The anode voltage drops slightly as the wavelength becomes shorter, to meet requirements in connection with the maximum permissible temperature of the anode terminal on the valve. When the anode voltage is constant, the temperature increases as the wavelength is decreased because of the higher capacitive currents in the valve and the skin effect at the terminal.

In connection with the high specific anode dissipation and in order to meet the demand for a glass envelope of the smallest possible dimensions, the envelope is made of hard glass which is able to withstand higher temperatures than the soft glass of which the bulbs of oxide-cathode valves were formerly made.

In this way the triodes TB 4/1250, TB 3/750, TB 2.5/300 (see fig. 4), as also the tetrodes QB 3.5/750 and QB 3/300 (fig. 5) have been evolved. To illustrate the resultant reduction in dimensions of the valve, the triodes TB 3/750, TB 4/1250, TB 2/500 and TB 3/1000 are depicted in fig. 215, and the tetrode QB 3.5/750 and pentode PB 3/800 in fig. 216.

Fig. 217 shows what can be attained with the triode TB 2.5/300 on wave-

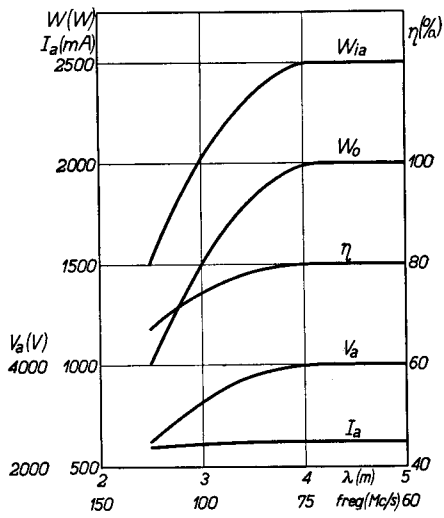

Fig. 218. Efficiency curve of the QB 3.5/750. The values are in respect of two controlled valves in a balanced circuit. Further, see remarks concerning the TB 2.5/300 (fig. 217).

lengths less than 3 metres, giving H.F. power and efficiency as function of the wavelength. The data refer to 2 valves working in a balanced oscillator circuit. Fig. 218 gives the same details in relation to two valves type QB 3.5/750.

In connection with the foregoing it should be remarked that, in the case of the tetrodes QB 3.5/750 and QB 3/300, effects of the self-inductance of the screen-grid lead are definitely noticeable in the wave range under review, so that it is necessary to employ condensers for series-tuning in these leads. This handicap has been removed in the design of the double tetrode QQE 06/40 (fig. 219), wherein series tuning is not necessary since the leads in question are kept sufficiently short by mounting the two valve systems in a common envelope. The method of construction of the QQE 06/40 is shown in fig. 220. A common oxide cathode is flanked on either side by a grid; the screen grid is common to both sections, but there are separate anodes.

The self-inductance between the screens and cathodes of the two halves is thus reduced to zero.

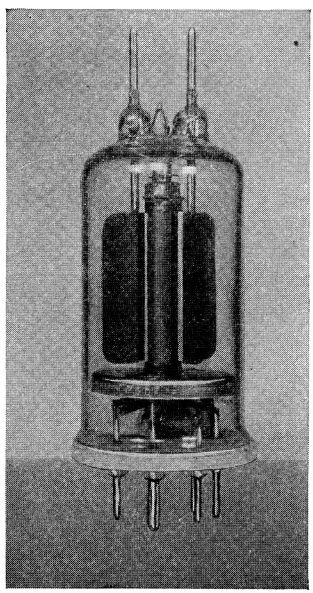

Fig. 219. The double tetrode QQE 06/40. For internal details see fig. 220, for efficiency curve fig. 221.

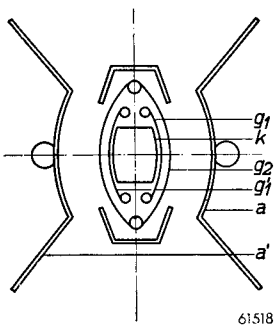

Fig. 220. Cross section of the electrode system of the QQE 06/40, comprising 2 control grids and two anodes, the cathode and screen grid being common to both sections.

This valve does actually give quite stable results at a wavelength of about 50 cm.; the output power as function of the wavelength is shown in fig. 221. The design of the tetrode QQC 04/15 is very similar, the only difference being that the valve has an oxide filament instead of an indirectly heated cathode.

Fig. 221 shows the output power and efficiency of this valve as function of the wavelength.

Fig. 223 is a photograph of a balanced oscillator employing two valves type TBW 6/6000. The cooler jackets of the water-cooled anodes are located in two tubes, which together form a Lecher system. The tuning device, consisting of a metal shorting plate, can be clearly seen. The disc seals of the grid are connected direct to a metal plate dividing the earthed metal housing of the transmitter into two parts. The upper compartment similarly contains a Lecher system, connected to the terminal of the centre tapping on the valve heater, and the tubes of this Lecher system contain the heater leads which are insulated from

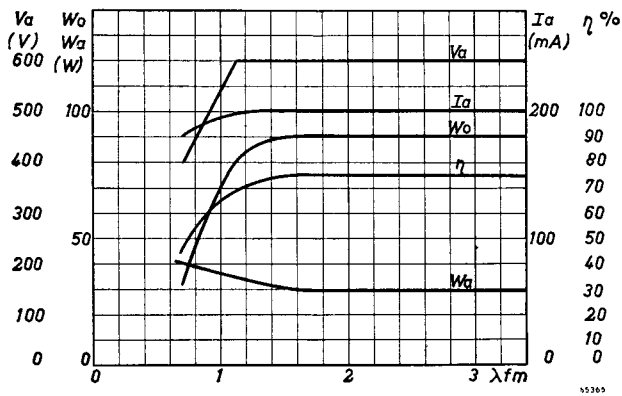

Fig. 221. Efficiency curve of the double tetrode QQE 06/40. As will be seen, the valve is effective at wavelengths below 1 metre.

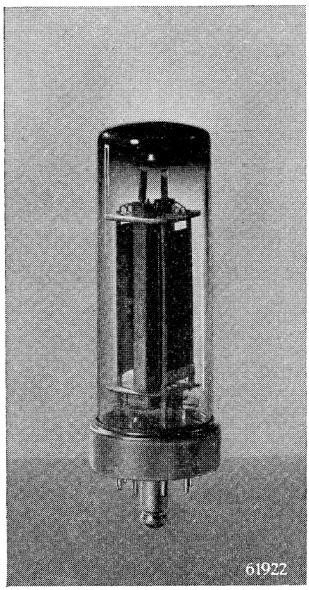

Fig. 222. The double tetrode QQC 04/15; the construction is the same as in the QQE 06/40, but the cathode is directly heated.

each other and also from the centre tap lead. An air flow is blown through the tubes of the heater part of the Lecher system, to cool the bottom of the valve. A metal plate ensures that no coupling can occur between the parts of the tubes in the heater system, above and below the tuning bridge. The ducts for the anode cooling-water are incorporated in the tubes that form the anode section of the Lecher system, and the ceramic cooling spiral is placed just below the oscillator; this arrangement ensures that the high voltages applied to the anode Lecher system cannot set up a heavy leak current to earth by way of the water. This oscillator delivers approximately 5 kW at a frequency of 220 Mc/s.

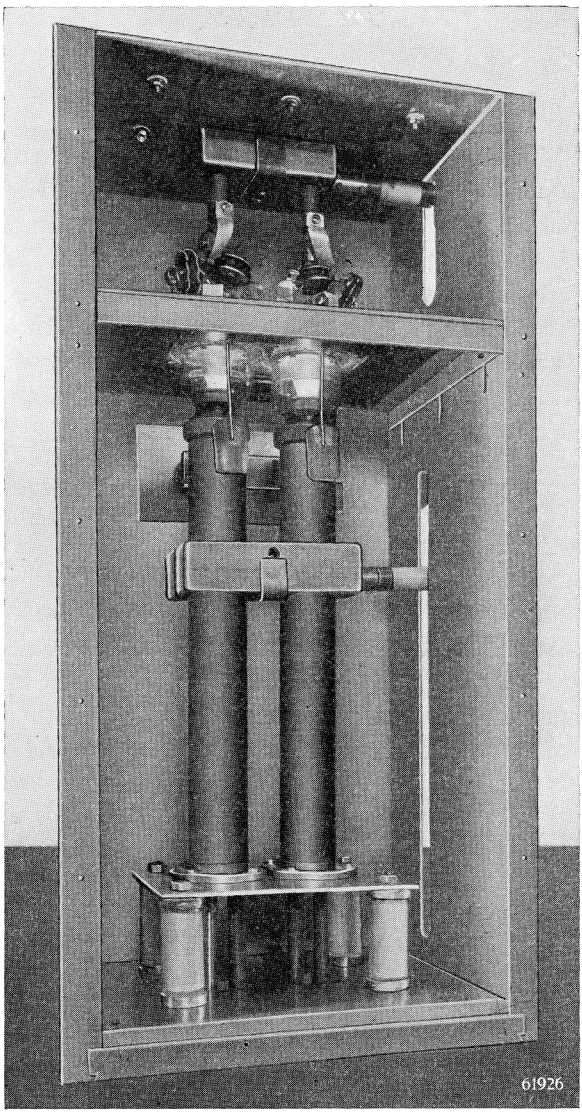

Fig. 223. Balanced oscillator incorporating two valves type TBW 6/6000. The output is 5 kW at a frequency of 220 Mc/s.

Appendix

§ 1. Simpson's law

According to Simpson's law, the area enclosed by a curve AB, the x axis and the ordinates AA_1 and BB_1 (see fig. 224) is determined by dividing the portion A_1B_1 of the x axis into an even number of equal parts ($2n$) and projecting ordinates from these points. The lengths of the ordinates are respectively: y_0, y_1, $y_2 \ldots . y_{2n}$, and if AB be the given curve, these can be measured from the graph. The length of each of the $2n$ sections into which the distance A_1B_1 is divided being h, this is equal to $(x_{2n} - x_o)/2n$. The area ABB_1A_1, as a very close approximation, is then:

$$O = \frac{h}{3}(y_o + 4y_1 + 2y_2 + 4y_3 + 2y_4 \ldots . 2y_{2n-2} + 4y_{2n-1} + y_{2n}),$$

provided that $2n$ is sufficiently high.

This formula depends for its accuracy on the assumption that the part of the curve where three points, P, Q and R, occur can be sufficiently closely approximated by the parabola drawn through those three points. The area of the strip PRR_1P_1 is then taken to be the area below the parabola in question. To calculate the area, the zero point of the system of co-ordinates is taken at Q_1; the abscissa axis is termed ξ (see fig. 225).

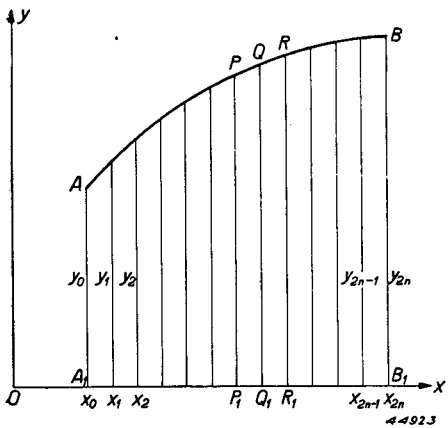

Fig. 224. Calculation of area employing Simpson's law.

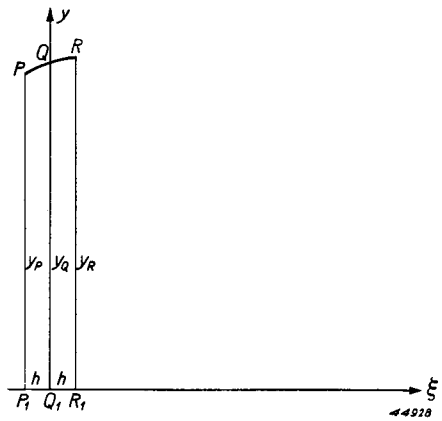

Fig. 225. Calculation of the area subtended by the parabola PQR.

For R_1, then $\xi = +h$; for P_1, $\xi = -h$. The ordinates P, Q and R are termed y_P y_Q and y_R.
The parabola through P, Q and R is of the universal form:

$$y = a\xi^2 + b\xi + c.$$

For Q, $\xi = 0$; $y = y_Q$, so that:

$$y_Q = c \quad \ldots\ldots\ldots\ldots \quad (1)$$

For R, $\xi = h$; $y = y_R$, and

$$y_R = ah^2 + bh + c \quad \ldots\ldots\ldots \quad (2)$$

For P, $\xi = -h$; $y = y_P$, and

$$y_P = ah^2 - bh + c \quad \ldots\ldots\ldots \quad (3)$$

From (1), (2) and (3), a, b and c are easily found:

$$ah^2 = {}^1/_2 (y_P - 2y_Q + y_R);$$
$$bh = {}^1/_2 (y_R - y_P); \; c = y_Q.$$

Now, the area

$$PRR_1P_1 = \int_{\xi=-h}^{\xi=+h} y\,d\xi = \int_{-h}^{+h} (a\xi^2 + b\xi + c)\,d\xi =$$
$$= \left| \frac{a}{3}\xi^3 + \frac{b}{2}\xi^2 + c\xi \right|_{-h}^{+h} = \frac{2}{3}ah^3 + 2ch,$$

or, employing the values of a and c found above:

$$\text{area } PRR_1P_1 = 2h\,(1/3\,ah^2 + c) = 2h\,[1/6\,(y_P - 2y_Q + y_R) + y_Q] =$$
$$= h/3\,(y_P + 4y_Q + y_R).$$

The area ABB_1A_1 in fig. 224 is equal to that of n similar double strips, and is therefore:

$$O = h/3\,(y_0 + 4y_1 + y_2) + h/3\,(y_2 + 4y_3 + y_4) + h/3\,(y_4 + 4y_5 + y_6) + \ldots\ldots + h/3\,(y_{2n-4} + 4y_{2n-3} + y2_{n-2}) + h/3\,(y_{2n-2} + 4y_{2n-1} + y_{2n}),$$ or:
$$O = h/3\,(y_0 + 4y_1 + 2y_2 + 4y_3 + 2y_4 + \ldots\ldots 2y_{2n-4} + 4y_{2n-3} + 2y_{2n-2} + 4y_{2n-1} + y_{2n}).$$

Applications

To illustrate the accuracy with which areas can be evaluated by means of Simpson's law, this law will now be applied to a number of known mathematical figures.

a) *Quarter circle* (fig. 226)
The abscissa OB is divided into $2n = 6$ equal parts; then $h = R/6$ and Pythagoras provides us with:

$$y_1 = \sqrt{R^2 - \left(\frac{1}{6}R\right)^2} = \frac{1}{6}R\sqrt{35}$$

$$y_2 = \sqrt{R^2 - \left(\frac{2}{6}R\right)^2} = \frac{2}{3}R\sqrt{2}$$

$$y_3 = \sqrt{R^2 - \left(\frac{3}{6}R\right)^2} = \frac{1}{2}R\sqrt{3}$$

$$y_4 = \sqrt{R^2 - \left(\frac{4}{6}R\right)^2} = \frac{1}{3}R\sqrt{5}$$

$$y_5 = \sqrt{R^2 - \left(\frac{5}{6}R\right)^2} = \frac{1}{6}R\sqrt{11}.$$

Further, $y_0 = R$; $y_6 = 0$.
According to Simpson's law:

$$O = \frac{R}{18}\left(R + \frac{4}{6}R\sqrt{35} + \frac{4}{3}R\sqrt{2} + 2R\sqrt{3} + \frac{2}{3}R\sqrt{5} + \frac{4}{6}R\sqrt{11} + 0\right)$$

or $O = 0.778\ R^2$.
The exact computation yields:

$$O = \frac{\pi}{4}R^2 = 0.785\ R^2,$$

which proves that the graphical result differs from the exact by only 1%.

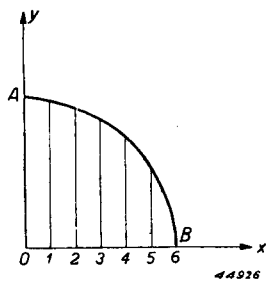

Fig. 226. To calculate the area of a quarter circle.

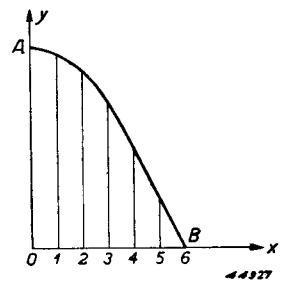

Fig. 227. To determine the area described by a cosine curve.

b) *Area in a cosine curve* (fig. 227)

In the cosine function, $OA = 1$, $OB = \pi/2$. Dividing OB into $2n = 6$ equal parts, we have $h = 15° = \pi/12$. The ordinates are obtained from the cosine table:

$y_0 = 1$; $y_1 = 0.9659$; $y_2 = 0.8660$; $y_3 = 0.7071$; $y_4 = 0.5000$; $y_5 = 0.2588$; $y_6 = 0$.

Simpson's law gives:

$$O = \frac{\pi}{36}(1 + 4 \,.\, 0.9659 + 2 \,.\, 0.8660 + 4 \,.\, 0.7071 + 2 \,.\, 0.5000 + \\ + 4 \,.\, 0.2588 + 0) = \frac{\pi}{36} \,.\, 11.4592 = 1.0000.$$

Exact calculation produces:

$$O = \int_{x=0}^{\pi/2} \cos x \, dx = \Big| \sin x \Big|_{0}^{\pi/2} = 1 - 0 = 1,$$

and the graphical result therefore agrees to the fourth decimal place.

c) *Area subtended by the curve* $y = e^x$ *between the ordinates* $x = 0$ *and* $x = 1$ (fig. 228)

Divide the space A_1B_2 into $2n = 2$ equal parts; then $h = {}^1/_2$. From tables, e^x is found to be:

x	$= 0$	$^1/_2$	1
e^x	$= 1$	1.6487	2.7183.

Therefore:

$$O = \frac{1}{6}(1 + 4 \,.\, 1.6487 + 2.7183) = \\ = \frac{1}{6} \,.\, 10.3131 = 1.7188.$$

Exact calculation gives:

$$O = \int_{x=0}^{1} e^x \, dx = \Big| e^x \Big|_{0}^{1} = e - 1 = 1.7183,$$

which represents a difference of only 0.03%.

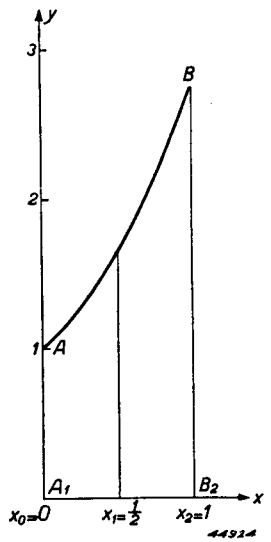

Fig. 228. To determine the area subtended by the curve $y = e^x$.

Let us now apply Simpson's law to determine the various components in a Fourier progression of graphically determined current impulses. In Chapter III it is shown that in a periodic current $i = f(\omega t)$, the d.c. component I_o and the amplitude of the first harmonic I_1 are determined by:

$$I_o = \frac{1}{2\pi} \int_o^{2\pi} f(\omega t)\, d(\omega t);$$

$$I_1 = \frac{1}{\pi} \int_o^{2\pi} f(\omega t) \cos \omega t\, d(\omega t).$$

However, the quantity $\int_o^{2\pi} f(\omega t)\, d(\omega t)$ is none other than the area between the curve $f(\omega t)$ and the abscissa axis, as limited by the ordinates, $\omega t = 0$ and $\omega t = 2\pi$. Even so, the quantity $\int_o^{2\pi} f(\omega t) \cos \omega t\, d(\omega t)$ represents the area lying between the curve $f(\omega t) \cos \omega t$, the abscissa axis and the ordinates $\omega t = 0$ and $\omega t = 2\pi$. Once $f(\omega t)$ has been determined graphically, the areas in question are computed by means of Simpson's law.

In the case of pulsating currents having a current angle of 2Θ (fig. 229), it must be noted that the area below the curve $\omega t = 0$ and $\omega t = 2\pi$ is equal to twice that of the half impulse between $\omega t = 0$ and $\omega t = \Theta$. For this reason, in applying Simpson's law it is not the part 0 to 2π that is divided into 2π equal sections, but the interval 0 to Θ; the result is then more accurate.

The quantity h is now equal to $\Theta/2n$, whereby Θ is to be expressed in radians; if, as is more usual, it is expressed in degrees, then:

$$h = \frac{\Theta^\circ}{2n} \cdot \frac{\pi}{180}.$$

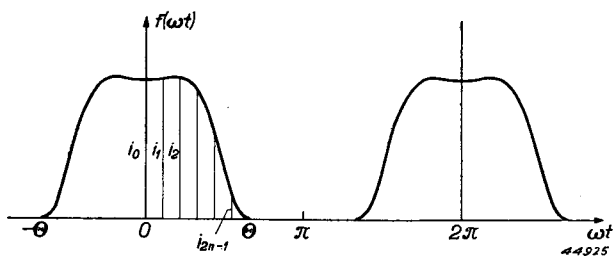

Fig. 229. To determine the d.c. component and harmonics of pulsating currents.

Let the ordinates at the different points of division be i_0, i_1,

$i_2 \ldots . i_{2n-1}, i_{2n}$; these are measured from the diagram. In this case $i_{2n} = 0$ and the direct current is:

$$I_0 = \frac{1}{\pi}\int_o^{\pi} f(\omega t)\, d(\omega t) = \frac{1}{\pi}\int_o^{\Theta} f(\omega t)\, d(\omega t) =$$

$$= \frac{1}{\pi}\cdot\frac{1}{3}\cdot\frac{\Theta^0}{2n}\cdot\frac{\pi}{180}(i_0 + 4i_1 + 2i_2 + 4i_3 + \ldots . + 2i_{2n-2} + 4i_{2n-1}), \text{ or:}$$

$$I_0 = \frac{\Theta^0}{180}\cdot\frac{1}{6n}(i_0 + 4i_1 + 2i_2 + 4i_3 + \ldots . + 2i_{2n-2} + 4i_{2n-1}).$$

To determine the first harmonic, each of the ordinates i_0, $i_1 \ldots .$ is multiplied by the relative value of cos ωt, and the new ordinates are termed i_0', i_1', $\ldots .$

Then:

$$I_1 = \frac{2}{\pi}\int_o^{\pi} f(\omega t)\cos\omega t\, d(\omega t) = \frac{2}{\pi}\int_o^{\Theta} f(\omega t)\cos\omega t\, d(\omega t) =$$

$$= \frac{2}{\pi}\cdot\frac{1}{3}\cdot\frac{\Theta^0}{2n}\cdot\frac{\pi}{180}(i_0' + 4i_1' + 2i'_2 + \ldots . + 2i'_{2n-2} + 4i'_{2n-1}), \text{ or}$$

$$I_1 = \frac{\Theta^0}{90}\cdot\frac{1}{6n}(i_0' + 4i_1' + 2i_2' + \ldots . + 2i'_{2n-2} + 4i'_{2n-1}).$$

Similar formulae may be derived in respect of the other harmonics. As an example of the application, let us take the impulse b in fig. 24 (chapter III, § 5): this is obtained from the load line b in fig. 22 in the following manner. The anode current i_a as function of the grid voltage v_g is determined from b, after which the appropriate values of ωt are calculated from $v_g = -275 + 500 \cos \omega t$: this furnishes the following table:

v_g	i_a	ωt
225	2400	0°
200	2340	18.2
175	2200	25.8
150	2020	31.8
125	1760	36.9
100	1450	41.4
75	1120	45.6
50	790	49.5
25	520	53.1
0	290	56.6
−25	70	60.0

ωt	i_a	
0°	2400	i_0
10°20′	2380	i_1
20°40′	2300	i_2
31°0′	2040	i_3
41°20′	1460	i_4
51°40′	610	i_5

The relation between i_a and ωt thus obtained is then the curve b in fig. 24, from which it appears that $\Theta = 62°$. Dividing the half impulse into $2n = 6$ equal parts, $h = 62°/6 = 10°20'$, and ordinates projected from the points of division give the figures shown in the accompanying table, as read from the diagram.
According to Simpson's law:

$$I_{a0} = \frac{62}{180} \cdot \frac{1}{18}(2400 + 4.2380 + 2.2300 + 4.2020 + 2.1460 + 4.610) =$$

$$= \frac{62}{3240} \cdot 30040 = 573 \text{ mA}.$$

To obtain I_{a1}, each value of i_a is then multiplied by its relative value of cos ωt.

ωt	i_a	cos ωt	i_a cos ωt	
0	2400	1.000	2400	i_0'
10°20′	2380	0.984	2340	i_1'
20°40′	2300	0.936	2150	i_2'
31°0′	2040	0.857	1750	i_3'
41°20′	1460	0.751	1095	i_4'
51°40′	610	0.620	380	i_5'

Then: $I_{a1} = \frac{62}{90} \cdot \frac{1}{18}(2400 + 4.2340 + 2.2150 + 4.1750 + 2.1095 +$

$+ 4.380) = \frac{62}{1620} \cdot 26770 = 1023$ mA.

§ 2 A.F. Class A amplifier

Although A.F. amplifiers do not fall within the general conception of "transmitting" valves, the following §§ will nevertheless be devoted to those valves which are used for the amplification of A.F. oscillations. The discussion will be confined to the calculation of input- and output power, efficiency and distortion, in so far as these properties are dependent on the characteristics of the valve, without touching upon the effect of A.F. transformers etc. as used in the amplifiers. We will take the case of the A.F. Class A amplifier as applied to the triode, this being the most commonly used type of valve for this purpose. Fig. 230 shows the circuit; the load consists of a resistance R across the secondary winding of the A.F. transformer, of which the primary is incorporated in the anode circuit.

It will be assumed that the transformer is "ideal", i.e. without leakage reactance and without ohmic resistance or capacitance; at the primary side the load resistance R is then equivalent to a resistance $R_a = (n_1/n_2)^2 R$, in which n_1 and n_2 are the numbers of turns of the primary and secondary of the transformer, respectively. This expression is then valid for all frequencies concerned.

The excitation voltage $V_{gp} \cos pt$ is usually derived from a microphone, possibly with one or more pre-amplifiers; the amplitude V_{gp} then assumes a number of different values. In the Class A amplifier, however, care is taken to prevent any flow of grid current and so avoid extra distortion: the grid voltage then answers to the expression:

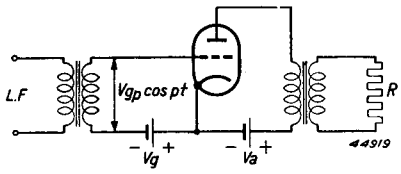

Fig. 230. Circuit diagram of an A.F. Class A amplifier.

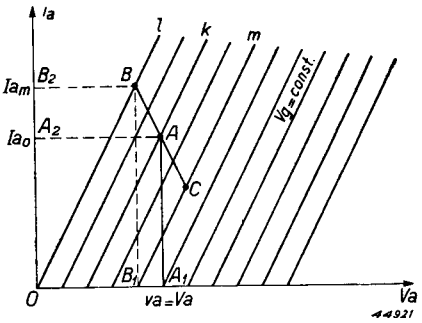

Fig. 231. Ideal characteristics of a triode, showing load line for Class A amplification, where the valve is not driven right up to the V_a axis.

$$v_g = V_g + V_{gp} \cos pt \leqq 0 \quad . \quad . \quad . \quad . \quad . \quad . \quad . \quad (1)$$

A. *Theory of straight-line characteristics*

Let us first review the idealized case of the straight characteristics (fig. 231):

$$i_a = S\,(v_g + Dv_a) \quad . \quad . \quad . \quad . \quad . \quad . \quad . \quad . \quad . \quad (2)$$

The characteristic in respect of $v_g = 0$ is then:

$$i_a = S\,Dv_a \quad , \quad . \quad . \quad . \quad . \quad . \quad . \quad . \quad . \quad . \quad . \quad (3)$$

which is the line l.

The grid bias V_g is so chosen with respect to the particular steady anode voltage V_a, that a certain standing current I_{ao} flows. In fig. 231 this condition is shown by the so-called zero signal or operating point A at the co-ordinates V_a and I_{ao} on the characteristic k and relative to the given grid voltage V_g.

Now, if the grid be excited in the above manner, the anode current will also vary with time, whereby:

$$i_a = I_{ao} + i_{a\sim} \quad \ldots\ldots\ldots\ldots \quad (4)$$

On the basis of the assumption concerning the transformer, only the component $i_{a\sim}$ will encounter the resistance R_a in the primary winding, in which a voltage drop will occur, equal to $i_{a\sim}R_a$, in which case the anode voltage becomes:

$$v_a = V_a - i_{a\sim}R_a \quad \ldots\ldots\ldots\ldots \quad (5)$$

Elimination of $i_{a\sim}$ in (4) and (5) then gives the relation between i_a and v_a under the particular conditions of excitation and load:

$$i_a = I_{ao} + \frac{V_a}{R_a} - \frac{v_a}{R_a}. \quad \ldots\ldots\ldots\ldots \quad (6)$$

This is a linear relation between i_a and v_a, in other words a straight line and, according to (6), $i_a = I_{ao}$ when $v_a = V_a$, that is, the straight line passes through the operating point A. The slope of this line is:

$$\frac{di_a}{dv_a} = -\frac{1}{R_a}$$

and is therefore dependent on the load resistance; the higher R_a becomes, the more gradual the slope. This line is termed the load line (see BAC in fig. 231).

Since the excitation potential and steady voltage on the grid are symmetrical, the portion AB of the load line is equal to section AC; the point C lies on the characteristic m which, in respect of k, is just as negative as l is positive with respect to k.

Let us now consider two possibilities:

a) The positive grid swing extends to the characteristic l, where $v_g = 0$ (point B); the negative swing C does *not* reach the v_a axis (see fig. 231).

b) The positive swing is as in a); the negative swing extends to the v_a axis (fig. 232).

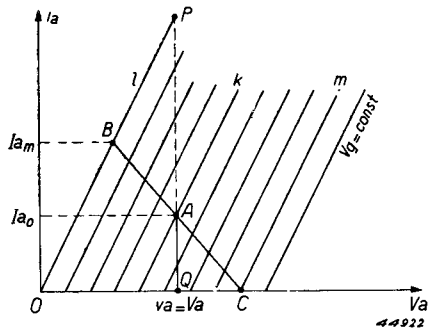

Fig. 232. As fig. 231, but running to the v_a axis.

Case a) From (3), the expression for l, and (6), that in respect of BC, the ordinate I_{am} at B is obtained by elimination of v_a:

$$I_{am} = \frac{SDR_a I_{ao} + SDV_a}{SDR_a + 1}.$$

The amplitude $I_{a\sim}$ of the a.c. component of the anode current is then:

$$I_{a\sim} = I_{am} - I_{ao} = \frac{SDV_a - I_{ao}}{SDR_a + 1} \quad \ldots\ldots \quad (7)$$

and the output power is:

$$W_0 = {}^1/_2\, V_{a\sim} I_{a\sim} = {}^1/_2\, I_{a\sim}{}^2 R_a = {}^1/_2\, R_a \left(\frac{SDV_a - I_{ao}}{SDR + 1}\right)^2 \quad \ldots \quad (8)$$

When $R_a = 0$ or ∞, $W_o = 0$, which will be obvious from fig. 231, for at $R_a = 0$, the load line BC is parallel to the i_a axis and the alternating anode voltage $V_{a\sim} = A_1B_1 = 0$; at $R_a = \infty$, BC runs parallel to the v_a axis and the alternating anode current is $I_{a\sim} = A_2B_2 = 0$.
At a certain value of R_a, W_o reaches a maximum, and differentiation thus yields:

$$R_a = \frac{1}{SD} \quad \ldots\ldots\ldots\ldots \quad (9)$$

It should be noted that, if the internal resistance R_i be introduced, Barkhausen's formula gives us:

$$SDR_i = 1,$$

so that the above value of R_a becomes:

$$R_a = R_i \quad \ldots\ldots\ldots\ldots \quad (9a)$$

The maximum power is then:

$$W_{0\,max} = \frac{(SDV_a - I_{ao})^2}{8\,SD} \quad \ldots\ldots\ldots \quad (10)$$

Apparently, then, this power increases according as the steady anode current I_{ao} becomes smaller, and this, too, is clearly seen from fig. 231: if the point A is moved down the line AA_1, the slope of BC remaining constant, with B on l, then $V_{a\sim} = A_1B_1$ and $I_{a\sim} = A_2B_2$ both increase. The lowest possible position of A, that is, the lowest possible value of I_{ao}, is reached when the point C falls on the v_a axis, since symmetrical setting of the anode current at that point is still just possible. In that event, it appears that:

$$I_{am} = 2\,I_{ao}, \text{ so that } I_{a\sim} = I_{ao}.$$

This value of I_{ao}, which we will term I_{aoo} is then calculable from (7):

$$I_{a\sim} = I_{aoo} = \frac{SDV_a - I_{aoo}}{SDR_a + 1},$$

therefore, having regard to (9):

$$I_{aoo} = \frac{SDV_a}{3} \quad \ldots\ldots\ldots\ldots \quad (11)$$

Expression (10) then becomes:

$$W_{0\,max} = \frac{1}{18} SDV_a^2 \quad \ldots\ldots\ldots \quad (12)$$

The input power is:

$$W_i = I_{aoo}\, V_a = \frac{1}{3} SDV_a^2 ,$$

and the relative max efficiency is:

$$\eta = \frac{W_{0\,max}}{W_i} = \frac{1}{6} = 16\frac{2}{3}\,\%.$$

Case b) The optimum value of R_a, i.e. $R_a = R_i$ found above, refers to the setting where the only limiting condition is $v_g \leqq 0$; if at the same time the load line extends down to the v_a axis (fig. 232), R_a will have a different optimum value, which is found in the following manner. As in a) above, the ordinate I_{am} at the point B is expressed by:

$$I_{am} = \frac{SDR_a I_{ao} + SDV_a}{SDR_a + 1}.$$

Now, according to fig. 232:

$$I_{am} = 2\, I_{ao},$$

so that:

$$2\, I_{ao} = \frac{SDR_a I_{ao} + SDV_a}{SDR_a + 1}.$$

Given I_{ao}, the value of R_a is obtained from:

$$R_a = \frac{SDV_a - 2\, I_{ao}}{SDI_{ao}} \quad \ldots\ldots\ldots \quad (13)$$

The amplitude of the alternating current is:

$$I_{a\sim} = I_{am} - I_{ao} = I_{ao},$$

and the output power:

$$W_0 = {}^1/_2\, I_{a\sim}{}^2\, R_a = {}^1/_2\, I_{ao}{}^2\, \frac{SDV_a - 2\, I_{ao}}{SDI_{ao}}, \text{ or:}$$

$$W_0 = {}^1/_2\, I_{ao}\, \frac{SDV_a - 2\, I_{ao}}{SD} \quad \ldots\ldots\ldots \quad (14)$$

Taking I_{ao} to be variable, W_0 reaches a maximum at that value of I_{ao}, which is given by:

$$\frac{dW_0}{dI_{ao}} = \frac{1}{2SD}\,(SDV_a - 4\, I_{ao}) = 0,$$

or:

$$I_{ao} = \frac{1}{4}\, SDV_a \quad \ldots\ldots\ldots \quad (15)$$

Geometrically, this means that if the ordinate QA is projected until it intersects at P the characteristic l in respect of $v_g = 0$, then $AQ = I_{ao} = 1/4\, PQ$, since, according to (3), l is expressed by:

$$i_a = SDv_a,$$

whilst in respect of the line PAQ, $v_a = V_a$; therefore $PQ = SDV_a = 4\, I_{ao}$.

The output power thus reaches maximum at:

$$W_{0\,max} = {}^1/_2 \cdot {}^1/_4\, SDV_a \cdot \frac{SDV_a - {}^1/_2\, SDV_a}{SD} = \frac{1}{16}\, SDV_a{}^2 \quad (16)$$

The input power is:

$$W_i = V_a I_{ao} = {}^1/_4\, SDV_a{}^2 \quad \ldots\ldots\ldots \quad (17)$$

and the efficiency:

$$\eta = \frac{W_0}{W_i} = 25\% \quad \ldots\ldots\ldots \quad (18)$$

Substitution of (15) in (13) then gives:

$$R_a = \frac{SDV_a - {}^1/_2\, SDV_a}{{}^1/_4\, (SD)^2\, V_a} = \frac{2}{SD} = 2R_i \quad \ldots\ldots \quad (19)$$

Summarizing, we now have the following:

a) Upper limit

$$R_a = R_i$$

$$W_{0\,max} = \frac{1}{18}\, SDV_a{}^2$$

$$W_i = \frac{1}{3}\, SDV_a{}^2$$

b) Upper and lower limit

$$R_a = 2\, R_i$$

$$W_{0\,max} = \frac{1}{16}\, SDV_a{}^2$$

$$W_i = \frac{1}{4}\, SDV_a{}^2$$

$$W_a = \frac{5}{18} SDV_a^2 \qquad W_a = \frac{3}{16} SDV_a^2$$

$$\eta = 16^2/_3\% \qquad \eta = 25\%.$$

The setting b appears to be the most satisfactory from every aspect and will therefore be used as the basis of the following discussion.
As already stated, the distance AQ in fig. 232 is equal to $^1/_4\ PQ$; this relation is independent of the choice of steady anode voltage V_a, so that, if the optimum location of the zero-signal point A is determined in respect of different anode-voltage values, the geometrical position of A will be on a straight line S (fig. 233), of which the slope is one quarter that of l, i.e. the characteristic for $v_g = 0$. The higher the anode voltage, the greater the input and output power, and anode dissipation. It should be noted, however, that the input power does not change if the valve is not excited, seeing that the direct anode current remains unchanged, but, as in that case the output power is zero, the whole of the input power is disposed of as anode dissipation. Therefore, when the excitation is removed, the above expression for W_a, viz. 3/16 SDV_a^2, changes to 1/4 SDV_a^2.

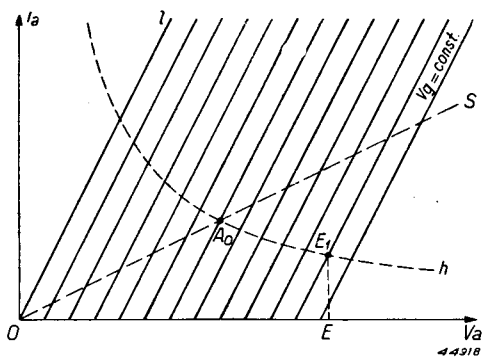

Fig. 233. For the setting shown in fig. 232, S indicates the geometrical position of the operating point and h is the hyperbola of the maximum anode dissipation.

This dissipation at the zero-signal point is a measure of the permissible anode potential, and it is represented in the i_a–v_a diagram in fig. 233 by the curve h; from the formula:

$$W_i = v_a i_a = W_{a\,max}$$

it follows that this curve is a hyperbola.
The point of intersection A_0 of S and h indicates the highest value of V_a which can be used under the conditions under review, viz. $R_a = 2\ R_i$ and having regard to the maximum permissible anode dissipation. The value of $V_{a\,max}$ follows from:

$$W_{a\,max} = {}^1/_4\ SDV_{a\,max}^2, \text{ or}$$

$$V_{a\,max} = 2\sqrt{\frac{W_{a\,max}}{SD}} = 2\sqrt{W_{a\,max}\,R_i} \quad \ldots\ldots \quad (20)$$

With $\eta = 25\%$, then:

$$W_{0\,max} = {}^1/_4\, W_{a\,max};\; W_i = W_{a\,max}.$$

If the anode potential is raised any higher than that which conforms to the point A_o in fig. 233, for instance OE, the standing anode current may be at most EE_1, where E_1 is a point on the hyperbola for the input power, and therefore also the dissipation at the operating point will be equal to the maximum permissible anode dissipation $W_{a\,max}$. The anode load R_a must then be greater than $2R_i$, and, in fact, so much the greater according as V_a is increased, as will be readily seen from figs. 232 and 233. The same result is obtained from (13) since, if I_{ao} be replaced by:

$$I_{ao} = \frac{W_{a\,max}}{V_a}, \quad \ldots\ldots\ldots\ldots \quad (21)$$

then:

$$R_a = \frac{V_a^2}{W_{a\,max}} - 2R_i \quad \ldots\ldots\ldots \quad (22)$$

In the case of the extreme operating point A_0, it may be said that, according to (20):

$$V_a^2 = 4\,W_{a\,max}\,R_i,$$

so that $R_a = 2R_i$, whilst at higher values of V_a, according to (22), R_a increases. On the basis of (21) and (22), the output power is now:

$$W_0 = {}^1/_2\, I_a^2{}_{\sim}\, R_a = {}^1/_2\, I^2{}_{ao} \cdot R_a = {}^1/_2\, \frac{W_{a\,max}^2}{V_a^2}\left(\frac{V_a^2}{W_{a\,max}} - 2R_i\right) =$$

$$= {}^1/_2\left(W_{a\,max} - 2\,\frac{W_{a\,max}^2\,R_i}{V_a^2}\right).$$

The input power is still:

$$W_i = W_{a\,max},$$

and the efficiency:

$$\eta = {}^1/_2\left(1 - 2\,\frac{W_{a\,max}\,R_i}{V_a^2}\right).$$

In the hypothetical case $V_a = \infty$,

$$\eta = 50\% \text{ and } W_a = {}^1/_2\, W_{a\,max}.$$

Summarizing, we then have:

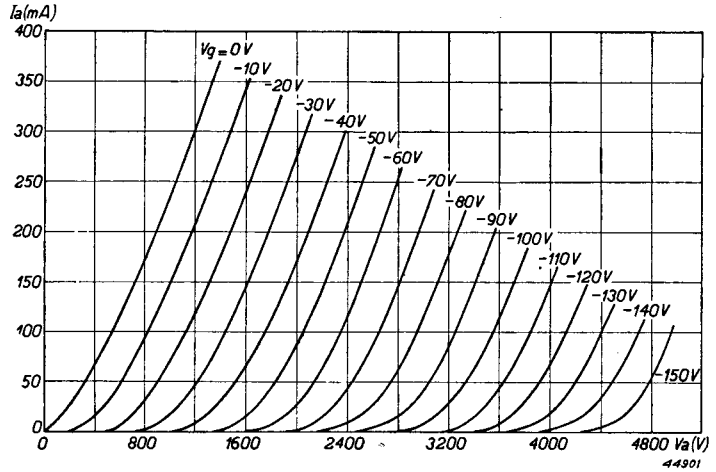

Fig. 234. Static I_a—V_a characteristics of a triode at $V_g \leqq 0V$.

$V_a \leqq 2\sqrt{W_{a\,max} \cdot R_i}$: the optimum value of $R_a = 2R_i$; the efficiency is 25%. The highest value of the output power is $^1/_4\, W_{a\,max}$.
$V_a > 2\sqrt{W_{a\,max} \cdot R_i}$: the optimum value of R_a is greater than $2R_i$; the efficiency is higher than 25%, but can never be more than 50%. The output power cannot exceed $^1/_2\, W_{a\,max}$.

B. *Theory of non-linear characteristics: distortion*

In practice, the static characteristics of a triode are not of the form shown in fig. 234; they are rather more curved, especially in the neighbourhood of the v_a axis. Fig. 234 shows the actual characteristics of a triode.

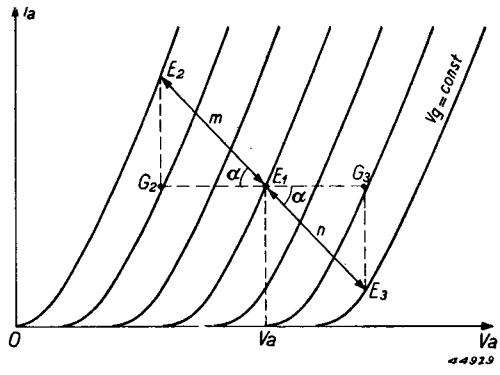

The load line representing a resistance R_a in the anode circuit will in this case, however, be a straight line also passing through the zero signal point E_1 (fig. 235), as shown by expressions (4), (5) and (6) in § 2.

Fig. 235. Load line for Class A amplification, in the I_a–V_a diagram of a triode having curved characteristics.

This load line gives the relation between anode current and both anode- and grid voltages and, since the development of the latter as a function of time is known (see (1), § 2), that of i_a as a function of time is known also. The form of the curve obtained is then as shown in fig. 236, being not fully sinusoidal, but slightly more pointed at the maxima than at the minima, due to the curvature of the static characteristic (fig. 235). The alternating anode current and also the voltage do not therefore present a true picture of the alternating grid potential, although this is otherwise the object of the A.F. amplifier; in effect, the amplifier is said to introduce a certain amount of distortion, and a measure of this distortion is given by a development of the anode current shown in fig. 236, in the form of a Fourier series:

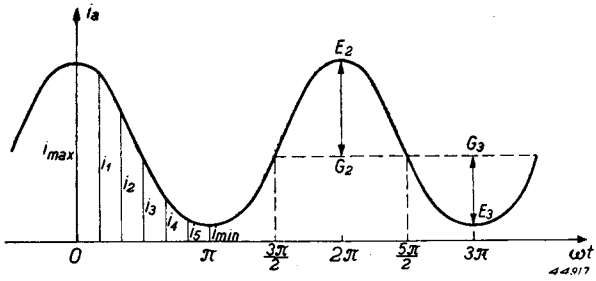

Fig. 236. Anode current as function of the time in the case of Class A amplification fig. 235.

$$i_a = I_{ao} + I_{a1} \cos \omega t + I_{a2} \cos 2\omega t + I_{a3} \cos 3\omega t + \ldots \quad (23)$$

Of those components that vary with time t, the only desirable one is that with frequency ω, that is: $I_{a1} \cos \omega t$, the other terms $I_{a2} \cos 2\omega t$ $I_{a3} \cos 3\omega t \ldots$. up to the highest harmonic being the cause of distortion. The quotient $I_{a2}/I_{a1} = d_2$ is known as the second harmonic distortion, $I_{a3}/I_{a1} = d_3$ the third harmonic distortion, etc. The total distortion is expressed by:

$$d = \sqrt{d_2^2 + d_3^2 + \ldots}$$

and it can be determined from the i_a curve (fig. 236) in the following manner. According to chapter III (see also Appendix, § 1), the amplitudes of the various components in (23) are expressed as:

$$I_{ao} = \frac{1}{2\pi} \int_0^{2\pi} i_a d(\omega t)$$

$$I_{a1} = \frac{1}{\pi} \int_0^{2\pi} i_a \cos \omega t \, d(\omega t)$$

$$I_{a2} = \frac{1}{\pi}\int_{o}^{2\pi} i_a \cos 2\omega t \, d(\omega t), \text{ etc.}$$

Further, as shown in § 1, the above integrals represent the areas enclosed by the curves $y = i_a(t)$, $y = i_a(t) \cos \omega t$; $y = i_a(t) \cos 2\omega t$, etc, between the given integration limits. These areas are determined by means of Simpson's law and, as the curves $i_a(t)$, $i_a(t) \cos \omega t$ etc. are symmetrical with respect to the point $\omega t = \pi$, it is sufficient to ascertain the area between the limits 0 and π and multiply the result by 2.
The interval 0 .... π is divided into, say, 6 equal parts, each $h = \pi/6$ in length (see fig. 236), and ordinates are then constructed at the points of division, these being: i_{max}, i_1, i_2, i_3, i_4, i_5, i_{min}.
Then:

$$I_{ao} = \frac{1}{\pi}\int_{o}^{\pi} i_a d(\omega t) = \frac{1}{\pi} \cdot \frac{h}{3}(i_{max} + 4i_1 + 2i_2 + 4i_3 + 2i_4 + 4i_5 + i_{min}) =$$

$$= \frac{1}{\pi} \cdot \frac{\pi}{18}(i_{max} + ... + i_{min}), \text{ or:}$$

$$I_{ao} = \frac{1}{18}[i_{max} + i_{min} + 4(i_1 + i_3 + i_5) + 2(i_2 + i_4)] \quad ..... \quad (23)$$

In calculating I_{a1}, the ordinates of the curve $i_a(t) \cos \omega t$ at the points designated must be determined; these are, in sequence:

i_{max}; $i_1 \cos 30° = {}^1/_2 i_1 \sqrt{3}$; $i_2 \cos 60° = {}^1/_2 i_2$; $i_3 \cos 90° = 0$;
$i_4 \cos 120° = {}^1/_2 i_4$; $i_5 \cos 150° = -{}^1/_2 i_5 \sqrt{3}$; $i_{min} \cos 180° = -i_{min}$.

Therefore:

$$I_{a1} = \frac{2}{\pi}\int_{o}^{\pi} i_a \cos \omega t \, d(\omega t) = \frac{2}{\pi} \cdot \frac{\pi}{18}(i_{max} + 2i_1\sqrt{3} + i_2 - i_4 - 2i_5\sqrt{3} - i_{min}),$$

or:

$$I_{a1} = \frac{1}{9}[i_{max} - i_{min} + 2\sqrt{3}(i_1 - i_5) + i_2 - i_4]. \quad .. \quad (24)$$

The ordinates of the curve $i_a(t) \cos 2\omega t$ are:

i_{max}; $i_1 \cos 60° = {}^1/_2 i_1$; $i_2 \cos 120° = -{}^1/_2 i_2$; $i_3 \cos 180° = -i_3$;
$i_4 \cos 240° = -{}^1/_2 i_4$; $i_5 \cos 300° = {}^1/_2 i_5$; $i_{min} \cos 360° = i_{min}$,

so that:

$$I_{a2} = \frac{1}{9}\,[i_{max} + i_{min} + 2\,(i_1 + i_5) - 4i_3 - (i_2 + i_4)]. \qquad (25)$$

The amplitudes of the other harmonics are found in the same manner, but for our purposes, I_{a3} and I_{a4} will be sufficient.

$$I_{a3} = \frac{1}{9}\,[i_{max} - i_{min} - 2\,(i_2 - i_4)]. \quad . \quad . \quad . \quad . \quad . \quad . \quad . \quad . \quad (26)$$

$$I_{a4} = \frac{1}{9}\,[i_{max} + i_{min} - 2\,(i_1 + i_5) + 4i_3 - (i_2 + i_4)] \qquad (27)$$

For the input power we then have $W_i = V_a\, I_{ao}$; the A.F. output power, as far as the first harmonic is concerned, is $W_{01} = {}^1/_2\, I_{a1}{}^2\, R_a$, and the total distortion, up to and including the fourth harmonic, is:

$$d = \frac{\sqrt{I_{a2}{}^2 + I_{a3}{}^2 + I_{a4}{}^2}}{I_{a1}}.$$

The above may now be illustrated by an example in which the choice of operating point and load resistance are taken into account.
Fig. 237 shows the I_a/V_a characteristics of the same triode as referred to in fig. 234 at values of $V_g < 0$ V, the line a being the dissipation hyperbola for 500 W, i.e. the maximum permissible dissipation for this valve.

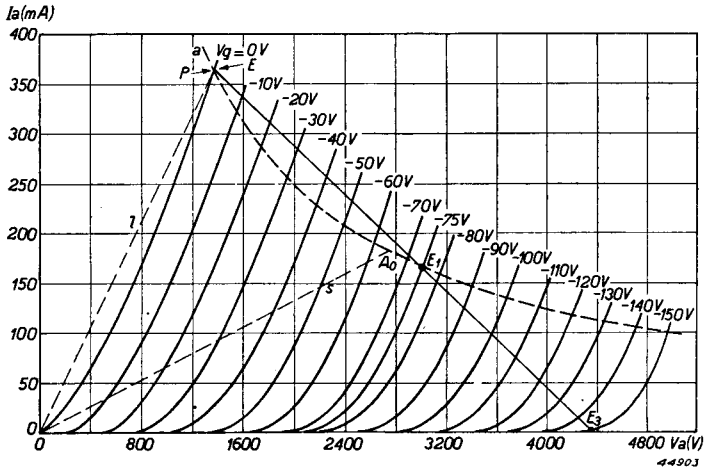

Fig. 237. I_a—V_a characteristics of the triode referred to in fig. 234, showing load line $E_2E_1E_3$ for class A amplification.

The optimum working point is obtained in the manner shown in fig. 233, but, as the characteristics are no longer straight, the method is more or less arbitrary. Through the point of intersection P of the curve $V_g = 0$ and the dissipation hyperbola a, the straight line l is drawn, through O, as shown by the line thus marked in fig. 233. The slope of the line s in fig. 237 is one quarter that of l; A_o is then the optimum operating point as in fig. 233.

Let us now find the class A setting, not for this operating point, which refers to an anode potential of 2750 V, but for a potential of 3000 V, such as is usual for this type of valve.
The zero signal point E_1 for this potential lies on the dissipation hyperbola, as also does the point E_1 in fig. 233; at that point $V_g = -75$ V, $I_a = 165$ mA. The excitation voltage will then be $V_{gp} = 75$ V, and the grid swing will lie between the limits $V_g = 0$ and $V_g = -150$ V. The load line, of which the lowest point in the ideal case (fig. 232) lies on the V_a axis, and which would therefore have to terminate at the foot of the curve for $V_g = -150$ V (to the left of E_3 in the figure), cannot be drawn since the distortion as a result of the sharp curve at the lower end of the static characteristic would be too great.
The fact that distortion will occur is shown by the circumstance that the portions E_1E_2 and E_1E_3 (fig. 237) on the load line are not equal, this being otherwise than in fig. 232 where $AB = AC$. This may be explained thus, that in fig. 236 the distance between the line G_2G_3 and the abscissa represents the standing current; due to distortion, the current amplitude E_2G_2 is greater than E_3G_3. The relative quantities are indicated in fig. 235 by the same letters and, since E_2G_2 and E_3G_3 are projections of E_1E_2 and E_1E_3 to the vertical axis, $E_1E_2 > E_1E_3$, because $E_2G_2 > E_3G_3$.
The ratio E_1E_2/E_1E_3 is a measure of the distortion, and, as will be seen presently, this distortion, assuming certain simplifications, can be calculated from:

$$d = {}^1/_2 \frac{1 - \frac{n}{m}}{1 + \frac{n}{m}}, \quad \ldots\ldots\ldots\ldots \quad (28)$$

where $m = E_1E_2$ and $n = E_1E_3$ (see fig. 235).
If it is required that d is to be less than, say, 5%, then $n/m > 9/11 = 0.82$,

and this is applied in relation to the load line E_2E_3 in fig. 237, where $E_1E_3/E_1E_2 = 0.83$. By means of this load line, after which:

$$R_a = \frac{V_{a\,max} - V_{a\,min}}{i_{a\,max} - i_{a\,min}} = \frac{4340 - 1380}{0.364 - 0.003} = 8200\ \Omega,$$

we can now determine the relation between i_a and v_g or dynamic characteristic; this is shown in fig. 238: E_1 is the zero signal point which occurs at $V_g = -75$ V, $I_a = 165$ mA.

As the dynamic characteristic is slightly curved, a sinusoidal grid potential superimposed on the direct voltage $V_g = -75$ V will not produce a fully sinusoidal anode current, in other words, distortion will be present.

The various values are then computed in the above manner for $V_{gp} = 75$ V: it is not necessary to construct the $i_a = f(t)$ curve as in fig. 236, as it is also possible to determine the values i_{max}, i_1 .... from fig. 238, knowing the grid voltage, $v_g = -75 + 75 \cos \omega t$. This furnishes the following table:

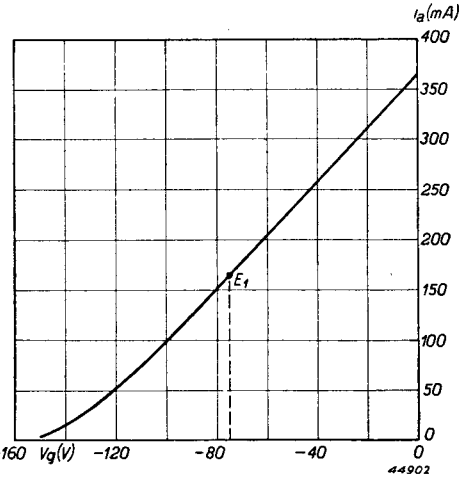

Fig. 238. Dynamic i_a/v_g characteristic of the triode represented in fig. 234 for A.F. class A operation in respect of the load line shown in fig. 237.

ωt	cos ωt	v_g	i_a
0°	1	0	364 = i_{max}
30°	0.866	—10	337 = i_1
60°	0.5	—37.5	264 = i_2
90°	0	—75	165 = i_3
120°	—0.5	—112.5	68 = i_4
150°	—0.866	—140	15 = i_5
180°	—1	—150	3 = i_{min}

From this it follows that:

$$I_{ao} = \frac{1}{18}[364 + 3 + 4(337 + 165 + 15) + 2(264 + 68)] = 172 \text{ mA}$$

$$I_{a1} = \frac{1}{9}[364 - 3 + 2\sqrt{3} \,.\, (337 - 15) + 264 - 68] = 186 \text{ mA}$$

$$I_{a2} = \frac{1}{9}[364 + 3 + 2 \,.\, (337 + 15) - 4.165 - (264 + 68)] = 8.8 \text{ mA}$$

$$I_{a3} = \frac{1}{9}[364 - 3 - 2 \,.\, (264 - 68)] = -3.4 \text{ mA}$$

$$I_{a4} = \frac{1}{9}[364 + 3 - 2 \,.\, (337 + 15) + 4.165 - (264 + 68)] = -1.0 \text{ mA},$$

$$W_i = V_a I_{ao} = 3000 \,.\, 172 \,.\, 10^{-3} = 516 \text{ W}$$
$$W_{o1} = {}^1/_2 \, I_{a1}{}^2 \, R_a = {}^1/_2 \,.\, (0.186)^2 \,.\, 8200 = 142 \text{ W}$$
$$W_a = W_i - W_{o1} = 374 \text{ W}$$
$$\eta = \frac{W_{o1}}{W_i} = 27.5\%$$
$$d = \frac{\sqrt{(8.8)^2 + (-3.4)^2 + (-1.0)^2}}{186} = 5.1\%.$$

It should be noted that the anode steady current I_{ao} is slightly higher than the anode current with zero signal, this being a direct result of the curvature of the dynamic characteristic. Finally, it may be shown that the distortion in fig. 235 is rendered by:

$$d = {}^1/_2 \,.\, \frac{1 - \frac{n}{m}}{1 + \frac{n}{m}} \quad \ldots\ldots\ldots\ldots \quad (28)$$

This formula applies only when the dynamic characteristic can be represented to a close approximation by an expression of the type:

$$i_a = a + b v_g + c v_g{}^2. \quad \ldots\ldots\ldots\ldots \quad (29)$$

Substitution of $v_g = V_g + V_{gp} \cos \omega t$ then gives:

$$i_a = a + b\,(V_g + V_{gp} \cos \omega t) + c\,(V_g + V_{gp} \cos \omega t)^2,$$

or in more detailed form:

$$i_a = a + bV_g + cV_g{}^2 + {}^1/_2 \, cV_{gp}{}^2 + (bV_{gp} + 2c\, V_g V_{gp}) \cos \omega t + {}^1/_2 \, cV_{gp}{}^2 \cos 2\omega t. \quad (30)$$

It thus appears that the distortion is caused only by the second harmonic. When $\omega t = 0$, $i_a = i_{max}$:

$$i_{max} = a + bV_g + cV_g^2 + {}^1/_2\, cV_{gp}^2 + bV_{gp} + 2cV_gV_{gp} + {}^1/_2\, cV_{gp}^2 \quad (31)$$

At $\omega t = \pi$, $i_a = i_{min}$:

$$i_{min} = a + bV_g + cV_g^2 + {}^1/_2\, cV_{gp}^2 - (bV_{gp} + 2cV_gV_{gp}) + {}^1/_2\, cV_{gp}^2, \quad (32)$$

whilst the standing current follows from (29), by substituting $v_g = V_g$

$$i_{00} = a + bV_g + cV_g^2 \quad . \quad . \quad . \quad . \quad . \quad . \quad . \quad . \quad . \quad (33)$$

From (31), (32) and (33) we then have:

$$i_{max} - i_{00} = cV_{gp}^2 + bV_{gp} + 2cV_gV_{gp} = V_{gp}\,(b + 2cV_g + cV_{gp}) \quad (34)$$

$$i_{00} - i_{max} = bV_{gp} + 2cV_gV_{gp} - cV_{gp}^2 = V_{gp}\,(b + 2cV_g - cV_{gp}) \quad (35)$$

The distortion is given by means of (30):

$$d = \frac{{}^1/_2\, cV_{gp}^2}{bV_{gp} + 2cV_gV_{gp}} = {}^1/_2\, \frac{cV_{gp}}{b + 2cV_g} \quad . \quad . \quad . \quad . \quad (36)$$

Now, in fig. 235:

$$E_2G_2 = i_{max} - i_{00} = m \sin a,$$
$$E_3G_3 = i_{00} - i_{min} = n \sin a,$$

so that, having regard to (34) and (35):

$$m = \text{constant}\,(b + 2cV_g + cV_{gp})$$
$$n = \text{constant}\,(b + 2cV_g - cV_{gp}),$$

where const. $= V_{gp}/\sin a$.
It then follows that:

$$m - n = \text{const.}\, 2cV_{gp};$$
$$m + n = \text{const.}\, 2\,(b + 2cV_g),$$

i.e.

$$\frac{m - n}{m + n} = \frac{cV_{gp}}{b + 2cV_g},$$

or, in view of (36):

$$\frac{m - n}{m + n} = 2d, \text{ that is,}$$

$$d = {}^1/_2 \cdot \frac{m - n}{m + n} = {}^1/_2 \cdot \frac{1 - \frac{n}{m}}{1 + \frac{n}{m}}.$$

§ 3. A. F. Class B amplifier

From the preceding §§ it has been seen that the efficiency of the Class A amplifier is always low and, although, as in the case of R.F. amplification, better results in this direction are obtained from Class B, it must be remembered that in the latter case an anode current passes through the valve which, in comparison with the excitation voltage, is considerably distorted, and this, of course, cannot be tolerated (see fig. 239). The answer is to be found in the balanced amplifier of which fig. 240 shows the circuit. The grid bias V_g is such that, at the given anode potential V_a, the anode current of the valves is, nearly enough, zero [1]. The signal voltage applied to the grid of one of the valves is in counter-phase with that on the other, the amplitude being the same: if the former potential be $V_{gp} \cos \omega t$, the second will be $-V_{gp} \cos \omega t$, and in practice this is put into effect by employing a driver transformer having a centre-tapped secondary winding, the grid bias being applied to the centre tap.

The primary side of the output transformer is likewise divided and the load R connected directly across the secondary winding. Assuming the characteristics of the valves to be identical, the current flowing through the load is practically sinusoidal, as shown by fig. 241. The curve a represents the signal voltage, and the arrows 1 and 2 indicate the direction in which the grids of the valves 1 and 2 (fig. 240) become less negative:

[1] Exact figures follow.

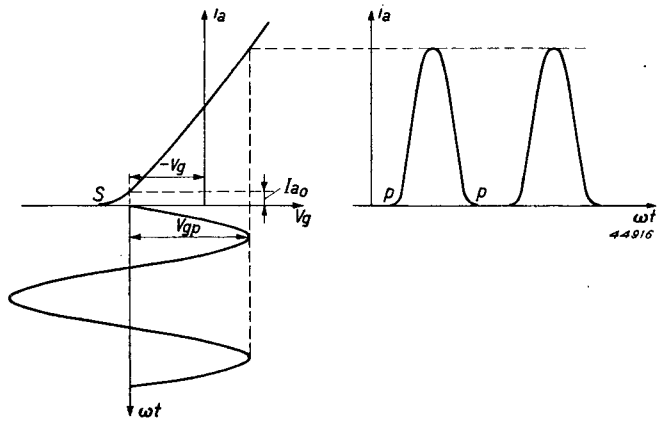

Fig. 239. Distortion of the anode current in an A.F. class B amplifier.

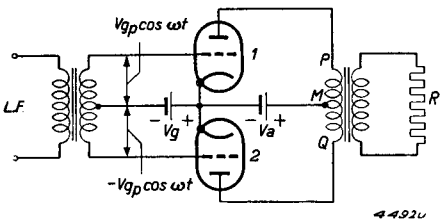

Fig. 240. Circuit of balanced A.F. amplifier.

at the grid of valve No. 2 this is one half-cycle later than in the case of valve No. 1. The anode currents of the two valves are indicated by *b* and *c*, and, by reason of the class B arrangement, their waveform is roughly that of half sines, with interruptions of a half cycle between each. The current impulses from valve No. 2 (curve *c*) appear one half cycle after those from valve No. 1 (curve *b*), because, according to *a*, the grid of valve 2 reaches its positive phase one half cycle after that of valve 1. The amplitude *c* is depicted pointing downwards, as the anode current of No. 2 passes through the primary side of the output transformer in the opposite direction to that of No. 1.

The potential on the secondary side of the output transformer and therefore also the current passing through the load resistance R, in keeping with the conception of the ideal transformer, are at any moment proportional to the currents in the primary. Apart from the transformation ratio, therefore, the secondary current is equal to the algebraic sum of the currents *b* and *c*, i.e. curve *d*, which is reasonably sinusoidal. Furthermore, due to the curvature of the static characteristic, more especially at the lower end (*S* in fig. 239), the anode current impulses flatten out at the extremities (at *p* in figs. 239 and 241, *b* and *c*). From fig. 241*d* it is seen that this flattening of the current in the secondary winding of

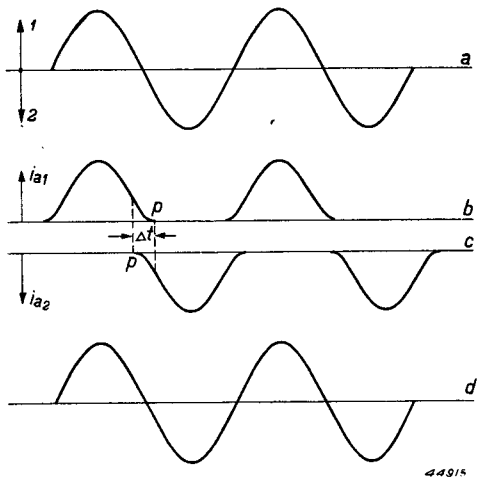

Fig. 241. Form of the current in the load resistance R of the Class B amplifier in fig. 240, in the presence of a standing current.
a) Excitation voltage.
b) Anode current of first valve.
c) Anode current of second valve.
d) Resultant current: the flattened ends *p* in *b* and *c* are counterbalanced in *d*.

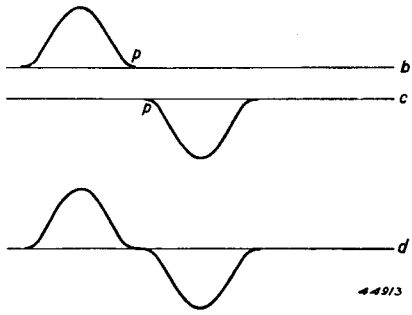

Fig. 242. As fig. 241, but with zero standing current; the flattened ends *p* at *b* and *c* are not counterbalanced in *d* and the anode current is accordingly distorted.

the transformer as produced by one of the valves is compensated by that of the other valve: this is however ensured only by a correct choice of standing anode current I_{a00}. For instance, if the grid bias were such as to produce no standing current, the anode current of the second valve would commence to flow only at the moment when that of the first becomes zero.

The condition shown in fig. 241 then changes to that of fig. 242; the flattened ends are no longer compensated and the form of the resultant current departs from the sinusoidal (fig. 242*d*).

As with the Class A amplification, the theory of straight line characteristics will be discussed first.

A. *Theory of straight line characteristics*

In the following, the method of calculation employed by C. J. de Lussanet de la Sablonière will be reviewed. The I_a–V_a characteristics will be assumed to be straight lines, as in chapter III (fig. 243): the load line is the straight line AB, and A is the point on the abscissa axis where $v_a = V_a$. The fact that the load line must be straight is borne out immediately by the consideration (see fig. 240) that the secondary load resistance R, on the primary side between P and M, as well as between Q and M, appears as a resistance $R_a=(n_1/n_2)^2 R$, in which n_1 is the number of turns in PM and QM respectively, and n_2 the number of turns on the secondary side. The anode current i_a of valve No. 1, flowing through MP thereby undergoes a voltage drop which is proportional to i_a, thus indicating that the load line is straight, and, further, since anode current commences to flow through valve No. 1 at the exact moment the current of valve No. 2 is zero, there is at that moment no voltage drop in the transformer, so that $v_a = V_a$ (point A, fig. 243).

If I_{ap} be the maximum value of the anode-current impulse of each valve, then the amplitude of the alternating anode potential will be $V_{ap} = I_{ap}R_a$.

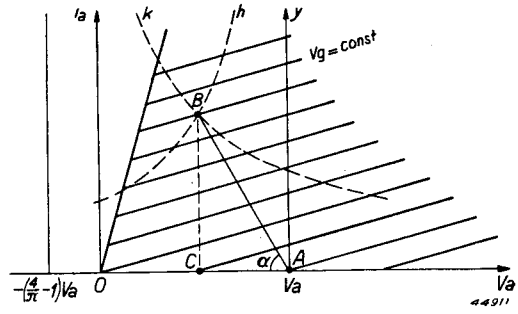

Fig. 243. Class B setting of triode with straight I_a–V_a characteristics. AB = load line; h = hyperbola of constant output power; k = hyperbola of constant anode dissipation.

In fig. 243, $BC = I_{ap}$; $AC = V_{ap}$ and R_a therefore equals cot. a. The first harmonic of the anode current, in accordance with fig. 19 (chapter III), is $I_{a1} = {}^1/_2\, I_{ap}$, and the direct anode potential, according to fig. 18 is $I_{ao} = 1/\pi\, I_{ap}$. For each valve, the output power is $W_o = {}^1/_2\, V_{ap} I_{a1} = {}^1/_4\, V_{ap} I_{ap}$, the input power is $W_i = V_a I_{ao} = 1/\pi\, V_a I_{ap}$ and the anode dissipation is $W_a = W_i - W_o = 1/\pi\, V_a I_{ap} - {}^1/_4\, V_{ap} I_{ap}$.

By means of the diagram, fig. 243, it is now possible to indicate clearly the amount of the output power and anode dissipation for the valve setting as at point B: introducing the fresh co-ordinate axes xAy, with A as origin and letting I_{ap} equal y, with $V_{ap} = x$, the output power will be $W_o = {}^1/_4\, xy$.

In this new system of co-ordinates, then, the line passing through all points of equal output power is an equilateral hyperbola through point B, of which axes Ax and Ay are the asymptotes; in fig. 243 this is the dotted line h.

The anode dissipation expressed in terms of x and y is:

$$W_a = \frac{V_a}{\pi}\, y - {}^1/_2\, xy = {}^1/_4\, y \left(\frac{4}{\pi}\, V_a - x\right).$$

This is similarly an equilateral hyperbola passing through B, but this time with the x-axis and straight line $x = 4/\pi\, V_a$ as asymptotes. This means that the centre point of the hyperbola in the figure lies on the negative v_a axis at a distance from O equal to $4/\pi\, V_a - V_a = (4/\pi - 1)\, V_a = 0.273\, V_a$. The line k is the dissipation hyperbola.

By constructing two sets of hyperbolas in the I_a/V_a diagram, one set for different values of W_o and the other for different values of W_a, the particular terminating point B of the load line at a given value of V_a can be immediately determined, for which W_o and W_a will have a certain pre-determined value. Further, given a constant value of W_a, the point

B can be so located as to give the most favourable values of W_o and therefore of η.
A practical method consists in drawing two sets of hyperbolas on tracing paper and moving them as desired over the characteristics.

B. *Theory of non-linear characteristics; distortion*

Consideration of figures 241 and 242 leads to the conclusion that in practice, even with zero signal in the class B condition, there is a certain anode current flowing in each valve, resulting in a time interval during which the valves function simultaneously. In fig. 241 this interval is indicated by Δt. The load line, which by reason of the purely ohmic load would be a straight line (such as AB in fig. 243) if the valves were working separately, then assumes a rather different form, and this will be the subject of our further discussion.
Fig. 244 reproduces that part of the family of characteristics which surrounds the quiescence point P. The direct anode voltage corresponding to this point is V_a and the grid potential is V_g. PM is the standing anode current: if the latter were zero, the load line, as in fig. 243, would be the straight line MN passing through M at a slope of $-1/R_a$; if on the other hand this standing current is not zero, but is, as in the present instance, equal to PM, the load line, *when only one valve is working*, is the line PQ, passing through P and parallel to MN, by virtue of the fact that the anode current always produces a proportional drop in the anode voltage.
If the second valve is working simultaneously in the manner already described, that is, in counter-phase with the first, the instantaneous anode potential of each valve (see fig. 240) is determined not only by its own anode current, but also by that of the other valve. In effect, the current i_{a2} in MQ sets up an induced current in the secondary winding of the transformer, and this in turn produces an induced voltage in winding MP of the first valve. Moreover, the anode cur-

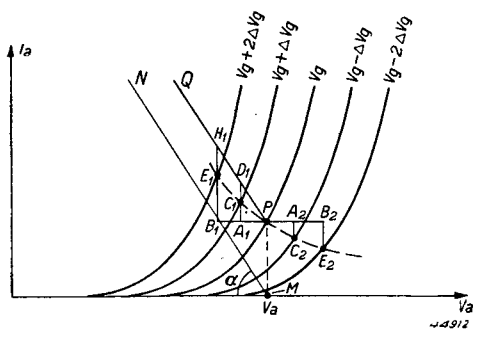

Fig. 244. Construction of the load line when both valves of a Class B amplifier are passing current simultaneously.

rents i_{a1} and i_{a2} of the two valves 1 and 2 work together from the point of view of anode voltage variations, for, when i_{a1} increases, i_{a2} decreases (owing to the action of the balanced circuit). Any increase in i_{a1}, however, is accompanied by a voltage drop at P, whilst a decrease in i_{a2} results in a voltage increase at Q and also, because of the balanced circuit, a voltage drop at P.

Let us designate by Δi_{a1} the increase in anode current in the first valve, by Δi_{a2} the decrease in the second valve — both as a result of a rise (or fall) in grid potential by an amount equal to ΔV_g — and by Δv_a the resultant decrease in anode potential of valve No. 1 (increase in valve No. 2): then $\Delta v_a = (\Delta i_{a1} + \Delta i_{a2})\, R_a$. This relationship is expressed in fig. 244. The points C_1 and C_2 on the characteristics for $V_g + \Delta V_g$ and $V_g - \Delta V_g$ respectively are so located that $PA_1 = PA_2$ and $C_1D_1 = A_2C_2$; if the diagram is drawn on millimetre graph paper, this setting is very readily found by trial and error. It will now be seen that $A_1C_1 = \Delta i_{a1}$; $A_2C_2 = \Delta i_{a2} = C_1D_1$, so that $A_1D_1 = \Delta i_{a1} + \Delta i_{a2}$. Since PQ is parallel to MN and its negative slope is therefore $1/R_a$, it may be said that $PA_1\,(= PA_2) = (\Delta i_{a1} + \Delta i_{a2})\, R_a = \Delta v_a$. The points C_1 and C_2 thus conform to the conditions representing simultaneous working of the valves and they are accordingly points on the load line. In the same manner it is possible to plot the points E_1 and E_2 on the $V_g + 2\Delta V_g$ and $V_g - 2\Delta V_g$ characteristics, whereby PB_1 is again equal to PB_2 and $E_1H_1 = B_2E_2$.
The load line around P then takes the form of the dotted line $E_1C_1PC_2E_2$; it curves gradually towards the right, to merge into the v_a axis and on the left into the line MN.
Once the load line has thus been established in the I_a–V_a diagram, the relation between i_a and v (the dynamic characteristic) can immediately be plotted, and an example is given in fig. 245 (curve $A_1B_1C_1$), in which the direct grid potential is equal to V_g at point P. It will be seen, in view of the flattening of the curve between B_1 and C_1, that the dynamic characteristic is not quite straight, but the supplementary action of the second valve practically counterbalances the effect of this bend in the characteristic from the aspect of distortion.

As far as the external circuit is concerned, it is as though the dynamic characteristic were actually the line $A_1B_1PB_2A_2$, obtained from the two valves in the manner shown in fig. 245. The curve $A_1B_1C_1$ of the

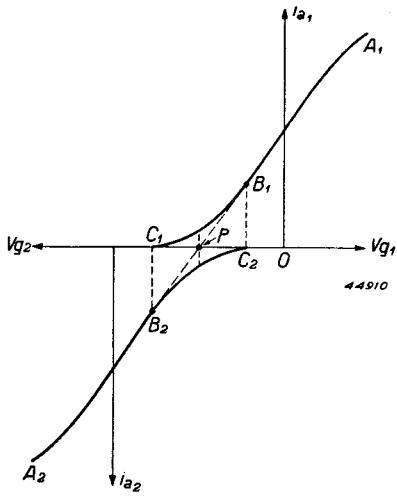

Fig. 245. Dynamic characteristics relating to Class B amplification.
$A_1B_1C_1$: dynamic characteristic of first valve.
$A_2B_2C_2$: dynamic characteristic of second valve.
$A_1B_1PB_2A_2$: combined dynamic characteristic.

first valve is rotated through an angle of 180° about P, to produce the characteristic $A_2B_2C_2$ of the second valve, and each ordinate of the dotted portion B_1PB_2 is then the algebraic sum of the appropriate ordinates of the curves B_1C_1 and B_2C_2.

The fact that the dynamic characteristic between B_1 and B_2 is represented in the external circuit by the dotted line in question follows from the fact that the currents i_{a1} and i_{a2} in the primary winding of the transformer (fig. 240) flow in opposite directions, producing the difference between the two currents in the secondary (see also fig. 241*b*, *c* and *d*).

From the dynamic characteristic obtained in this way we now calculate the input- and output power, anode dissipation, efficiency and distortion. Calling the excitation voltage a function of the time: $V_{gp} \cos \omega t$, we may write the anode current of the first valve (fig. 241*b*) in the form: —

$$i_{a1} = I_{ao} + I_{a1} \cos \omega t + I_{a2} \cos 2\omega t + I_{a3} \cos 3\omega t \; . \; . \; . \; . \qquad (1)$$

That of the second valve is 180° out of phase in time, so:

$$i_{a2} = I_{ao} + I_{a1} \cos (\omega t - 180°) + I_{a2} \cos 2 (\omega t - 180°) + \\ + I_{a3} \cos 3 (\omega t - 180°) + , \; .$$

or:

$$i_{a2} = I_{ao} - I_{a1} \cos \omega t + I_{a2} \cos 2\omega t - I_{a3} \cos 3\omega t + , \; . \qquad (2)$$

and the difference between the two currents is a measure of the current in the load resistance (see also fig. 241*b* and *c*, in which i_{a2} is shown opposed to i_{a1}); this is:

$$i = i_{a1} - i_{a2} = 2I_{a1} \cos \omega t + 2I_{a3} \cos 3\omega t + 2I_{a5} \cos 5\omega t + , \; . \qquad (3)$$

which shows that the distortion is caused only by the uneven harmonics.

The dynamic characteristic $A_1B_1PB_2A_2$ in fig. 245 is now worked out by means of (3) in conjunction with:

$$x = V_{gp} \cos \omega t, \quad \ldots \ldots \ldots \quad (4)$$

taking P as the origin of the system of co-ordinates.

To make possible a simple calculation of the amplitudes $2I_{a1} = a_1$, $2I_{a3} = a_3 \ldots$. of the various components, the method of Mouromtseff and Kozanowski is followed by drawing a line from P to the terminating point A_1 of the dynamic characteristic (see fig. 246) and ascertaining for a number of points x, the difference Δ between the ordinate of the dynamic characteristic and that of the straight line PA_1. Let A_1Q be designated by I_{ap}; then the equation for the straight line PA_1 will be:

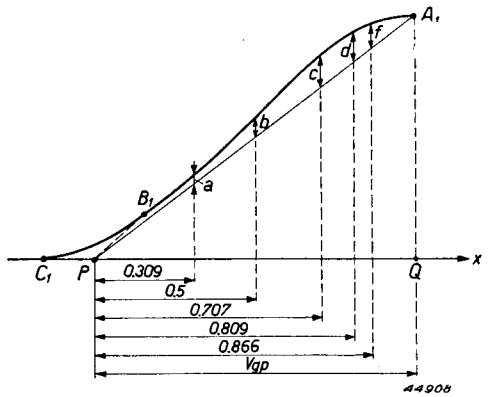

Fig. 246. Determination of the amplitudes of the harmonics from the ordinate-differences $\triangle$ of the dynamic characterastic $A_1\,B_1\,P$ and the straight line $A_1\,P$.

$$y = I_{ap} \cos \omega t\,, \quad \ldots \ldots \ldots \quad (5)$$

in which case the required difference between the ordinates is:

$$\Delta = i - y = a_1 \cos \omega t + a_3 \cos 3\omega t + a_5 \cos 5\omega t + \ldots - I_{ap} \cos \omega t \quad (6)$$

For the point A, $\omega t = 0$ and $\Delta = 0$, therefore:

$$0 = a_1 + a_3 + a_5 + \ldots - I_{ap}, \text{ or}$$
$$I_{ap} = a_1 + a_3 + a_5 + \ldots \quad \ldots \ldots \quad (7)$$

For P, $\omega t = 90°$ and naturally $\Delta = 0$.

Employing expression (7) for I_{ap}:

$$\Delta = a_3 (\cos 3\omega t - \cos \omega t) + a_5 (\cos 5\omega t - \cos \omega t) + a_7 (\cos 7\omega t - \cos \omega t) + \ldots$$

which can be written in the form:

$$\Delta = a_3 p_3 + a_5 p_5 + a_7 p_7 + \ldots$$

in which:

$$p_3 = -2 \sin 2\omega t \sin \omega t$$
$$p_5 = -2 \sin 3\omega t \sin 2\omega t$$
$$p_7 = -2 \sin 4\omega t \sin 3\omega t, \text{ etc.}$$

These coefficients may now be determined at $\omega t = 30°$, 36°, 45°, 60° and 72°, thus producing the following table, up to the eleventh harmonic:

ωt	30°	36°	45°	60°	72°
p_3	$-\frac{1}{2}\sqrt{3}$	— 1.1180	$-\sqrt{2}$	$-\frac{3}{2}$	— 1.1180
p_5	$-\sqrt{3}$	— 1.8090	$-\sqrt{2}$	0	+ 0.6910
p_7	$-\sqrt{2}$	— 1.1180	0	0	— 1.1180
p_9	$-\frac{1}{2}\sqrt{3}$	0	0	$-\frac{3}{2}$	0
p_{11}	0	0	$-\sqrt{2}$	0	0

The divisions of the x axis, determined by (4):

$$x = V_{gp} \cos \omega t,$$

then lie at:

0.309 V_{gp}; 0.5 V_{gp}; 0.707 V_{gp}; 0.809 V_{gp} and 0.866 V_{gp} (see fig. 249).

The differences will be termed in sequence a, b, c, d and f, in relation to which the following expressions apply, in accordance with the above:

$$\left.\begin{aligned} a &= -1.1180\,(a_3 + a_7) + 0.6910\,a_5 \\ b &= -\frac{3}{2}(a_3 + a_9) \\ c &= -\sqrt{2}\,(a_3 + a_5 + a_{11}) \\ d &= -1.1180\,(a_3 + a_7) - 1.8090\,a_5 \\ f &= -\frac{1}{2}\sqrt{3}\,(a_3 + a_9) - \sqrt{3}\,(a_5 + a_7) \end{aligned}\right\} \quad (8)$$

from which the unknown coefficients $a_3 \ldots . a_{11}$ can be easily solved, viz.

$$\left.\begin{aligned} a_5 &= 0.4\,(a - d) \\ a_7 &= \frac{b}{3} - 0.577\,f - a_5 \\ a_3 &= -0.4475\,(a + d) - {}^1/_2\,a_5 - a_7 \\ a_9 &= -\frac{2}{3}\,b - a_3 \\ a_{11} &= -0.707\,c - a_3 - a_5 \end{aligned}\right\} \quad (9)$$

I_{ap} being known, a_1 can be calculated from:

$$a_1 = I_{ap} - a_3 - a_5 - a_7 - a_9 - a_{11} \quad . \quad . \quad . \quad . \quad . \quad . \quad (9a)$$

The direct current flowing in each of the valves is determined not by the common characteristic A_1B_1P, but by the individual characteristic

$A_1B_1C_1$, except when the amplitude of the excitation voltage PQ (fig. 246) is high in comparison with the potential PC_1, in which case the latter may be replaced by the former to give a fairly close approximation to the direct current. From the practical point of view, this means that the impulse $CBAB'C'$ (fig. 247) is replaced by $PBAB'P'$, lying between $\omega t = -\pi/2$ and $+\pi/2$. In general, for a single valve:

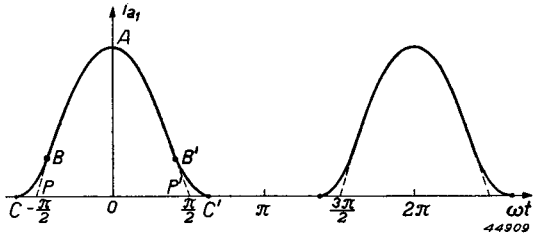

Fig. 247. Calculation of the D.C. component from the "combined impulse" $PBAB'P'$.

$$I_{ao} = \frac{1}{2\pi}\int_0^{2\pi} i_a d\omega t,$$

which, for reasons of symmetry, can be replaced by:

$$I_{ao} = \frac{1}{\pi}\int_0^{\pi/2} i_a d\omega t.$$

Substitution of expression (1) for i_a and subsequent integration then gives:

$$I_{ao} = \frac{1}{\pi}\left[\frac{\pi}{2} I_{ao} + I_{a1} - \frac{1}{3} I_{a3} + \frac{1}{5} I_{a5} - \frac{1}{7} I_{a7} + \frac{1}{9} I_{a9} - \frac{1}{11} I_{a11}\right],$$

so that:

$$I_{ao} = \frac{2}{\pi}\left[I_{a1} - \frac{1}{3} I_{a3} + \frac{1}{5} I_{a5} - \frac{1}{7} I_{a7} + \frac{1}{9} I_{a9} - \frac{1}{11} I_{a11}\right],$$

and, since

$$2I_{a1} = a_1;\ 2I_{a3} = a_3\ , \ldots$$

this becomes:

$$I_{ao} = \frac{1}{\pi}\left(a_1 - \frac{1}{3} a_3 + \frac{1}{5} a_5 - \frac{1}{7} a_7 + \frac{1}{9} a_9 - \frac{1}{11} a_{11}\right), \quad \ldots\ldots \quad (10)$$

from which the direct anode current may be calculated with the aid of formulae (9) and (9*a*).

At smaller amplitudes of the excitation voltage, this formula gives however inaccurate results, since the ends of the impulse, BC and $B'C'$ (fig. 247), then exert a relatively greater influence: in such cases I_{ao} is calculated by another method, for instance, by means of Simpson's law.

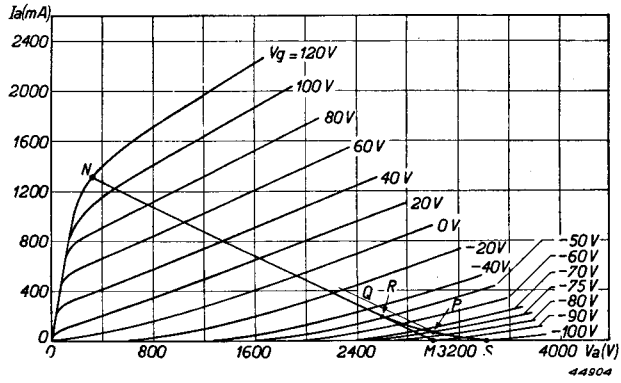

Fig. 248. I_a—V_a characteristics of the triode referred to in fig. 234, showing load line $NRPS$ for A.F. class B operation.

The output power per valve is:

$$W_o = \frac{1}{2} V_{ap1} I_{a1},$$

in which V_{ap1} is the peak value of the first harmonic of the alternating anode potential resulting from the combined action of the two valves. Therefore, if R_a be the anode resistance per half (in figs. 243 and 244 cot $a = R_a$), then

$$V_{ap1} = 2I_{a1}R_a = a_1 R_a,$$

so that:

$$W_o = \frac{1}{4} a_1^2 R_a \quad . \quad . \quad . \quad . \quad . \quad . \quad . \quad . \quad . \quad . \quad . \quad (11)$$

Input power, anode dissipation, efficiency and distortion are calculated along the same lines.

To illustrate the above, let us now compute the A.F. class B setting of the triode whose characteristics are shown in fig. 234.

Assuming that $V_a = 3000$ V, $V_g = -75$ V, the standing current is 65 mA: whether this choice of operating point is the correct one or not will appear later, when the dynamic characteristic has been plotted. The higher this standing current, the less the distortion at small amplitudes, but the more the class B setting passes over into class A/B which, especially at small amplitudes, means a reduction in efficiency.

The terminating point N of the load line will be placed on the character-

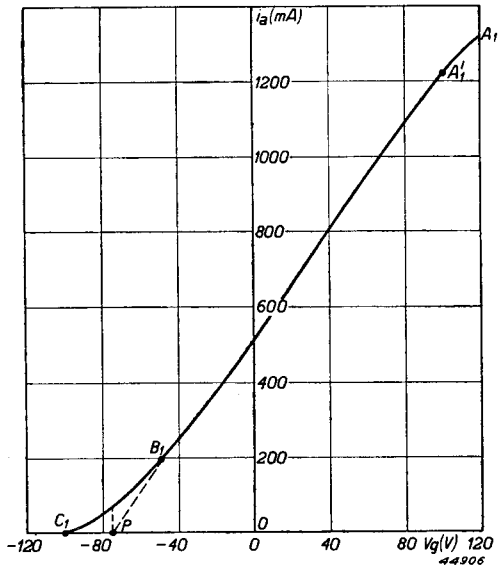

Fig. 249. Dynamic characteristic ($A_1B_1C_1$) relating to the load line in fig. 248. A_1B_1P is the combined characteristic.

istic for $V_g = +120$ V and as far as possible to the left to ensure high output and efficiency, although not too far, that is, on the limit characteristic, as this reduces the peak anode current too much (and therefore the output power also), whilst increasing distortion: the ultimate location must then be a compromise, for example $I_{ap} = 1320$ mA; $v_{a\,min} = 320$ V.

The grid voltage as a function of time will then be:

$$v_g\,(t) + -75 + 195 \cos \omega t.$$

The working line is plotted in the manner previously shown (see fig. 244); this will be $NRPS$. The anode resistance R_a is determined by the slope of the line MN:

$$R_a = \frac{V_a - v_{a\,min}}{I_{ap}} = \frac{3000 - 320}{1.320} = 2030 \text{ ohms.}$$

The relation between i_a and v_g can then be read from the load line, this being given in the following table and in fig. 249 (curve $A_1B_1C_1$):

V_g = 120 100 80 60 40 20 0 −20 −40 −50 −60 −70 −75 −80 −90 −100 V
I_a = 1320 1220 1090 950 800 660 520 380 250 190 140 90 65 40 20 0 mA.

The combined characteristic is then the line A_1B_1P, only half of which is shown (fig. 246): it will be seen that PB_1 lines up reasonably well with B_1A_1 thus showing that the choice of standing current is apparently correct.

Fig. 250 reproduces on an enlarged scale the differences Δ between ordinates of

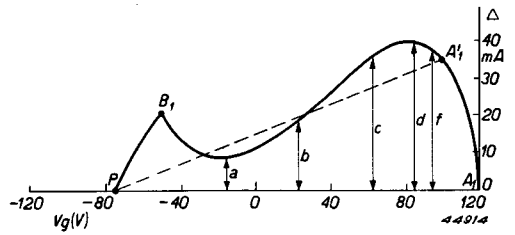

Fig. 250. Determination of the difference between the ordinates (Δ), relative to the dynamic characteristic in fig. 249.

this characteristic and the straight line A_1P, and from fig. 246 these values of Δ are found to be:

$a = 9$; $b = 18$; $c = 37$; $d = 40$; $f = 37$, which in conjunction with expression (9) gives:

$$a_5 = 0.4\,(9 - 40) = -12.4$$
$$a_7 = \frac{18}{3} - 0.577\,.\,37 + 12.4 = -3.0$$
$$a_3 = -0.4475\,.\,(9 + 40) + 6.2 + 3.0 = -12.8$$
$$a_9 = -\frac{2}{3}\,.\,18 + 12.8 = 0.8$$
$$a_{11} = -0.707\,.\,37 + 12.8 + 12.4 = -1.0.$$

Further, $I_{ap} = 1320$ mA, so that:

$$a_1 = 1320 + 12.8 + 12.4 + 3.0 - 0.8 + 1.0 = 1348 \text{ mA}.$$

Finally, (10) furnishes us with:

$$I_{ao} = \frac{1}{\pi}\,(1348 + 4.3 - 2.5 + 0.4 + 0.1 + 0.1) = 430 \text{ mA}.$$

The input power per valve is therefore:

$$W_i = V_a I_{ao} = 3000\,.\,0.430 = 1290 \text{ W},$$

the output power:

$$W_o = \frac{1}{4}\,a_1^2\,R_a = \frac{1}{4}\,(1.348)^2\,.\,2030 = 923 \text{ W},$$

the anode dissipation:

$$W_a = W_i - W_o = 367 \text{ W}.$$

The efficiency is:

$$\eta = \frac{W_o}{W_i} = \frac{923}{1290} = 71.5\%$$

and the distortion:

$$d = \frac{\sqrt{a_3^2 + a_5^2 + \ldots + a_{11}^2}}{a_1} = 1.35\%.$$

At other values of the excitation voltage the calculation is carried out in the same manner, but it must be remembered that the point A_1 (figs. 249 and 250) will then occupy another position, so that it becomes

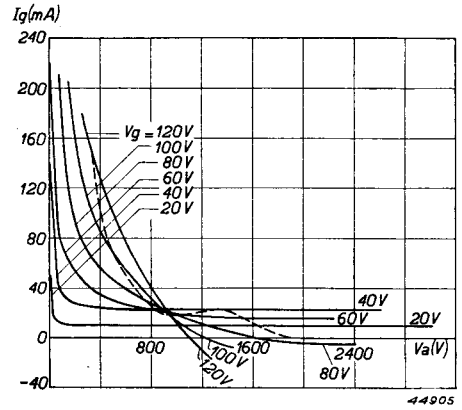

Fig. 251. I_g—V_a characteristics of the same triode as in fig. **234**; the broken line is the load line relating to A.F. class B operation shown in fig. **248**.

necessary to measure Δ at other points and in a slightly different way. For instance, if $V_{gp} = 175$ V, so that $v_{g\,max} = 100$ V, then the end of the characteristic will occur at A_1' (figs. 249 and 250): in fig. 250, Δ is therefore measured between the curves $A_1'B_1P$ and the straight line $A_1'P$, and further at points that will suit the lower value of V_{gp}, that is more to the left. From this example it will be seen that the Δ's can also be negative.

Finally, the grid current and control power must be computed. Fig. 251 shows the I_g–V_a characteristics of the triode represented in fig. 234: the load line in the I_a/V_a characteristics (fig. 248) gives the relation between the instantaneous values of v_g and v_a, and, by employing the I_g/V_a diagram, the relation between i_g and v_g can also be determined.

This gives the following table:

$v_g\,(t) =$	120	100	80	60	40	20	0 V
$v_a\,(t) =$	320	500	760	1050	1360	1640	1930 V
$i_g\,(t) =$	154	69	30	19	23	10	0 mA

which is shown graphically by the dotted line in fig. 251. The dynamic grid-current characteristic can then be plotted, viz. $i_g(t)$ as a function of $v_g(t)$, as shown in fig. 252, from which, in conjunction with the expression:

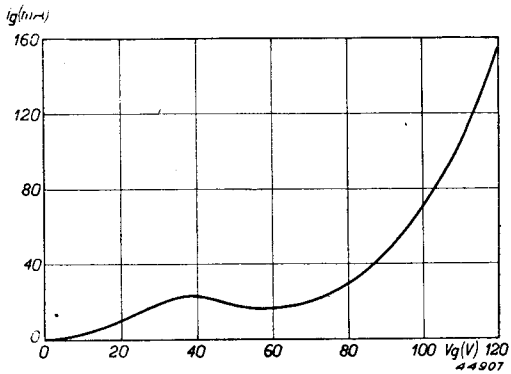

Fig. 252. Dynamic grid-current characteristic corresponding to the load line of fig. 251.

$$v_g(t) = -75 + 195 \cos \omega t$$

it is possible to determine $i_g = f(\omega t)$, this being the grid current impulse. Simpson's law next gives us the d.c. component and the first harmonic of the grid current in the manner described in § 1; thus:

$$I_{go} = 23.6 \text{ mA}; \; I_{g1} = 43.2 \text{ mA},$$

when the grid input power will be:

$$W_{gAF} = \frac{1}{2} V_{gp} \cdot I_{g1} = \frac{1}{2} \cdot 195.43.2 \cdot 10^{-3} = 4.2 \text{ W}.$$

§ 4. The use of constant-current characteristics

In chapters III to VII I_a — V_a characteristics at constant values of V_g were used. In principle I_a — V_g characteristics at constant values of V_a or V_g — V_a characteristics at constant values of I_a could also be used. In Anglo-American countries the latter characteristics are frequently used under the name of "constant current" characteristics. They may be derived from I_a — V_a characteristics by drawing lines I_a = constant and then determinating the points of intersection of those lines with lines V_g = constant.

Proceeding in this way we find the corresponding values of V_g and V_a. In practice more precise results can be obtained by first drawing lines V_a = constant in the I_a — V_a characteristics plot, thereby arriving at I_a — V_g characteristics for constant V_a. From the latter constant-current characteristics can be obtained by drawing lines I_a = constant. The reason for this cumbersome procedure is that for the major part I_a — V_a characteristics have a small slope, so that estimating the points of intersection of lines V_g = constant with lines I_a = constant is rather difficult. The I_a — V_a and constant-current characteristics of the Philips transmitting valve type TB3.5/750 are given in figs 253 and 254 respectively.

In both figures the same load line is depicted. The use of constant-current characteristics is a special advantage when these are used with R.F. valve settings, for which settings

$$v_a(t) = V_a - V_{ap} \cos \omega t \quad \ldots\ldots\ldots\ldots\ldots \quad (3,25)$$

and

$$v_g(t) = V_g + V_{gp} \cos \omega t \quad \ldots\ldots\ldots\ldots\ldots \quad (3,24)$$

(see chapter III, § 5, p. 45).

Eliminating cos ωt we find:

$$v_g(t)\, V_{ap} + va(t)\, V_{gp} = V_g\, V_{ap} + V_a\, V_{gp} \quad \ldots\ldots\ldots \quad (1)$$

Eq. (1) gives the relation between the momentary values of V_g and V_a, thus giving the equation of the load line in the constant-current characteristics plot. This load line, being given by a linear equation in V_a and V_g, is a straight line having a slope given by:

$$\frac{dv_g}{dv_a} = -\frac{V_{gp}}{V_{ap}} \quad \ldots\ldots\ldots\ldots\ldots\ldots\ldots \quad (2)$$

From (2) it is seen that the slope of the load line is a direct measure for the voltage amplification of the valve. The points of intersection of the load line with lines I_a = constant give the momentary values of the anode current. In the same way as for the I_a—V_a characteristics, $i_a = f(t)$, so the current pulse can be found with the help of equations (3,24) or (3,25), starting from the above-mentioned points of intersection. From the current pulse, the first harmonic and the d.c. anode current can be computed as in chapter III § 2. By using constant-current characteristics the values of

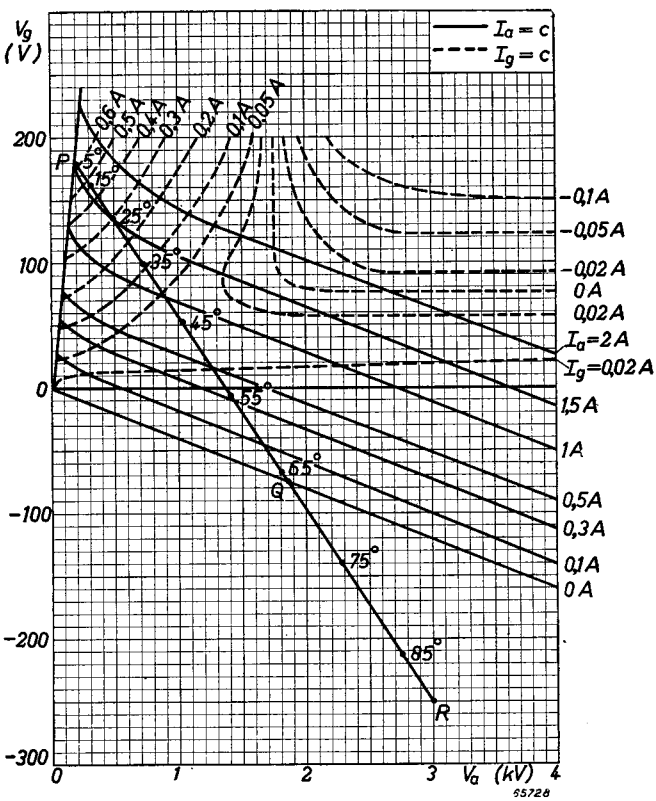

Fig. 253. Constant-current characteristics of the triode TB3.5/750 with the load line *PQR*.

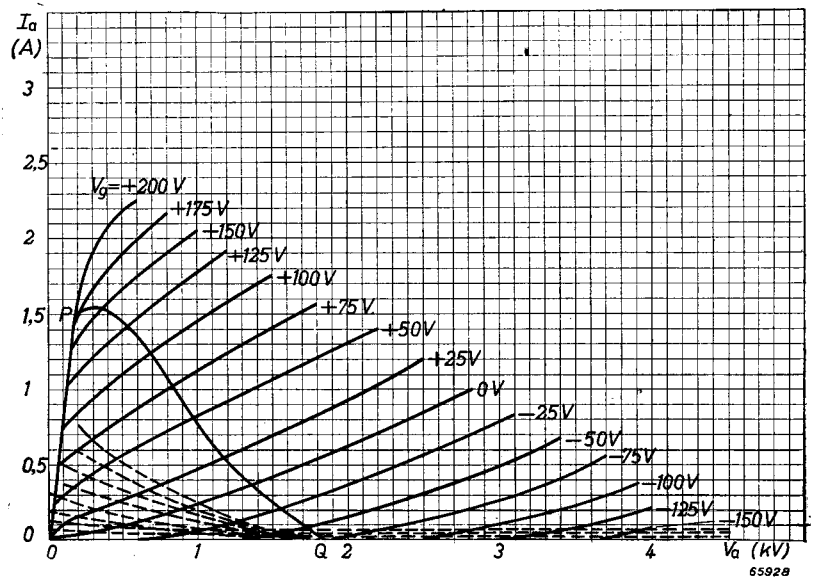

Fig. 254. I_a—V_a (and I_g—V_a) characteristics of the triode TB3.5/750 with the same load line (PQ) as in fig. 253.

I_{a1} and I_{a0} can be determined graphically in a rather simple way.

In § 1 of the appendix the determination of the area under a curved line (e.g. a current pulse) was shown to be performed with the help of Simpson's law. Instead of Simpson's law a different procedure, being somewhat less accurate but demanding fewer calculations, can be used. Looking again at fig. 224 we see that the part of the area lying below the curved line AB can be given with good degree of accuracy by:

$$0 = 2h\,(y_1 + y_3 + y_5 + \ldots\ldots y_{2n-3} + y_{2n-1}),$$

provided n is sufficiently large.

The validity of this formula is based on the assumption that that part of the curve AB upon which three successive points P, Q and R are lying can be approximated sufficiently by a straight line. The area of the strip $P\,.\,R\,.\,R_1\,.\,P_1$ is approximated as being that below the above-mentioned straight line. For the area below PQR it then follows from fig. 225, in which now $P.Q.R.$ is given as a straight line, that:

$$y_P h + \tfrac{1}{2}\,(y_Q - y_P)\;h + y_R h - (y_R - y_Q)\;h\;.\;\tfrac{1}{2} = y_Q h + \tfrac{1}{2}\,(y_P + y_R)\;h.$$

Now $y_Q = \frac{1}{2}(y_P + y_R)$, so that the area below PQR will be $2hy_Q$. The area below curve AB now consists of n strips of width $2h$; so we find:

$$0 = 2h\ (y_1 + y_3 + y_5 + \ldots\ldots\ldots\ldots y_{2n-3} + y_{2n-1})$$
$$= \frac{x_{2n} - x_0}{n}\ (y_1 + y_3 + y_5 \ldots\ldots\ldots y_{2n-3} + y_{2n-1}).$$

To illustrate the accuracy of this method we shall now calculate the area of a number of figures. To obtain a good comparison we divide the figures into the same number of strips as in § 1 of this appendix.

a. For the quarter circle (fig. 226) we then find:

$$y_{1/2} = \sqrt{R^2 - \left(\frac{R}{12}\right)^2} = \tfrac{1}{12}\ R\ \sqrt{143}$$

$$y_{3/2} = \sqrt{R^2 - \left(\frac{3R}{12}\right)^2} = \tfrac{1}{12}\ R\ \sqrt{135}$$

$$y_{5/2} = \sqrt{R^2 - \left(\frac{5R}{12}\right)^2} = \tfrac{1}{12}\ R\ \sqrt{119}$$

$$y_{7/2} = \sqrt{R^2 - \left(\frac{7R}{12}\right)^2} = \tfrac{1}{12}\ R\ \sqrt{95}$$

$$y_{9/2} = \sqrt{R^2 - \left(\frac{9R}{12}\right)^2} = \tfrac{1}{12}\ R\ \sqrt{63}$$

$$y_{11/2} = \sqrt{R^2 - \left(\frac{11R}{12}\right)^2} = \tfrac{1}{12}\ R\ \sqrt{23}$$

and hence:

$$0 = \frac{R}{6} \cdot \frac{R}{12}\ (\sqrt{143} + \sqrt{135} + \sqrt{119} + \sqrt{95} + \sqrt{63} + \sqrt{23}) = 3{,}165.$$

By integration we found in § 1 : $0 = \pi = 3.142$.
The deviation thus amounts to about 1.4%, as against 1% with Simpson's law.

b. For the cosine curve (fig. 227) we find:

$$y_{1/2} = \cos \frac{\pi}{24} = \cos \ 7.5°$$

$$y_{3/2} = \cos \frac{3\pi}{24} = \cos \ 22.5°$$

$$y_{5/2} = \cos \frac{5\pi}{24} = \cos \ 37.5°$$

$$y_{7/2} = \cos \frac{7\pi}{24} = \cos \ 52.5°$$

$$y_{9/2} = \cos \frac{9\pi}{24} = \cos \ 67.5°$$

$$y_{11/2} = \cos \frac{11\pi}{24} = \cos \ 82.5°$$

From this it follows that:

$$0 = \frac{1}{6} \cdot \frac{\pi}{2} (\cos \ 7.5° + \cos \ 22.5° + \cos \ 37.5° + \cos \ 52.5° +$$

$$\cos \ 67.5° + \cos \ 82.5°) = \frac{\pi}{12} \ 3.83064 = 1.0028.$$

Thus the deviation amounts to about 0.28 %, as compared with about 0.01 % with Simpson's law.

c. For the exponential curve (fig. 235) we find:

$$y_{1/2} = e^{1/4}$$

$$y_{3/2} = e^{3/4}$$

$$\text{Thus } 0 = \tfrac{1}{2} (e^{1/4} + e^{3/4}) = 1.7018.$$

By integration we found in § 1 : O = 1.7183, the deviation being about 1 %, as against 0.03 % with Simpson's law.
Although the deviations are greater than with Simpson's law, the approximation is sufficient, because the characteristics are not known with any greater accuracy.
We now turn back to the current pulse. From many calculations we found that as a rule 6 strips are enough for calculating the area below the current-pulse curves. Therefore we could divide the length of line

between $\omega t = 0$ and $\omega t = \theta$ into 6 equal parts. For the constant-current lines this means that we have to determine 6 points on the load line lying between

$$i_a = i_a \text{ max. and } i_a = 0$$

(corresponding to P and Q respectively).

The distance between the 6 points from the point P is to be $PQ \cos (2n + 1)\ \theta/12$, n being 0, 1, 2, 3, 4 and 5 successively. Adding the values of i_a corresponding to the points of intersection found from the constant-current characteristics and dividing by 6, we find the mean current over the time interval of the half current pulse.

To find the d.c. anode current we have to determine the mean value over a whole cycle, so that the value found above has to be multiplied by θ/π.

But there is a much simpler way than this.

With most R.F. class C settings θ has a value between about 60° and 70°, so that, if we divide the interval from $\omega t = 0$ to $\omega t = 90°$ into 9 parts of 10° each, about 6 parts will lie in the area of the current pulses. In this way the same degree of accuracy is obtained as with the method mentioned above.

If i_m is the symbol for the currents belonging to the points of intersection, the mean current in the interval between $\omega t = 0$ and $\omega t = 90°$ (according to the load line from P to R) is $\frac{\Sigma i_m}{9}$.

For the direct current we then find $\frac{2\Sigma i_m}{4 \times 9} = \frac{\Sigma i_m}{18}$.

The advantage of this procedure is that a division on a number of lines can be prepared in advance (e.g. on a piece of transparent paper). The length of the lines corresponds to the several load lines PR required for different valves under different conditions. Dividing into 9 equal parts of 10° gives points of intersection at 5°, 15°, 25°, 35°, 45°, 55°, 65°, 75° and 85° respectively.

Any line $P'R'$ can be marked with points lying at distances $P'R' \cos 5°$, $P'R' \cos 15°$, $P'R' \cos 25°$, $P'R' \cos 35°$, $P'R' \cos 45°$, $P'R' \cos 55°$, $P'R' \cos 65°$, $P'R' \cos 75°$ and $P'R' \cos 85°$ from P respectively. When this is done for a sufficient number of lines of different lengths there will always be a line $P'R'$, the length of which is the same as the load line PR in the constant-current characteristics. This can be carried out simply by drawing a cosine scale on a line $P'R'$, the length of which

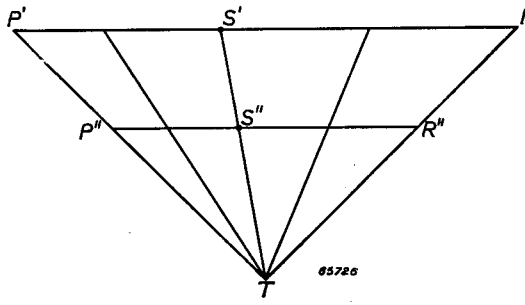

Fig. 255. Sketch illustrating the division of a load line $P''R''$ in a constant-current characteristics diagram.

corresponds to the longest line ever likely to be used. Taking the line $P'R'$ as the base of a triangle $P'R'T$ (see fig. 255) it is seen that for any line $P''R''$ running parallel to $P'R'$, the division is obtained in the same way as for the line $P'R'$.

The conformity of the triangles $P'S'T$ and $P''S''T$ yields:

$$P'S' : S'T = P''S'' : S''T \ldots\ldots\ldots\ldots 1).$$

In the same way, from the triangles $R'S'T$ and $R''S''T$ we obtain:

$$R'S' : S'T = R''S'' : S''T \ldots\ldots\ldots\ldots 2)$$

Dividing 1) over 2) we obtain:

$$P'S' : S'R' = P''S'' : S''R''.$$

In this way any line parallel to $P'R'$ is always divided in the same manner as the line $P'R'$.

When drawing the triangle with cos scale and parallel lines on transparent material it is easy to position the triangle $P'R'T$ on the load line PR in such a way that PR runs parallel to the base of the triangle and the ends of PR lie on the sides of triangle $P'R'T$.

The points of intersection of the radial lines running from T to the points of the cosine scale then give the points on PR where the value of the current is to be determined. To find the first harmonic I_{a1} it is necessary to multiply the above-determined values of i_m (according to e.g. (3,15)) by the values of cos ωt_m corresponding to i_m. Thus the first harmonic will be:

$$I_{a1} = \frac{2\Sigma i_m \cos \omega t_m}{18}.$$

To illustrate this we shall now calculate a R.F. class C setting with the help of constant-current characteristics. For this purpose we use the characteristics of the valve TB3/750 depicted in fig. 252.

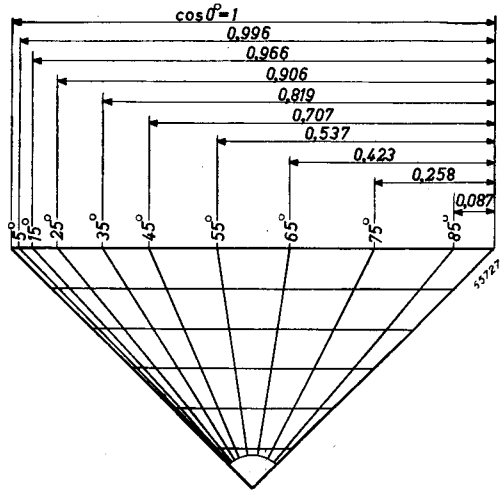

Fig. 256. Cosine scale for use when dividing any load line in a constant-current characteristics diagram.

With $V_{a\,g}\,3kV$, $V_g = -250$ $V_{gp} = 430$ V and driving the excitation to the line $V_g = V_a$, we find the load line PR.

On this line the points of intersection found with the help of the cosine scale are marked. From interpolation of the constant-current lines we find the following table:

ωt	i_a	$i_a \cos \omega t$	i_g
5°	1.50 A	1.49 A	0.60 A
15°	1.55	1.50	0.49
25°	1.50	1.36	0.30
35°	1.25	1.02	0.12
45°	0.72	0.51	0.04
55°	0.34	0.19	0.00
65°	0.02	0.01	0.00
75°	0.00	0.00	0.00
85°	0.00	0.00	0.00
	6.88	0.08	1.55

It follows that the d.c. anode current $I_{a0} = \frac{6880}{18} = 382$ mA.

The first harmonic $I_{a1} = \dfrac{2 \times 6080}{18} = 675$ mA.

Thus the input is: $W_1 = 3000 \times 0.382 = 1146$ W;

the output is: $W_0 = \frac{1}{2} \times 2820 \times 675 = 953$ W;

the anode dissipation is: $W_a = 193$ W.

The efficiency amounts to $\eta = \frac{953}{1146} \times 100 = 83.2\%$.

The grid current $ig_0 = \frac{1150}{18} = 86$ mA.

For the driving power we find $W_{RF} =$ abt $0{,}9 \times 430 \frac{86}{1000} = 33$ W.

The total cathode current amounts to 382 + 86 = 468 mA.
The grid dissipation will be $W_g = W_{ig} - i_{g0} V_g =$

$$33 - \frac{86}{1000} \times 250 = 11.5 \text{ W}.$$

Finally $ik_p = 1.49 + 0.62 = 2.11$ A.
For purposes of comparison we calculate the same setting with the help of the $I_a - V_a$ characteristics given in fig. 254.
For *va* and *vg* we have the equations:

$$V_a = 3000 - 2820 \cos \omega t$$

and

$$V_g = -250 + 430 \cos \omega t.$$

From this we find:

ωt	cos ωt	2820 cos ωt	V_a	430 cos ωt	V_g
5°	0.996	2805	195 V	428	178 V
15°	0.966	2710	290	416	166
25°	0.906	2560	440	390	140
35°	0.819	2310	690	352	102
45°	0.707	1995	1005	304	54
55°	0.573	1615	1385	246	-4
65°	0.423	1190	1810	182	-68
75°	0.258	728	2272	111	-139
85°	0.087	245	2755	37	-213

With the now known values of V_a and V_g we find (from interpolation between the lines *vg* = constant) from the *ia—va* characteristics:

ωt	i_a	i_a cos ωt	*vg*
5°	1,50 A	1,49 A	0,60 A
15°	1.55	1.50	0.49
25°	1.50	1.36	0.30
35°	1.25	1.02	0.12
45°	0.72	0.51	0.04
55°	0.34	0.19	0.00
65°	0.02	0.01	0.00
75°	0.00	0.00	0.00
85°	0.00	0.00	0.00

Thus it is seen that the use of constant-current characteristics and the cosine scale obviates the calculation of the 5 columns in the upper table.

In both cases the same points of intersection have been used for determining the current pulse. For the case of I_a — V_a characteristics, interpolations between lines V_g = constant can be omitted if, instead of using the same points of intersection as for the constant-current characteristics, we start from the points of intersection of the load line with lines V_g = constant. With the formul $a \cos \omega t = \frac{250 + vg}{430}$ the value of cos ωt can be determined for every value of vg; ωt then follows from a cosine table.

With the points of intersection found in this way we can then plot the current pulse $ia = f(\omega t)$. From the diagram the d.c. current and the first harmonic have to be found by graphical integration.

The use of constant-current characteristics is therefore the quicker way in the case of settings with tuned anode circuit.

PHILIPS TRANSMITTING VALVES AND RECTIFIERS FOR TRANSMITTERS

Summary of Technical Data

The following tables contain certain technical data the knowledge of which is indispensable to the correct working of the valves. Besides heater voltage and current, working currents, voltages and dissipation, and amplification factors, the more important details relating to R.F. Class C telegraphy, R.F. Class B Telephony and R.F. Class C anode modulation are also given.

In the case of the modulator valves, particulars are included of A.F. Class A and Class B settings; these modulators are triodes as specially employed in modulation amplifiers.

Finally, sundry details are provided of mercury vapour- or rare-gas filled rectifiers such as are frequently used in conjunction with the types of transmitting valves in question.

TYPE	V_f	I_f	V_a max.	V_{g2} max.	W_a max.	Full ratings		
						up to	W_o	η
	V	A	V	V	W	Mc/s	W	%
MAL 12/15	21.5	79	12 000	—	15 000	—	1 950	16
MAW 12/15						—	42 000	66
PAL 12/15	22	80	12 000	2 000	8 000	20	13 000	62
						20	4 000	33
						20	2 900	37
						20	7 500	70
PAW 12/15	22	80	12 000	2 000	12 000	20	15 900	61
						20	3 500	33
						20	2 900	37
						20	7 500	70
PB 1/150	10	3.25	1 750	775	70	—	300	69
PB 2/200	12	3.35	2 000	400	110	20	270	71
						20	45	29
						20	147	72
						20	124	69
						20	43	32
						—	400	70
PB 2/500	12	7.3	2 500	500	250	10	600	70
						20	90	26
						10	325	69
						20	100	28
						—	1 000	70
PB 3/800	12	8.5	3 000	600	450	10	1 200	72
						10	190	30
						10	580	71
						10	200	35
						—	1 600	69
PC 1.5/100	10	2	1 500	500	85	20	140	72
						20	34	29
						20	70	58
						20	30	30
PE 04/10 E	12	0.65	500	300	10	20	15	60
						20	4	31
						20	10	62
						20	2	33
PE 05/25	12.6	0.7	500	300	12	100	33	73
						100	6	33
						100	20	71
						55/165	9	43

[1]) Two valves. [2]) $V_{g2} = V_{g3}$

Class of service	Reduced ratings			Base	Dimensions	
	Freq.	W_o	η		max. diam.	max. length
	Mc/s	W	%		mm	mm
A mod.	—	2700	22		104	730
B mod. [1])					104	811
C telegr.	50					
B teleph.	50				234	525
C g_2g_3 mod.	50					
C ag_2 mod.	50					
C telegr.	50					
B teleph.	50				140	541
C g_2g_3 mod.	50					
C ag_2 mod.	50					
B mod. [1])				medium 5-pin	53	156
C telegr.	60	152	58			
B teleph.	60	35	25			
C ag_2 mod.	60	77	51	7 pins	63	169
C an. mod.	60	75	50	spec.		
C g_3 mod.	60	32	24			
B mod. [1])						
C telegr.	60	312	55			
B teleph.	60	50	22			
C ag_2 mod.	60	175	51	5 prongs	82	276
C g_3 mod.	60	45	22			
B mod. [1])						
C telegr. [2])	60	488	55			
B teleph.	60	67	21			
C ag_2 mod.				5 prongs	106	293
C g_3 mod.						
B mod. [1])						
C telegr.						
B teleph.				4 pins	66	252
C ag_2 mod.				spec.		
C g_3 mod.						
C telegr.	60	10	50			
B teleph.	60	2	17	medium	51	150
C ag_2 mod.	60	6.3	49	7-pin		
C g_3 mod.	60	1.8	20			
C telegr.	167	15	55			
B teleph.				8 spins	36.2	104.5
C ag_2 mod.				spec.		
C fr. mult.						

TYPE	V_f	I_f	V_a max.	V_{g2} max.	W_a max.	Full ratings		
						up to	W_o	η
	V	A	V	V	W	Mc/s	W	%
						20	45	69
E	12.6	0.65				20	11	31
PE 06/40 N	6.3	1.3	600	300	25	20	40	70
P	6.3	1.3				2/4	27	52
						—	100	71
						60	132	74
						60	23	34
PE 1/100	12.6	1.35	1 000	300	45	60	75	78
						60	27	37
						—	194	72
						120	375	75
						120	58	32
QB 3/300	5	6.5	3 000	600	125	120	300	79
						—	400	61
						75	1 000	80
						75	126	33
QB 3.5/750	5	14.1	4 000	600	250	75	510	75
						—	636	65
						60	8	62
QE 04/10	6.3	0.6	300	250	7.5	75/150	2.3	25
						50/150	1.5	19
						60	5.8	60
						186	20.8	65
						186	7.8	59
QQC 04/15	6.3	0.68	400	250	2×6 / 2×8 [3]	93/186	8	50
						62/186	10	38
						—	16	74
QQE 04/20	6.3	1.6	600	250	2×7.5	200	26 [4]	72
	12.6	0.8				200	17	76
						150	80	67
						150	45	66
QQE 06/40	6.3	1.8	600	250	2×20	50/150	24	40
						—	73	72

[1]) Two valves. [2]) $I_{g1} = 0$. [3]) Intermittent operation. [4]) $V_a = 500$ V.

Class of service	Reduced ratings			Base	Dimensions	
	Freq.	W_o	η		max. diam.	max.length
	Mc/s	W	%		mm	mm
C telegr. B teleph. C ag_2 mod. C fr. mult B mod. [1]	60 60 60	36 6.5 20	62 20 55	Med. 7-pin Med. 5-pin P	51 51 51	146 146 134
C telegr. B teleph. C ag_2 mod. C g_3 mod. B mod. [1]				Septar	49	110
C telegr. B teleph. C ag_2 mod. B mod. [1]	200	225	65	Giant 5-pin	62	130
C telegr. B teleph. C ag_2 mod. B mod. [1] [2]	120	500	67	Giant 5-pin	87	151
C telegr. C fr. mult. C fr. mult. C ag_2 mod.	175	10.8 [1]	42	B9G	38	78
C telegr. [3] C ag_2 mod. [3] C fr. mult. [3] C fr. mult. [3] B mod.	300	8	34	Con- tinental Loctal	32	100
C telegr. C ag_2 mod.	300	22	61	Septar	51	84
C telegr. C ag_2 mod. C fr. mult. B mod.	430 143/430	34 20	47 33	Septar	49	122

TYPE	V_f	I_f	V_a max.	W_a max.	Full ratings		
					up to	W_o	η
	V	A	V	W	Mc/s	W	%

Class of service	Reduced ratings			Base	Dimensions	
	Freq.	W_o	η		max. diam.	max. length
	Mc/s	W	%		mm	mm
C telegr. B teleph. C an. mod. C osc. [2]				spec.	118	306
C telegr. B teleph. C an. mod.					272	1 333
C telegr. B teleph. C an. mod.	20 20 20	125 000 40 000 56 000	65 30 66		272	1 393
C telegr. B teleph. C an. mod. B mod. [1]	20 20 20	10 500 2 000 6 000	72 33 75		194	471
C telgr. B teleph. C an. mod. B mod. [1]	75 20 20	3 500 3 300 6 000	51 33 75		95	495
C telegr. B teleph. C an. mod.					104 104	730 811
C telegr. B teleph. C an. mod.	37.5	25 000	62		280 226	618 714
C telegr. B teleph. C an. mod. B mod. [1]	300	18	27	A Med. 4-pin	69 69	174 170
C telegr. B teleph. C an. mod.	100	140	57	2 pins	63	174
C telegr. B teleph. C an. mod. B mod. [1]	150	250	46	2 pins	86	243

TYPE	V_f	I_f	V_a max.	W_a max.	Full ratings		
					up to	W_o	η
	V	A	V	W	Mc/s	W	%
TB 2.5/300	6.3	5.4	2 500	135	150	390	76
					150	65	34
					150	204	80
					—	530	71
TB 3/750	5	14.1	3 000	250	100	840	77
					100	140	36
					100	482	77
					—	1 100	75
TB 3/1000	12	8.5	3 000	500	20	1 200	72
					20	200	30
					20	720	72
					—	1 750	68
TB 3/2000	12	17	3 500	1 100	2	2 900	72
					2	600	35
					2	1 625	75
					—	3 300	66
TB 4/1250	10	9.7	4 000	450	100	1 450	76
					100	750	75
					—	1 830	77
TBL 6/6000	12.6	33	6 000	5 000	75	6 900	76
					75	1 900	32
					75	4 700	78
TBW 6/6000	12.6	33	6 000	6 000	75	6 900	76
					75	1 900	32
					75	4 700	78
TBL 12/100	18	196	15 000	45 000	15	108 000	75
					15	65 000	76
TBW 12/100	18	196	15 000	50 000[2]	15	108 000	75
					15	51 500	35
					15	65 000	76

[1]) Two valves. [2]) For B teleph. 100 kW.

Class of Service	Reduced ratings			Base	Dimensions	
	Freq.	W_o	η		max. diam.	max.length
	Mc/s	W	%		mm	mm
C telegr. B teleph. C an. mod. B mod. [1]	200	200	57	5 pins giant	62	132
C telegr. B teleph. C an. mod. B mod. [1]	143	425	61	5 pins giant	87	151
C telegr. B teleph. C an. mod. B mod. [1]	60 60	975 562	71 72	2 pins	106	262
C telegr. B teleph. C an. mod. B mod. [1]	20 20 20	2 600 520 1 300	70 32 74	2 pins	154	334
C telegr. C an. mod. B mod. [1]	120	875	63	spec.	118	213
C telegr. B teleph. C an. mod.	100	5 600	75		•122.5	200
C telegr. B teleph. C. an. mod.	220	2 850	50		70	256
C. telegr. C an. mod.	30 30	50 30	75 71		286	635
C telegr. B teleph. C an. mod.	30 30 30	50 — 30	75 — 71		240	710

TYPE	V_f	I_f	Peak inv. max.	I_o max.	Rectifier circuit
	V	A	kV	A	
DCG 1/250	4	2.5	3	0.25	single phase full wave 3 phase half wave 3 phase full wave
DCG 1.5/250	4	2.7	4.25	0.25	single phase full wave 3 phase half wave 3 phase full wave
DCG 4/1000$^{ED}_{G}$	2.5	4.8	10	0.25	single phase full wave 3 phase half wave 3 phase full wave
DCG 4/5000	4	6.75	13	1.25	single phase full wave 3 phase half wave 3 phase full wave
DCG 5/30	5	31	13	6	single phase full wave 3 phase half wave 3 phase full wave
DCG 5/5000$^{EG}_{GB}$	5	6.75	12	1.5	single phase full wave 3 phase half wave 3 phase full wave
DCG 6/6000	5	6.5	13	1	single phase full wave 3 phase half wave 3 phase full wave
DCG 9/20	5	12.5	21	2.5	single phase full wave 3 phase half wave 3 phase full wave
DCG 12/30	5	14	27	2.5	single phase full wave 3 phase half wave 3 phase full wave
DCX 4/1000	2.5	5	10	0.25	single phase full wave 3 phase half wave 3 phase full wave
DCX 4/5000	5	10	10	1.25	single phase full wave 3 phase half wave 3 phase full wave

Number of valves	V_{tr}	V_o	I_o	W_o tot.	Base	Dimensions	
						max. diam.	max. length
	kV	kV	A	kW		mm	mm
2	1.0	0.96	0.5	0.5			
3	1.2	1.4	0.75	1.1	A	48	115
6	2.1	2.8	0.75	2.2			
2	1.5	1.35	0.5	0.7			
3	1.7	2.0	0.75	1.5	A	49.5	137
6	3.0	4.1	0.75	3.0			
2	3.5	3.2	0.5	1.6	Edison	49.5	147
3	4.1	4.8	0.75	3.6	screw;	49.5	162
6	7.0	9.6	0.75	7.2	4 pins		
2	4.5	4.1	2.5	10.2	Goliath		
3	5.3	6.2	3.75	23.4	screw	53	221
6	9.1	12.5	3.75	46.8			
2	4.5	4.1	12	49			
3	5.3	6.2	18	112		220	581
6	9.1	12.5	18	225			
2	4.2	3.8	3	11.4	Goliath	52	235
3	4.9	5.8	4.5	26.1	screw; 4		
6	8.5	11.5	4.5	51.5	pins jumbo	51	217
2	4.5	4.1	2	8.3	4 pins		
3	5.3	6.2	3	18.8	spec.	120	242
6	9.1	12.5	3	37.5			
2	7.4	6.7	5	35	3 pins		
3	8.6	10.0	7.5	75	spec.	120	376
6	14.8	20.0	7.5	150			
2	9.5	8.6	5	43	3 pins		
3	11	12.9	7.5	97	spec.	120	383
6	19	25.8	7.5	194			
2	3.5	3.2	0.5	1.6			
3	4.1	4.8	0.75	3.6	4 pins	53	162
6	7.0	9.6	0.75	7.2			
2	3.5	3.2	2.5	8	4 pins		
3	4.1	4.8	3.75	18	jumbo	59	216
6	7.0	9.6	3.75	36			

INDEX